The Developmental and Evolutionary Roles of Isoforms of Regulator of G Protein Signalling 3 in Neuronal Differentiation.



Stephen John Fleenor
Jesus College

Thesis submitted for the degree of
Doctorate of Philosophy

The University of Oxford

Department of Physiology, Anatomy and Genetics

Trinity Term 2014

© 2014 Stephen John Fleenor

Acknowledgements

To say that this thesis is the product of my own ingenuity and hard work is, at best, an incomplete sentence. For the skills I learned, and the encouragement and inspiration that carried me through this journey, I owe a great many people my sincere gratitude.

First and foremost, I would like to thank Jo Begbie for, quite simply, always going above and beyond in her role as my supervisor. In this DPhil I found that RGS3 negatively regulates development of neurons. Jo, in every effort she made as my supervisor, exerted a diametrically opposite function in my own development. She was proactively involved in my project, and promoted my scientific development by encouraging me to attend talks, symposiums, and more conferences than a student could hope for (which were all the most treasured experiences of my DPhil – not the least of which were the very non-scientific exploits Jo encouraged in Warwick). In a similar vein, my scientific development is owed in large part to Cedric Patthey, whose prevalence in this thesis does not even begin to illuminate the extent to which we shared intellectual discourse. Cedric has been an invaluable partner in the RGS3 story, and a great friend.

I also would like to acknowledge the rest of the Begbie Lab, past and present. In particular, I would like to thank my four students: Raj Patel, Tom Booth, George Corfield, and Sonia Peh. Though they were not mentioned in this thesis, they all contributed to the project, and they all made the lab a lot more fun. There are many more people in and around Oxford who have helped and guided me, but among them I would like to particularly acknowledge Tam Sirey, who taught me cloning (very well, I should add!) and was one of the first people to fall in love with RGS3 and its isoforms.

I could never accept credit for a scientific achievement of this magnitude without acknowledging my seminal influences at the University of Texas. Ji-Hoon Lee showed me how to be organised, think big, and be a model graduate student. Lastly, I have to give much credit to Janice Fischer, my original mentor and dear friend. Janice showed me biology in all its majesty, and never ceased to believe in me. Were it not for Janice, I would not have experienced anything close to the scientific thrills and wonders that this DPhil and the UT years before it have given me.

This journey has been one of science, but it has been a personal adventure all the same. For the wonderful people in my life that have shared this journey with me, I am always grateful. Among them, I would like to especially thank my parents: my dad, for reminding me that the glory of now is far more important than the terror of then; and my mom, for forcing me to simplify my questions and keep an eye on the bigger picture ('so if I've got this right, you're trying to describe parts of the egg???').

Finally, words can only crudely express my gratitude to Kahlí, my wife and eternal partner. Forever and always, any achievement or lovely happenstance I ever come across will be because of her. She is the band on the gel; the beautiful and strange *in situ* stain; the ovation after giving a daunting talk. Every moment of my life, every pain and difficulty and resulting accomplishment, is wonderful and absolutely perfect, because she is by my side.

Declaration

The design, performance, and analysis of the work in this thesis, with the exceptions listed below, are wholly mine. The written presentation of the work in this thesis is wholly mine.

Exceptions:

- Figure 3.5. RNA extraction, FACS sorting, and transcriptome read analysis all performed by Dr Cedric Patthey (Umeå University, Sweden).
- Figure 3.7. E9.5 mouse embryos dissected by Dr Elizabeth Robertson (University of Oxford).
- Figure 3.8. E15.5 mouse embryo dissection, sectioning and *in situ* hybridisation performed with probes I generated by Dr Peter Oliver (University of Oxford).
- Figures 5.1, 5.2, 5.3, 5.4, 5.5, 5.6. Bioinformatic and transcriptomic analysis conducted by Dr Cedric Patthey.
- Figure 5.3. *In silico* substitution analysis and intron-exon boundary conservation conducted by Dr Cedric Patthey.
- Figure 5.8. RNA from amphioxus adults extracted by Dr Cedric Patthey.
- Figure 5.8. RNA from E6.0 chick embryos for RGS3hL cloning extracted by Alexandra Smith (University of Oxford, laboratory of Jo Begbie).



Stephen John Fleenor

23rd July 2014

Abstract

Fundamental to the complexity of the nervous system is the precise regulation in space and time of the production, maturation, and migration of neurons in the developing embryo. This is eloquently seen in the forming cranial sensory ganglia (CSG) of the peripheral nervous system. Placodes, which are transient pseudostratified neuroepithelia in the surface ectoderm of the embryo, are responsible for generating most of the neurons of the CSG. Placodal progenitors commit to the neuronal fate and delaminate from the epithelium as immature, multipolar neuroblasts. These neuroblasts reside in a staging area immediately outside the placode. Differentiation of the neuroblasts is intimately coupled to their adoption of a bipolar morphology and migration away from the staging area to the future site of the CSG. Thus the forming CSG is a highly tractable model to anatomically separate the three phases of a neuroblast's lifetime: from neuroepithelial progenitor (in the placode), to immature neuroblast (in the staging area), to mature neuron (in the migratory stream).

In this thesis, I used the forming CSG as a model to investigate the role of Regulator of G protein Signalling 3 (RGS3) in neuroblast commitment and differentiation. Promoters within introns of the RGS3 locus generate isoforms in which N-terminal sequences are sequentially truncated, but C-terminal sequences are preserved. Intriguingly, I found that expression of these isoforms in the forming CSG is temporally co-linear with their genomic orientation: longer isoforms are exclusively expressed in the progenitor placode; a medium isoform is expressed exclusively in the neuroblast staging area; and the shortest isoforms are expressed in the neuronal migratory stream. Furthermore, through loss- and gain-of-function experiments, I demonstrated that each of these isoforms plays

a specific role in the differentiation state in which it is expressed: placode-expressed isoforms negatively regulate neurogenesis; the neuroblast-expressed isoform negatively regulates differentiation; and the neuron-expressed isoforms negatively regulate neuronal migration. The negative regulatory role which all isoforms play in different cell-biological contexts is intriguing in light of the fact that they all share a C-terminal RGS domain, which canonically negatively regulates G protein signalling. Through domain mutation and deletion, I showed that the RGS and N-terminal domains are important for the function of each isoform. Thus temporally co-linear expression within the RGS3 locus generates later-expressed isoforms which lack the regulatory N-terminal domains of the earlier-expressed isoforms, giving them new license to perform different biochemical functions.

Lastly, I investigated the conservation and evolution of RGS3 and its isoforms. RGS3 was found to be present in all extant metazoans, and results from this thesis implicate it as the founding member of the R4 subfamily of RGS proteins. Furthermore, in the early vertebrate lineage, a critical domain was lost. This is intriguing in light of the fact that placodes in their stereotypic forms also emerged early in the vertebrate lineage. Ectopic overexpression of the full-length invertebrate RGS3 protein prevented pseudostratification of the vertebrate placode, suggesting that the domain loss in the early vertebrate lineage was important for the evolution of pseudostratified placodes and the expansion of the vertebrate nervous system.

In summary, the work in this thesis has uncovered a previously unseen model of transcriptional regulation of a single locus: intragenic temporal co-linearity. Furthermore, the demonstrated functions of this regulation have profound implications on

the generation and differentiation of vertebrate neurons, as well as the evolution of the vertebrate nervous system.

List of Abbreviations

aa	Amino Acid
BP	Basal Progenitor
bp	Base Pair
CDS	Coding Sequence
CNS	Central Nervous System
CP	Cortical Plate
CSG	Cranial Sensory Ganglia
DAG	Diacylglycerol
DIC	Differential Interference Contrast
DRG	Dorsal Root Ganglia
EGFP	Enhanced Green Fluorescent Protein
EMT	Epithelial-to-Mesenchymal Transition
ER	Endoplasmic Reticulum
ESN	Epidermal Sensory Neuron
EST	Expressed Sequence Tag
FB	Forebrain
GABA	γ-Aminobutyric Acid
GEF	Guanine Exchange Factor
GFP	Green Fluorescent Protein
GnRH	Gonadotropin-Releasing Hormone
GPCR	G Protein-Coupled Receptor
HB	Hindbrain
INM	Interkinetic Nuclear Migration
IPC	Intermediate Progenitor Cell
IZ	Intermediate Zone
kb	Kilobase Pair
LPA	Lysophosphatidic Acid
MB	Midbrain
MTN	Mesencephalic Trigeminal Nucleus
NCC	Neural Crest Cell
NFM	Neurofilament Medium chain
oRGC	Outer Radial Glial Cell
PDZ	PSD-95/Dlg/ZO-1
PH	Pleckstrin Homology
pH3	phosphorylated Histone H3
PNS	Peripheral Nervous System
PPR	Pre-Placodal Region
RACE	Rapid Amplification of cDNA Ends
RGC	Radial Glial Cell
RGS	Regulator of G protein Signalling
RGS3	Regulator of G protein Signalling 3
RPKM	Reads Per Kilobase per Megabase
SC	Spinal Cord
shRNA	Short-Hairpin RNA
SMART	Simple Modular Architecture Research Tool
SVZ	Subventricular Zone
UTR	Untranslated Region
VA	Vestibuloacoustic
VZ	Ventricular Zone

Table of Contents

Chapter 1. Introduction 18

Section 1.1 Evolution and Development of Vertebrate Sensory Neurons 19

Section 1.1.1 The Vertebrate Sensory Nervous System 19

Section 1.1.2 Dual Embryonic Origin of Vertebrate Sensory Neurons 21

Section 1.1.3 Derivatives of the Neural Crest 24

Section 1.1.4 Derivatives of the Neurogenic Placodes 27

Section 1.1.5 Evolution of NCCs and Placodes 32

Section 1.1.6 Behavioural Differences between NCC and Placode Neuronal Derivatives 43

Section 1.1.7 The Cranial Sensory Placodes as a Model for Neurogenesis, Differentiation and Migration in the CNS 50

Section 1.1.8 Discussion 57

Section 1.2 Regulator of G protein Signalling 3 (RGS3): a Candidate Regulator of Placodal Neurogenesis and Migration 60

Section 1.2.1 Identification of RGS3 60

Section 1.2.2 G Protein Signalling and its Regulation 63

Section 1.2.3 Roles of G Protein Signalling in Neurogenesis and Migration 69

Section 1.2.4 RGS3 Encodes Multiple Isoforms 70

Section 1.2.5 RGS3 and the Evolution of the R4 Subfamily of RGS Proteins 80

Section 1.2.6 Discussion 83

Section 1.3 Aims of This Thesis 84

Chapter 2. Materials and Methods 86

Section 2.1 Animal Models 86

Section 2.2 Molecular Biology 86

Section 2.2.1 PCR Amplification 86

Section 2.2.2 Rapid Amplification of cDNA Ends (RACE) 89

Section 2.3 Riboprobe Synthesis and *In Situ* Hybridisation 90

Section 2.4 Antibody Labelling 92

Section 2.5 *In Ovo* Electroporation 93

Section 2.6 Short-Hairpin RNA (shRNA) Design and Cloning 93

Section 2.7 Overexpression Design and Cloning 94

Section 2.8 Design and Cloning of Domain Deletion and Mutation Constructs for Overexpression 96

Section 2.9 Embryo Embedding and Sectioning 97

Section 2.10 Imaging 98

Section 2.11 Cell Counting Analyses 98

Section 2.12 Staging Area Length and Migration Analyses 99

Section 2.13 Quantitative Expression Analysis 101

Section 2.14 Phylogenetic Tree Construction 101

Section 2.15 Statistical Analysis 101

Chapter 3. Expression of Isoforms of RGS3 in Neuronal Development of Chick and Mouse 102

Section 3.1 Introduction 102

Section 3.2 Multiple Isoforms Are Generated by the RGS3 Locus 103

Section 3.2.1 RGS3 Isoforms Initiate at Predicted Promoter Sites 103

Section 3.2.2 Identification of RGS3 Isoforms Expressed in the Forming Chick Petrosal Ganglion 106

Section 3.2.3 Identification of Termini of 3' Untranslated Regions 110

Section 3.3 Spatiotemporally Co-Linear Expression of RGS3 Isoforms 113

Section 3.3.1 Qualitative Expression of RGS3 Isoforms in the Forming CSG 113

Section 3.3.2 Quantitative Expression in Mature CSG 118

Section 3.3.3 Expression of RGS3hL and/or C2PA in Pre-Placodal Cells 121

Section 3.4 Conservation of Expression of RGS3 Isoforms 123

Section 3.4.1 Expression in the Developing Mouse CSG 123

Section 3.4.2 The Forming Mouse Cerebral Cortex 128

Section 3.5 Differential RGS3 Isoform Expression in Other Neural Tissues 131

Section 3.6 Discussion 136

Section 3.6.1 Differential Developmental Expression of RGS3 Isoforms in Chick and Mouse 136

Section 3.6.2 Transcriptional Interference: a Potential Mechanism for the Regulation of RGS3 Isoform Expression 139

Chapter 4. Functional Analysis of RGS3 Isoforms in the Developing Chick Cranial Sensory Ganglia 144

Section 4.1 Introduction 144

Section 4.2 Knockdown of RGS3 Isoforms with Short-Hairpin RNA (shRNA) 145

Section 4.2.1 Design and Efficiency of shRNAs 145

Section 4.2.2 Morphological Effects on the Forming Epibranchial Ganglia 149

Section 4.2.3 Effects on Placodal Neurogenesis 152

Section 4.2.4 Effects on Placodal Neuroblast Differentiation 157

Section 4.2.5 Effects on Placode-Derived Neuronal Migration 162

Section 4.3 Overexpression of Each Isoform Individually 164

Section 4.3.1 Overexpression of RGS3L 168

Section 4.3.2 Overexpression of RGS3s 174

Section 4.3.3 Overexpression of RGS3hs 178

Section 4.4 Discussion 182

Section 4.4.1 Regulation of Progenitor Commitment in the Placode by RGS3hL and RGS3L 183

Section 4.4.2 Regulation of Neuroblast Differentiation by RGS3s 185

Section 4.4.3 Regulation of Neuronal Migration by RGS3hs 188

Chapter 5. On The Evolution of RGS3 191

Section 5.1 Introduction 191

Section 5.2 Evolution of RGS3 and the Expansion of the R4 Subfamily in Vertebrates 193
Section 5.2.1 Conservation of RGS3 in Metazoans 193
Section 5.2.2 Conservation of Isoform Generation in Metazoans 203
Section 5.2.3 Non-RGS3 R4 Members Emerged After Gnathostome Evolution 207
Section 5.3 Ectopic Overexpression of Amphioxus RGS3hL in the Vertebrate Placode 211
Section 5.4 Discussion 216
Section 5.4.1 RGS3hs and the Expansion of the R4 Subfamily 219
Chapter 6. Conclusions 221
Section 6.1 Temporal Co-linearity within the RGS3 Locus 221
Section 6.1.1 RGS3s 222
Section 6.1.2 RGS3hs and RGS4 224
Section 6.2 Evolution of RGS3 and the Placodes 225
Chapter 7. References 228

List of Figures

Figure 1.1. Neurons of the Vertebrate Sensory Nervous System. 20

Figure 1.2. Specification and Segregation of NCC and Placodal Domains. 23

Figure 1.3. Derivatives of NCCs. 26

Figure 1.4. Derivatives of the Neurogenic Placodes. 28

Figure 1.5. Metazoan Phylogeny. 34

Figure 1.6. Rudimentary Placode Structures in Amphioxus and Tunicates. 40

Figure 1.7. Neurogenesis, Differentiation and Migration from the Epibranchial and Trigeminal Maxillomandibular Placodes. 48

Figure 1.8. Neural Tube Formation and Neurogenesis in the Developing Cerebral Cortex. 54

Figure 1.9. A Microarray to Identify Regulators of Placodal Neurogenesis and Migration. 62

Figure 1.10. G Protein Signalling and its Regulation. 65

Figure 1.11. Isoforms of RGS3 in Human and Chicken. 72

Figure 1.12. RGS Proteins and Their Subfamilies. 82

Figure 2.1. Example Design of shRNA Oligos for Cloning. 94

Figure 2.2. Amplification Strategy for the RGS3LΔEF Construct. 97

Figure 2.3. Analysis of Staging Area Length and Migration. 100

Figure 3.1. Isoforms of RGS3 are Transcribed from Different Promoters at the Human Locus. 105

Figure 3.2. Identification of RGS3 Isoforms Expressed in Petrosal Placode-Associated Cells by 5' RACE. 109

Figure 3.3. Resolution of the 3' Untranslated Regions of RGS3 Isoforms. 112

Figure 3.4. Expression of RGS3 Isoforms in the Forming CSG. 117
Figure 3.5. Quantitative Expression of RGS3 Isoforms in Mature CSG. 120
Figure 3.6. Expression of RGS3hL/C2PA in Pre-Placodal Regions. 122
Figure 3.7. Expression of RGS3 Isoforms and RGS4 in the Developing Mouse CSG. 127
Figure 3.8. Expression of RGS3 Isoforms and RGS4 in the Developing Mouse Cortex. 130
Figure 3.9. Expression of RGS3 Isoforms Outside of the CSG. 135
Figure 3.10. Summary of Expression of RGS3 Isoforms. 136
Figure 3.11. Alignment of RGS3hL Exon 20 between Chicken, Mouse and Human. 143
Figure 4.1. Short-Hairpin RNA Design and Efficiency. 148
Figure 4.2. Effects of RGS3 shRNA-*CDS* on Epibranchial Ganglion Formation 151
Figure 4.3. Effects of RGS3 shRNA on the Production of Neuroblasts and Neurons. 154
Figure 4.4. Effects of RGS3 shRNA on Proliferation of Placodal Cells and Delaminated Neuroblasts. 156
Figure 4.5. Effects of RGS3 shRNA on the Spatiotemporal Transcriptional Programme of Placodal Derivatives. 159
Figure 4.6. Effects of RGS3 shRNA on Neuroblast Differentiation. 161
Figure 4.7. Effects of RGS3 shRNA on Neuronal Migration. 163
Figure 4.8. Constructs Designed for Individual Isoform Overexpression. 166
Figure 4.9. Ectopic Transcript Expression from Overexpression Constructs. 167
Figure 4.10. Overexpression of RGS3L Abolishes Neurogenesis. 170
Figure 4.11. Effects of RGS3L Overexpression on Epithelial Integrity. 173

Figure 4.12. RGS3s Overexpression Affects Spatial HuC/D Expression and Neuroblast Differentiation. 177
Figure 4.13. RGS3hs Overexpression Affects Neuronal Migration. 180
Figure 4.14. RGS3hs Overexpression Affects Neuronal Morphology. 181
Figure 5.1. Conservation of RGS3 in Vertebrates 195
Figure 5.2. Conservation of RGS3 in Invertebrates 200
Figure 5.3. Divergence of the PH and GEF Domains from Invertebrate RGS3. 201
Figure 5.4. Phylogenetic Comparison of R4 Subfamily Proteins. 202
Figure 5.5. Conservation of RGS3 Isoforms in Metazoans. 206
Figure 5.6. Conservation of R4 RGS Proteins in Vertebrates. 209
Figure 5.7. A Model for the Evolution and Expansion of the R4 Subfamily. 210
Figure 5.8. Ectopic Overexpression of Amphioxus RGS3hL Alters Morphology of the Vertebrate Placode. 215

List of Tables

Table 1.1. Aliases and Citations of RGS3 Isoforms 73

Table 1.2. Artificial/Partial Isoforms Used in RGS3 Experiments Previously..... 74

Table 2.1. Primers Used for 3' and 5' RACE 90

Table 2.2. Primers, Template Sizes, and Plasmid Information for RGS3 *In Situ* Hybridisation Constructs..... 91

Table 2.3. Primers, Template Sizes, and Plasmid Information for Non-RGS3 *In Situ* Hybridisation Constructs. 92

Table 2.4. Primary and Secondary Antibodies and Concentrations Used in This Thesis. 92

Table 2.5. shRNA Target Sequences Used in This Thesis. 94

Table 2.6. Primers Used for Amplification and Product Sizes of Wild-Type Overexpression Constructs..... 95

Table 2.7. Primers Used for the Generation of Domain Deletion and Mutation Constructs..... 97

Table 3.1. *In Situ* Hybridisation Probes and Positions on the Chicken RGS3 Locus 116

Table 3.2. *In Situ* Hybridisation Probes and Positions on the Mouse RGS3 Locus. 129

Chapter 1. Introduction

In the first section of this introduction I will describe the vertebrate sensory nervous system and its developmental origin from neural crest cells and placodes. I will then describe the derivatives of each of these cell types and the current understanding of their evolutionary origin from an invertebrate ancestor. Lastly, I will contrast their manners of neurogenesis and migration, and make a strong comparison between placodes and the neuroepithelium of the vertebrate central nervous system.

In the second section I will introduce how Regulator of G protein Signalling 3 (RGS3) was identified in the placodes and their derivative neurons. I will outline G protein signalling and its role in neurogenesis and neuronal migration. Then I will describe the isoforms of RGS3 and their differential functions. Lastly, I will contrast RGS3 with other members of the R4 subfamily and speculate on the evolution and expansion of this subfamily from a single invertebrate gene.

These two sections will introduce the basis for my investigations in this DPhil. In the third section, I will outline my aims with this DPhil and will summarise my principal findings.

Section 1.1 Evolution and Development of Vertebrate Sensory Neurons

Section 1.1.1 The Vertebrate Sensory Nervous System

The vertebrate sensory nervous system comprises a highly complex network of paired sense organs and sensory neurons (Figure 1.1). Multiple sensations are detected and relayed by different sensory neuron subtypes to the central nervous system (CNS) for processing. These include: olfaction; audition; gustation; touch, temperature, and pain; as well as unconscious sensations, such as balance, blood baro- and chemo-reception, heart rate and gut distension. The only sensations not conveyed by the sensory nervous system are visual inputs detected by the retina. These signals are relayed along the optic nerve, which forms as an off-shoot of the diencephalon.

All general sensations of the trunk are conveyed through the dorsal root ganglia (DRG). These ganglia comprise the cell bodies of primary sensory neurons. They are positioned bilaterally along the rostral-caudal axis of the spinal cord and project afferent axons from the periphery to the CNS.

In the head, olfaction is detected by the olfactory epithelium and relayed by the olfactory cranial nerve. All other sensations in the head are relayed by primary sensory neurons of the cranial sensory ganglia (CSG). Like the DRG, these ganglia comprise cell bodies of primary sensory neurons that relay signals from the periphery to the CNS. They are positioned bilaterally along the rostral-caudal axis of the hindbrain and the afferent axon bundles they project comprise several of the cranial nerves. The trigeminal ganglion associates with the Vth (trigeminal) nerve; the geniculate ganglion associates with the VIIth (facial) nerve; the vestibular and acoustic ganglia associate with the VIIIth (acoustic) nerve; the petrosal and superior ganglia associate with the IXth

(glossopharyngeal) nerve; and the nodose and jugular ganglia associate with the Xth (vagus) nerve.

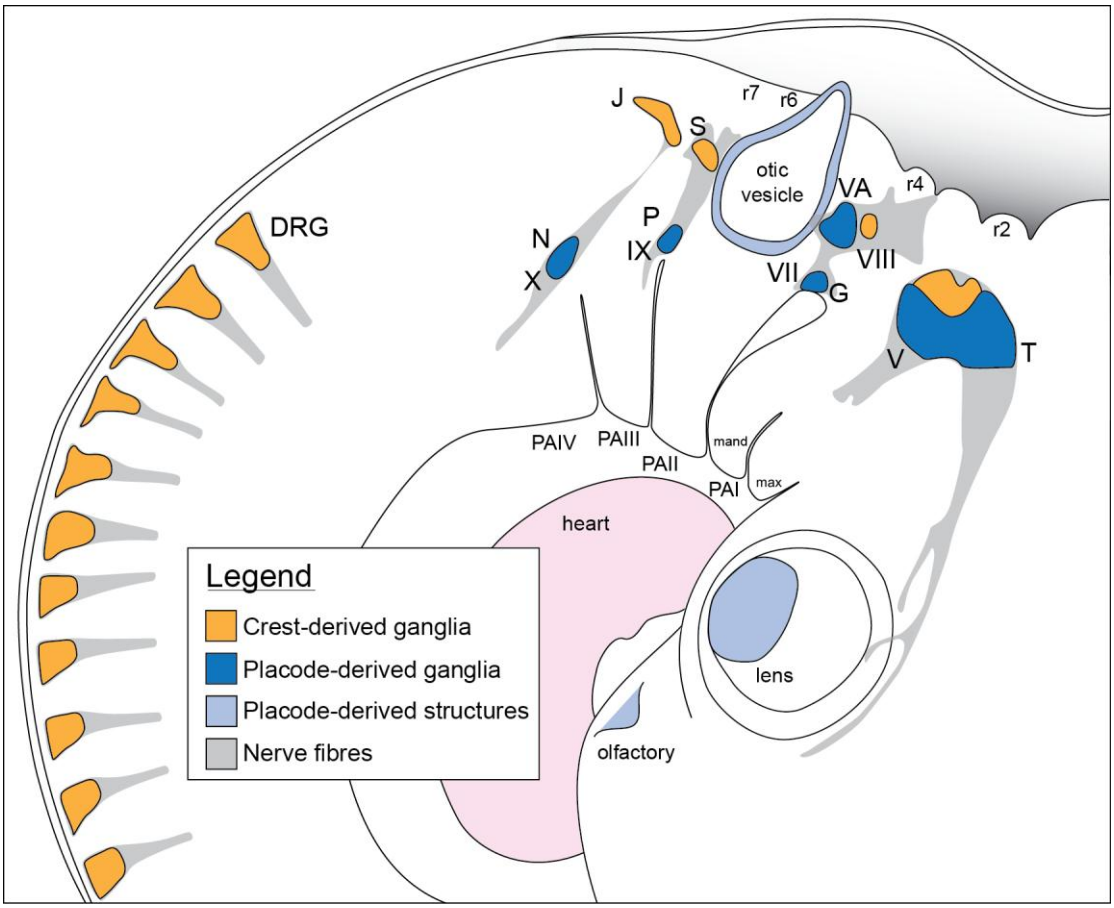


Figure 1.1. Neurons of the Vertebrate Sensory Nervous System.
Cartoon of a Hamburger-Hamilton stage 20 (HH20) (Hamburger and Hamilton, 1992) chick embryo depicting nerves (grey) and sensory ganglia of the developing peripheral nervous system. Cranial nerves V, VII, VIII, IX and X associate with the trigeminal (T), geniculate (G), vestibuloacoustic (VA), petrosal (P), superior (S), nodose (N), and jugular (J) ganglia. In the trunk, each dorsal root ganglion (DRG) and its associated nerve associates with a somite. The DRG and proximal cranial ganglia are neural crest-derived (orange), while the distal cranial ganglia are placode-derived (dark blue). In addition, placodes contribute the olfactory epithelium, the non-neural epithelium of the lens, and the otic vesicle (light blue), which gives rise to the inner ear. The heart is shown for embryonic reference, but its associated vessels and pericardial tissue are not shown. Adapted from (Kuratani et al., 1988).

Section 1.1.2 Dual Embryonic Origin of Vertebrate Sensory Neurons

The distinction between trunk and head sensory structures largely reflects a dual embryonic origin of vertebrate sensory neurons (Figure 1.1). In the trunk, DRG neurons are derived from neural crest cells (NCCs), a migratory stem cell population from the dorsal neural tube that gives rise to a diverse array of neural and non-neural cell types (Le Douarin and Kalcheim, 1999).

In the head, the more proximal neurons of the CSG are formed from NCCs (orange in Figure 1.1). However, many of the CSG neurons derive from the neurogenic placodes (blue in Figure 1.1) (D'Amico-Martel and Noden, 1983; Harlow and Barlow, 2007; Harlow et al., 2011; Thompson et al., 2010). Placodes are transient specialised regions of epithelia on the surface ectoderm that generate neural and non-neural derivatives (see Section 1.1.4).

While the CSG are comprised of NCC- and placode-derived neurons, these neurons are spatially separated. Relative to the position along the cranial nerve, NCC-derived neurons comprise the proximal components of the CSG and placode-derived neurons comprise the distal components of the CSG (D'Amico-Martel and Noden, 1983). In the case of the IXth and Xth nerves, the distal and proximal ganglia are separated. In the case of the Vth nerve, there is only one ganglion, but its proximal aspect is entirely NCC-derived and its distal aspect is entirely placode-derived (D'Amico-Martel and Noden, 1983). The geniculate ganglion is entirely placode-derived and does not have a proximal component (D'Amico-Martel and Noden, 1983; Harlow et al., 2011). The vestibular and acoustic ganglia of the VIIIth nerve are exceptional. Together they form a complex and do not have proximal or distal components. While it is clear that the entire acoustic ganglion and most of the vestibular ganglion are placode-derived, NCC-derived neurons

contribute to some of the vestibular ganglion (D'Amico-Martel and Noden, 1983; Freyer et al., 2011; Harlow et al., 2011).

Section 1.1.2.1 Embryonic Origins of NCC- and Placode-Derived Neurons are Spatially and Temporally Distinct

The embryonic origins of NCC- versus placode-derived neurons are distinct. While NCCs and placodes are both specified from a common border region lateral to the neural plate, this later segregates into lateral stripes of neural and non-neural ectoderm, respectively (Figure 1.2A) (Begbie, 2013; Patthey and Gunhaga, 2011). At early neurula stages, these regions abut each other, and different placodes are specified between anterior and posterior (Begbie, 2013; Patthey and Gunhaga, 2011). However, after neural tube closure at late neurula stages, pre-migratory NCCs are restricted medially to the dorsal neural tube and individually-specified placodes are positioned ventro-laterally on the surface of the embryo (Figure 1.2B) (D'Amico-Martel and Noden, 1983; Graham and Begbie, 2000).

During sensory neurogenesis, differentiated neuroblasts break away from the placodal epithelium and migrate into the embryo (toward the neural tube) to form the CSG. Cranial NCCs migrate throughout the head before the onset of placodal neurogenesis (Freter et al., 2013), but they do not differentiate into post-mitotic neurons of the proximal CSG until after the placode-derived distal CSG have formed (Figure 1.2C) (D'Amico-Martel, 1982; D'Amico-Martel and Noden, 1980; Hiscock and Straznicky, 1986; Thompson et al., 2010). The developmental origins of NCC- versus placode-derived CSG neurons are therefore very distinct, reflecting the developmental differences between NCCs and placodes themselves (see Section 1.1.6).

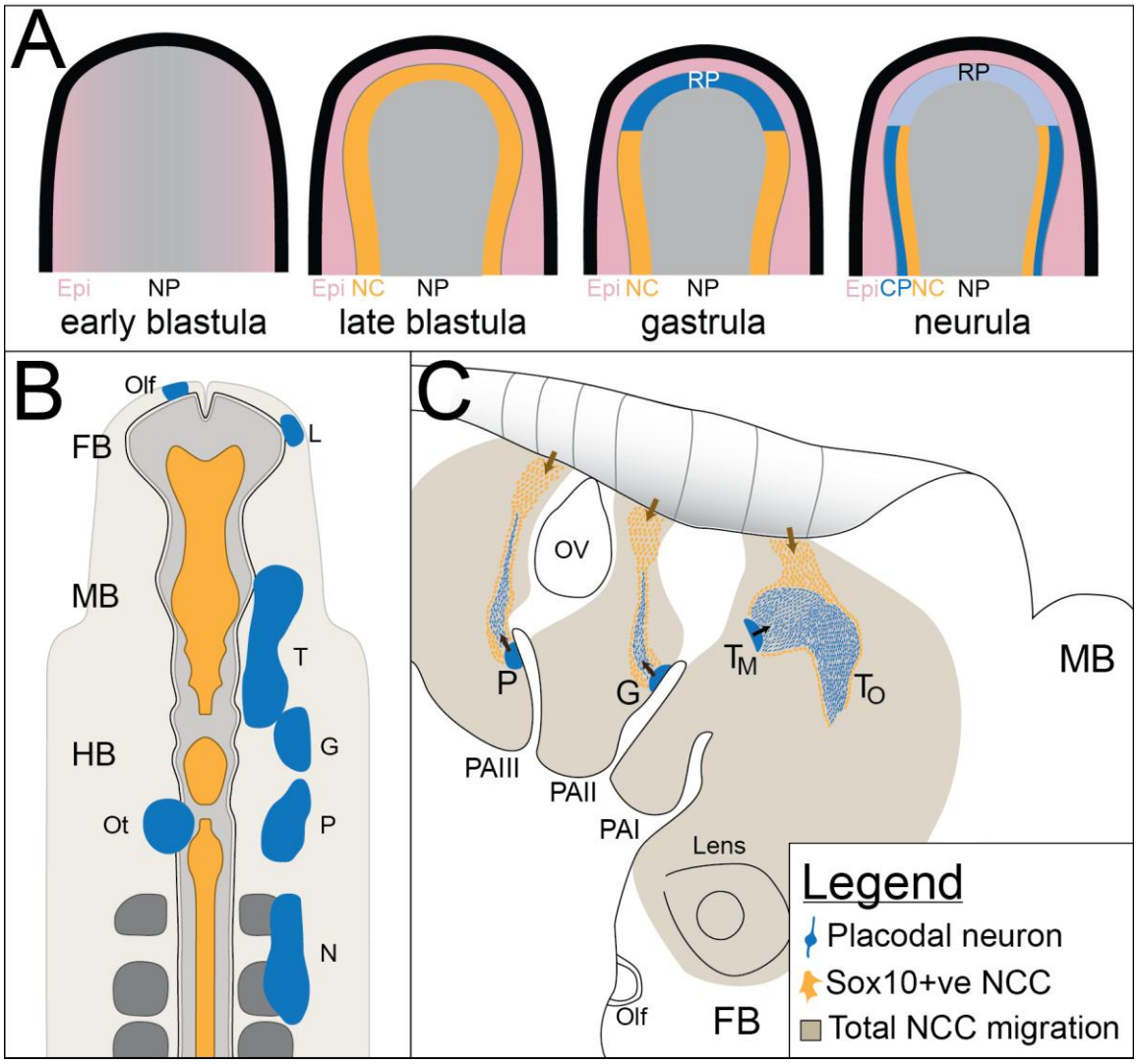


Figure 1.2. Specification and Segregation of NCC and Placodal Domains.
Figure legend on next page.

Figure 1.2. Specification and Segregation of NCC and Placodal Domains.
(A) Formation of the neural plate (NP) border. At early blastula stages, the NP is specified from surrounding ectodermal epidermal tissue (see Figure 1.8). A pre-neural crest (NC) domain forms at the lateral edges of the neural plate domain, followed by a pre-rostral placode (RP; later giving rise to the adenohypophysis, olfactory, and lens placodes) domain at the anterior ridge. At neurula stages, a pre-caudal placode (CP) domain forms at the lateral edge of the epidermis. Together the CP and RP domains comprise the pre-placodal region (PPR). *(B)* Fate map of an HH10 chick embryo showing the specified NC and pre-placodal domains segregated between the medial dorsal neural tube and the lateral surface ectoderm, respectively. Individual pre-placodal domains have also segregated. Note: the adenohypophyseal pre-placodal domain is not shown. Lateral line placodes are not present in amniotes. Each placodal domain develops bilaterally, and the contralateral domain for each is not shown. *(C)* HH18 chick embryo showing the pre-migratory origins of NCCs and placodes (indicated by brown and black arrows, respectively) are very segregated. NCCs have migrated throughout the head, but have yet to differentiate into neurons. A subset, marked by Sox10 expression, form structural corridors guiding the migration of placodal neurons (Freter et al., 2013) (see Section 1.1.6). Petrosal (P), geniculate (G), and trigeminal maxillomandibular (T_M) placodes are indicated in blue. The trigeminal ophthalmic (T_O) placode is lateral to the ganglion and is not distinguishable in wholemount. Nodose (N) placode is not shown. FB: forebrain; HB: hindbrain; L: lens; MB: midbrain; Olf: olfactory; Ot: otic; PAI-III: pharyngeal arches I-III. Adapted from (Begbie, 2013) *(A)* and (Fleenor and Begbie, 2014) *(B,C)*.

Section 1.1.3 Derivatives of the Neural Crest

In addition to sensory neurons of the peripheral nervous system (PNS), NCCs contribute a multitude of cell types. NCCs are initially specified as early as the late blastula stage from the neural (non-epidermal) component of the neural plate border (Figure 1.2A) (see Section 1.1.2.1) (Begbie, 2013; Patthey and Gunhaga, 2011). Around the time of neural tube closure, pre-migratory NCCs undergo an epithelial-to-mesenchymal transition (EMT) and migrate throughout the mesoderm along well-defined pathways (Begbie, 2013; Kulesa et al., 2010). While NCCs emigrate from all rostro-caudal levels of the neural tube between the midbrain to the caudal spinal cord (Figure 1.3A), rostral NCCs emigrate first.

In the head, NCCs flood through the mesoderm of the pharyngeal arches to give rise to bones and cartilage of the head and neck (Figure 1.2C) (Dupin et al., 2006). A later-migrating population of NCCs is more dorsally restricted, and largely does not contribute these derivatives (Baker et al., 1997). Both early- and late-migrating cranial NCCs are

capable of giving rise to neurons of the proximal CSG as well as neurons of the parasympathetic nervous system. Additionally, these give rise to melanocytes (Baker et al., 1997), the pigment-producing cells of the skin.

Vagal NCCs, which emigrate at the level of the first six somites, give rise to connective tissue of the heart and to neurons of the enteric nervous system (Begbie, 2013; Dupin et al., 2006). More caudally, along the rostro-caudal distance of the spinal cord, NCCs of the trunk contribute DRG and ganglia of the sympathetic nervous system (Figure 1.3B). DRG and sympathetic ganglia are formed from an early-migrating population of trunk NCCs which travel through the rostral sclerotome of each somite (Begbie, 2013). DRG form lateral to the neural tube, and sympathetic ganglia are positioned more ventrally, adjacent to the dorsal aorta. In addition, trunk NCCs give rise to chromaffin cells of the adrenal medulla, which are positioned above the kidneys. A later-migratory population of trunk NCCs travel along a more dorsolateral pathway and give rise to melanocytes (Begbie, 2013). Lastly, in both the head and trunk, NCCs contribute the Schwann cells and satellite glia associated with the peripheral nerves and ganglia, respectively.

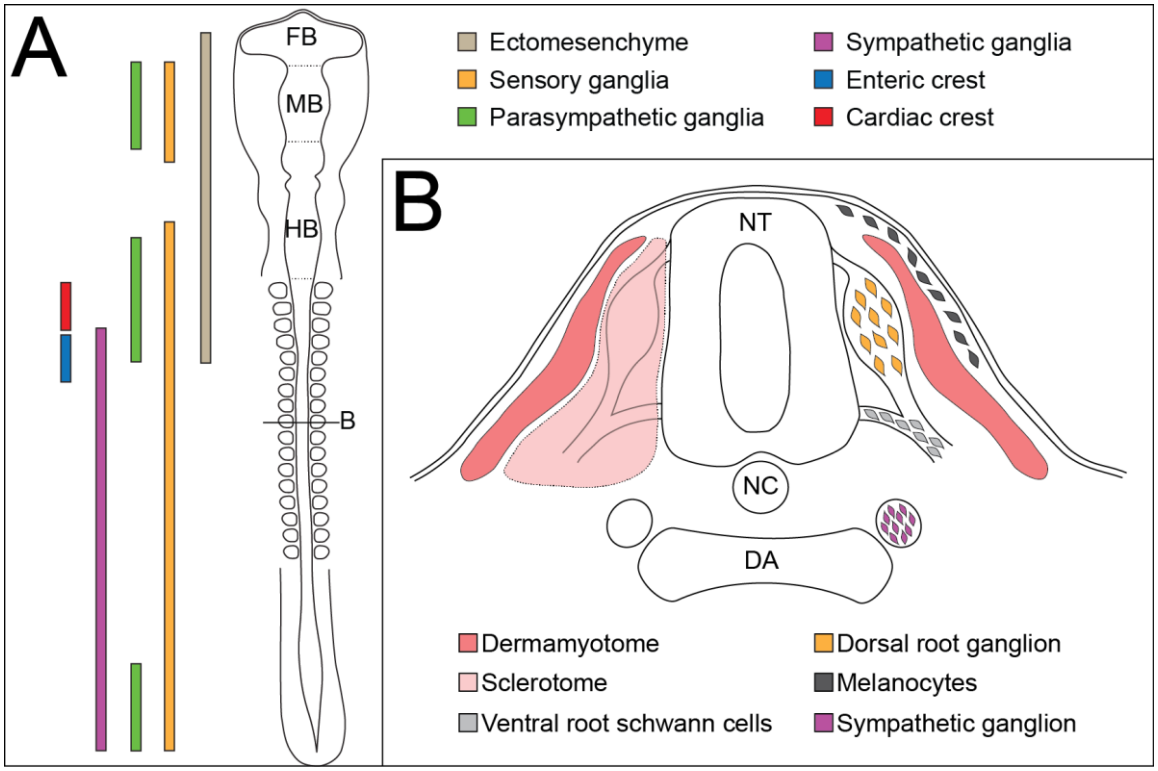


Figure 1.3. Derivatives of NCCs.
NCCs differentiate into different cell types along the rostro-caudal axis *(A)* as well as the dorso-ventral and medio-lateral axes *(B)*. In the head, ectomesenchymal NCCs give rise to musculature, bones and cartilage of the head and neck (not shown). In the trunk, an early migratory population travels through the sclerotome of the somite and gives rise to dorsal root ganglia, sympathetic ganglia, and Schwann cells. A later migratory population of NCCs travels between the surface ectoderm and the dermamyotome of the somite to give rise to melanocytes. Note: NCCs migrate bilaterally and give rise to contralateral structures. DA: dorsal aorta; FB: forebrain; HB: hindbrain; MB: midbrain; NC: notochord; NT: neural tube. Adapted from (Begbie, 2013).

Section 1.1.4 Derivatives of the Neurogenic Placodes

Placodes are specified from a horseshoe-shaped band lateral to the anterior neural plate of neurula stage embryos called the pre-placodal region (PPR) (Figure 1.2A) (see Section 1.1.2.1). This region is defined by fate maps in the chick which show its commitment to the placodal fate (Bhattacharyya et al., 2004; Pieper et al., 2011; Streit, 2002) as well as by its unique expression of Six and Eya genes (Grocott et al., 2012; Schlosser, 2006; Streit, 2007), which continues through the onset of placode induction.

Individual placodes, however, have distinct Pax gene expression identities and are induced by local signals from neighbouring tissues (Grocott et al., 2012; Schlosser, 2006; Streit, 2007). Furthermore, placodes are highly diverse in terms of the derivatives they produce. With the exception of the adenohyophyseal (pituitary) placode, which gives rise to endocrine cells of pituitary gland, and the lens placode, which invaginates to give rise to the non-neural lens, all of the placodes are neurogenic (Baker and Bronner-Fraser, 2001).

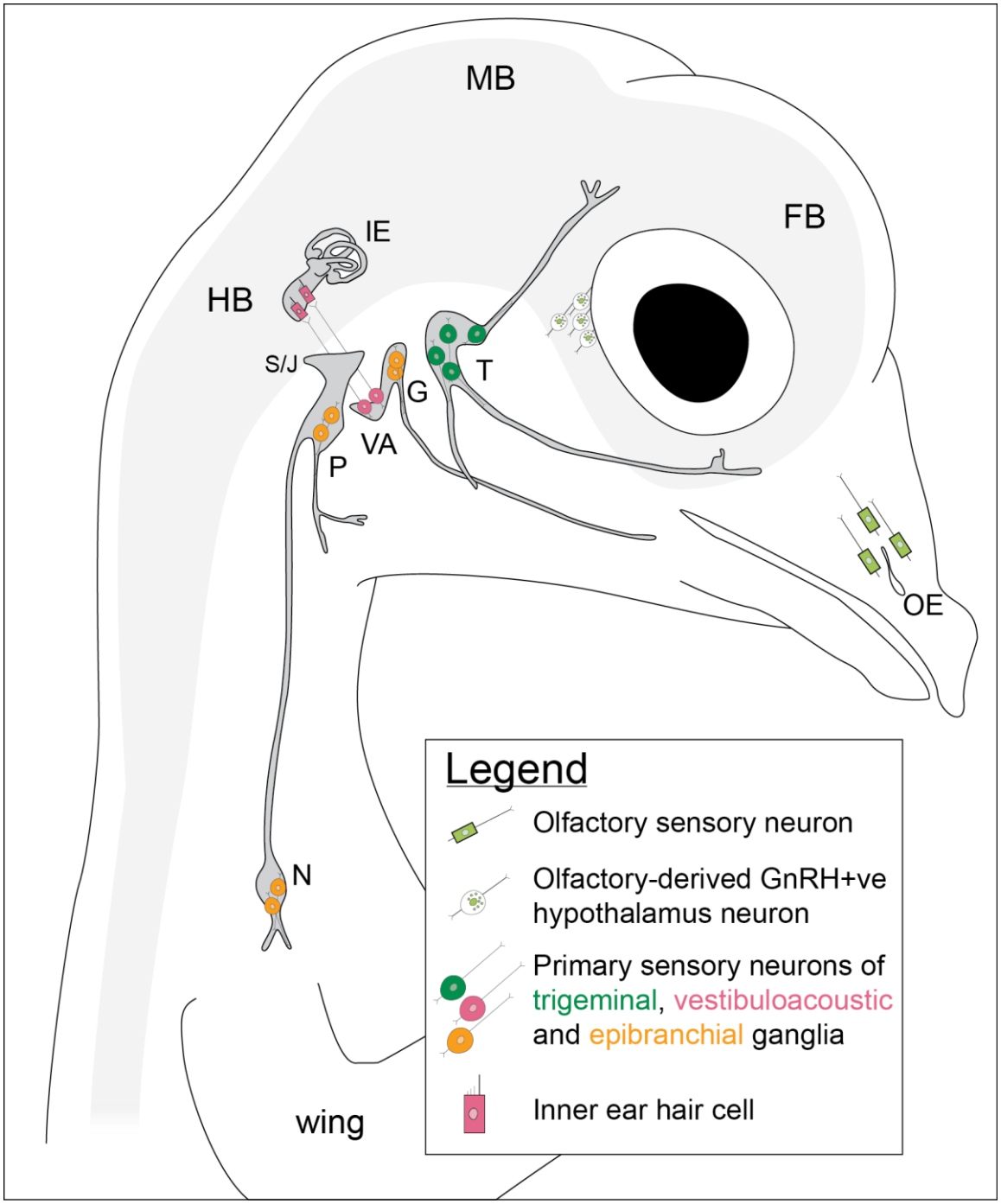


Figure 1.4. Derivatives of the Neurogenic Placodes.
Figure legend on next page.

Figure 1.4. Derivatives of the Neurogenic Placodes.
Embryonic day 12.0 (E12.0; HH38) chick embryo. Posterior placodes (cranial sensory placodes) generate primary sensory neurons of the trigeminal (T), geniculate (G), vestibuloacoustic (VA), petrosal (P) and nodose (N) ganglia. In addition, the otic placode contributes hair cells of the inner ear (IE), which are innervated by primary sensory neurons of the VA ganglion. Note: neurons of the proximal NCC-derived ganglia are not shown, but the superior/jugular (S/J) ganglionic complex is shown. The epithelium of the olfactory placode (OE) gives rise to epithelial olfactory sensory neurons as well as GnRH-positive cells, which migrate to and reside in the hypothalamus. Note: as this is an amniote embryo, derivatives of the lateral line placodes are not shown. CNS shown in grey. FB: forebrain; HB: hindbrain; MB: midbrain. Adapted from (D'Amico-Martel and Noden, 1983), (Streit, 2008) and (Patthey et al., 2014).

Section 1.1.4.1 The Olfactory Placode Generates Sensory and Non-Neural Cell Types

Of all the placodes, the olfactory placode is the most pluripotent. It invaginates to form the nasal epithelium, giving rise to supporting cells and glandular cells as well as olfactory sensory neurons. Prior to formation of the nasal epithelium, it also generates two populations of neurons which delaminate and migrate toward the CNS. In HH14 chick embryos, prior to placode invagination, an early population of neurons emigrates from the placode (Fornaro et al., 2001). Later, the olfactory placode also gives rise to gonadotropin-releasing hormone (GnRH)-positive neurons, which migrate into the CNS and reside in the hypothalamus. It is thought that the migration of the earlier population prefigures the olfactory nerve, providing a migratory tract for the later GnRH-positive neurons (Begbie, 2013; Fornaro et al., 2001).

Section 1.1.4.2 Posterior Placodes Generate Sensory Ganglia

Based on their initial specification from the PPR, placodes are broadly classified as anterior or posterior (or rostral and caudal, as indicated in Figure 1.2A) (see Section 1.1.2.1) (Streit, 2007). The anterior placodes include the adenohypophyseal, olfactory, and lens. The posterior placodes include the trigeminal, otic, and epibranchial series. Additionally, anamniote embryos possess a lateral line series of placodes which give rise to the mechano- and electroreceptive organs of the lateral line system (Schlosser, 2006).

The posterior placodes (henceforth referred to as the cranial sensory placodes) generate sensory neurons, which delaminate from the placodal epithelium on the surface of the embryo and migrate internally to form the CSG. These neurons are broadly divided between somatosensory and viscerosensory neurons. Somatic sensation generally involves sensory receptors on the surface of the body, and includes: mechanoreception (touch, hearing, and balance); thermoreception (temperature); nociception (pain); proprioception; and chemoreception. Visceral sensation involves innervation of internal organs, including taste buds, blood vessels and airways.

Section 1.1.4.2.1 The Trigeminal Ganglion

The trigeminal and vestibuloacoustic ganglia are responsible for somatic sensation. The trigeminal ganglion is responsible for general somatic sensation, relaying touch, temperature, and pain sensations in the face. It is comprised of two lobes: the ophthalmic, which innervates the skin of the face, the eyes and the nose; and the maxillomandibular, which branches to innervate the upper (maxillary) and lower (mandibular) jaw. These lobes are separated into distinct ganglia in developing anamniotes, reflecting the fact that they originate in development from two distinct placodes (Baker and Bronner-Fraser, 2001). The trigeminal placodes are molecularly distinct; for example, Pax3 is expressed in the ophthalmic but not in the maxillomandibular placode (Baker et al., 1999). In addition, the structure and neurogenic behaviour of the two placodes is quite distinct. The ophthalmic placode generates post-mitotic neurons from many small thickened foci; by contrast, the maxillomandibular placode produces mitotic neuroblasts from a continuous thickened field (Begbie, 2013; Begbie et al., 2002). The ophthalmic placode is located at the midbrain-hindbrain border and the maxillomandibular is located more ventrally.

Section 1.1.4.2.2 The Vestibuloacoustic Ganglion

The ganglia arising from the otic placode are collectively referred to as a single vestibuloacoustic ganglion. Prior to generation of sensory neurons, the otic placode invaginates to form the otic vesicle. This structure later gives rise to the entire mechanosensory and structural framework of the inner ear, including the hair cells that are innervated by sensory neurons of the VIIIth nerve. The patterning of the otic vesicle during inner ear formation has been widely studied (Groves and Fekete, 2012; Raft and Groves, 2014), as has the neurogenic programme specifying sensory neuron versus hair cell differentiation (Maier et al., 2014). Together, this network relays auditory and vestibular sensation. The neurons comprising the vestibuloacoustic ganglion emigrate from the anterior part of the otic vesicle.

Section 1.1.4.2.3 The Epibranchial Ganglia

The epibranchial series of ganglia, comprising (from rostral to caudal) the geniculate, petrosal and nodose, are responsible for visceral sensations. The geniculate ganglion primarily innervates taste buds, and the petrosal ganglion innervates taste buds as well as the carotid body and other visceral organs (Dauger et al., 2003). The nodose ganglion innervates a wide variety of targets, including blood vessels, airways, and the gastrointestinal tract (Zhuo et al., 1997). The epibranchial placodes crown the anterior aspect of each branchial arch, just posterior to the pharyngeal pouch (Figure 1.2B). In anamniotes, which possess additional caudal pharyngeal pouches, additional nodose placodes are present (Schlosser, 2006).

Section 1.1.5 Evolution of NCCs and Placodes

The intricate relationship between NCC and placodal derivatives in the head has raised intriguing questions about their co-evolution. Together the two populations generate most of the sensory structures of the vertebrate head, including the olfactory system, inner ear, and lens. In addition, NCCs give rise to the bone and cartilage of the head. In gnathostome vertebrates, which evolved after the divergence of agnathans such as lamprey and hagfish, NCCs give rise to jaws. Gans and Northcutt initially noted that while the cephalochordate amphioxus, which at the time was considered to be the closest living invertebrate relative, is confined to filter feeding, vertebrates are endowed with higher-order sensation that allows them to detect prey, and gnathostomes have the jaws to predate (Gans and Northcutt, 1983). These observations, coupled to the ostensible absence of NCCs and placodes in invertebrates, were the basis of 'The New Head Hypothesis' (Gans and Northcutt, 1983; Northcutt, 2005). This idea suggested the development of NCC- and placode-derived head structures as a necessary innovation in early vertebrates to evolve from a filter-feeding to predatory lifestyle.

Section 1.1.5.1 The Chordate Phylum in Metazoan Phylogeny

To investigate the evolutionary origins of placodes and NCCs, studies have focused on two extant taxa: the cephalochordate amphioxus, and the tunicate ascidians. Together with vertebrates, these taxa make up the Chordate phylum (Figure 1.5) (Maddison and Schulz, 2007). This phylum belongs to the superphylum Deuterostomia, which also contains two major phyla: echinoderms, comprised of sea urchins, starfish and sea cucumbers; and hemichordates, comprised of marine worms such as *Saccoglossus*. Deuterostomes make up bilateral animals along with protostomes, which contain: ecdysozoans, including arthropods and nematodes; and lophotrochozoans, including

annelids and molluscs. Bilateral animals, together with Cnidarians such as the jellyfish, comprise the Eumetazoa clade. Poriferans diverged early in metazoan evolution, prior to the divergence of Eumetazoans. Today members of this clade represent the most distant living relatives of vertebrates in the animal (metazoan) kingdom.

Based on morphological analyses, amphioxus was historically considered to be more closely related to vertebrates than tunicates. However, molecular phylogenetic comparisons show that tunicates are more closely related to vertebrates than amphioxus (Delsuc et al., 2006). Thus within chordates, vertebrates and tunicates are sister groups in a clade called olfactores, and cephalochordates share a more ancient common ancestor.

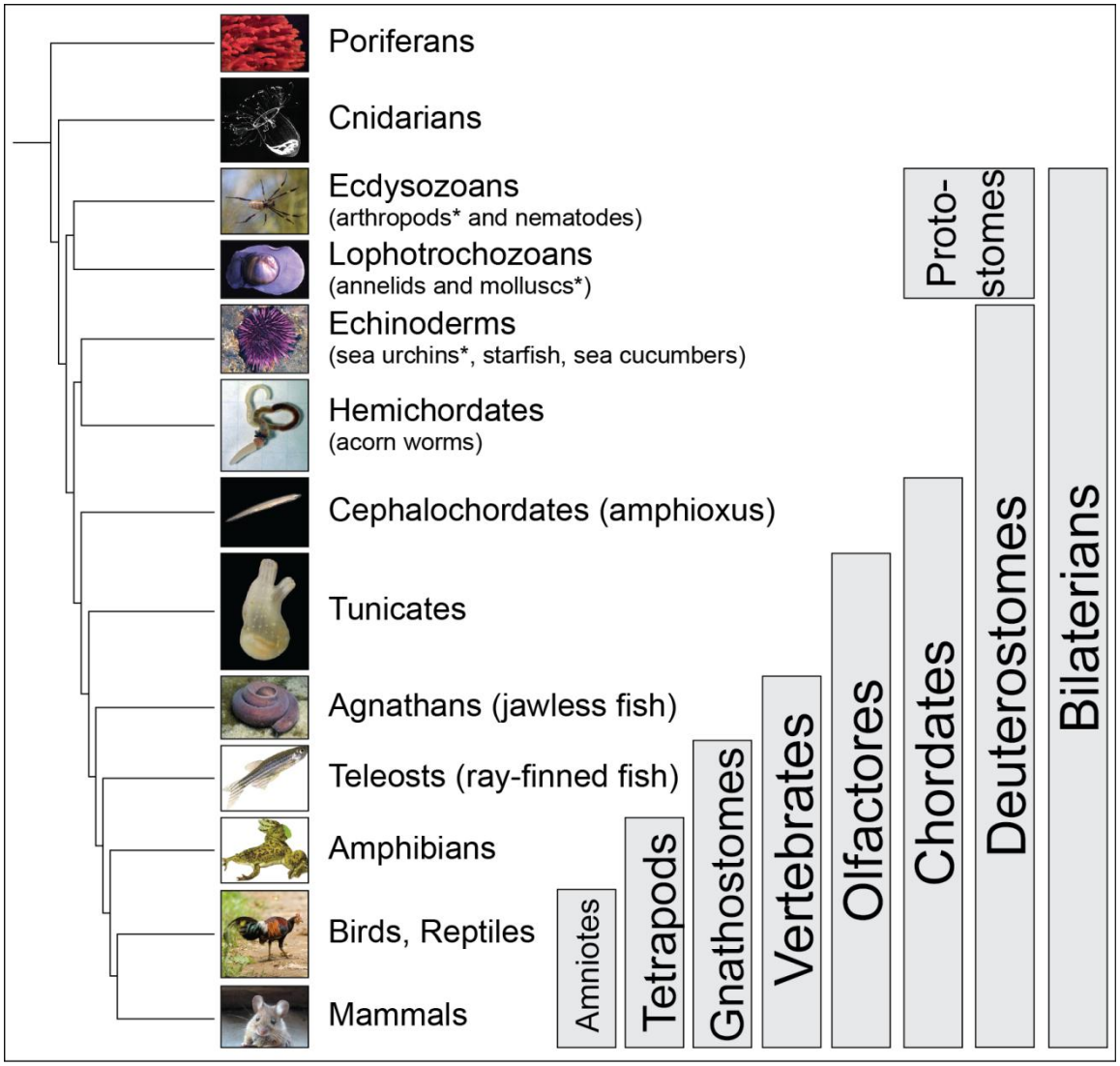


Figure 1.5. Metazoan Phylogeny.
The major taxa of modern animals are shown, with an emphasis on the divisions of chordates and vertebrates. Common aliases are indicated in brackets. The major clades of ecdysozoans, lophotrochozoans and echinoderms are listed in brackets underneath. The asterisked clade is pictured. Images courtesy of (Maddison and Schulz, 2007) and Google Images.

Section 1.1.5.2 Identification of Rudimentary Placodes in Invertebrate Chordates

The identification of homologous placodal structures in invertebrate chordates by means of anatomical and positional comparisons of amphioxus, tunicates, and fossils of extinct chordates has been controversial; and similarities between components of structures do not necessarily imply a common origin of those structures (Patthey et al., 2014). However, studies correlating conservation of gene expression with sensory ultrastructure in amphioxus and tunicates potentially reveal rudimentary placodes in invertebrate chordates.

Section 1.1.5.2.1 Amphioxus Epidermal Sensory Neurons Originate from a Placode-Like Domain

Amphioxus larvae contain epidermal sensory neurons (ESNs) which derive from a field of non-neural epithelium on the ventral surface ectoderm (Figure 1.6). This ventral field and the migratory neurons it produces express the NK-like homeobox transcription factor Tlx (Kaltenbach et al., 2009; Lu et al., 2012), homologues of which mark cranial sensory placodes and their derivative ganglia in vertebrates (Logan et al., 1998). Furthermore, ESNs express Brn3 (amphioxus Pou4) (Candiani et al., 2006), a POU-domain transcription factor expressed in neurons derived from the trigeminal and otic placodes of vertebrates, as well as their somatosensory neural derivatives (Artinger et al., 1998; Badea et al., 2012). ESNs born in this ectoderm migrate along the basal surface and re-integrate into the dorsal surface ectoderm (Figure 1.6) (Kaltenbach et al., 2009).

Some ESNs possess a basal axon which extends internally and innervates the CNS (as pictured, Figure 1.6). On their apical (external) surface, all ESNs protrude a single large cilium and many microvilli. Based on this ultrastructure, they are thought to be mechanoreceptors (Kaltenbach et al., 2009; Lacalli and Hou, 1999). Such an

ultrastructure resembles vertebrate hair cells. These cells, on the surface of the inner ear and lateral line organs, are derived from the otic and lateral line placodes, respectively (Schlosser, 2005) (see Section 1.1.4). Hair cells are also mechanoreceptors, characterised by a single large cilium ('kinocilium') and several microvilli ('stereocilia'). Like some amphioxus ESNs (Lacalli and Hou, 1999), hair cells do not possess an axon. However, other amphioxus ESNs possess an axon along with apical cilia, an ultrastructure not present in vertebrates (Patthey et al., 2014). This possibly represents an ancestral ultrastructure which diversified in vertebrate evolution (elaborated in Section 1.1.5.2.3).

Section 1.1.5.2.2 The Tunicate Atrial Primordium Resembles an Otic Placode

Tunicates, which are more closely related to vertebrates, also possess Brn3-positive ESNs at the dorsal and ventral midlines of the larval tail (Candiani et al., 2005; Mazet et al., 2005; Tang et al., 2013). Like amphioxus ESNs, these neurons are born in non-neural epidermis. However, these neurons do not migrate, and reside in their place of origin. Thus while they are sensory neurons which transcriptionally resemble amphioxus ESNs, they do not developmentally resemble placode-derived sensory neurons.

The head of tunicates might better suggest a pre-vertebrate origin of placodes. In larvae, bilateral epithelial primordia anterior and posterior to the brain give rise to the oral and atrial siphons of the adult, respectively. These primordia seem to resemble the anterior and posterior placodes of vertebrates, respectively (Figure 1.6) (Graham and Shimeld, 2013). Both express Six and Eya genes (Mazet et al., 2005), which mark the pre-placodal region (see Section 1.1.4). The more anterior oral primordium expresses Pitx, a marker of the anterior vertebrate placodes (Christiaen et al., 2002; Mazet et al., 2005).

The more posterior atrial primordium expresses FoxI (Mazet et al., 2005), Pax2/5/8 (Mazet et al., 2005; Wada et al., 1998), and Dlx (Irvine et al., 2007). These genes cooperate in a synergistic pathway to specify and maintain the otic placode downstream of FGF signalling (Hans et al., 2004; Mackereth et al., 2005). Consistently, formation of the atrial primordium depends on FGF signalling (Kourakis and Smith, 2007). Like vertebrate placodes, the atrial ectoderm thickens shortly after its induction (Mazet et al., 2005). In addition, like the otic placode (as well as the olfactory and lens placodes), the atrial primordium invaginates shortly after induction (Kourakis et al., 2010; Mazet et al., 2005). Furthermore, the forming atrial siphon expresses Neurogenin, the vertebrate homologue of which labels the placodes (Mazet et al., 2005) (and see Section 1.1.6.2.1).

If the atrial primordium is a true otic placode homologue, there should be conservation in the ultrastructure and function of its derivatives. Namely, cells should reside in the atrial siphon which resemble the mechanosensory hair cells of the inner ear and lateral line organs. There is some evidence of these cells. Ciliated sensory cells have been observed in the atrial siphon in scanning electron micrographs (Bone and Ryan, 1978; Burighel et al., 1998) and proposed to be mechanosensory. Furthermore, mechanosensation in the wall of the atrial siphon has been demonstrated in at least one tunicate (Mackie and Singla, 2003).

Section 1.1.5.2.3 Ancestral Diversity of Placode-Derived Sensory Neuron Subtypes

It is important to note that the diversity of vertebrate placode-derived sensory subtypes is far greater than that discovered in amphioxus or tunicates. The trigeminal, otic, epibranchial, and lateral line placodes all generate sensory neurons with free axon endings (non-ciliated), which either detect sensation directly or synapse with secondary

sensory cells (such as otic- and lateral line-derived hair cells). These neurons innervate a broad array of targets and relay a commensurate diversity of sensations.

Amphioxus and tunicates, and members of many other clades of Metazoa, have some mechanosensory neurons which are structured differently. Both clades contain axonless mechanoreceptors which resemble vertebrate hair cells; however, they also possess ciliated mechanoreceptors which project a basal axon. It is possible that the division of labour between hair cell mechanosensation and sensory neuron communication to the CNS occurred early in vertebrate evolution, with the separate non-ciliated sensory neuron diversifying to detect other (non-mechanosensory) sensations (Patthey et al., 2014).

It is unclear to what extent the transcriptional diversity of vertebrate sensory neuron subtypes is common to all chordates. In vertebrates, neurons positive for the somatosensory marker Brn3 derive from the otic, trigeminal and lateral line placodes (Artinger et al., 1998; Badea et al., 2012). Neurons positive for the viscerosensory marker Phox2 derive from the epibranchial placodes (Brunet and Pattyn, 2002) (see Section 1.1.6.2.1). Phox2-positive/Brn3-negative neurons have been identified in molluscs (lophotrochozoan protostomes), which diverged from Bilateria prior to deuterostomes (Figure 1.5). However these were only motor neurons, and no visceral sensory neurons of the PNS were seen (Nomaksteinsky et al., 2013). This suggests that while the specification of Brn3-positive somatic versus Phox2-postive visceral neurons is ancient, the division between these subtypes in sensory neurons is restricted to deuterostomes. Brn3 has been found to be expressed in ESNs of both amphioxus (Candiani et al., 2006) and tunicates (Candiani et al., 2005; Mazet et al., 2005; Tang et al., 2013), consistent with an ultrastructure which resembles somatosensory hair cells. Phox2 expression has not been investigated in amphioxus; in tunicates, Phox2 is not

expressed in ESNs, but is expressed in the atrial ectoderm of juveniles (Mazet et al., 2005). However, neither Phox2 nor Brn3 expression has been examined in sensory neurons of the adult atrial siphon, and the possibility cannot be ruled out that Phox2-, Brn3-double positive sensory neurons exist there.

However, the presence of Phox2 in the atrial ectoderm of tunicates suggests that the atrial primordium might possess epibranchial-like characteristics in addition to otic-like characteristics (Section 1.1.5.2.2). The epibranchial and otic placodes arise from a posterior placodal area (PPA) (Ladher et al., 2010). Like the atrial primordium (Kourakis and Smith, 2007), the PPA is induced by FGF, and it is only later divided into otic and epibranchial placodes by Wnt and BMP signalling, respectively (Ladher et al., 2010). Thus it is possible that the atrial primordium represents a proto-posterior placode in ancestral olfactores which gave rise to viscerosensory (epibranchial-like) Phox2-positive neurons and somatosensory (otic-, lateral line-like) mechanosensory neurons. In the ancestral vertebrate lineage, this placode would have separated into mechanosensory otic and lateral line placodes and Phox2-positive epibranchial placodes. However, transcriptional homology does not singularly define cell type homology (for example, see Section 1.1.5.3), and it is possible that Phox2 expression in the atrial ectoderm is not related to the specification of visceral sensory neurons. Since the viscerosensory identity of Phox2-positive cells in tunicates has not yet been determined, it is therefore possible that the viscerosomatic duality of PNS sensory neurons is unique to vertebrates.

Taken together, these data suggest a proto-placode epithelium in the most recent common ancestor of all chordates, but the diversification of placodes and their sensory neuron derivatives is largely a vertebrate novelty.

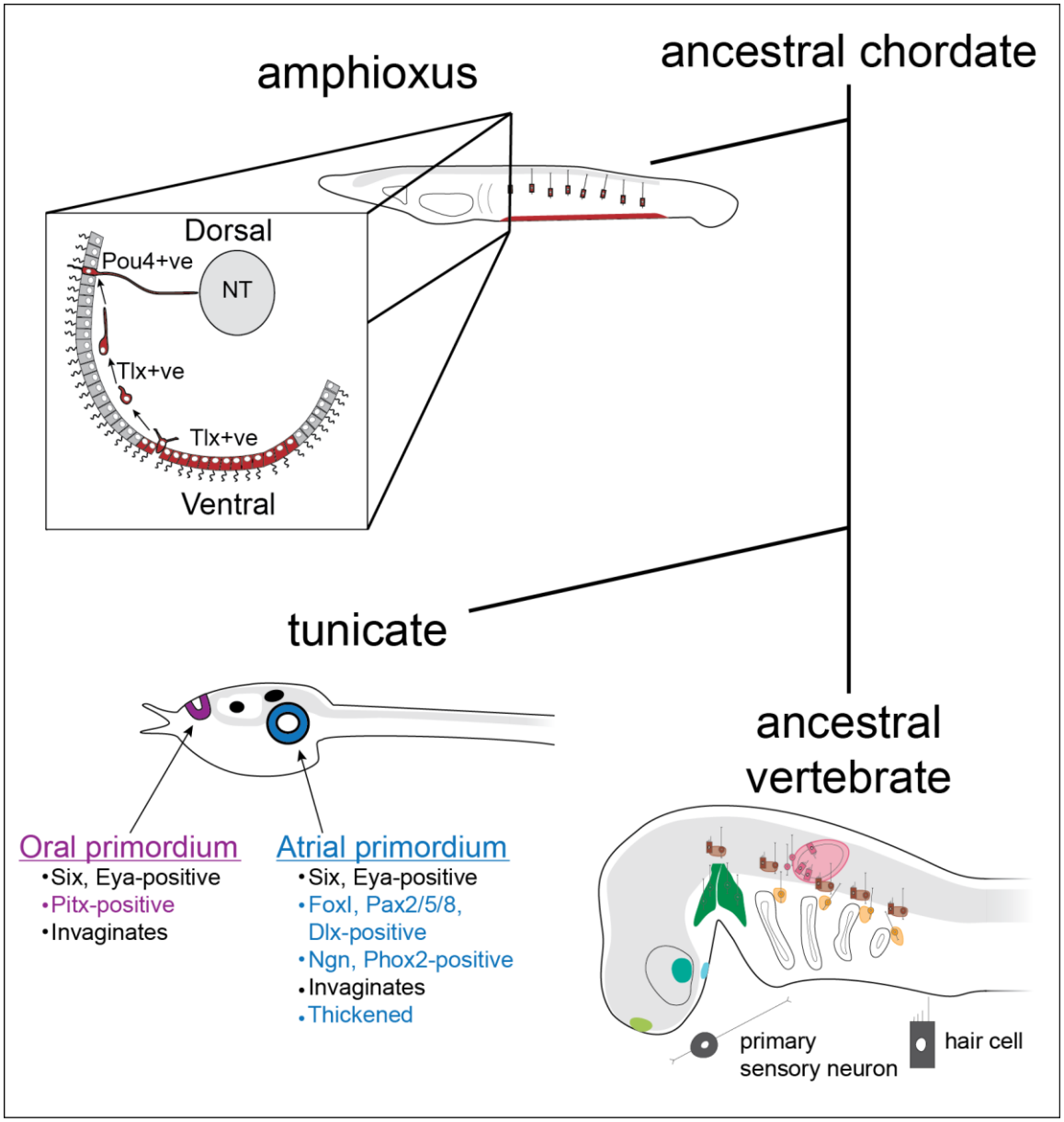


Figure 1.6. Rudimentary Placode Structures in Amphioxus and Tunicates.
In amphioxus, a ventral Tlx-positive field gives rise to neurons which migrate and re-integrate into the dorsal epidermis, where they down-regulate Tlx and up-regulate Pou4 (amphioxus Brn3). Like other epidermal cells, these neurons possess a single large cilium ('kinocilium'), but also have microvilli. On their basal (internal) surface, they protrude an axon which innervates the neutral tube (NT). In tunicates, larvae possess primordia of the oral and atrial siphons. Both contain characteristics of anterior and posterior vertebrate placodes, respectively. In addition, the atrial primordium is thickened and expresses epibranchial marker Phox2. Regardless of whether these structures are truly derivatives of a proto-placode in ancestral chordates, it is clear the vertebrate clade has expanded the diversity of its placodes and neuronal derivatives dramatically. Namely, posterior placodes generate primary sensory neurons with free nerve endings and ciliated hair cells which lack afferent axons. Vertebrate placodes are colour-coded. Light green: olfactory; blue: adenohypophysis; turquoise: lens; dark green: trigeminal; brown: lateral line; pink: otic; orange: epibranchial. Adapted from (Patthey et al., 2014), (Kaltenbach et al., 2009) and (Graham and Shimeld, 2013).

Section 1.1.5.3 Identification of Rudimentary NCCs in Invertebrate Chordates

The diversity of NCC derivatives in vertebrates is vast, and the extent of this diversity is novel to vertebrates. Invertebrate chordates possess some of these cell types, such as sensory neurons and pigment-producing cells; however the identification of rudimentary NCCs requires the identification of developmental homology of proto-NCC behaviour in addition to homology of derivatives.

In an effort to identify rudimentary NCCs, gene regulatory networks have been assembled characterising the molecular signature of vertebrate NCCs (Sauka-Spengler et al., 2007). When applied to amphioxus, however, no such molecularly homologous cell type was found (Meulemans and Bronner-Fraser, 2007). Instead, many genes important during the differentiation programme of NCCs to cartilage were expressed in mesoderm derivatives (Meulemans and Bronner-Fraser, 2007). Some genes were found to be expressed in the amphioxus lateral neural plate (Meulemans and Bronner-Fraser, 2007); but these are more likely to reflect conservation of dorsal-ventral patterning along the chordate neural tube (Donoghue et al., 2008).

Recently, however, a multipotent cell in the tunicate *Ciona intenstinalis* has been identified which resembles a rudimentary NCC (Abitua et al., 2012). This cell is fated to become the pigment-producing otolith by the activation of Mitf; or the non-pigment-producing ocellus by the repression of Mitf from FoxD, which is activated by Wnt7. A very similar mechanism is present in vertebrates in differentiating NCCs into melanophores versus iridophores, respectively (Curran et al., 2010). Thus this cell might be homologous to NCCs, as evidenced by similarities in its gene regulation and in the derivatives to which it gives rise; but unlike NCCs, this cell is non-migratory. This is due to the absence of expression of the epithelial-to-mesenchymal transition (EMT)-

inducing gene Twist (Thiery et al., 2009; Yang et al., 2004). When Twist was ectopically activated downstream of Mitf, the cell underwent EMT and became highly migratory (Abitua et al., 2012). Collectively this provides very strong evidence for the existence of a rudimentary NCC in tunicates (Butts and Graham, 2013).

However, there has not been a homologous cell type identified in amphioxus, suggesting that this cell type emerged in the chordate lineage after the divergence of amphioxus. In addition, the absence of other obvious proto-NCC types in invertebrate chordates suggests that rudimentary NCCs in their most multipotent form arose in ancestral vertebrates.

Section 1.1.5.4 Summary

Investigations in amphioxus and tunicates have revealed developmental structures which share many characteristics of vertebrate placodes. In amphioxus, a ventral Tlx-positive epidermal region generates migratory ESNs. In tunicates, a thickened ectodermal primordium invaginates and gives rise to neurons which structurally resemble ESNs and might be mechanosensory. Vertebrate mechanosensation is conducted by non-neural placode-derived hair cells, and relayed by primary sensory neurons with free axon endings. This suggests that while rudimentary placode structures likely existed in ancestral chordates, the diversification of sensory neuron subtypes is a vertebrate novelty. No rudimentary NCC types have been identified in amphioxus, and only one has been identified in tunicates. The specification and gene expression of this cell type is homologous to the vertebrate melanocyte precursor, but unlike the vertebrate NCC, this cell type is not migratory. However, it does have the gene regulatory network in place to undergo EMT when induced ectopically. This suggests that at least one rudimentary NCC type was present in the most recent common ancestor between tunicates and

vertebrates. However, like placodes and their derivatives, the diversification of NCC types is a vertebrate innovation.

Section 1.1.6 Behavioural Differences between NCC and Placode Neuronal Derivatives

NCCs and placodes both contribute sensory neurons. However, the manner by which these two populations generate sensory neurons is markedly different. NCCs and placodal derivatives both migrate to their final destination, but there are key differences in how they migrate. NCCs leave the neural tube by undergoing an EMT (Strobl-Mazzulla and Bronner, 2012), whereas placode-derived neurons do not (Graham et al., 2007). Furthermore, NCC migration has been highly characterised by the attraction and repulsion of chemotactic guidance cues (Kulesa et al., 2010). Candidate screening in our laboratory (unpublished) as well as a microarray (see Section 1.2.1) have shown that many chemotactic receptors are not expressed in placode-derived neurons; in fact, placodes secrete the CXCR4 ligand SDF-1, whereas cranial NCCs express the receptor (Theveneau et al., 2010).

However the main difference in sensory neurogenesis between these populations is the point along their migratory trajectories at which they begin to differentiate. NCCs emigrate as multipotent progenitors, giving rise to sensory neurons only after reaching their final destinations. By contrast, placodal cells break down the basement membrane and migrate into the embryo as neuroblasts/neurons, and are committed to their sensory neuronal fate before leaving the placode.

Section 1.1.6.1 Neuronal Differentiation of NCCs by Environmental Cues

There is evidence that NCCs are induced to the sensory neuron fate by the new environment to which they migrate. It is clear that in the trunk, DRG formation does not begin until NCCs have reached the site of the mature ganglion. An early population of Neurogenin-2-positive NCCs have been shown in the mouse and chick to migrate to the site of the mature ganglion, around which later NCCs coalesce to form a ganglion (George et al., 2010; Ma et al., 1999; Montelius et al., 2007; Rifkin et al., 2000; Zirlinger et al., 2002). The cue for migratory NCCs to differentiate into DRG neurons is likely released laterally from the neural tube. Insertion of a silastic barrier between the neural tube and newly migrating NCCs prevents DRG formation in the chick, but does not prevent formation of the more ventrally localised sympathetic ganglia (Kalcheim and Le Douarin, 1986).

There is also some evidence NCCs are fated to become sensory neurons prior to migration. One study suggested a pre-programmed sensory fate of NCCs prior to EMT, based on: the early onset of expression of GDF7, a BMP family member, in the dorsal neural tube prior to migration; and the ability of GDF7 to induce sensory neuron differentiation *in vitro* (Lo et al., 2005). However, the same study showed the capacity of GDF7-expressing NCCs to give rise to sensory neurons as well as neurons of the autonomic (sympathetic and parasympathetic) ganglia. Furthermore, in the head of the chick embryo, NCCs do not express Neurogenin-1 until after migrating (Thompson et al., 2010).

Section 1.1.6.2 Neuronal Differentiation of Cranial Sensory Placodes

Section 1.1.6.2.1 Transcriptional Pathway

Unlike NCCs, derivatives of the cranial sensory placodes express Neurogenins before migrating toward the future sensory ganglia (Abu-Elmagd et al., 2001; Begbie et al., 2002; Fode et al., 1998). By all measures, placodal derivatives are neuronal from the outset. Placodal cells commit to the neuronal fate by expressing Delta-1 (Begbie et al., 2002) downstream of Neurogenin activity (Fode et al., 1998; Ma et al., 1998). Delta-1 is a transmembrane ligand which activates the Notch pathway in neighbouring progenitors, laterally inhibiting them from the neuronal fate in order to maintain the progenitor pool (Chitnis et al., 1995; Henrique et al., 1995) (Figure 1.7B).

Upon commitment to the neuronal fate, placodal cells initiate a differentiation programme that is promoted by Neurogenin (Figure 1.7B) (Fode et al., 1998; Ma et al., 1998). This includes: the basic Helix-Loop-Helix transcription factors NeuroD and NeuroM (also referred to as NeuroD4 and Math3), two paralogues of the *Drosophila* proneural gene Atonal (Bertrand et al., 2002); and Islet-1, a Lin11/Isl-1/Mec-3 (LIM) domain-containing protein required for sensory, motor, and pancreatic cell differentiation (Bach, 2000; Bertrand et al., 2002). These genes are expressed in the committed placodal cells (henceforth referred as 'neuroblasts') and retained throughout their differentiation (Abu-Elmagd et al., 2001; Begbie, 2008; Fode et al., 1998; Freter et al., 2013; Krüger and Braun, 2002; Ma et al., 1998; Zou et al., 2004).

Visceral-versus-somatic identity is established at these early stages of neuronal differentiation. Somatosensory neuroblasts of the trigeminal and otic placodes express Brn3a (Anderson, 1999; Artinger et al., 1998; Fedtsova and Turner, 1995) downstream of Neurogenins (Anderson, 1999), which is required for their future survival (Xiang et al.,

1996). Viscerosensory neuroblasts of the epibranchial placodes initiate a pathway parallel to the Neurogenin pathway with expression of Phox2a (Fode et al., 1998), which sequentially promotes expression of Phox2b (Pattyn et al., 1997). Like Brn3a, both genes are required later for the neurons' survival (Morin et al., 1997; Pattyn et al., 1999).

Section 1.1.6.2.2 Differentiation of Neuroblasts to Neurons

The first action of committed neuroblasts is to translocate their cell bodies to the basal surface of the placode and delaminate (Figure 1.7A) (Blentic et al., 2011; Graham et al., 2007). Importantly, with the exception of derivatives of the trigeminal ophthalmic placode, which are post-mitotic (see Section 1.1.4.2.1), these neuroblasts have yet to exit the cell cycle (Begbie et al., 2002; Blentic et al., 2011; Graham et al., 2007). Furthermore, while they express early neural markers, they do not express the more mature neural markers such as SCG10 (Fode et al., 1998; Krüger and Braun, 2002; Ma et al., 1998; Zou et al., 2004) and HuC/D (Abu-Elmagd et al., 2001; Blentic et al., 2011).

Neuroblasts reside in a 'staging area' immediately outside of the placode. Their migration away from this staging area is concurrent with their differentiation into post-mitotic, SCG10-positive/HuC/D-positive neurons (Begbie et al., 2002) (and see above references). The migratory stream of post-mitotic neurons emanating from the staging area extends to the dorsal neural tube (where the nerves will innervate the hindbrain) (unpublished observation in our laboratory). Later in development, the stream will coalesce into a ganglion with an afferent connection to the CNS. During formation of the CSG, the neuroblasts and post-mitotic neurons derived from the placode are constantly spatially separated between the staging area and the migratory stream, respectively.

Morphological differences are also observed between neuroblasts and neurons. Labelling of placodal derivatives with Green Fluorescent Protein (GFP) shows that neuroblasts are round and unpolarised, with many short projections, while neurons are bipolar with long projections (Figure 1.7A) (Graham et al., 2007). Furthermore, neuroblasts exhibit differences in localisation of the neural-specific intermediate filament protein neurofilament-medium chain (NFM) (Figure 1.7B). In immature neuroblasts, this protein localises into thick globules (Blentic et al., 2011; Graham et al., 2007). In differentiated neurons, this protein is assembled into filaments and labels the neuronal projections of the forming nerve (Abu-Elmagd et al., 2001; Begbie et al., 1999; Begbie and Graham, 2001; Blentic et al., 2011; Fode et al., 1998; Thompson et al., 2010).

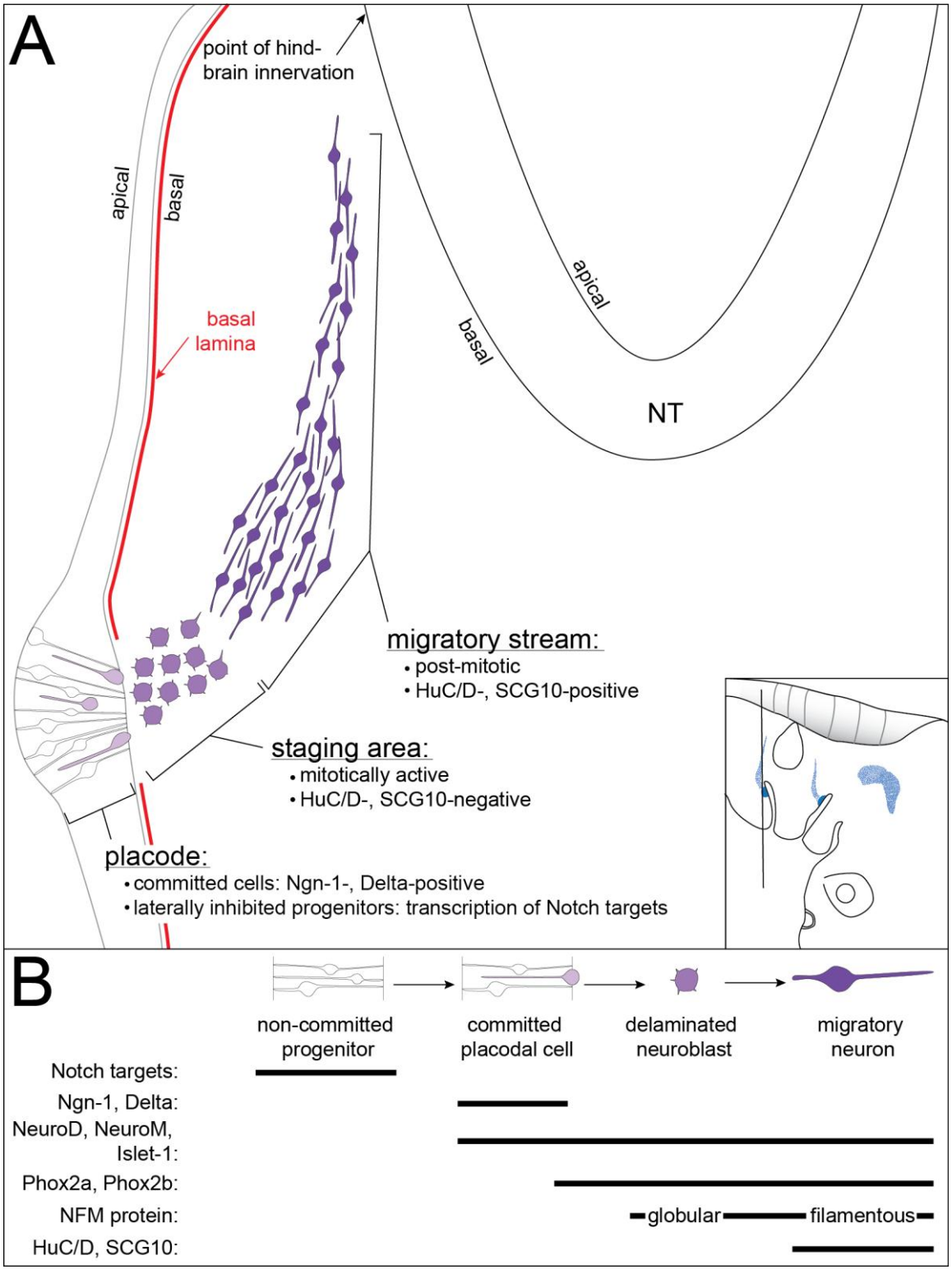


Figure 1.7. Neurogenesis, Differentiation and Migration from the Epibranchial and Trigeminal Maxillomandibular Placodes.
Figure legend on next page.

Figure 1.7. Neurogenesis, Differentiation and Migration from the Epibranchial and Trigeminal Maxillomandibular Placodes.
(A) A diagrammatic representation of a transverse section at the axial level of the petrosal epibranchial placode (wholemount in inset) reveals spatial domains corresponding to the three phases of a neuroblast's differentiation programme. Uncommitted progenitors as well as recently committed neuroblasts are present in the placode. The basement lamina immediately below the placode is broken down, allowing committed neuroblasts to leave the epithelium. Neuroblasts exiting the placode emerge into the staging area, where they possess a round, unpolarised morphology, are mitotically active, and are HuC/D/SCG10-negative. When neuroblasts leave the staging area, they become HuC/D/SCG10-positive, post-mitotic, and morphologically bipolar as they migrate toward the dorsal neural tube (NT). *(B)* Spatial separation of the expression pathway of neuronal differentiation. In addition to differential gene expression, NFM protein changes from globular to filamentous organisation as differentiated neurons project bipolar processes.

Section 1.1.6.3 Neuronal Migration of Placode-Derived Neurons

NCCs migrate as mesenchymal stem cells to their final destinations, then differentiate into neurons. Placode-derived neurons are committed to the neuronal fate from the outset of migration. They do not seem to rely on guidance cues (see Section 1.1.6), but they do rely on cranial NCCs to migrate to the correct destinations. Cranial NCCs migrate prior to placodal neurogenesis and form structural corridors to guide their migration (Freter et al., 2013). Such corridors have been identified surrounding the rostral migratory stream from the subventricular zone to the olfactory bulb (Sun et al., 2010) as well as in the thalamocortical tract from early-migrating neurons derived from the ventral telencephalon (López-Bendito et al., 2006). In the absence of these corridors, placodal neurogenesis proceeds and ganglia are formed; however these ganglia are improperly positioned along the rostral-caudal axis and fail to innervate the hindbrain (Begbie and Graham, 2001; Blentic et al., 2011; Osborne et al., 2005). In addition, placodal neurons migrate robustly *in vitro* on NCCs or on Fibronectin, an extracellular matrix protein secreted by NCCs, but migrate poorly on mesoderm (Blentic et al., 2011; Freter et al., 2013). Together this suggests that NCC corridors generate a permissive migratory environment for placodal migration. It is unclear to what extent placodal neurons depend on NCC-secreted Fibronectin *in vivo* as a substrate for migration.

However, placodal neurons are seen clustered together in fixed tissue (Blentic et al., 2011) (schematised in Figure 1.7A). This suggests they might engage in chain migratory behaviour such as the neurons of the rostral migratory stream (Sun et al., 2010), where neurons use each other as a substrate. Further studies using time-lapse imaging of placode-derived neurons are necessary to confirm this chain migration.

Section 1.1.6.4 Summary

Neuronal differentiation of NCCs and placodal derivatives in space and time is notably different. NCCs migrate as mesenchymal stem cells and differentiate into neurons once reaching their final destination. Placodal cells initiate the differentiation programme prior to leaving the epithelium, and fully mature into post-mitotic neurons after leaving the neuroblast staging area. Thus, the three phases of neuronal differentiation of placodal cells, from progenitor to neuroblast to neuron, are separated in space and time.

Section 1.1.7 The Cranial Sensory Placodes as a Model for Neurogenesis, Differentiation and Migration in the CNS

Considering the above observations, placodal neurogenesis more closely resembles that of the CNS than of NCCs. Like neurons derived from the placodes, neurons within the CNS commit to the neuronal fate before migrating to their final destinations. This is perhaps related to the fact that, like placodes, nearly all neurons of the CNS are born in an epithelium: the neural tube. (The only CNS neurons not born in the neural tube are the GnRH-positive neurons contributed by the olfactory placodes) (see Section 1.1.4.1). In the head, the neural tube gives rise to the forebrain, midbrain, and hindbrain (from rostral to caudal) (Figure 1.8B). In the trunk, the neural tube gives rise to the spinal cord (Figure 1.8B).

Section 1.1.7.1 Formation of the Neural Tube

The neural tube is characterized by a stereotypic pseudostratified columnar morphology in all vertebrates (Figure 1.8A). Cytoplasmic processes of each cell span the entire epithelium, but cell bodies are distributed at different positions along the apicobasal axis. At the end of gastrulation, ectodermal epithelial cells elongate along the apicobasal axis, giving rise to the pseudostratified morphology in a structure called the neural plate (Colas and Schoenwolf, 2001; Miyata, 2008). (This is true of amniotes. In amphibians, a second cell layer develops above the ectoderm, generating a thickened bi-laminar neural plate) (Colas and Schoenwolf, 2001). During neurulation, the neural plate apically constricts in its centre and its lateral edges elevate and converge together to form the neural tube. The apical surface lines the luminal surface of this tube (called the ventricular surface), and the basal surface lines the interface between the neural tube and mesoderm (called the pial surface). By late neurulation, the neural tube divides into morphologically visible segments along the rostral-caudal axis, forming the primitive forebrain, midbrain, hindbrain, and spinal cord (Figure 1.8B).

Section 1.1.7.2 Cell Divisions in the Neural Tube

Cells of the neural plate and early neural tube are self-renewing stem cells, and the tissue is collectively called a neuroepithelium (Götz and Huttner, 2005). Neuroepithelial cells translocate their nuclei up and down the apicobasal axis in a process referred to as interkinetic nuclear migration (INM). INM is intimately tied to phases of the cell cycle. Before S phase, the cell bodies translocate to the basal surface. Before M phase, the cell bodies translocate to the apical surface, where they divide.

Neuroepithelial cell divisions initially give rise to two daughter neuroepithelial cells. However, around the onset of CNS neurogenesis in rodents (approximately E10),

neuroepithelial cell divisions begin to generate radial glial cells (RGCs) (Götz and Huttner, 2005). RGCs are proliferative and resemble neuroepithelial cells, but assemble different apical junctions and express astroglial markers (Götz and Huttner, 2005). RGC divisions can generate two daughter RGCs, one daughter RGC and one daughter neuron, or two daughter neurons.

Section 1.1.7.3 Neuronal Migration in the Neural Tube

RGCs maintain apical and basal attachments. Unlike neuroepithelial cells, INM movements of RGCs do not extend to the basal surface of the neuroepithelium. Instead, INMs occur within a domain at the apical surface called the ventricular zone (VZ).

Neurons lose their apical and basal attachments, and migrate basally. Many neurons then migrate parallel to the ventricular surface to distribute throughout the CNS. This migration can take place along the dorso-ventral axis or along the rostro-caudal axis and is referred to as tangential migration (Figure 1.8B, red arrow) (Marín et al., 2010). In mammals, the developing dorsal forebrain (which gives rise to the cerebral cortex) is largely populated by neurons that do not migrate tangentially but radially (Figure 1.8B). That is, they migrate past the VZ and continue migrating basally to populate the cortical plate (CP). During development, the CP expands as more and more neurons are produced. New-born neurons migrate to the most superficial (pial) surface, creating an 'inside-out' layered structure in which older neurons are deeper within the cortex (Marín et al., 2010).

Section 1.1.7.4 Basal Progenitors of the Developing Cerebral Cortex

In addition to neurons, RGCs also give rise to basal progenitors (BPs) (Götz and Huttner, 2005). The majority of investigation of BPs has been in the developing cortex; however,

BPs have been identified in the midbrain, hindbrain and spinal cord (Haubensak et al., 2004). Like neurons, basal progenitors detach from the apical surface and migrate basally. However, they do not migrate into the CP; they instead reside in a layer between the CP and VZ called the subventricular zone (SVZ). BPs were initially identified in the murine cortex as intermediate progenitor cells (IPCs) (Figure 1.8B). These cells resemble neurons in that they are committed to the neuronal fate and they lose their apical and basal attachments. However, they are still mitotic, and most undergo one round of cell division to give rise to two post-mitotic neurons (Haubensak et al., 2004; Miyata et al., 2004; Noctor et al., 2004). They express the T-domain transcription factor Tbr2, but not radial glial marker Nestin or post-mitotic neuronal marker β-tubulin (Englund et al., 2005). The daughter neurons produced from IPC divisions migrate radially away from the SVZ and contribute to the CP (Miyata et al., 2004; Noctor et al., 2004).

Another BP exists in small proportions in the murine cortex called ‘outer radial glial cells’ (oRGCs) (Figure 1.8B) (Wang et al., 2011). oRGCs are detached from the apical surface, but maintain a basal attachment. Unlike IPCs, oRGCs undergo multiple rounds of division in order to expand the progenitor pool (Lui et al., 2011). Intriguingly, oRGCs exist in much greater proportions in the developing primate cortex, suggesting a mode for the expansion and gyrification of the primate cortex compared to rodents (Florio and Huttner, 2014; Lui et al., 2011; Molnár, 2011).

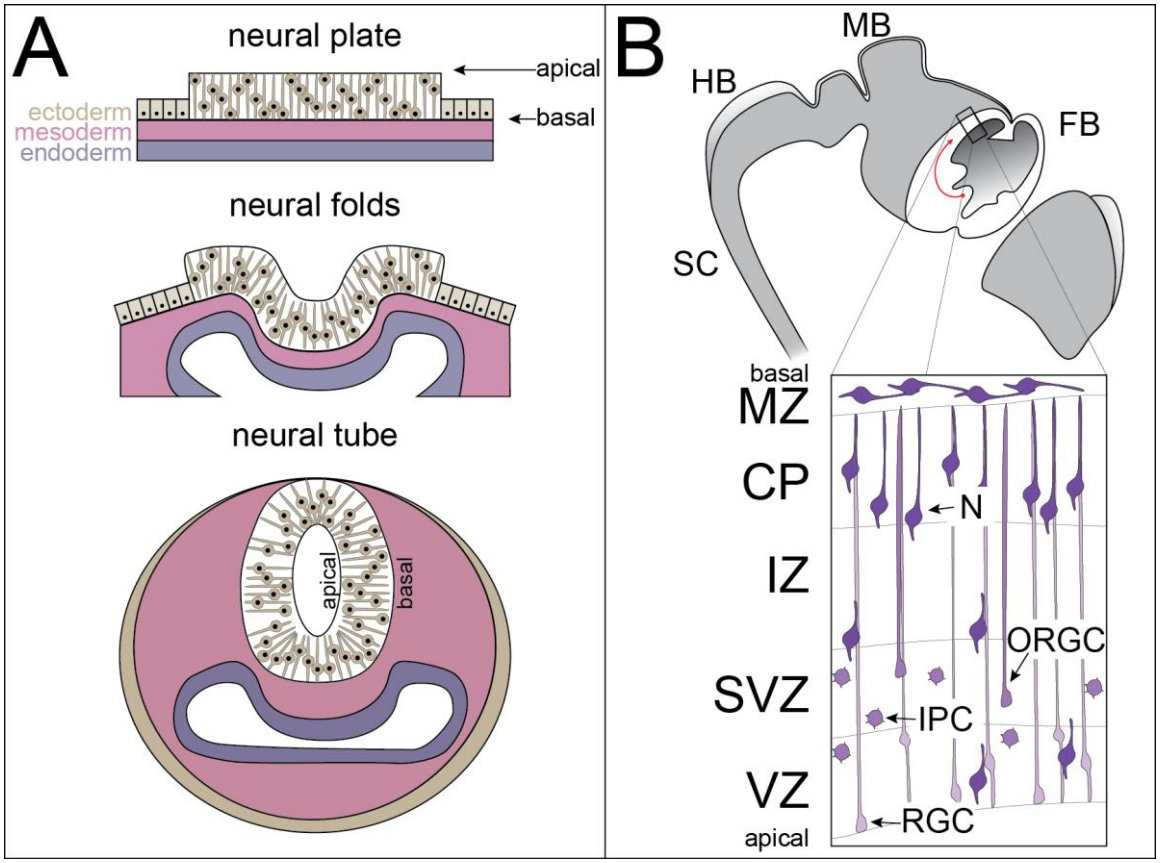


Figure 1.8. Neural Tube Formation and Neurogenesis in the Developing Cerebral Cortex. *(A)* Cross section of a gastrula/neurula-stage embryo showing the forming neural tube. The neural plate forms from a thickening in the ectoderm of gastrula-stage embryos, producing a pseudostratified epithelium. The neural plate apically constricts in its centre and the lateral edges elevate, producing the neural folds. Neurulation occurs as these folds close together to form the neural tube. *(B)* The neural tube constricts at stereotypic locations along the rostro-caudal axis, forming the subdivisions of the central nervous system. In the dorsal forebrain, the cerebral cortex forms from the migration of neuroblasts and neurons in different layers. Radial glial cells (RGCs) stretch from the apical to basal surfaces, but their cell bodies remain in the ventricular zone (VZ). Intermediate progenitor cells (IPCs) mostly reside in the subventricular zone (SVZ) where they undergo one round of division to give rise to two neurons. Additionally, the SVZ hosts the cell bodies of outer radial glial cells (ORGCs), which maintain a basal process but detach apically, and undergo multiple rounds of self-renewal. Neurons (N) are born in the VZ and SVZ, and migrate past the intermediate zone (IZ) to increasingly superficial layers of the cortical plate (CP). Such migration along the apico-basal axis is referred to as radial migration. Tangential migration occurs perpendicularly to the apico-basal axis, either ventro-dorsally (illustrated with red arrow) or rostro-caudally. In the developing cortex, tangentially migrating neurons travel through the IZ (not shown). In addition, tangentially migrating Cajal-Retzius cells migrate to the marginal zone (MZ) superficial to the CP prior to the onset of radial migration in the cortex. FB: forebrain; HB: hindbrain; MB: midbrain; SC: spinal cord.

Section 1.1.7.5 Parallels between the Cranial Sensory Placodes and Developing Cerebral Cortex

Many parallels exist between placodes and the neural tube. Cranial sensory placodes are, by all measures, neuroepithelia. They are thickened, pseudostratified ectoderm (Graham et al., 2007). Like the neural tube, divisions in the placode occur at the apical surface (Graham et al., 2007). They have a basement lamina at their basal surface (Blentic et al., 2011; Graham et al., 2007), and express apical markers Par-3 and aPKC at their apical surface (unpublished observation in our laboratory). Lastly, neurogenesis is also similar between the placodes and neural tube. Both initiate differentiation programmes that include expression of Neurogenins, NeuroD, NeuroM (Mattar et al., 2008), and HuC/D (Englund et al., 2005) (and see Section 1.1.6.2.1).

The cranial sensory placodes share closer similarity to the developing cerebral cortex than any other region of the neural tube. Pax6 is expressed in the VZ of the cortex (Götz et al., 1998; Walther and Gruss, 1991); its paralogue, Pax2, is expressed in the epibranchial placodes (Baker and Bronner-Fraser, 2000). Neuroblasts emanating from the placodes resemble IPCs in that both are mitotic yet neural fate-restricted. IPCs of the cortex undergo only one round of division to generate two post-mitotic neurons (Haubensak et al., 2004; Miyata et al., 2004; Noctor et al., 2004). Likewise, divisions are infrequently seen in the neuroblast staging area outside the placode (Begbie et al., 2002; Blentic et al., 2011; Graham et al., 2007). Furthermore, placodal neuroblasts exhibit multiple, short projections and are unpolarised. Similarly, IPCs in the SVZ also exhibit a multipolar morphology (Noctor et al., 2004).

Section 1.1.7.6 Differences between the Cranial Sensory Placodes and Developing Cerebral Cortex

There are important differences between the cranial sensory placodes and the cortex. For example, IPCs of the SVZ express Tbr-2 (Englund et al., 2005), whereas neuroblasts of the cranial sensory placodes do not (Ryan et al., 1998) (and unpublished work in our laboratory). The largest difference however between cranial sensory placodes and the cortex is in the migration of their neuronal derivatives.

Section 1.1.7.6.1 Neuronal Migration

Differentiated cortical neurons migrate using radial glial fibres as a substrate (Marín et al., 2010). Radial glia are not present along the migratory tract of placode-derived neurons, and the migratory behaviour of neurons derived from the cranial sensory placodes seems to more closely resemble that of the rostral migratory stream (see Section 1.1.6.3). Furthermore, cortical neurons migrate within an epithelium: as they migrate farther into the CP, the epithelium expands. Placode-derived neurons, by contrast, delaminate from the basal surface of the placodal epithelium and migrate through NCC mesenchyme (Blentic et al., 2011; Graham et al., 2007). Lastly, differentiated cortical neurons as well as IPCs exhibit a multipolar morphology as they pass through the SVZ toward the CP (Tabata and Nakajima, 2003). In the placodes, however, no unpolarised cells express markers of post-mitotic differentiation such as HuC/D (Blentic et al., 2011).

Section 1.1.8 Discussion

NCCs and placodes have often been associated together for three reasons. First, placodes and NCCs fate-map from a common origin at the neural plate border (Figure 1.2A). However the neural plate border emerges in the chick embryo at HH4, and by the time the cranial sensory placodes initiate neurogenesis (HH12-15), the placodes have segregated to the lateral non-neural ectoderm embryologically distant from the neural tube (Figure 1.2B,C).

Second, together placodes and NCCs generate all sensory neurons of the PNS. This is important, and the similarities and differences between NCC- versus placode-derived sensory neurons are only beginning to be understood. For example, neurons of the DRG and trigeminal ganglia are somatosensory. One study identified few differences in gene expression between DRG and trigeminal ganglia, but it did not discriminate between placode- versus NCC-derived neurons of the trigeminal ganglion (Eng et al., 2007). Furthermore, the segregation of NCC- and placode-derived neurons between proximal and distal CSG (respectively) suggests distinct functions for these neurons.

Third, NCCs and placodes in their diversified and stereotypic forms are unique to vertebrates. However, rudimentary NCCs and placodes have been identified in invertebrate chordates, muddying their initial characterisation as a vertebrate novelty (Gans and Northcutt, 1983). Also, NCCs and placodes do not appear to have co-evolved. Sensory neuron-generating rudimentary placodes have been identified in tunicates and cephalochordates, but sensory neuron-generating rudimentary NCCs have not.

On this final point, it is interesting to note that the telencephalon, which gives rise to the cerebral cortex, is a vertebrate novelty (Rétaux et al., 2013). Placodes likely existed in

ancestral chordates, but their diversification is also novel to vertebrates. In this respect, and in regard to development, the placodes which generate CSG (the cranial sensory placodes) more closely resemble the developing cortex than NCCs. Both are neuroepithelia which generate cells committed to the neuronal fate. NCCs, by contrast, are mesenchymal, and express markers of neuronal commitment after migrating. The cortex generates post-mitotic neurons as well as mitotic neuroblasts. The placode generates neuroblasts, at least some of which are mitotic, which share many characteristics of cortical neuroblasts, except for the absence of Tbr2 expression.

There are some key distinctions between cranial sensory placodes and the developing cerebral cortex. Namely, while cortical neurons expand the epithelium as they migrate, placodal neuroblasts break away from the basement membrane and leave the epithelium. However, this difference makes the cranial sensory placode advantageous as a model system to investigate fundamental principles of neuronal differentiation and migration. The cortex has VZ, SVZ and CP layers subdividing radial glial progenitors, intermediate progenitors, and differentiated neurons. But the separation of these layers is not precise (Figure 1.8B). Pax6- and Nestin-positive radial glial nuclei are enriched in the VZ but present in the SVZ; Tbr2-positive intermediate progenitors are enriched in the SVZ but present in the VZ; and differentiated neurons are mingled throughout the SVZ as well as the CP (Englund et al., 2005). Further complicating this blurred division is the fact that radial glial progenitors also generate post-mitotic neurons in the VZ, and outer radial glial progenitors self-renew in the SVZ.

By contrast, the separation between progenitors, neuroblasts and neurons is much more tractable in the placodes. Because progenitors are epithelial, they remain in the placodal epithelium. All committed neuroblasts leave the epithelium and reside in a staging area

immediately outside the placode. None of these neuroblasts differentiate without leaving the staging area; in fact, this area is defined by absence of HuC/D. Finally, differentiated neurons form a migratory stream which progresses away from the staging area toward the dorsal hindbrain. The neurons migrating in this stream are not travelling through a neuroepithelium as in the cortex, so principles of migration learned in the placode-derived neurons do not directly translate to cortical migration *per se*. However, because a glial/neuronal architecture is absent from the placodal migratory stream, investigations about the nature of placode-derived neuronal migration answer questions about the intrinsic migratory mechanisms of neurons. In support of this idea, neurons of the rostral migratory stream, which are similarly removed from a neuroepithelial substrate, form chains of migration which resemble the pattern of placode-derived neurons (see Section 1.1.6.3).

The processes of progenitor commitment, neuroblast differentiation, and neuronal migration continue from the cranial sensory placodes as a steady stream over the course of about two days of chick embryo development (Blentic et al., 2011). Thus examining embryos fixed at a stage of peak placodal neurogenesis provides a very clear separation of the three phases of a neuroblasts's lifetime: from progenitors, to immature neuroblast, to mature neuron.

Section 1.2 Regulator of G protein Signalling 3 (RGS3): a Candidate Regulator of Placodal Neurogenesis and Migration

Section 1.2.1 Identification of RGS3

While the fundamental differentiation programme of placodal neuroblasts is understood (Neurogenin-1/2 → NeuroD, NeuroM → SCG10, HuC/D) (Section 1.1.6.2.1), little is known about the genes involved in controlling the rate and manner of placodal neurogenesis, differentiation and/or neuronal migration.

To identify molecules upregulated during generation and migration of placode-derived neurons, a microarray was previously conducted (unpublished). Tissue containing the head mesenchyme adjacent to the pre-placodal ectoderm of the presumptive geniculate placode of HH13 chick embryos was compared to tissue containing the neural derivatives of the geniculate placode and adjacent head mesenchyme of HH17 chick embryos (Figure 1.9). Sox10-positive NCCs are present in the head mesenchyme at the axial level of the geniculate placode by HH13 but remain undifferentiated through HH17 (Freter et al., 2013; Thompson et al., 2010), and no known expressional changes occur in non-placodal surface ectoderm during this period. Aside from placodal neurogenesis, the only major change to this tissue between HH13 and HH17 is the production of blood vessels. Thus the former tissue served as a background to subtract surrounding embryonic structures. The only major changes accounted for were then associated with the production and migration of placodal neural derivatives and angiogenesis.

Of 873 reads identified with a fold change greater than 2.0, 490 were found to be upregulated and 383 were found to be downregulated. Reads were manually annotated to specific genes, beginning with the most upregulated reads, and genes known to be involved in angiogenesis were eliminated. After accounting for repeated reads of the

same gene, 117 upregulated genes were sorted into functional categories. Some genes were expected, such as NeuroD (fold change: +19.36) and HuD (fold change: +14.74). Of the genes not previously investigated in the cranial sensory placodes, 28 were further screened by *in situ* hybridisation to determine placodal derivative-specific staining. Four were seen to be expressed in NCCs, and one was found in blood vessels. However, 14 genes were found to be expressed specifically in the forming CSG, representing: transcription factors; genes involved in general and neuronal migration; and genes involved in intracellular signalling (Figure 1.9).

We hypothesised that intracellular signalling molecules might play important roles in the regulation of placodal neurogenesis and migration. Four of the molecules found to be expressed in the forming CSG were previously demonstrated to be involved in intracellular signalling. Among these, Regulator of G protein Signalling 3 (RGS3) stood out as a promising candidate because of its titular role in G protein signalling, which is broadly implicated in neurogenesis and neuronal migration (elaborated in Section 1.2.3).

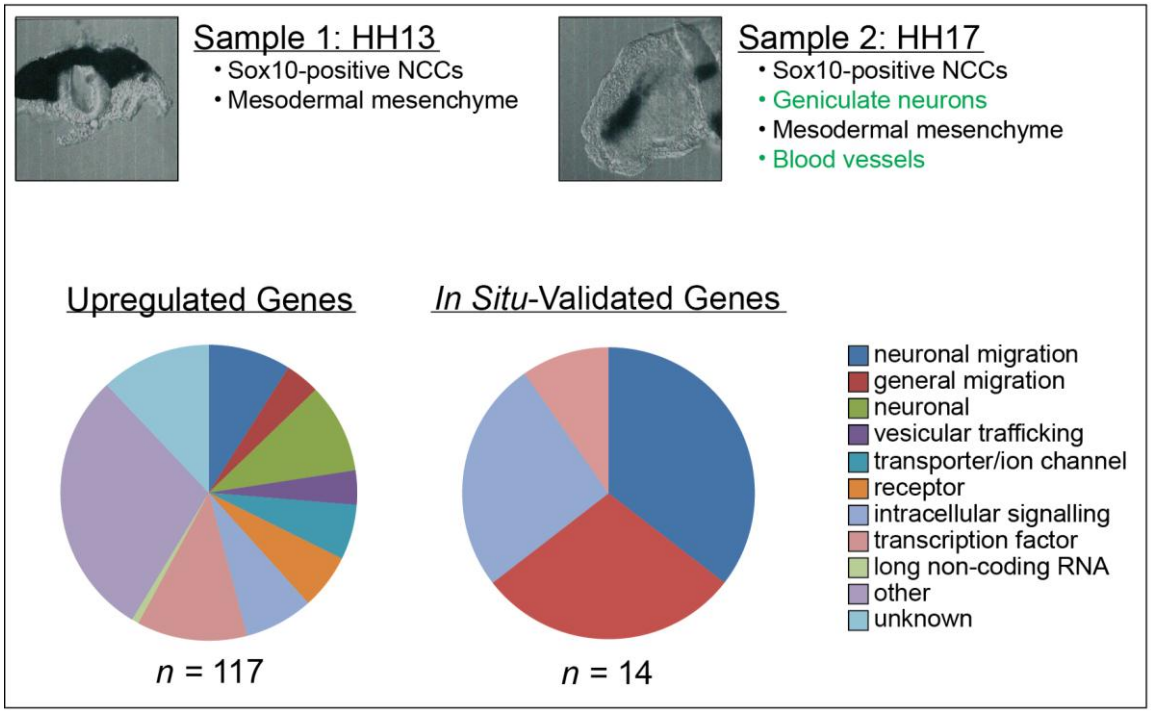


Figure 1.9. A Microarray to Identify Regulators of Placodal Neurogenesis and Migration. *(Top)* Transverse slices of HH13 and HH17 chick embryos were taken at the axial level of geniculate placode. The primary embryonic differences between these tissues are the presence of the induced geniculate placode and its neural derivatives, and blood vessels. Three slices per stage were used to extract RNA for microarray analysis (*bottom*), and representative slices were used for *in situ* hybridisation (shown) with Sox10 (HH13) or Phox2b (HH17) to demonstrate presence of NCCs and placode-derived neurons, respectively. Micrographs courtesy of Jo Begbie. *(Bottom)* After accounting for repeated reads and reads corresponding to angiogenesis, the 117 most-upregulated reads were sorted into functional categories (left). 28 of these were chosen for validation by *in situ* hybridisation; of these, 14 were found to be expressed in the forming CSG (right).

Section 1.2.2 G Protein Signalling and its Regulation

Section 1.2.2.1 General Overview

RGS3 contains a regulator of G protein signalling (RGS) domain, which canonically inhibits G protein signalling (Figure 1.10). G proteins have three subunits (α, β, and γ) which form a complex and associate with the membrane (Alberts et al., 2002). This complex is stable as long as Gα is bound to GDP. When this GDP is replaced by GTP, the heterotrimer dissociates between a GTP-bound Gα and a Gβγ heterodimer. The heterotrimer is generally thought to be inactive, and the dissociated Gα and Gβγ heterodimer activate downstream signalling cascades. Gα possesses an intrinsic GTPase activity, meaning it tends toward its GDP-bound, heterotrimeric state.

G protein-coupled receptors (GPCRs) are seven-pass transmembrane proteins which stimulate G protein signalling. They act as guanine exchange factors (GEFs) on Gα, replacing GDP with GTP (Alberts et al., 2002). Non-ligand binding 'orphan' receptors exist, but most GPCRs bind ligands on their extracellular surface. Ligand binding activates the GEF activity on the cytosolic surface of the GPCR, thereby dissociating the heterotrimer and activating the downstream pathway.

G protein signalling is negatively regulated by RGS proteins. Like RGS3, these proteins contain an RGS domain, which binds Gα and enhances its intrinsic GTPase activity up to 100-fold (Watson et al., 1996). This serves to rapidly attenuate the effect of GPCR activation by promoting formation of the inactive heterotrimer.

G protein signalling constitutes the most diverse and polygenic signalling pathway in eukaryotes. GPCRs alone comprise one of the largest families in the mammalian proteome, comprising 358 non-olfactory genes in humans (Sharman et al., 2013). 16

Gα's, five Gβ's, and 14 Gγ's are also encoded by the human genome (Milligan and Kostenis, 2006). Lastly, mammals possess 36 different RGS genes (Bansal et al., 2007). While diverse roles of the Gβγ heterodimer are beginning to be understood (Smrcka, 2008), the majority of work on G protein signalling has focused on the role of Gα. In the following two sections, I will describe two Gα signalling pathways that have been highly characterised.

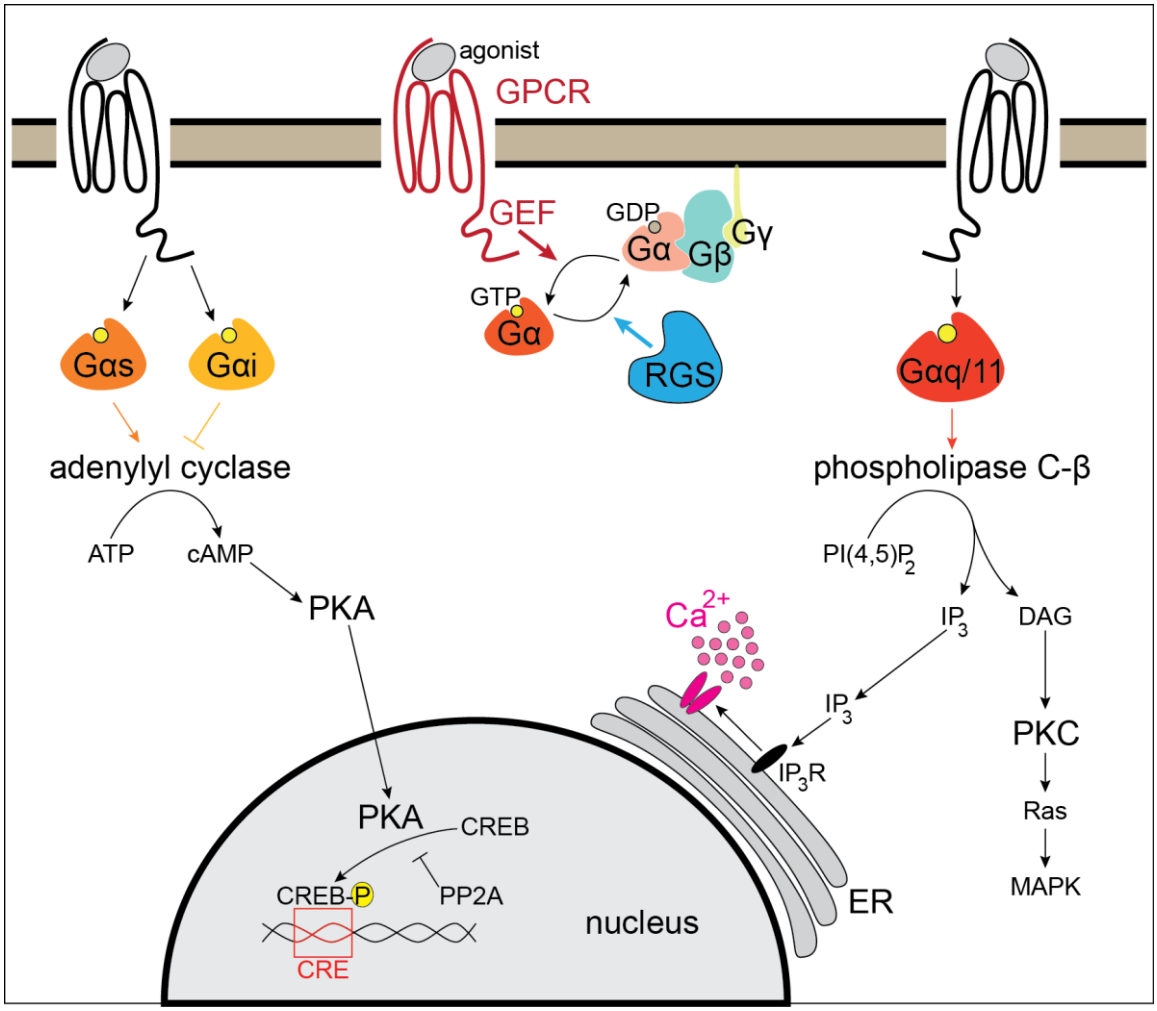


Figure 1.10. G Protein Signalling and its Regulation.
Heterotrimeric G proteins are positively and negatively regulated by guanine exchange factors (GEFs) and regulators of G protein signalling (RGSs), respectively. G protein-coupled receptors (GPCRs) are seven-pass transmembrane proteins that act as GEFs at their cytosolic surface. Upon agonist binding to an extracellular site, GPCRs exchange GDP bound to the Gα subunit for GTP. Binding of GTP by Gα induces a conformational change that promotes dissociation of Gα from the Gβγ heterodimer. The dissociated Gα-GTP is free to translocate about the cell and is active. RGSs antagonise Gα activity by promoting the intrinsic GTPase activity of Gα. This causes dephosphorylation of GTP into GDP and reassembly of the inactive heterotrimer. There are two main pathways stimulated by Gα subunits. The cAMP pathway (left) initiates with cyclic AMP (cAMP) production by adenylyl cyclase, which is activated by Gαs (stimulatory) or inhibited by Gαi (inhibitory). cAMP binds to a regulatory subunit of protein kinase A (PKA) and activates it, allowing it to translocate into the nucleus where it phosphorylates CRE binding protein (CREB). Phosphorylated CREB binds to DNA at cAMP response element (CRE) sequences and mediates downstream transcription. Protein phosphatase 2A dephosphorylates CREB, antagonising the pathway. The IP_3/DAG pathway (right) initiates with the cleavage of $PI(4,5)P_2$ into IP_3 and diacylglycerol (DAG) by phospholipase C-β, which is activated by Gαq/11. IP_3 binds to IP_3 receptors on the surface of the endoplasmic reticulum (ER), stimulating the release of intracellular Ca^{2+}, which serves as a secondary messenger for a multitude of downstream pathways. DAG activates protein kinase C (PKC) at the plasma membrane (not shown), which phosphorylates (among other substrates) the small GTPase Ras. Ras activates the mitogen associated protein kinase (MAPK) cascade, leading to downstream transcription.

Section 1.2.2.2 cAMP Signalling Downstream of Gαs and Gαi

Cyclic AMP (cAMP) is a modified form of AMP which is broadly used as a secondary messenger. cAMP is synthesised from ATP by the catalytic activity of adenylyl cyclase (Figure 1.10). When dissociated from the G protein heterotrimer, stimulatory Gα (Gαs) binds to adenylyl cyclase and activates it (Lodish et al., 2000). Gαs is activated by the β-Adrenergic GPCR, which is activated by the hormone ligands epinephrine or norepinephrine.

cAMP can activate membrane ion channels, but it most often influences the cell by activating protein kinase A (PKA) (Lodish et al., 2000). PKA translocates into the nucleus and phosphorylates the transcription factor CREB. Phosphorylated CREB is active and able to bind DNA at cAMP response element (CRE) sites, activating expression of target genes.

Adenylyl cyclase is also negatively regulated by a second Gα, inhibitory Gα (Gαi). The GPCRs specific to Gαi are activated by the prostaglandin E1 and adenosine ligands (Lodish et al., 2000). Downstream, CREB and other PKA targets are inhibited by protein phosphatases: mainly, protein phosphatase 2a (PP2A) (Alberts et al., 2002).

Section 1.2.2.3 Effectors Downstream of Gαq Signalling

Phospholipase C-β (PLC-β) is an enzyme linked to the plasma membrane activated by Gαq/11 downstream of the muscarinic acetylcholine GPCRs (Figure 1.10). PLC-β cleaves the membrane lipid phosphatidylinositol 4,5-bisphosphate ($PI(4,5)P_2$) to generate inositol triphosphate (IP_3) and diacylglycerol (DAG) (Alberts et al., 2002). These two molecules engage in separate downstream pathways. IP_3 binds to a receptor on the surface of the endoplasmic reticulum (ER), stimulating the release of its Ca^{2+} stores.

Ca^{2+}, in turn, is a widespread secondary messenger with numerous downstream targets. DAG binds and activates protein kinase C (PKC) on the plasma membrane. PKC phosphorylates a number of downstream substrates, including the mitogen-activated protein kinase (MAPK) effector Ras (Sánchez-Fernández et al., 2014).

Gαq also activates several other downstream effectors. Most notably, it activates the RhoGEFs, which act as GEFs to stimulate the Rho GTPases (Sánchez-Fernández et al., 2014). Rho GTPases, including RhoA, Rac and CDC42, have enormously diverse roles in cytoskeletal dynamics, cell polarity, migration, and even gene expression (Etienne-Manneville and Hall, 2002).

Section 1.2.2.4 RGS Activity of RGS3

RGS3 negatively regulates signalling through a multitude of GPCRs, namely: interleukin receptors (Bowman et al., 1998; Druey et al., 1996); muscarinic M2 (Jaén and Doupnik, 2005; Jaén and Doupnik, 2006; Melliti et al., 1999; Toro-Castillo et al., 2007) and M3 receptors (Anger et al., 2007; Anger et al., 2004; Karakoula et al., 2008; Tovey and Willars, 2004; Wang et al., 2002); and endothelin receptors (Anger et al., 2008; Chahdi and Sorokin, 2010; Cho et al., 2003; Dulin et al., 2000; Dulin et al., 1999).

Downstream of these receptors, RGS3 has also been shown to bind Gαi (Dulin et al., 1999; Yau et al., 2008) and Gαq/11 (Chen et al., 2014; Dulin et al., 1999; Neill et al., 2001; Niu et al., 2002) and directly enhance their intrinsic GTPase activity (Scheschonka et al., 2000; Vogt et al., 2007). RGS3 is highly specific to these Gα proteins, as overexpression of RGS3 has no effect on the GTPase activity of Gαs, Gαz or Gα12/13 (Scheschonka et al., 2000). Furthermore, this regulation can be pinned down to the

function of the RGS domain, as deletion or mutation abrogates this effect (Scheschonka et al., 2000; Vogt et al., 2007).

Because RGS activity promotes formation of the inactive heterotrimer, RGS3 effectively inhibits Gβγ activity as well. Like Gαq/11, the Gβ1γ2 heterodimer activates PLC-β, stimulating IP_3 production and MAPK activation (Shi et al., 2001; Vogt et al., 2007). Transfection of RGS3 attenuates this activation. Mutation of the RGS domain of RGS3 at Gα-binding residues does not perturb this attenuation (Shi et al., 2001), suggesting a direct role of RGS3 in regulating Gβγ independent of its Gα-regulatory function. This regulation is also seen on Gβγ inward-rectifying K^+ (GIRK) channels, which are inhibited by transfection of RGS3 (Doupnik et al., 1997; Jaén and Doupnik, 2005).

Section 1.2.3 Roles of G Protein Signalling in Neurogenesis and Migration

Section 1.2.3.1 GPCRs

GPCRs are broadly expressed in the adult CNS and are essential for a multitude of neurophysiological processes. In addition, many members have important roles in neuronal development. An increasing number of GPCRs are being identified as having important roles in neurogenesis, including (but not limited to): the (LPA) receptor (Fukushima, 2004; Geach et al., 2014); the Wnt receptor, Frizzled (Bielen and Houart, 2014); orphan receptors such as GPRC5B (Kurabayashi et al., 2013); and recently, the extracellular matrix adhesion receptor GPR56 (Bae et al., 2014).

Further, chemotactic GPCRs mediate neuronal migration in a variety of contexts (Marín et al., 2010). Additionally, GPCR receptors of neurotransmitters, such as glutamate (Jansson and Akerman, 2014) and cannabinoids (Zhou et al., 2014), have also been shown to play critical roles in neuronal migration during development.

Section 1.2.3.2 RGS3

RGS3 negatively regulates neurogenesis in the ventricular zone of the cerebral cortex (Qiu et al., 2010; Qiu et al., 2008). This effect is dependent on the RGS activity of RGS3, as mutation of the RGS domain results in normal migration into the CP (Murai et al., 2010). Furthermore, the activity of RGS3 in cortical neurogenesis has been shown to act upstream of Gαi2, as an RGS-insensitive construct (Gαi2QL) occludes the negative regulatory activity of RGS3 (Murai et al., 2010). Lastly, RGS3 associates with Ephrin-B in cerebellar granule cells, where it might also regulate chemotaxis (Lu et al., 2004; Lu et al., 2001) (elaborated in Section 1.2.4.3.2).

Section 1.2.4 RGS3 Encodes Multiple Isoforms

Section 1.2.4.1 The Human RGS3 Locus

RGS3 belongs to the RGS family of proteins by virtue of its RGS domain. This domain is approximately 120 amino acids (aa) in length (Koelle and Horvitz, 1996) and is conserved throughout Eukarya (Sierra et al., 2002). The RGS3 gene, however, encodes a full-length protein product of 1198 aa with several other domains (Kent et al., 2002). This gene has been mapped to 153.0 kilo-base pairs (kb) and spans 25 coding exons (Kehrl et al., 2002; Kent et al., 2002). From 5' to 3', these exons encode: a C2 domain, which binds Ca^{2+} and associates with different types of lipids in the plasma membrane (Nalefski and Falke, 1996); a PSD-95/Dlg/ZO-1 (PDZ) domain, which binds to short peptide motifs to facilitate protein-protein interactions (Lee and Zheng, 2010); an EF Hand domain, which binds to Ca^{2+} and can induce conformational change in tertiary protein structure (Lewit-Bentley and Réty, 2000); and a C-terminal RGS domain.

Multiple isoforms are produced at the RGS3 locus (Figure 1.11) (Kehrl et al., 2002). These include the full-length isoform, which we have termed RGS3hL (previously referred to as C2PA-RGS3) (Kehrl et al., 2002; Lu et al., 2004). In addition, four other protein-coding transcripts are produced. Three of these isoforms share the four 3'-terminal exons of RGS3hL, encoding the RGS domain and the entire 3' untranslated region (UTR). However, the 5'-termini of these isoforms are progressively truncated: RGS3L encodes only the PDZ domain, EF Hand domain and the RGS domain; RGS3s encodes the EF Hand domain and the RGS domain; and RGS3hs encodes only the RGS domain. Each of these isoforms contains one unique upstream exon. For RGS3s, this exon contains no coding sequence and comprises the entirety of its 5' UTR. For RGS3L and RGS3hs, this exon encodes the entire 5' UTR as well as 18 and 140 unique aa,

respectively. In the latter case, the extension of the coding sequence in the RGS3hs-specific exon to 140 aa is unique to primates. Only the terminal 21 aa are homologous to the unique RGS3hs-specific exons of other mammals and vertebrates (Kent et al., 2002).

Lastly, the RGS3 locus also produces an upstream isoform encoding only the C2 and PDZ domains, termed C2PA (Kehrl et al., 2002). In addition to possessing a unique 5' exon that encodes the 5' UTR and the first 26 aa, C2PA possesses a unique 3' exon, which encodes 34 aa, a stop codon, and a 3' UTR. While other isoforms exist at the human locus, these five are conserved throughout vertebrate evolution (see Chapter 5).

Section 1.2.4.2 The Chicken RGS3 Locus

RGS3L, RGS3s and RGS3hs have previously been identified in the chicken (Kent et al., 2002; Tosetti and Dunlap, 2004; Tosetti et al., 2003), but evidence suggests RGS3hL and C2PA are also expressed. First, upstream genomic sequence encodes the homologous exons of RGS3hL and C2PA (Kent et al., 2002), producing a total locus of 69.0 kb (Figure 1.11). Additionally, an EST has been identified which corresponds to the shared upstream sequences of RGS3hL and C2PA (ChEST268e2) (Boardman et al., 2002). RGS3hL is putatively comprised of 1036 aa and is encoded by 25 exons.

The nomenclature of RGS3 isoforms has been highly inconsistent throughout the literature, with 'long' or 'short' titles assigned to different isoforms in different publications (Table 1.1). In addition, truncated isoforms have been cloned as artefacts of amplification and erroneously labelled as naturally occurring (Table 1.2). To avoid confusion and to speak in absolute terms of the function of each isoform, the nomenclature previously used in the chicken (Tosetti and Dunlap, 2004; Tosetti et al., 2003) and listed in Table 1.1 will be applied to this thesis.

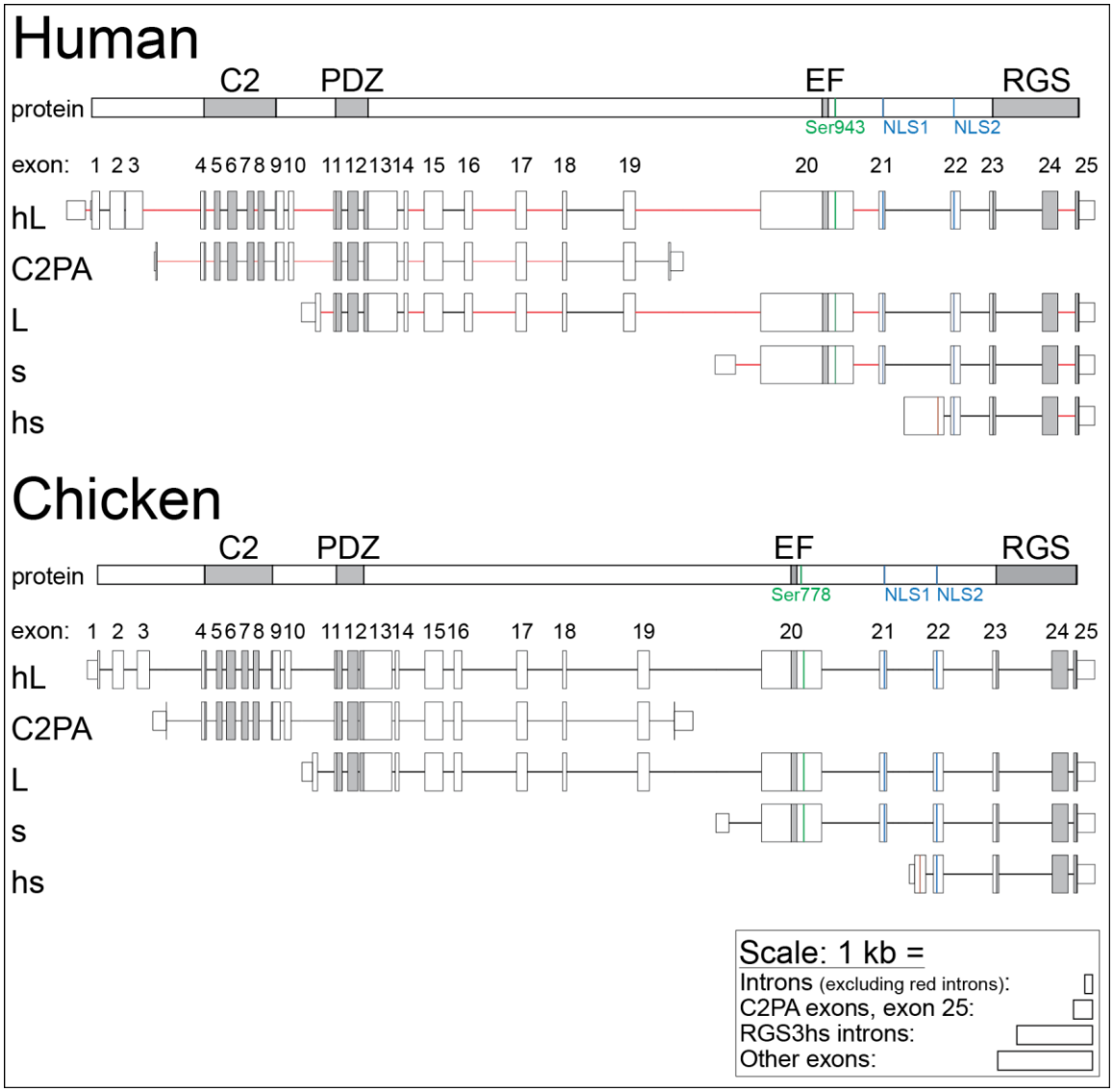


Figure 1.11. Isoforms of RGS3 in Human and Chicken.
The full-length RGS3 protein (RGS3hL) of both human and chicken contains a C2, PDZ, EF Hand, and RGS domain and is encoded by 25 exons (boxes). Untranslated regions (UTRs) are shown as thinner than coding regions. In humans, an additional 5' exon exists encoding most of the UTR (not labelled). The exon-intron boundaries relative to the position in the aa sequence are conserved, as are the positions of each domain (grey). The primary difference between the human and chicken proteins is the elongation of exon 20 at the 5' end to include an additional 114 aa. In addition, the unique exon of RGS3hs in primates extends to 140 aa (while the corresponding chicken exon only encodes 38 aa), and no 5' UTR has been detected. However, the terminal 21 aa is conserved in all vertebrates (indicated by red lines). The 14-3-3-binding serine (corresponding to Ser264 of human RGS3s) is indicated in green (see Section 1.2.4.3.3). The two nuclear localisation sequences (NLSs) identified in (Dulin et al., 2000) are indicated in blue. The human RGS3 locus is considerably larger, owing in large part to larger introns (horizontal lines). For this reason, introns in red have been reduced in length not to scale. The scale legend shows the lengths of 1.0 kb of sequence for each type of genomic element.

Table 1.1. Aliases and Citations of RGS3 Isoforms
RGS3hL is termed in this thesis. C2PA is universally recognised without any other aliases. RGS3L, RGS3s, and RGS3hs reference based on (Tosetti and Dunlap, 2004; Tosetti et al., 2003).

Isoform	Alias	References
RGS3hL	C2PA-RGS3	(Kehrl et al., 2002; Lu et al., 2004)
RGS3L	PDZ-RGS3	(Cho et al., 2003; Costigan et al., 2003; Hirabayashi et al., 2002; Kehrl et al., 2002; Lu et al., 2004; Lu et al., 2001; Meyer et al., 2004; Moratz et al., 2004; Murai et al., 2010; Qiu et al., 2010; Qiu et al., 2008; Shi et al., 2012)
	SRB-RGS (rat)	(Ikeda et al., 2001; Ikeda et al., 2007)
RGS3s	RGS3	(Anger et al., 2008; Anger et al., 2007; Anger et al., 2004; Benzing et al., 2000; Bowman et al., 1998; Castro-Fernández et al., 2003; Castro-Fernández et al., 2004; Chahdi and Sorokin, 2010; Chatterjee et al., 1997a; Chatterjee et al., 1997b; Chen et al., 2014; Costigan et al., 2003; Doupnik et al., 1997; Druey et al., 1996; Dulin et al., 2000; Dulin et al., 1999; Grüning et al., 1999; Hao et al., 2006; Karakoula et al., 2008; Ladds et al., 2007; Melliti et al., 1999; Neill et al., 2001; Niu et al., 2002; Reif and Cyster, 2000; Schreiber et al., 2001; Shi et al., 2012; Shi et al., 2001; Tatenhorst et al., 2004; Toro-Castillo et al., 2007; Tovey and Willars, 2004; Wang et al., 2002; Ward and Milligan, 2005; Yau et al., 2008)
	RGS3L	(Cho et al., 2003; Mittmann et al., 2002; Mittmann et al., 2001; Moratz et al., 2004; Vogt et al., 2007)
RGS3hs	RGS3S (human)*	(Cho et al., 2003; Kehrl et al., 2002; Moratz et al., 2004)
	RGS3s (mouse)	(Anger et al., 2007; Anger et al., 2004; Jaén and Doupnik, 2005; Jaén and Doupnik, 2006; Reif and Cyster, 2000)
	Rgs3**	(Freisinger et al., 2010)

*The primate RGS3hs isoform is larger than other vertebrates because of 140 aa encoded in the unique first exon. The terminal 21 aa of this exon, beginning with a methionine, is conserved in vertebrates. 'RGS3s,' identified in mouse, encodes only these 21 aa in its unique exon.
**Zebrafish (*Danio rerio*) RGS3hs-KYLER isoform. Teleosts lack the HTMKE exon, and mammals lack the KYLER exon (see Section 3.2.2 and Section 5.2.2.1). The authors stated that the start codon is 10 base pairs (bp) downstream of the start of the common exon of RGS3hs, creating a 173 aa protein homologous to the artificial 168 aa RGS3S construct (Table 1.2). However, their experiments injected full-length RNA which encodes the in-frame start codon in the unique exon, creating a 205 aa protein containing the KYLER sequence.

Table 1.2. Artificial/Partial Isoforms Used in RGS3 Experiments Previously
With the exception of RGS3NT, which was purposefully designed, these isoforms were originally believed to be naturally occurring. However, their 5' termini are within exons, suggesting that they are artefacts of amplification.

Isoform	Notes	References
RGS3T	Truncated form of human RGS3s lacking N-terminal 313 aa; start is inside first coding exon of RGS3s (RGS3hL exon 20).	(Benzing et al., 2000; Castro-Fernández et al., 2003; Chatterjee et al., 1997b; Druey et al., 1996; Dulin et al., 2000; Neill et al., 2001; Toro-Castillo et al., 2007)
RGS3CT	Alias of RGS3T.	(Scheschonka et al., 2000; Shi et al., 2001)
RGS3NT	First 313 aa of human RGS3s.	(Scheschonka et al., 2000; Shi et al., 2001; Toro-Castillo et al., 2007)
RGS3S	Final 168 aa of all isoforms; starts with 4^{th} aa of 1^{st} common exon of RGS3hs. Not to be confused with RGS3S of Table 1, which is a natural alias of RGS3hs.	(Mittmann et al., 2002; Mittmann et al., 2001)* (Vogt et al., 2007)
RGS3ss	Truncated chicken RGS3s immediately after EF Hand domain.	(Tosetti and Dunlap, 2004; Tosetti et al., 2003)
MeRGS3L	Named Medaka RGS3-like, but published sequence is actually most similar to mammalian RGS13.	(Itoh et al., 2005)

*Nomenclature used to refer to an appropriately-sized RT-PCR expression band. Most likely detected endogenous RGS3hs.

Section 1.2.4.3 Functions of Each Isoform

Section 1.2.4.3.1 RGS3hL and C2PA

To date, no functional role of RGS3hL has been described. Its expression in adult mice has been shown to be widespread, with particular enrichment in testes (Kehrl et al., 2002). Similarly C2PA, which shares the C2 and PDZ domains but not the downstream domains, was initially identified in spermatocytes of the testes (Linares et al., 2000). This could reflect a role of C2PA in meiosis, as it has also been found to be upregulated in mouse ovaries after the initiation of meiosis (Olesen et al., 2007). Interestingly, though C2PA lacks the C-terminal RGS domain, it colocalises with a CREB-binding protein (see Section 1.2.2.2) after heat shock, whereas RGS3L (lacking the C2 domain but possessing the PDZ and downstream domains) does not (Hirabayashi et al., 2002).

Section 1.2.4.3.2 RGS3L

The majority of focus on RGS3L has been through its physical and functional interaction with Ephrin-B1. Ephrin-B1 is classically described as a transmembrane ligand for the axon pathfinding repellent receptor EphB (O'Leary and Wilkinson, 1999). However, it has been shown more recently to play important roles in neuroepithelial integrity (Arvanitis et al., 2013) and neurogenesis (Qiu et al., 2008).

In the cortex, RGS3L and Ephrin-B1 are both specifically expressed in the VZ, and RGS3L co-immunoprecipitates with Ephrin-B1 from cortical tissue (Lu et al., 2001). This interaction occurs at a motif on the C-terminus of Ephrin-B1, where the PDZ domain of RGS3L binds. Co-overexpression of RGS3L and Ephrin-B1 in the VZ reduces the frequency of cells migrating into the CP (Murai et al., 2010; Qiu et al., 2008). This is likely due to decreased neurogenesis, since Ephrin-B1 (Qiu et al., 2008) or

RGS3L knockout (whilst retaining RGS3s and RGS3hs) (Qiu et al., 2010) results in increased cell cycle exit and neuronal differentiation.

There is also evidence that RGS3L might interact with Ephrin-B1 during GPCR-mediated chemotaxis. RGS3L and Ephrin-B1 proteins colocalise in cerebellar granule cells (Lu et al., 2001). Overexpression of Ephrin-B1 prevents the migratory response of dissociated cerebellar granule cells by SDF-1, a ligand of the GPCR CXCR4. Co-overexpression of the PDZ domain of RGS3L, however, abrogates this effect (Lu et al., 2004; Lu et al., 2001). While the PDZ domain by itself was expected to act as a competitive inhibitor of endogenous RGS3L (which contains an RGS domain and, presumably, regulates CXCR4 transduction), the results could also relate to perturbation of other endogenous binding partners. For example, in addition to RGS3L, several other PDZ domain-containing proteins bind (Lin et al., 1999) and colocalise (Torres et al., 1998) with Ephrin-B proteins. Furthermore, the PDZ domain of RGS3L is promiscuous. In addition to binding Ephrin-B proteins, the PDZ domain of RGS3L binds the synaptic cell adhesion molecule Neuroligin and the AMPA receptor subunit GluR2 (Meyer et al., 2004).

RGS3L has been shown to diverse play roles in the non-neural context. In cell culture, RGS3L was shown to be an important component of the canonical Wnt cascade by promoting β-catenin stability, in a manner dependent on the PDZ and RGS domains (Shi et al., 2012). In addition, RGS3L can bind the DNA-binding and hinge domains of the nuclear oestrogen receptor and negatively regulate its transcription factor activity (Ikeda et al., 2001; Ikeda et al., 2007).

Section 1.2.4.3.3 RGS3s and RGS3hs

Human RGS3s was the first RGS3 isoform to be identified (Druey et al., 1996), and the most widely studied. RGS3s, and to a lesser extent RGS3hs, are broadly implicated in the regulation of G protein signalling (all findings described in Section 1.2.2.4 involved only RGS3s and/or RGS3hs). Interestingly however, while RGS3s and RGS3hs both encode the RGS domain, they can exert differential effects on G protein signalling. For example, human RGS3s was found to negatively regulate murine lymphocyte chemotaxis following stimulation by the interleukin-8 (IL-8) agonist, in a manner more efficient than human RGS1 (Bowman et al., 1998). By contrast, lymphocyte chemotaxis was less effectively inhibited by mouse RGS3hs than by mouse RGS1, when stimulated with BLC, ELC or SDF-1 agonists (Reif and Cyster, 2000). While this could reflect species differences or differential selectivity to chemotactic GPCRs of RGS1, it could also relate to the N-terminal sequences encoded by RGS3s but not RGS3hs.

These N-terminal sequences could alter specificity or function of the RGS domain, or affect subcellular localisation of the protein. In support of the latter idea, while RGS3s localised to the cytoplasm of human embryonic kidney cells, a construct lacking the N terminus was expressed in all subcellular compartments (Toro-Castillo et al., 2007). In addition, the N-terminus of RGS3s was sufficient to translocate from the cytoplasm to the plasma membrane upon induction by endothelin-1 (ET-1) or a Ca^{2+} ionophore in human mesangial cells (Dulin et al., 1999). Lastly, two nuclear localisation sequences (NLSs) are present between the EF Hand and RGS domains (Dulin et al., 2000). RGS3s encodes both of these NLSs, but RGS3hs encodes only one of these (see Figure 1.11). Human RGS3s localised to the cytoplasm of Chinese hamster ovary (CHO) cells, but a truncated construct, RGS3T (see Table 1.2), which lacks the first 313 aa of RGS3s but

retains both NLSs, specifically localised to the nucleus (Dulin et al., 2000). This suggests that the first 313 aa of RGS3s actively target the protein away from the nucleus.

Alternatively, the N-terminal sequences of RGS3 could alter the function of the RGS domain. RGS3s contains a serine residue in its N-terminus (Ser264 of human RGS3s) which is not present in RGS3hs. When this serine is phosphorylated, it is bound by 14-3-3ζ (Niu et al., 2002; Ward and Milligan, 2005), a member of the 14-3-3 family of proteins which are ubiquitously expressed in eukaryotes and bind to and regulate a multitude of proteins (Obsilova et al., 2014). This binding negatively regulates the RGS activity of RGS3s (Schreiber et al., 2001) by preventing Gα binding (Niu et al., 2002). Structural analysis has shown that 14-3-3 binding sterically hinders the interaction between the RGS domain and Gα (Rezabkova et al., 2010; Rezabkova et al., 2011).

In addition, RGS3s contains an EF Hand domain, which changes conformation upon Ca^{2+} binding. While this function could be as simple as buffering intracellular Ca^{2+} concentrations, it could also exert a conformation change elsewhere in the protein (Lewit-Bentley and Réty, 2000; Skelton et al., 1994). The EF Hand domain of RGS3s was previously shown to be essential to inhibit γ-aminobutyric acid (GABA)-induced attenuation of Ca^{2+} (Tosetti and Dunlap, 2004; Tosetti et al., 2003). When stimulated with GABA, dissociated DRG neurons inhibited Ca^{2+} influx, presumably via a mechanism downstream of the G protein-coupled $GABA_B$ receptor. This effect was abrogated by RGS3s but not by an EF Hand-deletion construct. The authors thus proposed a feedback mechanism in which the $GABA_B$ receptor inhibits Ca^{2+} influx, and Ca^{2+} in turn activates RGS3s in order to attenuate this inhibition. Intriguingly however, the EF Hand domain of the yeast trehalase enzyme Nth1 has recently been shown to be essential for 14-3-3 binding to neighbouring phosphorylated serines (Kopecka et al.,

2014). Interestingly, the EF Hand domain of this protein is 30 aa from the 14-3-3-binding serine residue. Consistently, the 14-3-3-binding serine of human and chicken RGS3s is also 30 aa downstream of the EF Hand domain (Figure 1.11). Thus, it is also possible that the EF Hand domain of RGS3s responds to Ca^{2+} and interacts with 14-3-3 proteins in order to negatively regulate RGS function.

Taken together, these data suggest that while RGS3s retains the RGS capability of RGS3hs, its N-terminal sequences can alter its localisation and/or conformation. This regulation, in turn, can alter the substrate specificity or activity of RGS3s in order to differentially regulate G protein signalling. It is notable, however, that RGS3s has also been shown to negatively regulate TGFβ signalling independent of its RGS domain by binding to Smad3 at its N-terminus (Yau et al., 2008). Thus the N terminus of RGS3s is highly important for its function, both in modulation of RGS activity and in RGS-independent roles.

Section 1.2.4.4 Summary

Like all other RGS proteins, RGS3 encodes an RGS domain. However, it also encodes several other domains and motifs which have been shown to play very diverse roles. It is interesting that, with the exception of C2PA, all RGS3 isoforms encode the C-terminal RGS domain. This implies that each isoform exerts RGS function, but the activity, selectivity and localisation of each isoform depends on its N-terminal domains.

Section 1.2.5 RGS3 and the Evolution of the R4 Subfamily of RGS Proteins

The RGS family of proteins comprises 36 mammalian genes which, based on sequence homology of the RGS domain, can be divided into nine subfamilies (Figure 1.12) (Bansal et al., 2007). These subfamilies likely arose in metazoan evolution from the duplication of ancestral founding members, since the intron-exon boundaries within the primary amino acid sequence are highly conserved within each subfamily (Sierra et al., 2002).

RGS3 is a member of the R4 subfamily, additionally comprising RGS1, 2, 4, 5, 8, 13, 16, 18, and 21 (Bansal et al., 2007). R4 proteins are stereotypically characterised by a C-terminal RGS domain, and most have a neighbouring amphipathic helix motif (Sierra et al., 2002). Aside from RGS3, all other R4 proteins contain no more than 85 aa N-terminal to the RGS domain. RGS3 thus stands out as a striking exception in this subfamily, encoding a total of 1,072 aa N-terminal to the RGS domain.

In this regard, RGS3hs much more closely resembles other R4 subfamily members than do other RGS3 isoforms. This raises the intriguing possibility that other R4 subfamily members ancestrally contained upstream sequences and isoforms which were lost in evolution. The expansion of the R4 subfamily occurred during the two rounds of whole-genome duplication early in vertebrate evolution between the emergence of tunicates and jawed vertebrates (Sierra et al., 2002). It was originally thought that R4 genes emerged from duplication of the RZ subfamily, because (a) this subfamily is conserved throughout Metazoa; (b) the RGS domain of R4 proteins is most closely related to that of RZ proteins; and (c) the RGS domains of R4 and RZ genes share a conserved intron-exon boundary (Sierra et al., 2002).

However, an ‘R4 RGS-like’ open reading frame has since been identified in the amphioxus genome, suggesting a pre-vertebrate origin of the R4 subfamily (Suurväli et al., 2013). Intriguingly, Simple Modular Architecture Research Tool (SMART) analysis of this peptide sequence (Entrez ID: 7220373) identifies 979 aa upstream of the putative RGS domain, including a putative PDZ domain (Schultz et al., 1998). Thus it is possible that the R4 subfamily expanded from a pre-vertebrate origin, and while RGS3 retained the N-terminal sequences of this gene in addition to the RGS domain, other R4 members only retained the RGS domain.

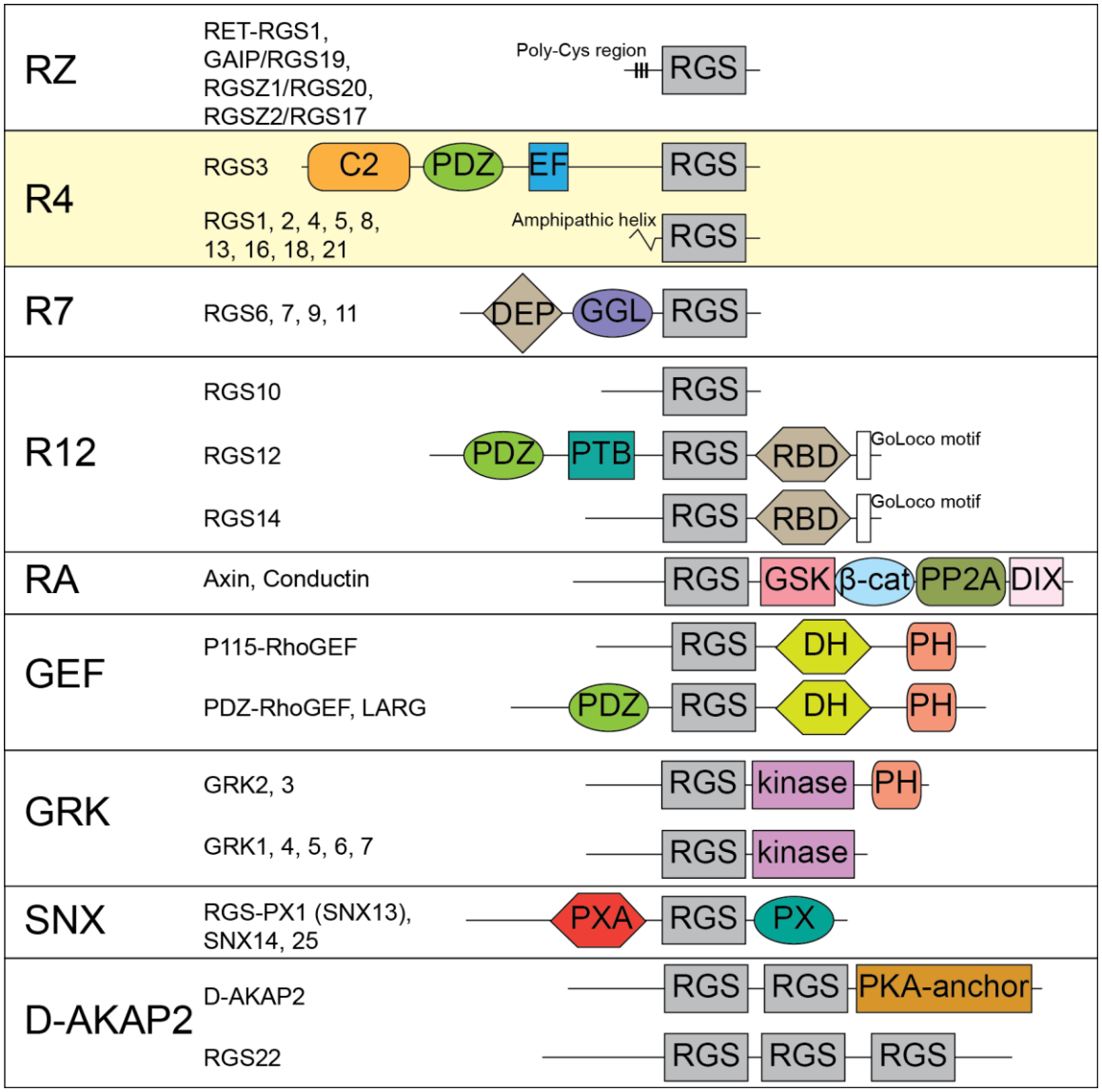


Figure 1.12. RGS Proteins and Their Subfamilies.
RGS proteins can possess several domains outside of the RGS domain, but the R4 and RZ subfamilies stereotypically possess little more than a C-terminal RGS domain. RGS3 is a stark exception within the R4 subfamily (highlighted), containing an N-terminal C2, PDZ, and EF Hand domain. β-cat: β-catenin-binding; DEP: dishevelled/EGL-10/pleckstrin; DH: Dbl homology; DIX: dishevelled homology; GGL: Gγ-like; GSK: glycogen synthesis kinase 3β-binding; PH: pleckstrin homology; PP2A: protein phosphatase 2A domain; PTB: phosphotyrosine binding; PX: phosphatidylinositol-binding; PXA: PX-associated domain; RBD: Ras-binding domain. Adapted from (Bansal et al., 2007).

Section 1.2.6 Discussion

G protein signalling is broadly implicated in neurogenesis and neuronal migration. The complexity of the developing nervous system is owed in part to the biochemical diversity of this signalling pathway. Components of G protein signalling are polygenic (especially GPCRs), creating specific permutations for each cell type or even subcellular compartment. In addition, the presence of RGS proteins presents a layer of regulation which fine-tunes the pathway downstream of GPCRs.

Adding to this complexity is the production of multiple isoforms from the RGS3 locus, each containing a C-terminal RGS domain (except for C2PA) and increasingly truncated N termini. These N-terminal sequences can exert numerous regulatory functions on the RGS domain, and can even function independently of the RGS domain (Yau et al., 2008). Thus the role of 'RGS3' in a given cell type (such as placode-derived neurons) can only be considered in the context of every individual role of every isoform expressed in that cell type.

Lastly, RGS3 seems to represent a critical component of the evolution of the R4 subfamily of RGS proteins. RGS3 is the only member of the R4 subfamily with a significantly extended N terminus, including a PDZ domain. An amphioxus R4-like protein similarly encodes a long N terminus which also includes a PDZ domain. However, this is the only invertebrate R4 gene discovered. This suggests that the evolution and expansion of the R4 subfamily is intricately linked to the evolution of vertebrates.

Section 1.3 Aims of This Thesis

The cranial sensory placodes and their derivative neurons comprise a spatiotemporally tractable model to dissect the principles of neurogenesis, differentiation and neuronal migration. However, the molecular regulation of these processes in the placodes remains elusive. Based on its role in G protein signalling, which is broadly implicated in neurogenesis and neuronal differentiation, RGS3 potentially plays an important role in the placodes. Moreover, the evolution of the R4 subfamily of RGS proteins (to which RGS3 belongs) accompanied the evolution of vertebrates as well as the emergence of placodes in their stereotypic form.

In this thesis, I aimed to elucidate the role(s) of isoforms of RGS3 in cranial sensory placodes, using the forming petrosal ganglion in the developing chick embryo as an experimental model system. Specifically, I sought to:

- characterise the unique expression patterns of isoforms of RGS3 across the cranial sensory placodes and during differentiation and migration of neurons;
- knock down and overexpress RGS3 isoforms to determine the roles of these proteins in progenitors, neuroblasts and neurons;
- characterise the evolution of RGS3 and the R4 subfamily of proteins, as well as the function of the invertebrate R4-like protein in the vertebrate placode.

To address these aims, I first characterised the expression patterns of isoforms of RGS3 using *in situ* hybridisation probes specific to each isoform. Looking at transverse sections through the placode and forming ganglion, I analysed the precise onset and

termination of expression of each isoform in the epithelial progenitor, immature neuroblast, and mature neuronal states. To investigate conservation of this expression in other species and neuronal types, I conducted homologous *in situ* hybridisations on the forming CSG and cerebral cortex of mouse embryos. I next used short-hairpin RNA targeting the shared 3' sequences to simultaneously knock down all isoforms (except C2PA) in the placodes and their neuronal derivatives. To determine the specific role of each isoform, I overexpressed RGS3L, RGS3s, and RGS3hs individually. I further dissected the domain dependence of each isoform through overexpression of constructs with targeted deletions or mutations. Lastly, in collaboration with Dr Cedric Patthey (Umeå University, Sweden), the conservation of RGS3 and the evolution of RGS proteins were analysed. A distinct domain difference was observed between invertebrate and vertebrate RGS3, which led me to test the function of the invertebrate RGS3 in the vertebrate placode.

Chapter 2. Materials and Methods

Section 2.1 Animal Models

Fertilised eggs of *Gallus gallus domesticus* hens were purchased from Winter Egg Farm (Hertfordshire, UK) and incubated to the indicated HH stages at 38°C in a humidified incubator and fixed in MEMFA (0.1M Mops; 2 mM EGTA; 1 mM MgSO4; 3.7% formaldehyde) overnight at 4°C.

Wild-type E9.5 mouse embryos were collected and fixed in 4% paraformaldehyde by Dr Elizabeth Robertson (University of Oxford). Coronal and sagittal sections of E15.5 mouse embryos were provided by Dr Peter Oliver (University of Oxford).

Section 2.2 Molecular Biology

Products amplified by polymerase chain reaction (PCR) from first-strand cDNA pools were purified using the PureLink® PCR Purification kit (Life Technologies, Renfrewshire, UK; catalogue number: K3100-01). Products amplified from plasmids were separated on a gel and purified using the Qiagen Qiaquick Gel Extraction kit (Manchester, UK; catalogue number: 28704). All products were purified into 30.0 µl diethylpyrocarbonate (DEPC)-treated double-distilled water (ddH_2O).

Section 2.2.1 PCR Amplification

Section 2.2.1.1 DNA Polymerases

For *in situ* hybridisation constructs and colony screening, unless otherwise indicated, I used Taq or REDTaq DNA Polymerase (Sigma Pharmaceuticals, Hertfordshire, UK; catalogue numbers D1806 or D4309, respectively). For RACE and amplification of

overexpression constructs, I used Phusion® High-Fidelity DNA Polymerase (New England Biolabs (NEB), Hertfordshire, UK; catalogue number M0530S).

Section 2.2.1.2 Tissue Dissection and RNA Extraction, and cDNA Synthesis

Unless otherwise indicated, cDNA was synthesised from RNA extracted and purified as follows. Using a flame-sharpened tungsten needle, 3-4 pharyngeal regions (from the level of the first somite to the midbrain/hindbrain boundary) were dissected from HH18 chick embryos into 50 µl TRIzol® reagent (Life Technologies; catalogue number: 15596-026). Immediately after collecting samples into TRIzol®, tissues were homogenised using RNase/DNase-free pestles. 950 µl TRIzol® and 200 µl chloroform were added to the samples, and the aqueous phase was separated following centrifugation. RNA was purified by ethanol precipitation and resuspension in 20 µl DEPC-ddH_2O. Purity and concentration were determined using a NanoDrop® ND-1000 Spectrophotometer (Thermo Fisher Scientific, Cheshire, UK). First-strand cDNA was synthesised in triplicate using the Cloned AMV First-Strand cDNA Synthesis kit (Life Technologies; catalogue number: 12328-032) using 0.5 µg RNA per reaction and the oligo-dT primer.

Section 2.2.1.3 Amplification Settings

Section 2.2.1.3.1 Taq Polymerase

10X PCR Buffer with 15mM $MgCl_2$ (Sigma):	5.0 µl
10 mM dNTPs (Roche, Sussex, UK):	1.0 µl
10 µM sense (forward) primer:	1.0 µl
10 µM antisense (reverse) primer:	1.0 µl
Sigma Taq* (5.0U or 1.0U/µl):	0.25 µl or 2.5 µl
First-strand cDNA template**:	4.0 µl
DEPC-ddH_2O:	to 50.0 µl

*Sigma Taq (catalogue number D1806) was at 5.0U/µl, and Sigma REDTaq (catalogue number D4309) was at 1.0U/µl.
**For PCR colony screening, dissociated bacteria replaced template.

Thermocycler Settings:

Initial Denaturation:	94°C, 4 minutes
30 Cycles:	
Denaturation:	94°C, 1 minute
Annealing:	see below*, 2 minutes
Elongation:	72°C, see below**
Final Elongation:	94°C, 10 minutes

Annealing temperature set to 4°C below the lowest melting temperature (T_M) of either primer, calculated as T_M = 4(number of Gs + number of Cs) + 2*(number of As + number of Ts).
**Elongation time set to 1 minute per kb of desired product.

Section 2.2.1.3.2 Phusion® Polymerase

5X Phusion® HF Buffer (NEB):	10.0 µl
10 mM dNTPs (Roche):	1.0 µl
10 µM sense (forward) primer:	1.5 µl
10 µM antisense (reverse) primer:	1.5 µl
NEB Phusion® HF (2.0U/µl):	0.5 µl
First-strand cDNA template:	4.0 µl
DEPC-ddH_2O:	31.5 µl

Initial Denaturation:	98°C, 30 seconds
30 Cycles:	
Denaturation:	98°C, 8 seconds
Annealing:	see below*, 20 seconds
Elongation:	72°C, see below**
Final Elongation:	98°C, 8 minutes

*Annealing temperature calculated using the NEB T_M Calculator (https://www.neb.com/tools-and-resources/interactive-tools/tm-calculator).
**Elongation time set to 30 seconds per kb of desired product.

Section 2.2.2 Rapid Amplification of cDNA Ends (RACE)

Section 2.2.2.1 Tissue Dissection and RNA Extraction

RNA was extracted from the petrosal placode and derivatives as follows. Transverse slices ~200-300 µm thick were cut immediately caudal to the otic vesicle using a flame-sharpened tungsten needle. The junctions between surface ectoderm and neural tube were broken, and the neural tube and notochord were removed from the sample. Underlying endoderm and ventral (pharyngeal arch) ectoderm were similarly removed. 4-8.5 pairs of tissue were dissected and kept in DEPC-treated phosphate buffered saline (PBS) on ice before RNA purification. Tissue was homogenised by pipetting and RNA was purified using the Qiagen RNeasy Mini Kit (catalogue number: 74004) into 30.0 µl DEPC-treated ddH_2O and confirmed for purity using a NanoDrop® ND-1000 Spectrophotometer.

Section 2.2.2.2 RACE

RACE was conducted using the Invitrogen GeneRacer™ kit (catalogue number L1500-D1; Life Technologies) using 7.0 µl RNA (450-960 ng). A provided oligo-dT primer was used to synthesise first-strand cDNA from purified RNA from above (for 3' RACE) or GeneRacer™ RNA Oligo-ligated RNA (for 5' RACE). One round of gene-specific PCR was followed by a second round of nested PCR (for amplification settings, see Section 2.2.1.3) using the primers listed in Table 2.1. Second-round products were collectively purified using the PureLink® PCR Purification kit and cloned into pCR4Blunt-TOPO (Life Technologies; catalogue number: K289520). Colonies were PCR screened using T7 forward and T3 primers (provided by pCR4Blunt-TOPO kit) with 45°C annealing temperature and 2 minute elongation time (see Section 2.2.1.3). Products were run on a 1.0% agarose gel and colonies of distinct sizes were miniprepped

using the Qiagen Spin Miniprep kit (catalogue number: 27106), and then submitted for sequencing with Source Bioscience Plc (Nottingham, UK).

Table 2.1. Primers Used for 3' and 5' RACE

Primer Name	Sequence (5'→3')
P_{UP} Gene-Specific rev	TGTTCTGGCCCCGCTTGCCAATCT
P_{UP} Nested rev	CCTGCACACGGACTGGGGAGTCACA
P_{DOWN} Gene-Specific rev	GGCCCTGAAAGCTGCGAGCCCATA
P_{DOWN} Nested rev	GCCGGAAAATCCCCAGCCGGTTCT
3' Gene-specific fwd	CCCCCGCTTCCTCCGCTCTGA
3' Nested fwd	CCAGAAGAAAGCCAGCTCCCCGCTGTA

Section 2.3 Riboprobe Synthesis and *In Situ* Hybridisation

Templates for riboprobe synthesis were amplified using primers indicated in Table 2.2 and Table 2.3. Unless otherwise indicated, templates were amplified with Taq polymerase (Section 2.2.1.3.1) and cloned into pGEM-T (Promega, Southampton, UK; catalogue number: A3600) using cDNA described in Section 2.2.1.2. For amplification of mouse riboprobe templates, cDNA was prepared as described in Section 2.2.1.2 from RNA extracted from E9.5 mouse embryos (provided by Dr Robertson) and purified into 30.0 µl DEPC-ddH_2O using the Qiagen RNeasy Mini Kit. Plasmids containing templates were submitted for sequencing as in Section 2.2.2.2 to confirm sequence fidelity and to check orientation of sequence in the vector. 2.0 µg plasmid was linearised using the restriction enzymes listed in Table 2.2 and Table 2.3 and purified into 30.0 µl DEPC-ddH_2O using the PureLink® PCR Purification kit. 6.0-9.0 µl of purified linearised plasmid were used in an *in vitro* transcription reaction using the dioxigenin (DIG)-labelled rNTPs and the polymerase listed in Table 2.2 and Table 2.3. *In situ* hybridisation was carried out as described previously (Henrique et al., 1995) on wholemount embryos.

Table 2.2. Primers, Template Sizes, and Plasmid Information for RGS3 *In Situ* Hybridisation Constructs.
Amplification primers and vector into which PCR product was cloned is listed. Enzymes used to linearise (cut) and *in vitro* transcribe (RNAP) are also listed. RGS domain probe corresponds to the coding sequence of RGS3hs used for overexpression (Table 2.6). The ChEST456e1 template cloned into pBSKII had previously been obtained in our laboratory. Note: the exon20a antisense primer was erroneously designed. The G indicated in red is not endogenous, and should be an A.

Name	Sequence (5'→3')	Size (bp)	Vector	Cut	RNAP
RGS3hL	s: ATGGAACTGTCACAAAACGA	269	pGEM-T	NcoI	SP6
	a: TTCCCCTTCACCTGTGAAGG				
C2PA	s: ACTGCTGGCCAGCCTGTCCCTCCTG	181	pGEM-T	NcoI	SP6
	a: GAAGGTGGTGAGGCAGAAGGAAGCT				
C2 domain	s: GGCCAGCTGAAGCTGTCTAT	476	pGEM-T	NotI	T7
	a: GATATCCTGGCCCTCACACG				
RGS3L	s: CAGTTTGACTGGGGTTTGTTCC	163	pGEM-T	NcoI	SP6
	a: GCCGGTATCTCCGCTCCGA				
PDZ	s: GGAGTGATGGGCTAATGCTA	703	pGEM-T	NcoI	SP6
	a: TGCTTGGTGATGTTCTCAGC				
RGS3s	s: ACTGCCTGACACAGACATTAATAACG	137	pGEM-T	NotI	T7
	a: CAGATGTGGGCTCAGTTGCA				
RGS3hs-HTMKE	s: AGAGCGCAGTGCCGGGC	171	pGEM-T	NotI	T7
	a: TCCTTCATGGTGTGCCGG				
ChEST 456e1	Cloned in (Boardman et al., 2002).	741	pBSKII	NotI	T3
exon20a	s: ATGCTGGAGACGGACGC	350	pGEM-T	NotI	T7
	a: TCCAGGTAGTTCTCGTCGCT				
exon20b	s: ATGATCGAGACGTCGGGC	311	pGEM-T	NcoI	SP6
	a: GAGGTCTCCTCCCCTTCATC				
RGS domain	s: ATGAAGAACCGGCTGGGG	545	pCR4	SpeI	T7
	a: TCCATGTAAACACGCAGCTC				
3' terminus	s: GCGCGTTCCCTAGCAGC	250	pGEM-T	NotI	T7
	a: ACCTATGACCATGACAATGCA				
Musm-PDZ	s: TGCCAGACCACACAGATCAT	613	pGEM-T	NotI	T7
	a: CAAAGCTCATGCAGCCAATA				
Musm-s	s: AAGCAAGAGAGCCAAGCCTC	274	pGEM-T	NcoI	SP6
	a: CCAAGTTCCCCAGAGGAGC				
Musm-e20	s: GCCTACCCTCTCAGGAGTCA	493	pGEM-T	NcoI	SP6
	a: AAGGGATAGCCCAGGTGGAT				
Musm-hs	s: AGTCATCCGGCCAGGATTC	220	pGEM-T	NotI	T7
	a: TCCTTCATGGTGTGCCGCC				
Musm-RGS	s: TCCTTCAAGCCTACCTCGGA	418	pGEM-T	NotI	T7
	a: GCGGGGGACTCATCTTCTTC				

Table 2.3. Primers, Template Sizes, and Plasmid Information for Non-RGS3 *In Situ* Hybridisation Constructs.
Amplification primers and vector into which PCR product was cloned is listed. Enzymes used to linearise (cut) and *in vitro* transcribe (RNAP) are also listed.

Name	Sequence (5'→3')	Size (bp)	Vector	Cut	RNAP
RGS4-CDS	s: GCCGGCCACTTGCTTAAAAA	567	pGEM-T	NotI	T7
	a: CATGAGCGTGGGCTCTTTTG				
RGS4-3'UTR	s: AGCTATCAGGCACTGGGAGA	574	pGEM-T	NotI	T7
	a: AGTATGAGCAGAGCCCAGGA				
EphrinB1	s: GTCATGAAAGTGGGGCAGGA	448	pGEM-T	NcoI	SP6
	a: GTAGTGCGGGCAGTAGTTGT				
EphrinB2	s: CCCCAAGTTCCTTCCTGGAC	535	pGEM-T	NotI	T7
	a: ACTGGAATGCCCAGCCTTAC				
LPAR1	s: GCAGGGCTGGCCTACTTTTA	621	pGEM-T	NcoI	SP6
	a: TGAATTCTGCCAGGAGCAGG				
LPAR2	s: CAACGAGTCGGTGGGTTTCT	421	pGEM-T	NotI	T7
	a: GATCATGACGCGTTGGTTGG				
Musm-RGS4	s: GACATGAAACATCGGCTGGG	554	pGEM-T	NcoI	SP6
	a: AGACCAGGGAAGTGCAGTCT				

Section 2.4 Antibody Labelling

Wholemount antibody staining was carried out as described in (Thompson et al., 2010).

Antibodies and the concentrations at which they were used are listed in Table 2.4.

Table 2.4. Primary and Secondary Antibodies and Concentrations Used in This Thesis.

Primary Antibodies

Antibody	Ig	Animal	Manufacturer	Cat. No.	Concentration
GFP	G	Rabbit	Life Technologies	A11122	1:500
GFP	G	Rat	BioLegend (London, UK); or Nacalai Tesque (Nijo Karasuma, Japan)	338002; 04404-84	1:1000
HuC/D	G	Mouse	Life Technologies	A-21271	1:500
Islet-1/2	G	Mouse	DSHB (U Iowa, USA)	39.4D5	1:500
NFM	G	Mouse	Life Technologies	RMO-270	1:5000
NFM	G	Rabbit	Abcam (Cambridge, UK)	ab9034	1:500
pH3	G	Rabbit	Millipore (Watford, UK)	06-570	1:500

Secondary Antibodies

Antibody	Ig	Animal	Manufacturer	Cat. No.	Concentration
Alexa-488 Rat	G	Goat	Life Technologies	A11006	1:500
Alexa-488 Rabbit	G	Goat	Life Technologies	A11008	1:1000
Alexa-555 Mouse	G	Donkey	Life Technologies	A31570	1:1000
Alexa-568 Mouse	G	Goat	Life Technologies	A11004	1:1000
Alexa-647 Rabbit	G	Donkey	Life Technologies	A31573	1:1000

Section 2.5 *In Ovo* Electroporation

Electroporation in the chick embryo has previously been shown to be highly efficient with little perturbation on global gene expression (Farley et al., 2011). HH11-13 embryos were electroporated *in ovo* using a BTX® Electro Square Porator™ ECM830 with 4 pulses at 10V, 5 ms each. Egg shells were re-sealed and embryos were incubated a further 18-26 hours to HH16-18. Short-hairpin RNA (shRNA) and pMES overexpression vectors were introduced at 2.0 µg/µl. A chicken β-actin-GFP expression construct was co-electroporated at 0.4 µg/µl with shRNA vectors. DNA mixes were prepared with 0.05% Fast Green dye and 0.01% carboxymethyl cellulose (CMC; provided by Dr Patthey).

Section 2.6 Short-Hairpin RNA (shRNA) Design and Cloning

The RGS3L full-length mRNA sequence was input into three design engines: the Whitehead Institute siRNA Design Engine (http://sirna.wi.mit.edu/home.php); the Genscript siRNA Target Finder (https://www.genscript.com/ssl-bin/app/rnai); and the Life Technologies BLOCK-iT^{TM} RNAi Designer (https://rnaidesigner.lifetechnologies .com/rnaiexpress/). Engines were run at default settings. shRNA sites were aligned to the chicken mRNA database with the basic local alignment search tool (BLAST) (Altschul et al., 1990). shRNA sites were selected based on common findings between the three engines and/or lowest amount of contiguous base pairs aligned to the shRNA sequence from off-target gene products. Sequences selected contained two endogenous 5' A residues followed by 19 bp, as recommended by the user manual of the p*Silencer*^{TM} 2.1-U6 Hygro vector (Life Technologies; catalogue number: AM5760M), into which the shRNA constructs were cloned. To clone shRNAs, complementary sense and antisense oligos were ordered which would anneal to form double-stranded DNA with overhanging

BamHI and HindIII restriction sites. An example construction of these oligos is shown in Figure 2.1. Oligos were annealed and cloned as according to the p*Silencer*™ 2.1-U6 Hygro user manual. shRNA target sequences are listed in Table 2.5.

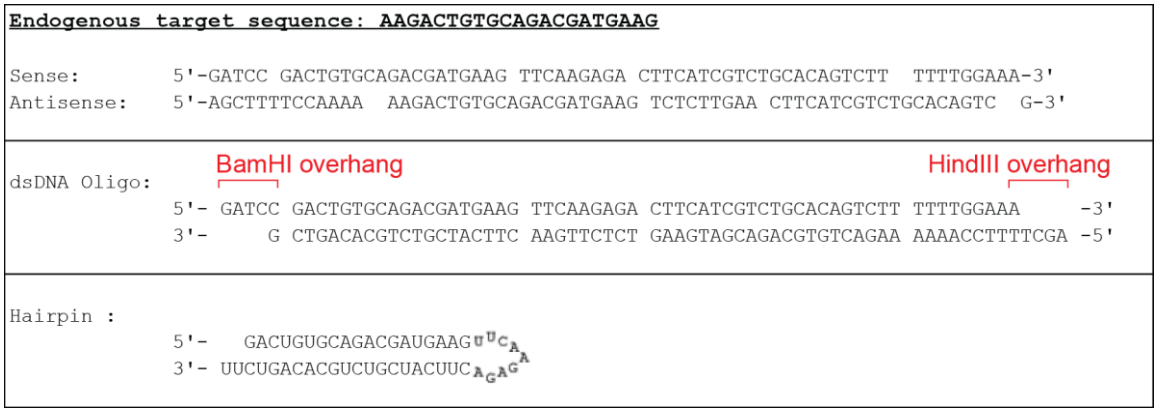


Figure 2.1. Example Design of shRNA Oligos for Cloning.
Sense and antisense sequences were inserted into oligo templates (top) and ordered. After annealing, oligos contained single-stranded overhangs which complement the BamHI and HindIII restriction sites (middle). The final transcribed secondary structure for the shRNA is shown at bottom. This particular example is of sh678 (Table 2.5).

Table 2.5. shRNA Target Sequences Used in This Thesis.

Site Name (Figure 4.1)	**Sequence (5'→3')**
sh678	AAGACTGTGCAGACGATGAAG
sh881	AAGCAGGACTATCCAGGTGAC
sh1997 (shRNA-*CDS*)	AAGCTCTCAAGTGGGGGGAGT
sh2172	AAGATCTTTGCGGAGTACATC
sh2929	AAACCCTCGTTCCCAATTTAC
sh3300 (shRNA-*3'UTR*)	AAGCATCTCTGCAGCTAGCAA
Control shRNA	AACAGTCGCGTTTGCGACTGG

Section 2.7 Overexpression Design and Cloning

Sense primers beginning with the start codons described in the text (Section 4.3) were used with a common antisense primer ending 38 bp into the 3' UTR to amplify overexpression constructs (Table 2.6). For amphioxus RGS3hL (Brala RGS3hL), a similar sense primer initiating at the start codon was designed, as well as an antisense primer ending 34 bp into the 3' UTR. PCR products were cloned into pCR4, which was

subsequently digested with EcoRI, gel-separated, and purified into 30.0 µl DEPC-ddH_2O. pMES (provided by Paul Kulesa, Stowers Research Institute, USA) was EcoRI digested in parallel and purified with the PureLink® PCR Purification kit into 30.0 µl DEPC-ddH_2O. Ligations were performed with T4 DNA Ligase (NEB) using a 6:1 insert:vector molar ratio for 10 minutes at room temperature. Colonies were screened using a gene-specific antisense primer and a sense primer specific to pMES ('pMES MCS fwd', Table 2.6). Positive colonies were prepped and submitted for sequencing (Source Bioscience) with overlapping vector and gene-specific primers to ensure sequence fidelity and proper orientation.

Table 2.6. Primers Used for Amplification and Product Sizes of Wild-Type Overexpression Constructs.
Start codons at the beginning of sense primers are indicated in red. For chicken products (ie, all except Brala), the same antisense primer was used with different sense primers. The product size for each reaction is listed next to the sense primer. RGS3hs primers are identical to those for the RGS domain probe in Table 2.2. Additionally, the 'pMES MCS fwd' primer used in colony screening is listed.

Primer Name	**Sequence (5'→3')**	**Product Size** (bp)
RGS3hL fwd	ATGGAACTGTCACAAAACGA	3149
RGS3L fwd	ATGAACCGCTTCAATGGACT	2438
RGS3s fwd	ATGCTGGAGACGGACGC	1265
RGS3hs fwd	ATGAAGAACCGGCTGGGG	545
RGS3 3'UTR rev	TCCATGTAAACACGCAGCTC	
Brala RGS3hL fwd	ATGGATGTGCCACAGAGTCC	3631
Brala RGS3hL rev	CCTCGGGTTAGCTTGTGTTT	
pMES MCS fwd	TCTGGCGTGTGACCGGCG	

Section 2.8 Design and Cloning of Domain Deletion and Mutation Constructs for Overexpression

The RGS3sΔEF construct was cloned by performing two PCRs in parallel, one immediately upstream and one immediately downstream of the EF Hand domain (Figure 2.2). Importantly, the antisense primer of the upstream reaction (P2) additionally contained antisense sequences which aligned to the region immediately downstream of the EF Hand domain, and the inverse was true for the sense primer of the downstream reaction (P3; Table 2.7). A RGS3LΔEF construct was first cloned, using 'RGS3L fwd' (P1; Table 2.6) and P2 in one reaction, and P3 and '3'UTR rev' (P4; Table 2.6) in the other reaction. This produced two PCR products with overlapping sequences upstream and downstream of the EF Hand domain. A final PCR was performed combining these products as template and using P1 and P4 to construct the full-length construct. This PCR product was gel-separated, purified, and cloned into pCR4. A subsequent PCR using 'RGS3s fwd' and '3'UTR rev' and with RGS3LΔEF as template generated the RGS3sΔEF construct, which was cloned into pCR4 and subsequently subcloned into pMES as in Section 2.7.

The RGS3LN740A was generated in a similar manner, using 20 bp primers corresponding to P2 and P3 of Figure 2.2 which flanked the N740 codon and contained two bp substitutions (AAT to GCT). Two parallel PCRs were performed as above, and a final PCR used 'RGS3L fwd' and '3'UTR rev' as P1 and P4, respectively (Table 2.6). This product was purified and cloned into pCR4 and used as template for RGS3sN740A and RGS3hsN740A. All three N740A constructs were subcloned into pMES as in Section 2.7.

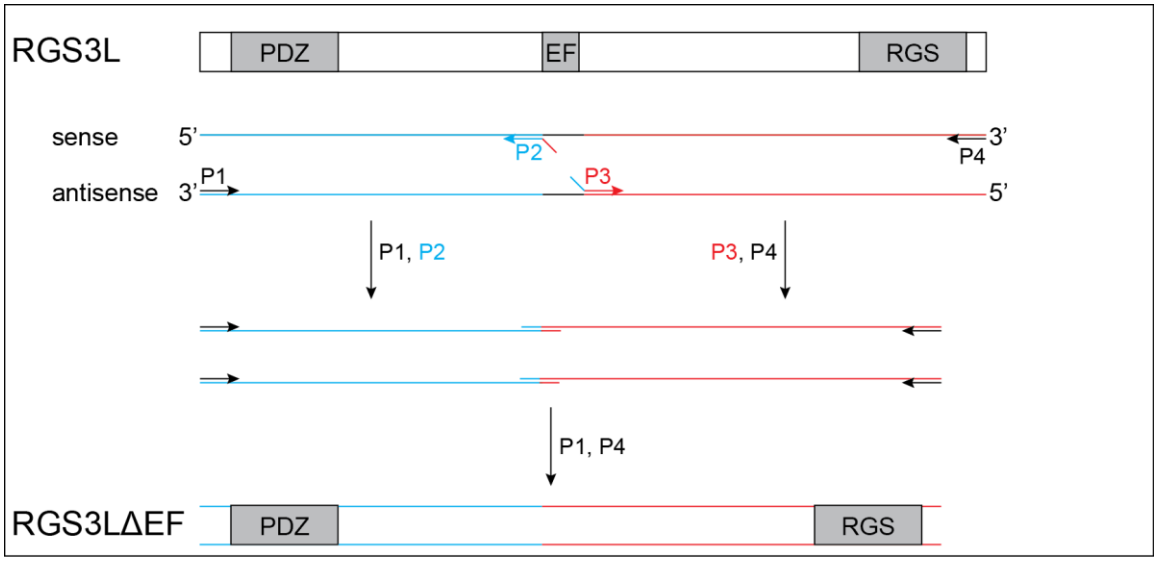


Figure 2.2. Amplification Strategy for the RGS3LΔEF Construct.
Two parallel reactions were performed using primers complementing the sequences upstream (P1, P2) and downstream (P3, P4) of the EF Hand domain. The antisense P2 primer contained 5' sequence which complemented the sequences immediately downstream of the EF Hand domain, and the sense P3 primer contained 5' sequence which encoded the sequences immediately upstream of the EF Hand domain (see Table 2.7). The products of these reactions were combined as template for a P1/P4 reaction, which generated the full-length RGS3L product lacking an EF Hand domain (RGS3LΔEF).

Table 2.7. Primers Used for the Generation of Domain Deletion and Mutation Constructs.
For the ΔEF primers, the upstream complement is indicated in blue, and the downstream complement is indicated in red. For the N740A primers, the mutated residues are in lowercase.

Primer Name	Sequence (5'→3')
RGS3 ΔEF upstream rev (P2)	TCTCGATCATATCGTCCTCTTCTTCGTCATCC
RGS3 ΔEF downstream fwd (P3)	AGAGGACGATATGATCGAGACGTCGGGCTG
RGS3 N740A fwd	AAGGAGGTGgcTCTGGACTC
RGS3 N740A rev	GAGTCCAGAgcCACCTCTTC

Section 2.9 Embryo Embedding and Sectioning

Embryos were embedded in a 15% gelatin/15% sucrose PBS solution and fixed in MEMFA overnight at 4°C. Fixed blocks were sectioned transversely (unless otherwise stated) at 100 µm intervals for antibody-labelled embryos or 50 µm intervals for *in situ* hybridisation-labelled embryos.

Section 2.10 Imaging

Confocal analysis of transverse sections of antibody-labelled embryos was performed at 20X magnification on a Zeiss LSM710 microscope, unless otherwise indicated. 1.44 µm intervals were acquired. 3D-reconstruction was performed using ImageJ version 1.47q software. DIC imaging of wholemount embryos and sections was performed at 4X and 20X magnification, respectively, using an Olympus BX51 compound light microscope. These images were captured with a Retiga-2000R Fast1394 camera and acquired using Simple PCI Version 6.5.2.0 software.

Section 2.11 Cell Counting Analyses

For counting of total neuroblasts and neurons following shRNA electroporation (Figure 4.3), Islet-1/2-positive cells (in which nuclei were specifically labelled) were visualised and counted using the multipoint selection tool in ImageJ. Every sixth confocal Z image was analysed to create a depth in the Z plane of 8.64 µm, ensuring nuclei (which I measured to average ~6 µm in diameter) were not counted twice.

A similar approach was used to count GFP/pH3-double positive cells (Figure 4.4). GFP localises to all subcellular compartments, whereas αpH3 specifically labels M-phase nuclei. GFP and pH3 channels were overlaid in ImageJ and double-positive cells in every sixth Z image were counted. GFP-positive cells in the non-placodal surface ectoderm were not counted.

Neuroblast differentiation analysis (Figure 4.6 and Figure 4.12) required the overlay of GFP, NFM and HuC/D channels. αHuC/D labels the cytoplasm but is excluded from the nucleus (Figure 4.14C), so GFP-/HuC/D-double positive cells were counted by the presence of αGFP and exclusion of αHuC/D in the nucleus in every sixth Z image. In the

HuC/D-negative staging area, GFP-positive cells were sufficiently separated to distinguish individually. All GFP-positive cells counted in the staging area were also NFM-positive, indicating they were neuroblasts. HuC/D positive (GFP-positive and negative) neurons were counted similarly in every sixth Z image for analysis in Figure 4.10.

Section 2.12 Staging Area Length and Migration Analyses

For staging area length and migration analyses, the total distance from the ventral-most delaminated neuroblast outside the placode to the point of innervation for CSG axons (visualised with αNFM as the exit point for CNS motor axons (Thompson et al., 2010)) was drawn in Adobe Illustrator version 16.0.3 (Figure 2.3). For the length of the staging area (Figure 4.5L and Figure 4.12C), a line was drawn along the total distance line to the first HuC/D-positive cell body. For the migration analyses, (Figure 4.7A and Figure 4.13C) lines were drawn from the base of the total line to the cell body and terminus of its leading projection, respectively. The lengths of each line were measured and divided by the length of the total line to normalise the distances. For projection length analysis (Figure 4.7B, Figure 4.14A), the raw distance of the leading cell body was subtracted from the raw distance of its projection.

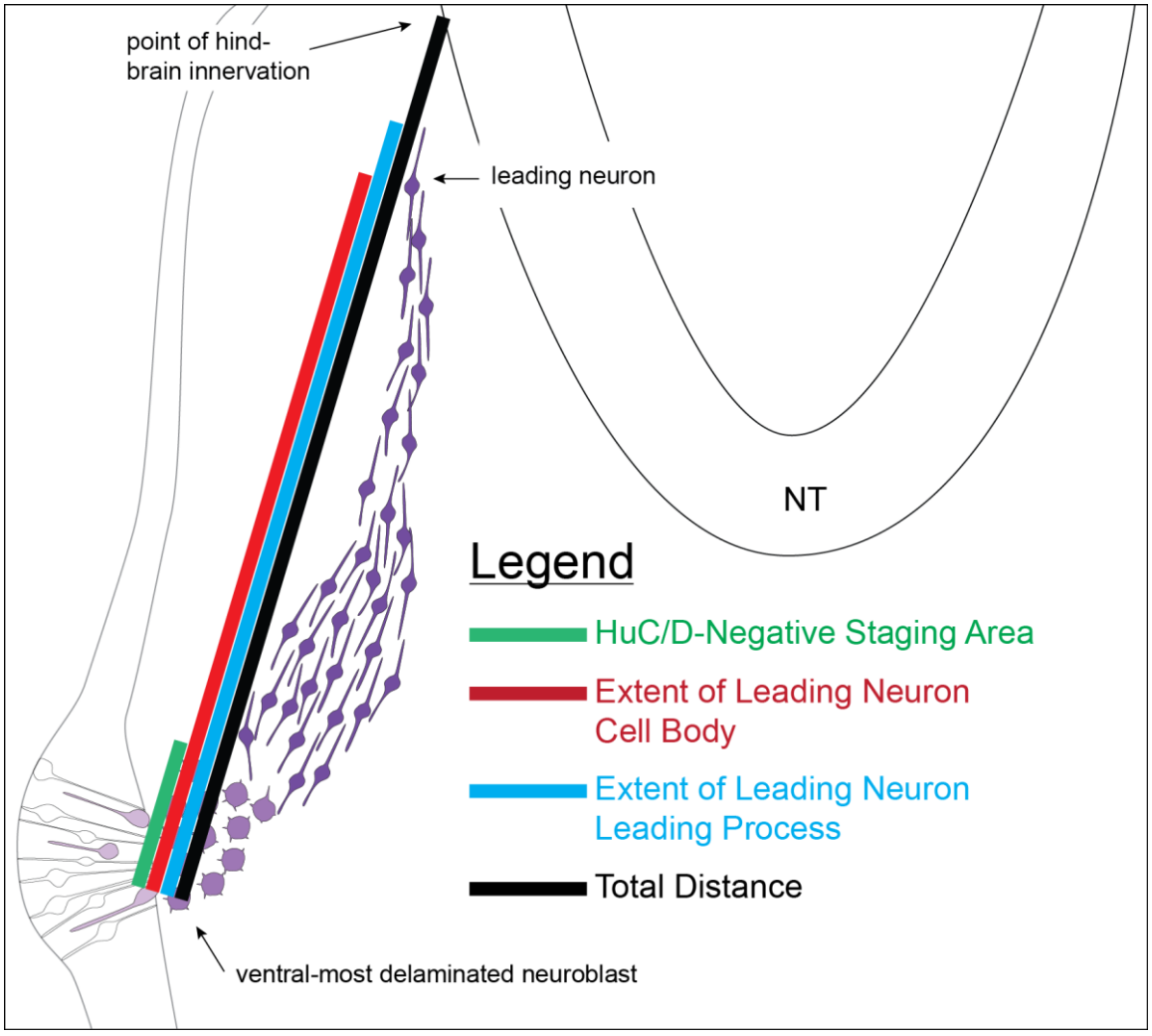


Figure 2.3. Analysis of Staging Area Length and Migration.
To normalise for size differences between embryos, a total distance line was drawn in Adobe Illustrator (black) from the ventral-most delaminated neuroblast to the point of hindbrain innervation (arrows). Other measurements were drawn from the base of this line (the ventral-most delaminated neuroblast) to the point of interest: the first HuC/D-positive neuron (green), the position of the cell body of the farthest-migrated neuron (red), or the position of the terminus of the projection of the farthest-migrated neuron (green). These measurements were divided by the total distance to calculate a percentage of the migratory stream.

Section 2.13 Quantitative Expression Analysis

CSG were previously dissected, antibody labelled, and FACS sorted by Dr Patthey as described in Section 3.3.2. RNA was extracted and whole-transcriptome sequenced. Duplicated repeats likely produced as an artefact of sequencing amplification were removed. Read counts for particular transcripts were normalised per kb in length of the transcript per megabases of mapped reads as RPKM values. These values were further normalised using the Differential Expression Seq package (DEseq) (Anders and Huber, 2010), which is widely used to account for variation in datasets. For analysis of RGS3hs-HTMKE levels versus RGS3hs-KYLER levels, only reads mapping to the unique exons of these transcripts were used.

Section 2.14 Phylogenetic Tree Construction

For the phylogenetic tree of the R4 family, an alignment of the RGS domain was generated using the Multiple Alignment using Fast Fourier Transform (MAFFT) software (Katoh and Standley, 2013) and trimmed manually. The maximum likelihood methodology was implemented in the MEGA5 software (Tamura et al., 2011) using the JTT substitution model. All other parameters were set to default.

Section 2.15 Statistical Analysis

Statistical analysis was performed in Microsoft Excel using a Student's one-tailed T-Test. *p* values less than 0.05 were considered significant, while those greater than or equal to 0.05 were considered insignificant.

Chapter 3. Expression of Isoforms of RGS3 in Neuronal Development of Chick and Mouse

Section 3.1 Introduction

The differential generation of isoforms of RGS3 has been known for some time (Kehrl et al., 2002). However, the expression of RGS3 isoforms has mostly been investigated in cell culture, and rare expression studies in the embryo have failed to discriminate between isoforms by using probes common to three or more isoforms (Lu et al., 2001; Norlin and Berghard, 2001). Following microarray analysis, RGS3 expression in the forming CSG of the chick embryo was confirmed using an antisense probe generated against an expressed sequence tag (EST), ChEST456e1 (Boardman et al., 2002) (Section 1.2.1). This probe aligned to a region encoding most of the RGS domain and the 3' UTR, recognising all isoforms except C2PA (see Figure 3.4A). Thus it was not clear which isoforms (if not all) contribute to this staining. Furthermore, the staining with this probe was only superficially analysed, and it was not clear whether it stained the placode and/or neuroblast staging area in addition to migratory neurons of the forming CSG.

In this chapter, I sought to dissect the differential expression of RGS3 isoforms in the forming chick CSG. Furthermore, I sought to differentiate staining between the progenitor placode, neuroblast staging area, and neuronal migratory stream. To achieve this, I designed and cloned various regions of the RGS3 locus, including regions specific to each isoform, and generated antisense probes. *In situ* hybridisation was carried out with these probes on wholemount embryos, which I sectioned for more precise analysis. I focused my analysis on transverse sections of the forming petrosal ganglion, a model system in which the placode, immature neuroblasts, and mature neurons are clearly

spatially separated (Figure 1.7). Lastly, I sought to determine the conservation of these expression patterns in other species and neuronal tissues. To achieve this, I designed and cloned homologous probes for *in situ* hybridisation on mouse embryos. I carried out *in situ* hybridisation with these probes to E9.5 mouse embryos in wholemount, and sectioned these embryos as in the chick. In addition, in collaboration with Dr Peter Oliver (University of Oxford), I analysed the staining of these probes on the forming cerebral cortex. Comparison of these patterns, and their implications for the maturation of neurons in the embryo, will be discussed in the final section.

Section 3.2 Multiple Isoforms Are Generated by the RGS3 Locus

Section 3.2.1 RGS3 Isoforms Initiate at Predicted Promoter Sites

Before determining the differential expression of RGS3 isoforms, I first sought to determine the nature of their production. Isoforms can be differentially produced by alternative splicing or by transcription from alternative promoters. The fact that the C2PA, RGS3L, RGS3s, and RGS3hs isoforms encode N-terminal truncations of RGS3hL and are each only unique at their 5' ends by the presence of one exon suggests the latter. If this hypothesis is true, the promoter driving expression of each isoform should be embedded within an intron of RGS3hL. This would produce pre-mRNA with a unique splice donor site that could be spliced to the acceptor site on the next RGS3hL exon, generating a unique 5' exon not present in RGS3hL.

To determine whether RGS3 isoforms are transcribed from different promoters, I analysed annotations of the human RGS3 locus on the UCSC genome browser (Kent et al., 2002) (Figure 3.1). Two sets of annotations were analysed: methylation signatures of

lysine 4 of histone H3 (H3K4), and CpG islands. H3K4 trimethylation marks are associated with transcriptionally permissive chromatin (Santos-Rosa et al., 2002; Schneider et al., 2004), especially when compared to a depletion of H3K4 monomethylation (Heintzman et al., 2007). CpG islands, which are non-methylated, GC-rich regions of DNA, are similarly associated with transcription initiation (Deaton and Bird, 2011; Gardiner-Garden and Frommer, 1987). H3K4 trimethylation and monomethylation marks were displayed on the UCSC genome browser from datasets across seven different human cell lines from the ENCODE Data Coordination Center (Bernstein et al., 2012). CpG island annotations were displayed on the UCSC genome browser based on unpublished prediction software from G Miklem and L Hillier.

I found three broad peaks of H3 K4 trimethylation, each corresponding precisely to the start of the unique exons for RGS3L, RGS3s, and RGS3hs (red arrowheads, Figure 3.1B,C). Additionally, I observed troughs of H3 K4 monomethylation associated with each peak of H3 K4 trimethylation across these cell lines. A more subtle H3 K4 trimethylation peak corresponded to the start site of C2PA. However, I also observed a CpG island annotated in this region (Figure 3.1B). Taken together, these data suggest that C2PA, RGS3L, RGS3s and RGS3hs isoforms are differentially transcribed from distinct downstream promoters.

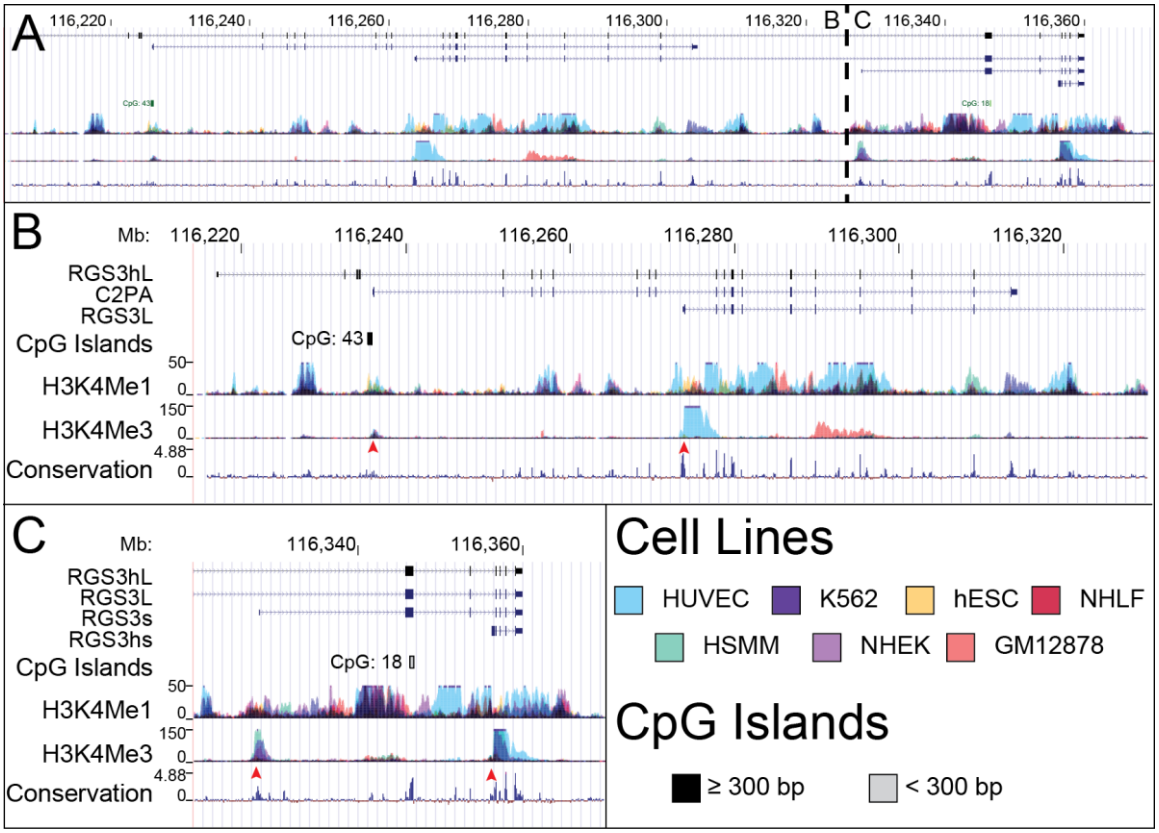


Figure 3.1. Isoforms of RGS3 are Transcribed from Different Promoters at the Human Locus.
(A) View of the entire human RGS3 locus, adapted from (Kent et al., 2002). Megabase positions along chromosome 19 are indicated at top. Dashed line indicates division of the locus, magnified in *(B)* and *(C)*. The browser has been configured to display tracks of CpG islands (see text for credit), H3 K4 mono- and trimethylation (H3K4Me1 and H3K4Me3, respectively), and conservation of DNA sequence across 100 vertebrates annotated by the PhyloP software (Pollard et al., 2010). *(B)* Magnification of the 5' end of the RGS3 locus, showing predicted promoter marks at the start of C2PA and RGS3L (red arrowheads). For C2PA, a minor H3K4Me3 peak accompanies a CpG island. For RGS3L, the start site is associated with a major H3K4Me3 peak. *(C)* Magnification of the 3' end of the RGS3 locus, showing major H3K4Me3 peaks at the start sites of RGS3s and RGS3hs. GM12878: lympoblastoid cells; hESC: human embryonic stem cell; HSMM: human skeletal muscle myoblasts; HUVEC: human umbilical vein endothelial cells; K562: leukemia cells; NHEK: epidermal keratinocytes; NHLF: normal human lung fibroblasts.

Section 3.2.2 Identification of RGS3 Isoforms Expressed in the Forming Chick Petrosal Ganglion

I next sought to determine which (if not all) RGS3 isoforms are expressed in the forming CSG of the chick embryo. The chicken RGS3 gene models on the UCSC and Ensembl genome browsers currently only display the RGS3L, RGS3s and RGS3hs isoforms (Flicek et al., 2014; Kent et al., 2002). A chicken model for RGS3hL was prepared by Dr Patthey based on a transcriptomic dataset which he previously acquired (see Section 3.3.2). It was thus additionally imperative that I characterised the chicken C2PA isoform.

I decided to achieve both of these aims by carrying out 5' Rapid Amplification of cDNA Ends (RACE), which identifies the 5' termini of isoforms from an RNA pool. This technique involves replacing 5' methylguanosine caps on mRNA with an RNA oligo, reverse-transcribing this RNA, and amplifying cDNA using an oligo-specific sense primer and an gene-specific antisense primer. This technique is highly sensitive to non-specific amplification, a problem alleviated by using very pure tissue. To specifically isolate the forming petrosal placode and neural derivatives, I dissected transverse slices of HH18 chick embryos containing the petrosal placode, non-placodal surface ectoderm, and the mesenchyme outside of the placode, including its neural derivatives. RNA was extracted from this tissue for RACE. Because amplification of shorter products is more efficient, two primers were separately used to identify the start exons of the downstream (RGS3s and RGS3hs) and upstream (C2PA and RGS3L) isoforms: P_{UP} and P_{DOWN}, respectively (Figure 3.2A).

Three distinctly sized RACE products were generated with the P_{DOWN} primer: 885 bp, 321 bp, and 256 bp, respectively (Figure 3.2C). The 885 bp product was assigned to

RGS3s because it contained a unique exon followed by the six terminal coding exons of RGS3hL (Figure 3.2C,E). The unique exon encoded in this RACE product encoded an in-frame start codon which encodes an additional N-terminal seven aa. In human, this unique exon is entirely non-coding, and the start codon begins with the first nucleotide of the first shared coding exon (exon 20 of RGS3hL; see Figure 1.11) (Chatterjee et al., 1997a).

The 321 bp and 256 bp products were assigned to RGS3hs as they contained the four terminal coding exons of RGS3hL, but each contained a unique 5' exon. Analysis of the 321 bp product showed that the unique exon encoded a 5' UTR and 39 aa of the open reading frame (Figure 3.2C,E). The last 22 of these 39 aa aligned to the unique coding sequence of human RGS3hs with 73% similarity, indicating that this isoform is chicken RGS3hs. By virtue of the conserved C-terminal five aa of its unique exon, HTMKE, I have termed this isoform RGS3hs-HTMKE.

Analysis of the 256 bp product showed that its unique exon encoded a 5' UTR and 19 aa of open reading frame (Figure 3.2C,E). While a homologous exon could not be found in eutherian mammals, homologous exons in non-eutherian mammals, amphibians, teleosts, cartilaginous fish, and agnathans (jawless fish) were identified by aligning the amino acid sequence to translated genomes with BLAST (see Section 5.2.2.1). The C-terminal five aa of its unique exon are KCLER, though the conserved sequence in evolution is KYLER (see Figure 5.5B). For this reason, I have termed this isoform RGS3hs-KYLER. RGS3hs-KYLER and RGS3hs-HTMKE proteins are only unique from one another by virtue of their unique exon sequences (19 and 39 aa, respectively). Because evidence suggests these proteins do not perform different biochemical functions (discussed in

Section 5.4.1), henceforth I will use the name RGS3hs when referring to both isoforms collectively.

Two RACE products were generated with the P_{UP} primer: 776 bp and 426 bp, respectively (Figure 3.2B). The 776 bp product was assigned to C2PA because it contained a unique exon upstream of RGS3hL exon 4 (Figure 3.2D). The unique exon encoded a 5' UTR and 28 aa of open reading frame. These 28 aa are 62% similar to the unique 5' coding sequences of human C2PA, confirming that this RACE product is indeed the 5' terminus of chicken C2PA.

The 426 bp product contained a unique exon immediately upstream of the common exon on which the primer aligned (exon 11 of RGS3hL) (Figure 3.2B,D). This exon encoded a 5' UTR and 18 aa of coding sequence. These 18 aa are 100% identical to the unique 5' coding sequences of human RGS3L and to those of the previously-identified chicken RGS3L (GenBank accession NM_204459), confirming that this RACE product is the 5' terminus of chicken RGS3L. In addition, this RACE product extended its 5' UTR 53 bp past the 5' terminus of the previously-identified RGS3L, suggesting that this previous product is truncated as an artefact of amplification.

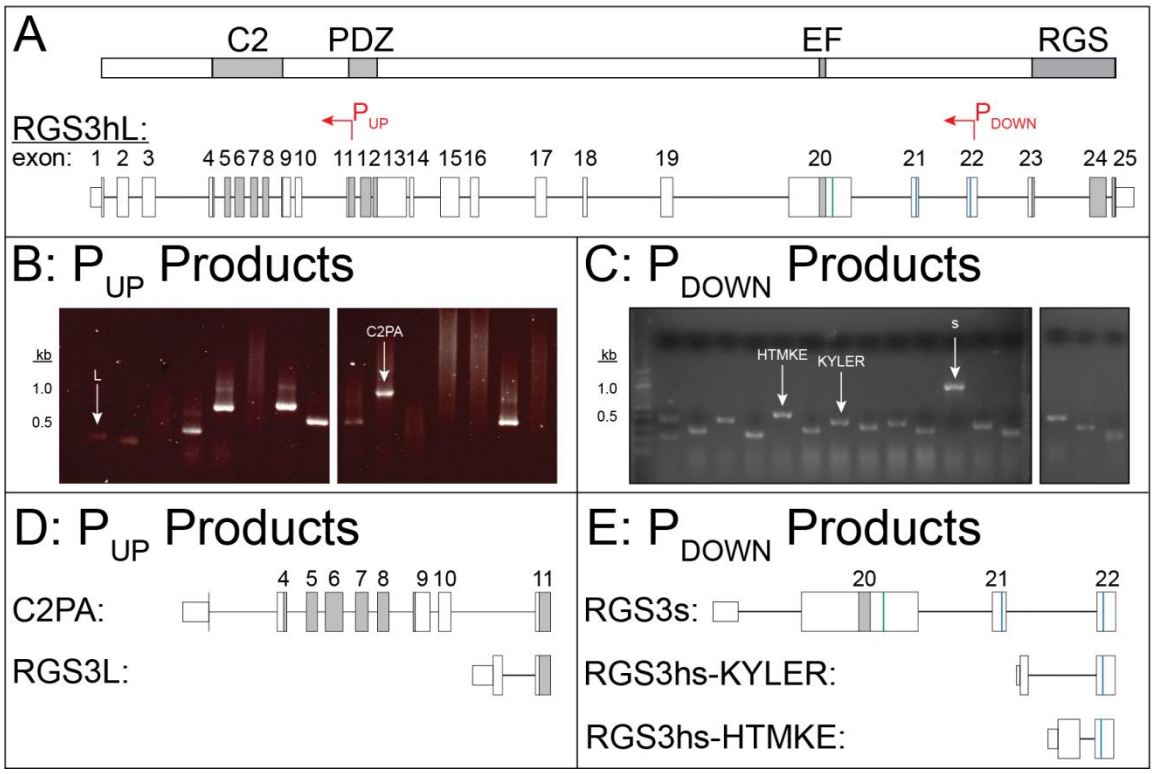


Figure 3.2. Identification of RGS3 Isoforms Expressed in Petrosal Placode-Associated Cells by 5' RACE.

(A) P_{UP} and P_{DOWN} antisense primers were designed against exons 11 and 22 of RGS3hL to identify the 5' termini of upstream and downstream isoforms, respectively. *(B,C)* 5' Rapid Amplification of cDNA Ends (RACE) was performed, generating products of several different sizes as visualised on an agarose gel. Products representing several different sizes were sent for sequencing. Products which aligned to RGS3 isoforms are indicated. *(D,E)* Sequencing of the bands indicated in *(B)* and *(C)* confirmed that these products corresponded to RGS3 isoforms (see text for details). This was the first identification of RGS3hs-KYLER expression in chicken. The only other species in which it has shown to be expressed is Zebrafish (Freisinger et al., 2010).

Section 3.2.3 Identification of Termini of 3' Untranslated Regions

I next sought to characterise the 3' terminus of each isoform. In the human gene model, RGS3hL, RGS3L, RGS3s and RGS3hs all share a common 3' UTR. In the original chicken gene model, however, RGS3L, RGS3s, and RGS3hs were reported to have progressively truncated 3' UTRs (Figure 3.3). Because microRNAs preferentially bind the 3' UTR of transcripts (Robins and Press, 2005), this model was intriguing as it could hypothetically represent a mode of differential post-transcriptional regulation. Alternatively, this model could have been assembled based on artefactual truncations during amplification. I explored this possibility by conducting 3' RACE using a common sense primer in the coding sequence of the final exon of all isoforms (exon 25 of RGS3hL; see Figure 1.11). Only one product was identified which extended to the length of the RGS3s 3' UTR, and no product corresponding to the length of the reported RGS3hs 3' UTR was identified. Because shorter templates are more highly favoured for amplification, and RGS3hs is definitely expressed (as determined by 5' RACE (Figure 3.2C,E) and *in situ* hybridisation (Figure 3.4)), these data suggest that the 3' UTR of RGS3hs is likely not truncated relative to RGS3s.

In the 3' UTR of RGS3L, immediately downstream of the reported extent of RGS3s, is an A-rich region (27/36 bp) which could have strong affinity to the oligo-dT primer used in reverse transcription. Thus the 3' RACE product, and the previously reported extent of the RGS3s 3' UTR, could have been generated from non-specific binding by the oligo-dT primer. Downstream of the A-rich region is a further 250 bp before a second, final A-rich region. To determine if RGS3s and RGS3hs contain this terminal 250 bp, I performed *in situ* hybridisation using an antisense probe which recognized this region (which I have termed '3' terminus'). I found that the staining of this probe extended

dorsally to include the placode and the migratory neural stream, as well as the vestibuloacoustic and trigeminal ganglia (which were not seen with RGS3L or RGS3s expression; Figure 3.4). Based on my later confirmation of the exclusive expression of RGS3L and RGS3s inside of the placode and neuroblast staging area (Figure 3.4), respectively, I concluded that the 3' UTR of RGS3hs-HTMKE extends to the terminus of RGS3L. The RGS3s and RGS3hs sequences, including extension of the 3' UTRs to this 250 bp region, have since been validated by the RefSeq database (accessions NM_001281935.1 and NM_001281937.1, respectively).

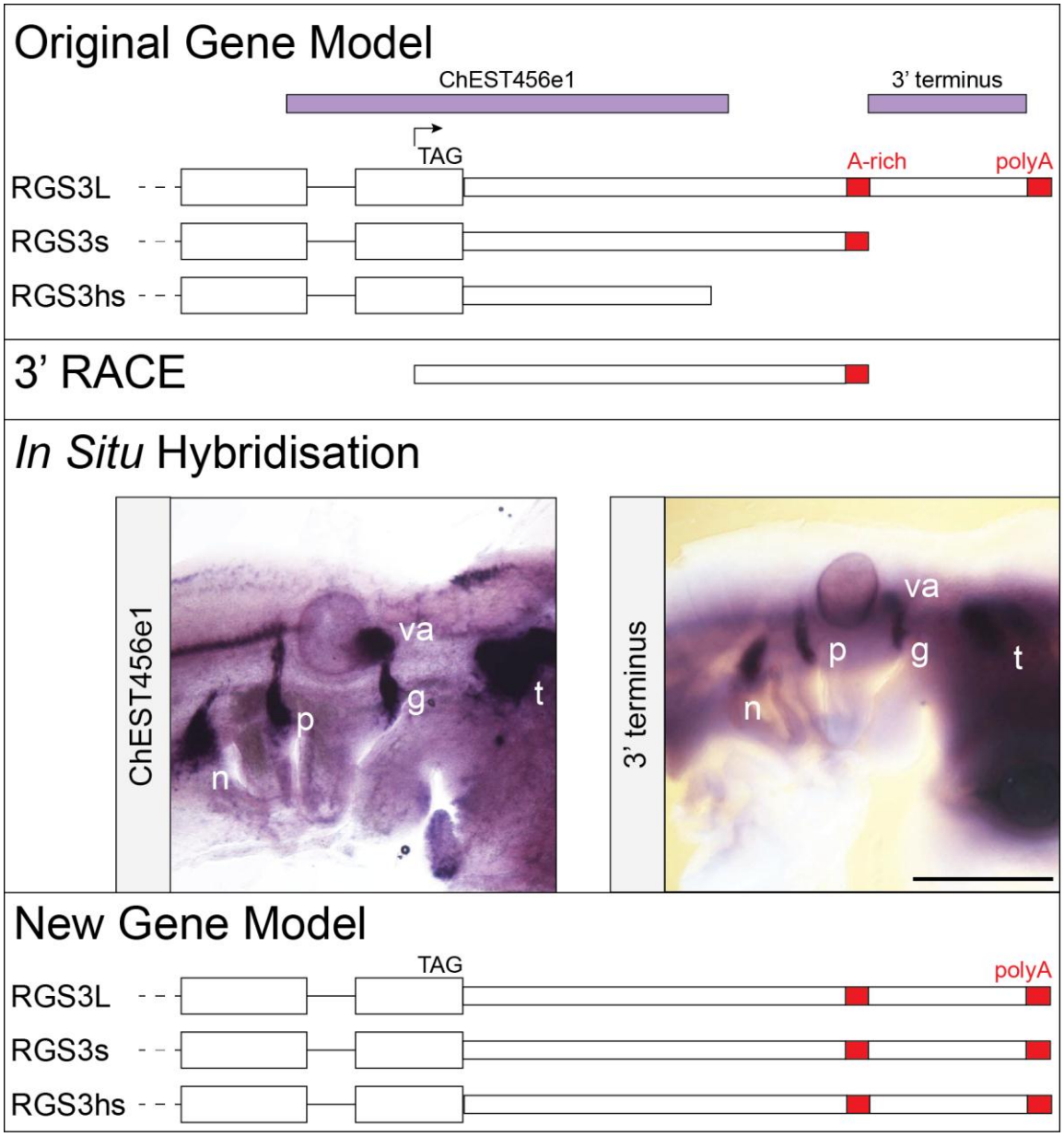


Figure 3.3. Resolution of the 3' Untranslated Regions of RGS3 Isoforms.
The original chicken RGS3 gene prediction showed shorter isoforms with truncated 3' UTRs relative to RGS3L. 3' RACE using the sense primer shown generated only one product which extended to the length of the original RGS3s prediction. This terminus is A-rich however, and could complement the oligo-dT primer used in amplification. To determine whether the extended 3' terminus of RGS3L is present on other isoforms, I designed an *in situ* hybridisation probe that would align to the 250bp downstream of the predicted RGS3s terminus. This probe stained identically to the probe which recognised all isoforms (ChEST456e1), confirming a new gene model in which all isoforms extend their 3' UTRs to the length of RGS3L. Scale: 500 µm.

Section 3.3 Spatiotemporally Co-Linear Expression of RGS3 Isoforms

Section 3.3.1 Qualitative Expression of RGS3 Isoforms in the Forming CSG

The transcription of C2PA, RGS3L, RGS3s, and RGS3hs-HTMKE from different promoters in human suggests that they may be subject to differential regulation and expression. To determine whether RGS3 isoforms are differentially expressed in the forming CSG, I turned to the petrosal placode and its neural derivatives, which is an ideal model to separate placodal progenitors, delaminated neuroblasts, and migratory neurons (Figure 1.7A). The expression of RGS3 in the forming CSG was previously identified in wholemount following microarray analysis (Section 1.2.1) using an EST-based probe which recognises RGS3hL, RGS3L, RGS3s, RGS3hs-HTMKE, and RGS3hs-KYLER (Figure 3.3; Figure 3.4I; henceforth referred to as ChEST456e1). To determine the whether this probe stained progenitors and neuroblasts in addition to neurons of the forming CSG, I performed *in situ* hybridisation using the ChEST456e1 probe on HH18 chick embryos, a stage of robust neurogenesis from the petrosal placode (Blentic et al., 2011). Analysis of transverse sections through the petrosal placode and migratory stream showed that the placode, neuroblast staging area, and neuronal migratory stream were all stained. This means that RGS3hL, RGS3L, RGS3s, RGS3hs-HTMKE, and/or RGS3hs-KYLER could be expressed in any or all of these areas. In addition, the RACE products identified in Section 3.2.2 (including C2PA) were amplified from tissue containing the petrosal placode as well as its neural derivatives. Together these data implicate the expression of any or all RGS3 isoforms in placodal progenitors, staging area neuroblasts, and/or migratory neurons of the forming petrosal ganglion.

To address which isoforms were expressed in which differentiation states of the forming petrosal ganglion, I designed *in situ* hybridisation probes that would uniquely identify each isoform (see Table 3.1).

Section 3.3.1.1 RGS3hL, C2PA and RGS3L

Analysis using probes for the unique sequences of RGS3hL, C2PA, and RGS3L all showed expression restricted to the epibranchial placodes (Figure 3.4 B,C,E, respectively). Consistently, this staining was seen with two probes recognising common sequences: one which recognised the shared coding sequences of RGS3hL and C2PA upstream of RGS3L (termed 'C2 domain'; Figure 3.4D and Table 3.1), and one which recognised the shared coding sequences of all three isoforms (termed 'PDZ'; Figure 3.4F and Table 3.1). In transverse sections, I found that staining with the PDZ probe was restricted to the placodal epithelium, and with no labelling of neuroblasts or migrating neurons (Figure 3.4J).

Section 3.3.1.2 RGS3s

Analysis using the unique probe for RGS3s showed expression was also restricted to the epibranchial placodes (Figure 3.4G). In transverse sections, however, this probe stained only the basal surface of the epithelium where neuroblasts delaminate from the placode, and the staging area where the neuroblasts reside (Figure 3.4K). Neurons which had left the staging area did not stain with this probe, suggesting the expression of RGS3s is highly specific to immature, committed neuroblasts. This staining was also seen with two other probes aligning to the first common coding exon of RGS3s (RGS3hL exon 20), recognising RGS3hL, RGS3L, and RGS3s (exon20a and exon20b; Figure 3.4N and O, respectively; see Table 3.1). Analysis of transverse sections of embryos stained with

either of these probes showed staining in the placode (as expected according to RGS3hL and RGS3L expression, above) as well as the neuroblast staging area, but not the migratory neurons (not shown).

Section 3.3.1.3 RGS3hs-HTMKE

Unlike the other isoforms, the staining from the RGS3hs-HTMKE probe (Figure 3.4H) was not unique to the epibranchial placodes. I also observed staining in the neurons of the trigeminal and vestibuloacoustic. Analysis of transverse sections showed that, like the RGS3s probe, the RGS3hs-HTMKE probe stained the neuroblast staging area. Unlike RGS3s however, staining was excluded from the placode, suggesting that the isoform is expressed in neuroblasts later than RGS3s. This staining was partially obscured by mesenchyme of the pharyngeal arches that were also labelled. However, the differentiated neurons leaving the staging area were detectable, though staining was less enriched in the migratory stream than in the staging area. Furthermore, development of this stain for a shorter exposure time (pictured in Figure 3.4L) labelled outside of the placode and the migratory stream, but not the pharyngeal arches, confirming that staining outside of the placode corresponded to the neuroblast staging area.

Section 3.3.1.4 RGS3hs-KYLER

I was unable to design a probe specific to RGS3hs-KYLER because its 5' exon is too short for *in situ* detection (61 bp). Instead, I compared the staining pattern from the RGS3hs-HTMKE probe to that of the ChEST456e1 probe, which recognised RGS3hs-HTMKE as well as RGS3hs-KYLER, RGS3hL, RGS3L and RGS3s (see Table 3.1). As expected from the above *in situ* stainings and as mentioned in Section 3.3.1, this probe stained the placode, neuroblast staging area, and neurons (Figure 3.4I,M). However,

unlike the RGS3hs-HTMKE probe, this probe was equally enriched between the neuroblast staging area and the migratory stream (Figure 3.4M). A similar wholemount pattern was seen with two probes aligning to the same set of transcripts: one recognising the common coding sequence of both RGS3hs isoforms (termed the 'RGS domain' probe; Figure 3.4P, see Table 3.1); and the 3' terminus probe previously used to assemble the gene model for the 3' UTRs (Figure 3.3 and Figure 3.4P,Q). Together this suggests the staining in the migratory stream was due to RGS3hs-KYLER in addition to RGS3hs-HTMKE expression.

Table 3.1. *In Situ* Hybridisation Probes and Positions on the Chicken RGS3 Locus

Probe Name	Exons Aligned	Isoforms Recognised	Figure 3.4 Wholemount Image
RGS3hL	RGS3hL e1-3	RGS3hL only	B
C2PA	C2PA unique	C2PA only	C
C2 domain	RGS3hL e4-10	RGS3hL, C2PA	D
RGS3L	RGS3L unique	RGS3L only	E
PDZ	RGS3hL e13-19	RGS3hL, C2PA, RGS3L	F; section: J
RGS3s	RGS3s unique	RGS3s only	G; section: K
exon20a	RGS3hL e20	RGS3hL, RGS3L, RGS3s	N
exon20b	RGS3hL e20-21	RGS3hL, RGS3L, RGS3s	O
RGS3hs-HTMKE	RGS3hs-HTMKE unique	RGS3hs-HTMKE only	H; section: L
RGS domain	RGS3hL e22-25	RGS3hL, RGS3L, RGS3s, RGS3hs-HTMKE, RGS3hs-KYLER	P
ChEST456e1	RGS3hL e24-25	RGS3hL, RGS3L, RGS3s, RGS3hs-HTMKE, RGS3hs-KYLER	I; section: M
3' terminus	RGS3hL e25	RGS3hL, RGS3L, RGS3s, RGS3hs-HTMKE, RGS3hs-KYLER	Q

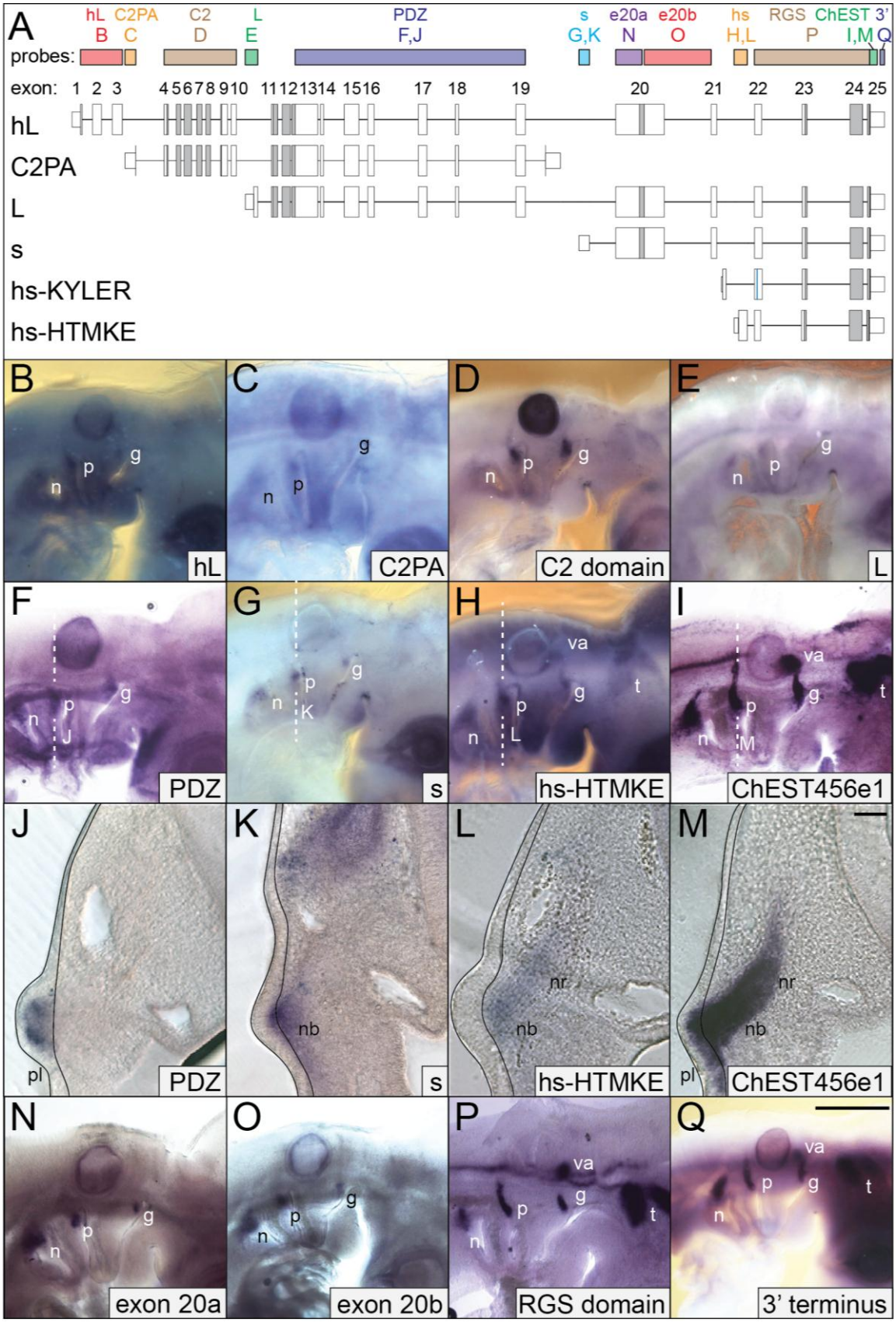


Figure 3.4. Expression of RGS3 Isoforms in the Forming CSG.
Figure legend on next page.

Figure 3.4. Expression of RGS3 Isoforms in the Forming CSG.
Wholemount embryos *(B-M)* were used to perform *in situ* hybridisation with the probes aligning to the RGS3 locus in *(A)*. Staining associated with the geniculate (g), petrosal (p) and nodose (n) placodes was observed for all probes in *(B-I)*. In addition, the trigeminal (t) and vestibuloacoustic (va) ganglia were labelled by probes in *(J-M)*. *(N-Q)* Transverse sections of embryos in *(F)*, *(G)*, *(J)*, and *(L)*, respectively, at the axial level of the petrosal placode showed sequential expression of RGS3 isoforms. Black lines indicate outlines of surface ectoderm, including the thickened placode. RGS3hL, C2PA and RGS3L probes all stained the placode (pl) exclusively *(O)*. The RGS3s probe stained neuroblasts (nb) at the basal surface of the placode and in the staging area. The RGS3hs-HTMKE probe labelled neuroblasts in the staging area (but not at the basal surface of the placode) and post-mitotic neurons (nr). The probe aligning to RGS3hL, RGS3L, RGS3s, RGS3hs-HTMKE, and RGS3-KYLER showed robust staining in the placode (pl), neuroblasts (nb), and neurons (nr). $n \geq 3$ embryos for each probe. Scale bar in *(M)*: 50 µm. Scale bar in *(Q)*: 500 µm.

Section 3.3.2 Quantitative Expression in Mature CSG

To confirm the presence of RGS3hs-KYLER expression in CSG neurons and its abundance relative to RGS3hs-HTMKE, I asked Dr Patthey to examine a dataset he previously generated. Dr Patthey had dissected CSG in an effort to profile the transcriptomes of each ganglion. Because rostral ganglia develop prior to caudal ganglia, these were dissected at different developmental stages. Trigeminal ophthalmic, trigeminal maxillomandibular, and vestibuloacoustic ganglia were dissected from HH18 chick embryos; and petrosal and nodose ganglia were dissected from HH23 chick embryos. Due to technical constraints, the geniculate ganglion was not dissected. Neurons were labelled with an antibody against the neuronal intermediate filament NFM (see Section 1.1.6.2.2) and purified using fluorescence activated cell sorting (FACS). mRNA was then extracted from these cells and reverse transcribed, and triplicate samples were sent for whole-transcriptome sequencing.

Dr Patthey aligned sequencing reads to unique 5' exons of each RGS3 isoform using BLAST. RGS3hL, C2PA, RGS3L, and RGS3s were all expressed at basal levels in all ganglia, consistent with the absence of *in situ* hybridisation staining in placode-derived neurons (not shown). By contrast, RGS3hs-HTMKE and RGS3hs-KYLER were

enriched to levels comparable to the post-mitotic neural marker HuD (Figure 3.5). These levels were not enriched in the viscerosensory petrosal or nodose ganglia compared to the somatosensory trigeminal ophthalmic, trigeminal maxillomandibular, or vestibuloacoustic (VA) ganglia, indicating there was not a visceral versus somatic identity of these isoforms.

The sequencing reads for trigeminal and vestibuloacoustic ganglia are from HH18 embryos (the same stage at which *in situ* hybridisation staining was conducted), so the expression levels in Figure 3.5 directly relate to staining seen in Figure 3.4 (Section 3.3.1). For the petrosal and nodose ganglia to be at a comparable stage of development, they were dissected at HH23. Therefore it cannot be ruled out that HH23 ganglia have different relative levels of RGS3hs-KYLER and RGS3hs-HTMKE compared to HH18 ganglia, and these levels do not complement the *in situ* hybridisation data *per se*. However, considering that RGS3hs-KYLER and RGS3hs-HTMKE stain with similar intensity in all ganglia at HH18 (Figure 3.4H,I,L,M,P,Q), they are likely to be at comparable levels in all cranial sensory placode-derived neurons at all stages.

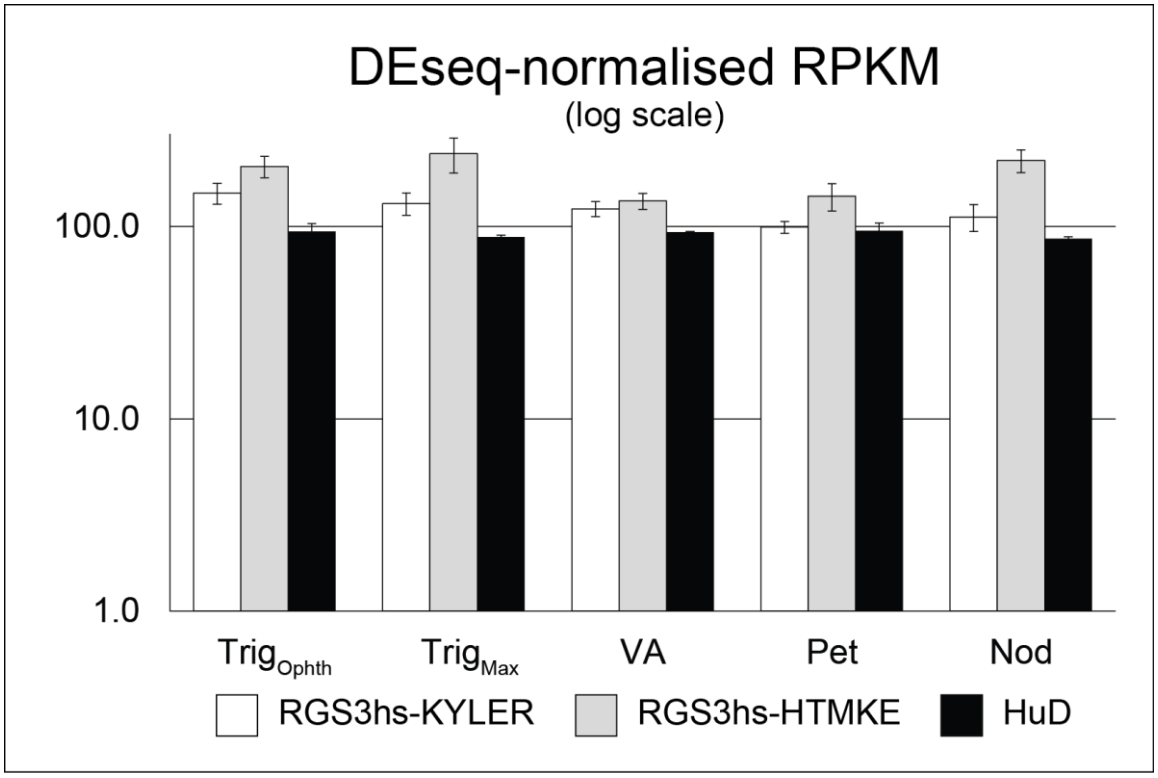


Figure 3.5. Quantitative Expression of RGS3 Isoforms in Mature CSG.
Transcriptome sequencing reads per kilobase pair per million reads (RPKM) were DEseq-normalised and averaged across triplicate samples of each ganglion. RGS3hs-KYLER and RGS3hs-HTMKE were found to be abundant in these samples, comparable to that of post-mitotic marker HuD. However, neither isoform was enriched relative to the other, and all ganglia had similar levels of reads, suggesting that these isoforms do not relate to a visceral versus somatic identity. Note: trigeminal ophthalmic ($Trig_{Ophth}$), trigeminal maxillomandibular ($Trig_{Max}$), and vestibuloacoustic (VA) ganglia were extracted from HH18 embryos, while petrosal (Pet) and nodose (Nod) ganglia were extracted from HH23 embryos.

Section 3.3.3 Expression of RGS3hL and/or C2PA in Pre-Placodal Cells

The RGS3L expression I observed in the placodal epithelium would be consistent with its playing a role like that previously demonstrated in the maintenance of cortical neuroepithelial progenitors (Qiu et al., 2010). However, a developmental role of RGS3hL and C2PA has not been investigated. In staining embryos with the C2 domain probe (Figure 3.4D; Table 3.1), which aligns to RGS3hL and C2PA, I observed a strong expression in the epibranchial placodes of HH15 embryos (Figure 3.6C). At this stage, neurogenesis in the petrosal and nodose placodes is in its infancy (Blentic et al., 2011). I hypothesised that this staining might relate to an early role of RGS3hL and/or C2PA in placode organisation, prior to the onset of neurogenesis. To investigate this, I carried out *in situ* hybridisation with the C2 domain probe on HH11-13 embryos, a stage at which the epibranchial pre-placodal domain has separated from the otic pre-placodal domain, but individual placodes have yet to initiate neurogenesis (Freter et al., 2013; Ladher et al., 2010).

In younger embryos (HH11-12^{-}), I observed staining on the lateral surface ectoderm, rostral to the otic vesicle (Figure 3.6A). In older embryos (HH12-13), I observed staining in this position as well a domain of lateral surface ectoderm caudal to the otic vesicle, near the cleft between the second and third pharyngeal arches (Figure 3.6B). Intriguingly, this staining resembles that of pro-epibranchial markers Sox3 (Ishii et al., 2001) and Pax2 (Groves and Bronner-Fraser, 2000; Ladher et al., 2010). Fate-mapping studies of cells in this region confirm that they give rise to the epibranchial placodes (Ishii et al., 2001). In addition, the invaginating otic vesicle was seen to be stained, characteristic of Pax2 but not Sox3 expression. Staining was also observed in the rostral forebrain and the isthmus of the midbrain/hindbrain boundary (Figure 3.6A,B), which

will be elaborated upon in Section 3.5. By HH15, when the petrosal and geniculate placodes are specified and neurogenic, robust staining was observed (Figure 3.6C). At this stage staining was additionally seen in the floorplate of the forebrain and the olfactory placodes (Figure 3.6C; elaborated in Section 3.5). Collectively, these data show an early expression of RGS3hL and/or C2PA in the pro-epibranchial and pro-otic ectodermal domains, suggesting an early role in the organisation of these placodes.

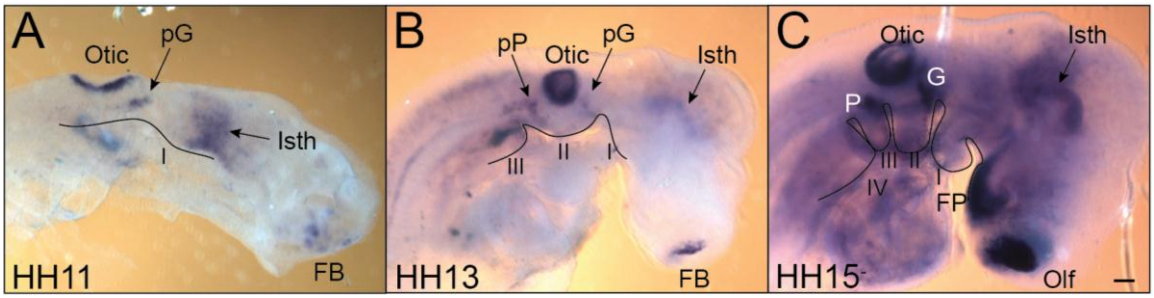


Figure 3.6. Expression of RGS3hL/C2PA in Pre-Placodal Regions.
HH11-13 embryos were *in situ* hybridised with a probe which recognised the shared coding sequence between RGS3hL and C2PA (n=4). In younger embryos *(A)*, staining could be seen in the invaginating otic placode, the isthmus (Isth), and the rostral forebrain (FB). In addition, a staining pattern rostral to the otic placode which resembled cells fated to form the geniculate placode (pG) (Ishii et al., 2001). In older embryos *(B)*, staining which resembled pre-petrosal (pP) areas was also seen. It was not clear whether staining on the third arch was ectodermal (corresponding to a pre-nodose area) or from underlying tissue. By HH15-16 (n=4), staining could be seen in the geniculate (G) and petrosal (P) placodes, stereotypically crowning pharyngeal arches II and III. In addition, these embryos displayed robust staining in the olfactory placode (Olf) and the floorplate (FP) of the forebrain. Rostral forebrain staining in *(C)* is underneath the plane of view. Scale bar in *(C)*: 100 µm.

Section 3.4 Conservation of Expression of RGS3 Isoforms

Section 3.4.1 Expression in the Developing Mouse CSG

To investigate the conservation of differential isoform expression across species, I designed three probes: one which would recognise the unique exon of RGS3hs-HTMKE (referred to as the 'Musm-hs' probe; Figure 3.7D,H; Table 3.2); one which would recognise the unique exon of RGS3s (referred to as the 'Musm-s' probe; Figure 3.7C,G; Table 3.2); and one which would recognise the shared coding sequence of RGS3hL, C2PA, and RGS3L (referred to as the 'Musm-PDZ' probe; Figure 3.7B,F; Table 3.2), homologous to the PDZ probe I used in the chick (Figure 3.4F,J; Table 3.1). Probes were cloned from RNA extracted from the hindbrain region of E9.5 mouse embryos (provided by Elizabeth Robertson, University of Oxford). I carried out *in situ* hybridisation with these probes on E9.5 mouse embryos (provided by Elizabeth Robertson).

Section 3.4.1.1 RGS3hL, C2PA and RGS3L

As in chick, the staining I observed with the PDZ probe was only associated with the epibranchial placodes and no other cranial sensory placodes (n=3; Figure 3.7B). In transverse sections, I found this staining enriched in the placodal epithelium, consistent with the observations in chick embryos (Figure 3.7F; see Figure 3.4F,J).

Section 3.4.1.2 RGS3s

As in the chick embryo, the RGS3s stain was specific to the epibranchial placodes (Figure 3.7C; n=4). However, contrary to the exclusive staining of the neuroblast staging area observed in the chick (Figure 3.4K), transverse sections showed RGS3s staining in mouse embryos to be absent from the staging area and present in the migratory stream (Figure 3.7G). This staining was consistent with two probes I generated: one which

recognised the coding sequence common to RGS3hL, RGS3L and RGS3s (referred to as 'Musm-e20'; see Figure 3.7A and Table 3.2); and one which recognised the shared coding sequence of RGS3hL, RGS3L, RGS3s and RGS3hs-HTMKE (referred to as 'Musm-RGS'; see Figure 3.7A and Table 3.2). With these probes, staining was seen in forming ganglia some distance from the placode (n=3 for both; staining not shown), as seen with the RGS3s probe. Stain development was stopped on these embryos after a similar length of exposure to that of the RGS3s probe, which was considerably shorter to that of RGS3hs-HTMKE or RGS3hL/C2PA/L (approximately six hours compared to 144 hours with RGS3hL/C2PA/L and 53 hours with RGS3hs-HTMKE), suggesting that this stain corresponded to RGS3s expression.

Section 3.4.1.3 RGS3hs-HTMKE

Like in chick embryos, staining with the RGS3hs-HTMKE probe appeared to label mesenchyme of the pharyngeal arches around and ventral to the placode. In addition, staining appeared in the dorsal mesenchyme adjacent to rhombdomeres 4-6 of the hindbrain. However, no staining was detected in the placodes, neuroblasts or neurons of any of the cranial sensory ganglia.

Section 3.4.1.4 RGS4

Together these data suggest conservation of expression of RGS3hL, C2PA and/or RGS3L in the epibranchial placodes, but reveal important species differences in expression of RGS3s and RGS3hs-HTMKE. In the chick, RGS3s is expressed in the neuroblast staging area but downregulated in the differentiated migratory stream. In the mouse, the inverse is true. RGS3hs-HTMKE is enriched in neuroblasts in the chick but is expressed in the differentiated migratory stream. In the mouse, RGS3hs-HTMKE

expression was not detected in any placodal derivatives. These findings are summarised in Figure 3.10.

In light of these differences, it is interesting that eutherian mammals including mouse do not possess an RGS3hs-KYLER isoform (see Section 3.2.2). Intriguingly, RGS4, a fellow R4 subfamily member, is expressed in the forming mouse CSG (Grillet et al., 2003; Grillet et al., 2005). RGS4 is encoded by five exons. The aa sequence encoded by the latter four exons is highly homologous to the final four exons of all RGS3 isoforms. The aa sequence encoded by the first exon is highly similar to that of RGS3hs-KYLER across evolution (see Figure 5.5B). This suggests that RGS4 and RGS3hs-KYLER might share a common ancestral origin (see Section 5.2.3), and that RGS4 expression in the mouse might replace a requirement for RGS3hs-KYLER. To test this hypothesis, I designed and cloned an RGS4 probe and carried out *in situ* hybridisation on E9.5 embryos (23-27 somites; n=4). Like the probes recognising all isoforms in chick embryos (Figure 3.4I,M,P,Q), the RGS4 stain developed quickly and with an extremely low background (Figure 3.7E). In transverse sections, RGS4 was seen to label the migratory stream and the neuroblast staging area. This suggests that RGS4 expression in the forming CSG (and potentially other developing tissues) relieved selective pressure during mammalian evolution to retain RGS3hs-KYLER. If this is true, it would suggest that the inverse is true in developing birds: the presence of RGS3hs-KYLER in the forming CSG and other tissues would replace the requirement for RGS4 expression. To test this, I cloned two probes recognising the coding sequence and the 3' UTR of chicken RGS4, and carried out *in situ* hybridisation with them on HH16 and HH18 embryos. At either stage, and with either probe, no staining was detected in the forming CSG. However, staining was observed in the dorsal NCC adjacent to rhomdomere 2 of the

hindbrain, demonstrating that the probes were capable of detecting endogenous transcripts (not shown).

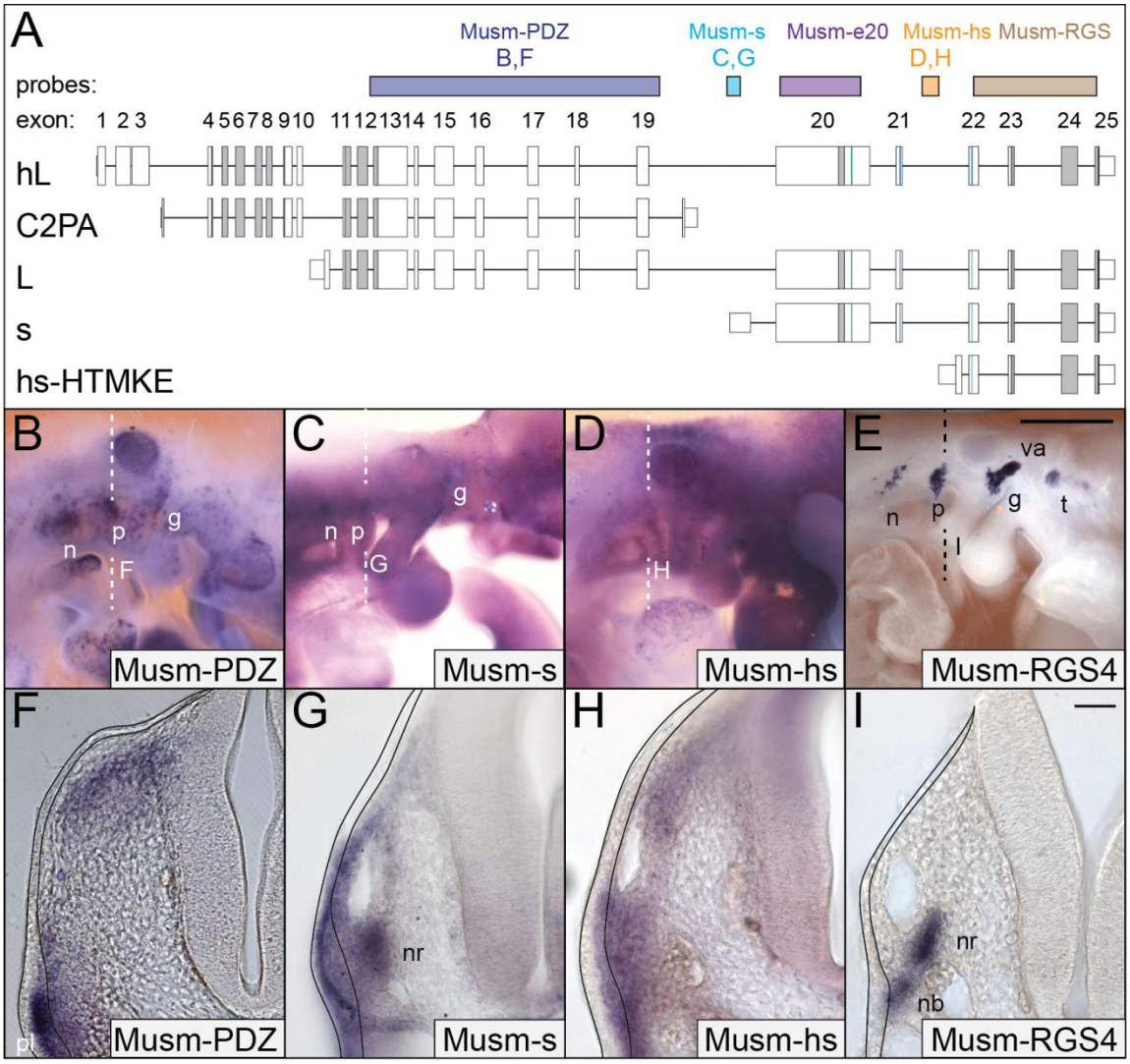


Figure 3.7. Expression of RGS3 Isoforms and RGS4 in the Developing Mouse CSG.
(A) The mouse RGS3 locus, showing its five isoforms (mice lack an RGS3hs-KYLER isoform) and corresponding *in situ* hybridisation probes. Two probes overlapping coding sequences of RGS3hL, RGS3L, and RGS3s, and RGS3hL, RGS3L, RGS3s, and RGS3hs-HTMKE, respectively, are shown but the stained embryos are not pictured (see text). The probe specific to RGS3hL, C2PA, and RGS3L *(B)* labelled the nodose (n), petrosal (p) and geniculate (g) placodes. In transverse sections *(F)*, it was seen to be enriched in the placodal (pl) epithelium. The probe specific to RGS3s *(C)* labelled ganglia associated with the epibranchial placodes. In transverse sections *(G)*, staining enriched in the post-mitotic neurons (nr) could be seen. Note: the full apico-basal width of the placode in this section extends in a different focal plane, and epithelial outlines (black lines) are drawn to accommodate this width. Cranial sensory placodes or their derivatives were not labelled by the RGS3hs-HTMKE probe, either in wholemount *(D)* or in transverse sections *(H)*. The probe specific to RGS4 labelled the epibranchial ganglia as well as the vestibuloacoustic (va) and trigeminal (t) ganglia *(E)*. In transverse sections *(I)*, this staining localised to neuroblasts (nb) and neurons. Scale bar in *(E)*: 500 µm. Scale bar in *(I)*: 50 µm.

Section 3.4.2 The Forming Mouse Cerebral Cortex

I next investigated whether differential expression of RGS3 isoforms is conserved across other neural tissues. The developing mouse cerebral cortex served as an apt model, given its spatial separation of VZ progenitors, SVZ neuroblasts and CP neurons and its parallels with placodal neurogenesis (see Section 1.1.7.5). A probe which aligned to RGS3hL, C2PA and RGS3L was previously shown to label the VZ of E16.5 mice (Lu et al., 2001), consistent with the later-demonstrated role of RGS3L in cortical neurogenesis (Qiu et al., 2010). Expression patterns of RGS3s and RGS3hs-HTMKE, however, have not been investigated.

I collaborated with Dr Peter Oliver (Department of Physiology, Anatomy and Genetics, University of Oxford), who carried out *in situ* hybridisation on coronal and sagittal sections of E15.5 mouse embryos. The Musm-PDZ, Musm-s, and Musm-hs probes (Figure 3.8A and Table 3.2) which I had previously designed and cloned were used (Section 3.4.1). Consistent with previous reports (Lu et al., 2001) and labelling of the placodes of chick and mouse embryos, staining with the PDZ probe was highly specific to the VZ (Figure 3.8C).

The Musm-s probe did not show specific staining in the VZ or SVZ, but there was a clear signal in the CP (Figure 3.8D).

The Musm-hs probe did not label any layer of the cortex (Figure 3.8E), but it did label ectomesenchymal derivatives in the head, showing that it was capable of detecting endogenous transcripts (not shown).

Finally, Dr Oliver carried out *in situ* hybridisation using the Musm-RGS4 probe which I had previously designed and cloned. This probe was examined on the forming mouse

CSG to determine if the loss of RGS3hs-KYLER from the eutherian mammalian genome had been replaced by expression of RGS4, which encodes a similar amino acid sequence (Section 3.4.1.4). Similar to the labelling of CSG neurons seen in E9.5 embryos (Figure 3.7E,I), the Musm-RGS4 probe labelled the CP with extremely low background in other layers (Figure 3.8F).

Taken together, these stains reflect the findings in the developing mouse CSG. This suggests that the same RGS3/RGS4 transcriptional differentiation programme employed in the mouse CSG is also employed in the mouse cortex. Interestingly, a different programme is employed in the chick CSG. These findings are summarised in Figure 3.10. The significance of this observation in terms of transcriptional regulation of the RGS3 locus will be discussed in Section 3.6. Lastly, these data provide an interesting insight into the developmental relationship between RGS3hs-KYLER and RGS4 in evolution, and this will also be elaborated upon in Section 3.6.

Table 3.2. *In Situ* Hybridisation Probes and Positions on the Mouse RGS3 Locus.

Probe Name	Exons Aligned	Isoforms Recognised	Figure 3.7 Wholemount Image
Musm-PDZ	RGS3hL e13-19	RGS3hL, C2PA, RGS3L	B; section: F
Musm-s	RGS3s unique	RGS3s	C; section: G
Musm-e20	RGS3hL e20	RGS3hL, RGS3L, RGS3s	Not shown
Musm-hs	RGS3hs-HTMKE unique	RGS3hs-HTMKE	D; section: H
Musm-RGS	RGS3hL e22-25	RGS3hL, RGS3L, RGS3s, RGS3hs-HTMKE	Not shown

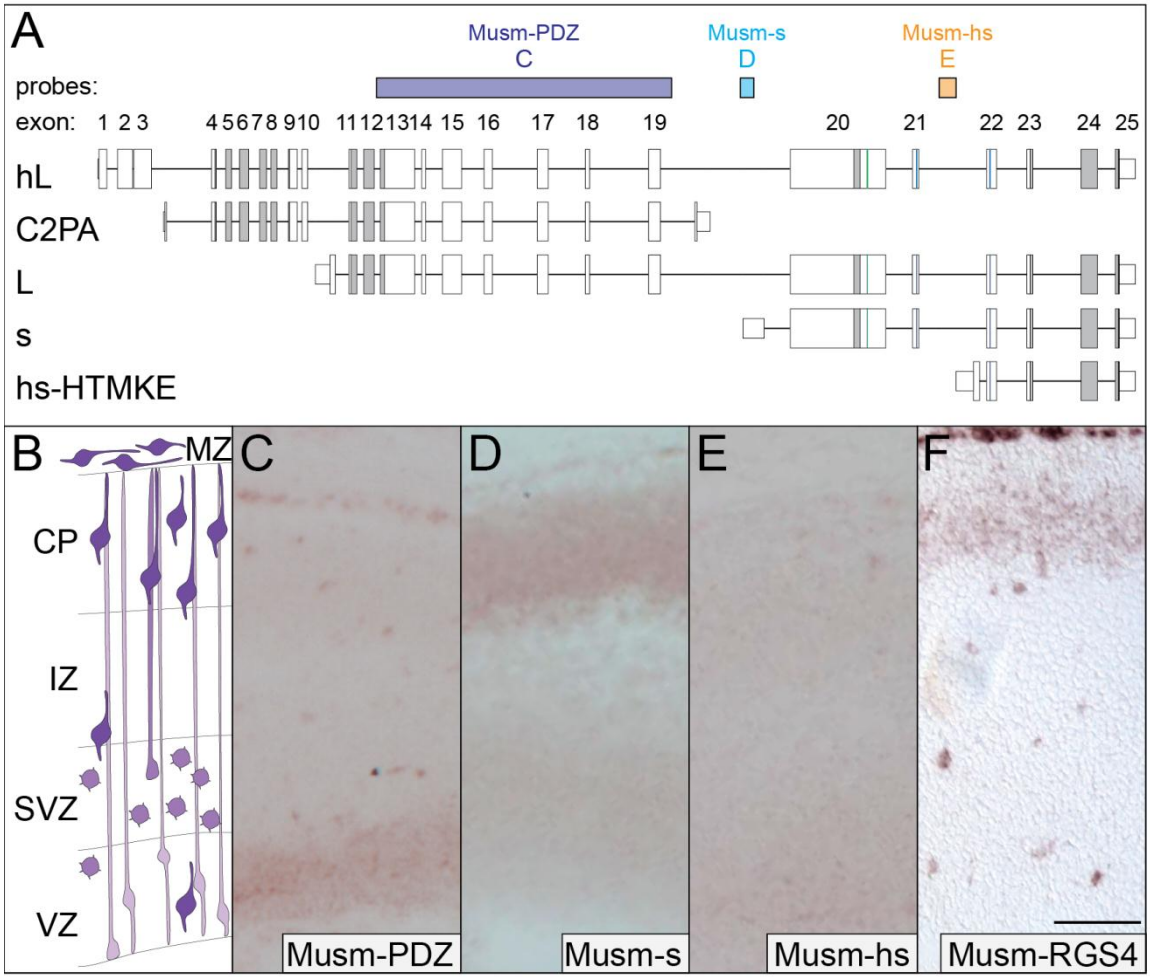


Figure 3.8. Expression of RGS3 Isoforms and RGS4 in the Developing Mouse Cortex.
(A) The mouse RGS3 locus, showing its five isoforms (mice lack an RGS3hs-KYLER isoform) and corresponding *in situ* hybridisation probes. *(B)* Schematic representation of a coronal section of the developing cerebral cortex, with radial glia (light purple), intermediate progenitors (purple), and post-mitotic neurons (dark purple) shown amongst the four layers: ventricular zone (VZ), subventricular zone (SVZ), intermediate zone (IZ), and cortical plate (CP). *(C-F)* Coronal sections of E15.5 mouse embryos *in situ* hybridised with Musm-PDZ *(C)*, Musm-s *(D)*, Musm-hs (*E)*, and Musm-RGS4 *(F)*. Musm-PDZ staining was enriched in the VZ, and Musm-s staining was enriched in the CP. Musm-hs staining was not seen in any layers. Musm-RGS4 staining was enriched in the CP, with extremely low background in other layers. In addition, Musm-RGS4 staining was seen in neurons of the mantle zone (MZ). Scale bar in *(F)*: 50 µm.

Section 3.5 Differential RGS3 Isoform Expression in Other Neural Tissues

In the above investigations of differential isoform expression in the forming CSG and cortex (Section 3.3.1, Section 3.4.1, and Section 3.4.2), I also observed differential isoform expression in other neural tissues.

Section 3.5.1.1 RGS3hL, C2PA, and RGS3L

As mentioned, RGS3hL, C2PA, and RGS3L expression in HH18 embryos was seen in the epibranchial placodes. The PDZ probe, recognising RGS3hL, C2PA, and RGS3L (Figure 3.4A; Table 3.1), also strongly stained the otic vesicle (Figure 3.4F). This was initially considered to be artefactual trapping of stain, since the stain was not specific to any region of the otic epithelium (for example, the neurogenic anterior portion which gives rise to vestibuloacoustic neurons; see Section 1.1.4.2.2). However, considering the very specific staining of the C2 domain probe (which recognised RGS3hL and C2PA; Figure 3.4A; Table 3.1) early in otic placode induction (Section 3.3.3; Figure 3.6A,B), it seems likely that this stain reflected real expression of RGS3hL and/or C2PA.

Outside of the cranial sensory placodes, the PDZ probe also showed expression in the olfactory placode. This staining was seen as early as HH15 (seen with the C2 domain probe in Figure 3.6C), a stage at which the olfactory placodes are newly specified and neurogenic, but have yet to invaginate (Bhattacharyya and Bronner-Fraser, 2008; Fornaro et al., 2001). Whether this expression is specific to neural progenitors is unclear however, since post-mitotic olfactory neurons reside in the epithelium as well as progenitors (see Section 1.1.4.1). This probe was lastly seen in two domains of the forebrain. It strongly stained the floor plate of the rostral diencephalon (seen with the C2 domain probe in Figure 3.6C), a region of critical importance in patterning the

dorsoventral axis of the CNS during development (Placzek and Briscoe, 2005). In addition, the PDZ probe appeared to label the rostral end of the anterior neural ridge (seen with the C2 domain probe in Figure 3.6A,B), a region important for patterning the forebrain (Wilson and Houart, 2004).

The C2 domain probe stained all of the same structures as the PDZ probe, suggesting that expression of RGS3hL and/or C2PA are responsible for the staining outside the epibranchial placodes. Furthermore, all of these structures were labelled with the ChEST456e1, RGS domain, or 3' terminus probes which recognised all variants except C2PA (Figure 3.9A; see Figure 3.4A and Table 3.1), suggesting that RGS3hL expression is responsible for this labelling. In HH11-13 chick embryos, the RGS3hL/C2PA probe also labelled the midbrain/hindbrain boundary. This region, called the isthmus, functions as an FGF-secreting organiser to specify midbrain versus hindbrain identity (Nakamura et al., 2005). The signal-to-noise ratio of the individual RGS3hL, C2PA, or RGS3L isoform *in situ* hybridisations was too low to detect expression outside of the epibranchial placodes, so it is unclear which (if not all) of these isoforms are expressed in non-epibranchial structures. However, it is notable that staining with any probes recognising RGS3hL, C2PA, or RGS3L, in the chick or mouse embryos, was specific to tissues fated or specified as neuroepithelia.

Section 3.5.1.2 RGS3s

The RGS3s probe was remarkably specific to neuroblasts from the epibranchial placodes, and was not seen anywhere else in chick or mouse embryos (Section 3.3.1.2, Section 3.4.1.2, and Section 3.4.2).

Section 3.5.1.3 RGS3hs-HTMKE

As mentioned (Section 3.3.1), the RGS3hs-HTMKE probe labelled neuroblasts and neurons of the epibranchial as well as vestibuloacoustic and trigeminal CSG of chick embryos, but did not label any other neural populations. In mouse embryos, no neural populations were labelled at E9.5 or E15.5 (Section 3.4.1.3 and Section 3.4.2).

Section 3.5.1.4 RGS3hs-KYLER

RGS3hs-KYLER is not present in the mouse genome, and its unique exon in the chicken is too short for detection with *in situ* hybridisation. Because the only other isoform-specific probes did not label any neurons outside the CSG, I inferred that any staining outside the CSG with the ChEST456e1, RGS domain, or 3' terminus probes, which recognised all variants except C2PA (see Figure 3.4A and Table 3.1), was attributed to RGS3hs-KYLER expression.

In addition to the CSG, these probes labelled other sensory neuron populations (Figure 3.9A). Expression was found in the DRG of the trunk and the mesencephalic trigeminal nucleus, a collection of midbrain primary sensory cell bodies that associate with the trigeminal nerve and relay proprioceptive sensations (Lazarov, 2007).

Finally, these probes also labelled non-sensory neuronal populations. They labelled the motor neurons of the ventral neural tube of the rostral spinal cord and hindbrain (Figure 3.9B,C). They also stained the rhombic lip, which generates deep cerebellar nuclei and cerebellar granule cells (Green et al., 2014) (Figure 3.9A).

Section 3.5.1.5 RGS4

RGS4 was not found in any neural populations in the chick at the stages examined. In E9.5 mouse embryos, RGS4 was seen in the CSG (Figure 3.7E,I), and weakly in some motor neurons of the hindbrain (not shown); however the development of this stain was stopped with low background, and it is possible that further development of the stain would label other populations. In sagittal sections of E15.5 mouse embryos, RGS4 was seen in the forming DRG (not shown), confirming previous investigations in E10.0 mouse embryos (Grillet et al., 2003; Grillet et al., 2005). RGS4 expression in these reports was also observed in the locus coeruleus, the main noradrenergic centre of the brain, as well as the motor neurons of the ventral neural tube, but these structures were not present in the plane of our sagittal sections, so we could not confirm these reports. Taken with the inferred expression of RGS3hs-KYLER from the previous section, these data suggest potentially very diverse roles of RGS3hs-KYLER in the chick, and RGS4 in the mouse, in different neuronal contexts.

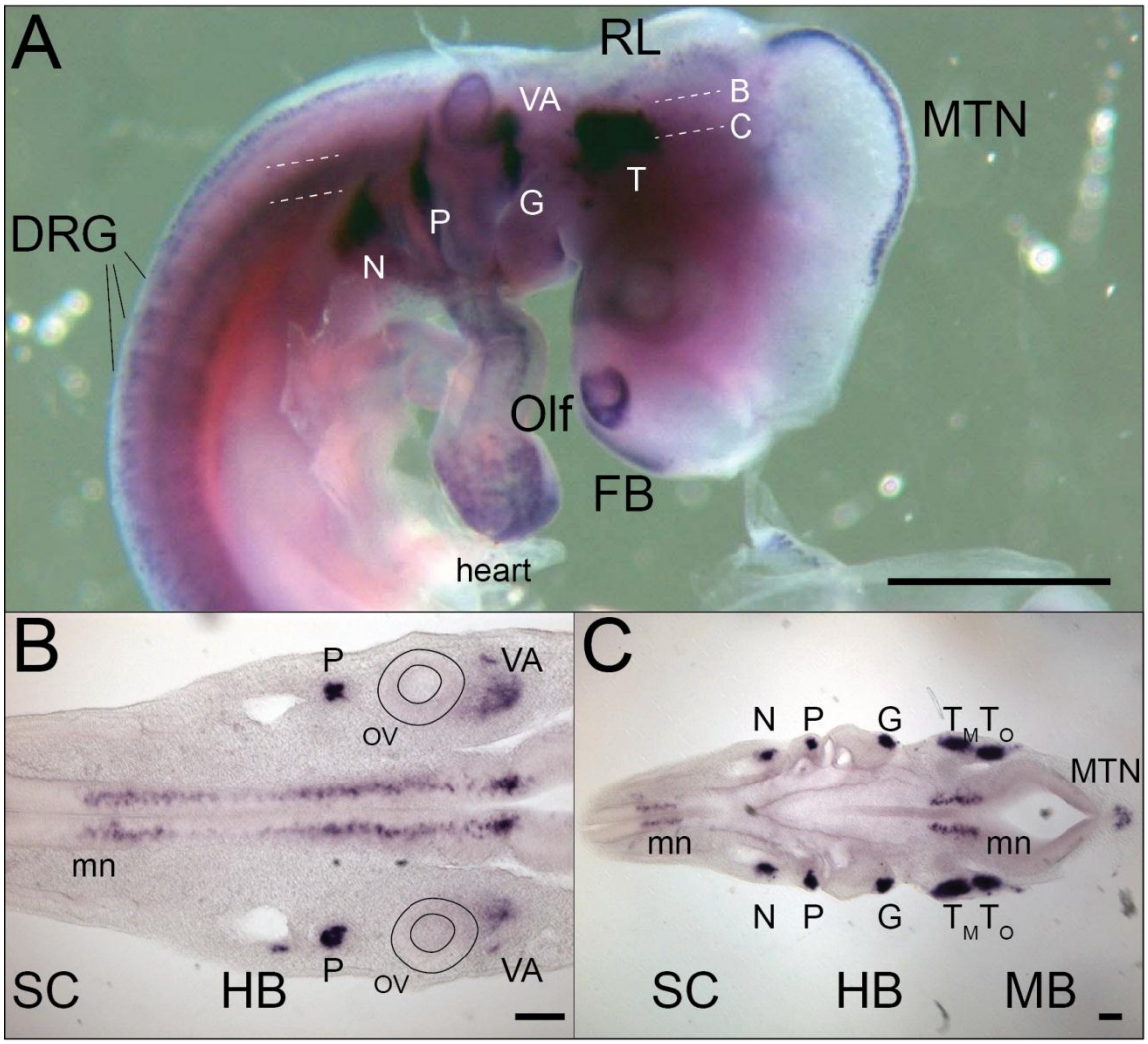


Figure 3.9. Expression of RGS3 Isoforms Outside of the CSG.
Head and rostral trunk of an HH18 chick embryo *in situ* hybridised with the ChEST456e1 probe, which recognised RGS3hL, RGS3L, RGS3s, and both RGS3hs isoforms (see Figure 3.4A and Table 3.1). *(A)* Olfactory (Olf), rostral forebrain (FB), and floor plate of the forebrain (underneath the field of view) expression were detected by this probe as well as the probe specific to RGS3hL and C2PA (the C2 domain probe; see Figure 3.4A and Table 3.1; Figure 3.6B,C), suggesting this staining relates to RGS3hL expression. The heart was detected by the PDZ probe (which recognised RGS3hL, C2PA, and RGS3L; see Figure 3.4A and Table 3.1) but not the C2 domain probe, suggesting that this staining relates to RGS3L expression. The RGS3hs-HTMKE probe (see Figure 3.4A and Table 3.1) stained all of the CSG, but had markedly weaker staining. In addition to strong staining in the CSG, this probe exhibited staining in the mesencephalic trigeminal nucleus (MTN), the rhombic lip (RL), and the dorsal root ganglia (DRG). *(B)* A coronal section through the dorsal CSG shows the petrosal (P) and vestibuloacoustic (VA) ganglia, caudal and rostral to the otic vesicle (OV), respectively. In addition, motor neurons (mn) of the ventral neural tube are labelled. *(C)* A more ventral coronal section shows the remainder of the CSG, as well as neurons of the MTN and motor neurons of the spinal cord (SC) and rostral hindbrain (HB). G: geniculate; MB: midbrain; N: nodose; T_M: trigeminal maxillomandibular; T_O: trigeminal ophthalmic. Scale bar in *(A)*: 500 µm. Scale bars in *(B,C)*: 100 µm.

Section 3.6 Discussion

Section 3.6.1 Differential Developmental Expression of RGS3 Isoforms in Chick and Mouse

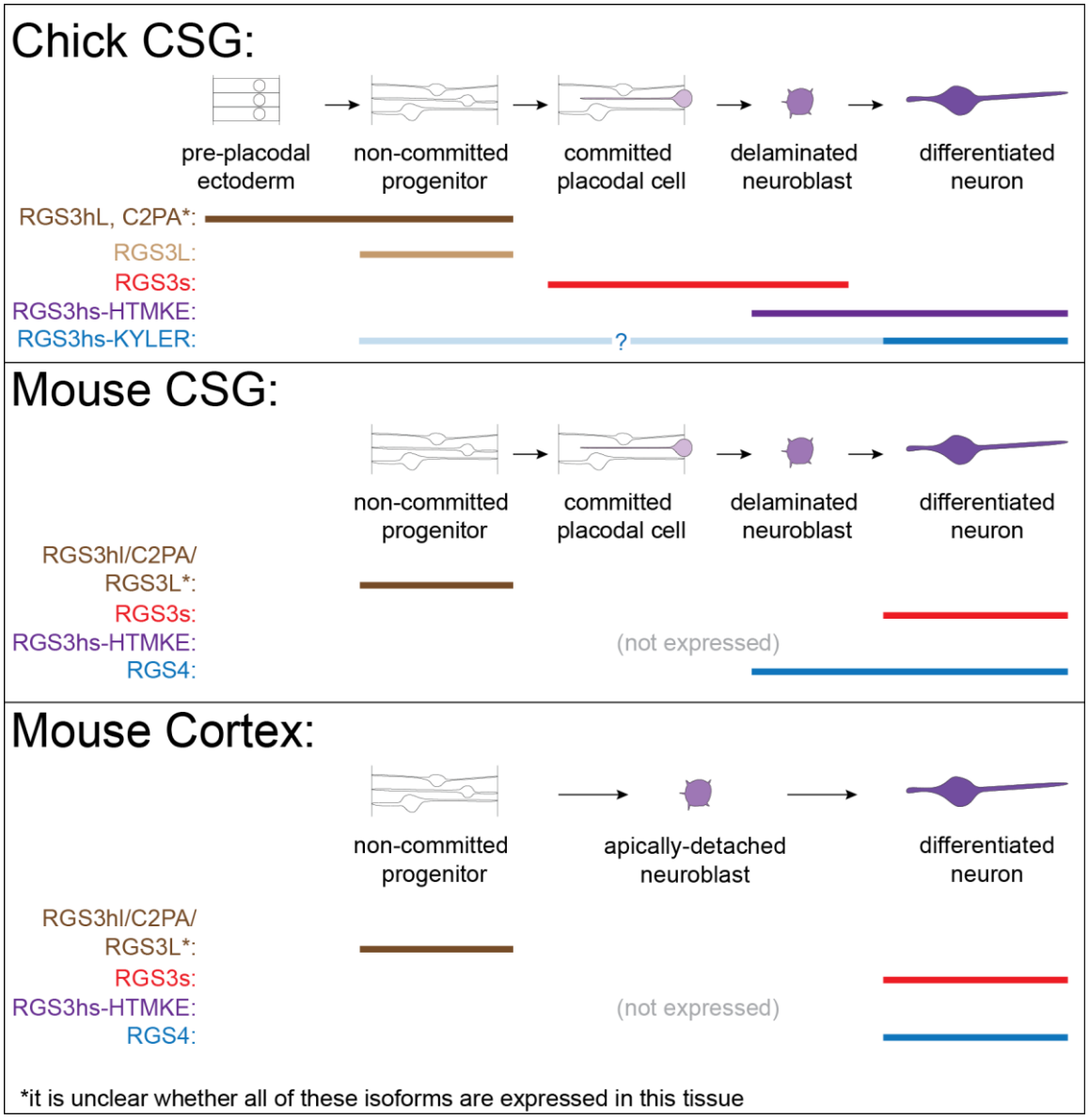


Figure 3.10. Summary of Expression of RGS3 Isoforms.
Figure legend on next page.

Figure 3.10. Summary of Expression of RGS3 Isoforms.
RGS3 isoforms are sequentially expressed in different vertebrate phyla and in different neuronal tissue. However, the patterns of expression are different between species. In the chick CSG, RGS3hL and/or C2PA are expressed in pre-placodal ectoderm (it is not known whether other isoforms are expressed here as well). In the placode, RGS3hL, C2PA, and RGS3L are all expressed. RGS3s is expressed in committed neuroblasts of the basal placode and staging area. RGS3hs-HTMKE is expressed in the staging area and differentiated neurons. It is unclear whether RGS3hs-KYLER is expressed in the placode or staging area, but it is expressed in differentiated neurons. In the mouse CSG, a probe recognising RGS3hL, C2PA and RGS3L labels the placodal epithelium as in chick. RGS3s is expressed in differentiated neurons. RGS3hs-HTMKE is not expressed, but RGS4, which is similar in amino acid sequence to RGS3hs-KYLER, is expressed in delaminated neuroblasts and differentiated neurons. A very similar expression pattern is observed in the mouse cortex, with the exception that RGS4 is not expressed in the SVZ (which houses neuroblasts) and is only seen in the CP.

Collectively, these data suggest temporal sequential expression of RGS3 isoforms in chick and mouse, and in the forming epibranchial CSG as well as the forming cortex (Figure 3.10). In the forming CSG of chick embryos, RGS3hL and/or C2PA are expressed in pre-placodal ectoderm of HH11-13 embryos (Figure 3.6A,B). RGS3hL, C2PA and RGS3L are all expressed in the induced placodes of HH16-18 embryos (Figure 3.4). This expression pattern could relate to either non-committed progenitors or newly committed progenitors, as seen with early pro-neural markers Delta-1 and Ngn (Figure 1.7B). However, the expression of RGS3hL and/or C2PA in pre-placodal ectoderm, prior to the onset of neurogenesis, suggests that these proteins play a role in non-committed epithelium. RGS3s is expressed in neuroblasts at the basal surface of the placode and in the staging area (Figure 3.10). Such an expression is seen with later neurogenic markers such as Phox2a and Phox2b (Figure 1.7B). However, expression of these genes continues after the neuroblasts differentiate, whereas RGS3s is downregulated. In fact, this is the only marker identified which specifically labels neuroblasts of the cranial sensory placodes. This implies an important function of RGS3s expression in neuroblasts.

Lastly, RGS3hs-HTMKE and RGS3hs-KYLER are expressed in differentiated neurons (Figure 3.10). RGS3hs-HTMKE is also expressed in the neuroblast staging area, but not at the basal surface of the placode, suggesting that its expression initiates later than RGS3s. It is not clear whether RGS3hs-KYLER is expressed in immature neuroblasts, since expression of RGS3hs-KYLER from this study can only be deduced by the process of elimination using a probe which recognises the shared 3' terminus (Figure 3.4I,M). However, expression of mouse RGS4 might provide some insight, since its amino acid sequence resembles RGS3hs-KYLER (Figure 5.5B and Section 5.2.3). RGS4 was found to be expressed in neuroblasts and neurons of the forming mouse CSG (Figure 3.7E,I). By contrast, RGS4 was not expressed in any neuronal populations of the chick embryo (Section 3.4.1.4), and mouse does not have an RGS3hs-KYLER isoform. This suggests that RGS4 expression in neurons of the mouse embryo might replace RGS3hs-KYLER expression in neurons of the chick embryo, and vice versa. While a similar amino acid sequence does not predicate conserved expression (for example, RGS3s; see below), a highly similar protein sequence suggests a conserved biochemical function, and a role of RGS4 in immature neuroblasts of mouse embryos hypothetically should be similar to a role of RGS3hs-KYLER in immature neuroblasts of chick embryos. This will only be confirmed by detection of RGS3hs-KYLER in neuroblasts of chick embryos. The unique exon of RGS3hs-KYLER is too short for detection with traditional *in situ* hybridisation; however, locked nucleic acids are capable of detecting specific transcripts with recognition motifs of 12-24 bp (Darnell et al., 2010), and this could provide a method of detecting the specific expression of RGS3hs-KYLER in chick embryos.

There were key differences identified in this study in the expression of RGS3 isoforms in chick and mouse (Figure 3.10). While RGS3s expression was restricted to placode-

derived neuroblasts of the chick embryo, it was restricted to placode-derived neurons of the mouse embryo. Furthermore, while RGS3hs-HTMKE was expressed in CSG neuroblasts and neurons of the chick embryo, it was not expressed in any neurons of the mouse embryo. Interestingly, an identical pattern of expression was seen in the mouse cortex. RGS3hL/C2PA/RGS3L was expressed in the VZ, which houses progenitors; RGS3s was expressed in the CP, which houses neurons; and RGS3hs-HTMKE was not expressed. This suggests that the functions of RGS3 isoforms are similar in the forming CSG as in the developing cortex.

An absence of RGS3hs-HTMKE in CSG and cortical neurons of mice could be explained by a degeneration of the neural-specific enhancer(s) which govern its expression in other species (such as the chick). However, the switch in expression of RGS3s from neuroblasts to neurons in the avian to mammalian lineages (respectively) suggests an alteration in the function of the gene product. Consistent with this idea, the first common exon of RGS3s, exon 20 of RGS3hL, is expanded in mouse and human by 114-164 aa (Figure 3.11). It is possible that these novel amino acids are responsible for regulation or subcellular localisation of the protein, changing substrate specificity for its RGS domain (this idea is elaborated upon in Section 6.1.1).

Section 3.6.2 Transcriptional Interference: a Potential Mechanism for the Regulation of RGS3 Isoform Expression

Importantly, in every system investigated, the sequence of expression of these isoforms is co-linear with their genomic orientation. In the chick, RGS3hL/C2PA expression precedes placode induction in pre-placodal ectoderm. In the induced placode, expression of both of these isoforms is retained, and RGS3L is also expressed. Upon commitment to the neuroblast fate, these isoforms are downregulated, and RGS3s is upregulated.

RGS3hs-HTMKE is also upregulated in neuroblasts, but not neuroblasts at the basal surface of the placode, suggesting it comes on later. In the mouse, RGS3hL/C2PA/RGS3L is expressed in the placode and VZ, and RGS3s is expressed in differentiated neurons of both tissues. Expression of RGS3 isoforms in these contexts is thus a model of temporal co-linearity. Temporal co-linearity has been classically described as a progressive activation in space and time of genes within Hox clusters in a sequence identical to their orientation along the chromosome. In the HoxD cluster of mice, for example, telomeric HoxD genes activate before centromeric HoxD genes (Soshnikova and Duboule, 2009). One model proposed for this manner of regulation is progressive chromatin remodelling, with non-permissive centromeric chromatin gradually opening up for transcription (Soshnikova and Duboule, 2009). However, while temporal co-linearity across the Hox cluster involves regulation of multiple genes, temporal co-linearity of RGS3 isoform expression occurs within a single gene. To our knowledge, this is the first characterisation of such a phenomenon.

This implicates the regulation of RGS3 isoforms as inherently different from Hox genes. Because longer isoforms have open reading frames which continue to the 3' terminus of shorter isoforms (except C2PA), repression of expression of shorter isoforms by means of chromatin remodelling would prevent transcription of the full sequence of longer isoforms. Thus, the progressive chromatin remodelling model proposed for the Hox cluster cannot be true for the RGS3 locus. Instead, the regulation of RGS3 isoforms might be explained by an inverse model: expression of longer isoforms prevents transcription initiation of shorter isoforms. In this model, transcription of longer isoforms is like traffic on a motorway, preventing the entrance of cars (initiating RNA polymerase) on downstream entrance ramps (promoters). This mechanism of

transcriptional interference has been shown previously by preventing transcription termination of an upstream gene and thus preventing initiation of transcription of the downstream gene (Greger et al., 2000; Gummalla et al., 2014; Shearwin et al., 2005).

For this to apply to the RGS3 locus, transcription from upstream and downstream promoters cannot overlap. RGS3L and RGS3s expression does not overlap, suggesting termination of RGS3L transcription is necessary to allow initiation of RGS3s transcription. RGS3s is expressed in the basal placode as well as the staging area whereas RGS3hs-HTMKE is expressed in the staging area and differentiated neurons, suggesting that its expression initiates later. RGS3s and RGS3hs-HTMKE expression does overlap in the staging area, but this could relate to RGS3s transcripts retained in the cytoplasm after the initiation of RGS3hs-HTMKE transcription. An evolutionary complement to this hypothesis is the fact that in the mouse CSG and cortex, where RGS3hs-HTMKE is not expressed, RGS3s expression comes on later in differentiated neurons, suggesting the absence of RGS3hs-HTMKE allows it to be expressed later. Lastly, RGS3hL and/or C2PA are expressed in pre-placodal ectoderm prior to placode induction. However, it is not clear which of these isoforms are expressed in this tissue (if not both); nor have I investigated the expression of RGS3L, RGS3s, or either RGS3hs isoform in these early stages. Such an investigation is thus paramount to further understand the nature of RGS3 intragenic temporal co-linearity.

However, there are important incompatibilities with a mechanism of transcriptional interference at the RGS3 locus. First, the start of RGS3hs-HTMKE transcription is downstream from the start of RGS3hs-KYLER transcription, and the transcriptional interference model would dictate that expression of the former should be interfered by expression of the latter. However, the expression patterns of RGS3hs-HTMKE and

RGS3hs-KYLER overlap in the forming chick CSG, and the expression of either does not appear to be downregulated as late as HH23 (Section 3.3.2). Furthermore, in the placode of HH18 embryos, RGS3hL, C2PA, and RGS3L are all expressed. The presence of RGS3hL and/or C2PA transcripts could be retained from early transcription in pre-placodal ectoderm, but a qualitative argument against this idea is the apparently robust staining using the RGS3hL/C2PA probe on HH18 embryos (Figure 3.4D) compared to HH15 embryos (Figure 3.6C). Lastly, a mechanism of transcriptional inference would imply that the locus is constantly occupied, and thus these genes are highly expressed (Shearwin et al., 2005). An understanding of the extent to which this mechanism applies to the RGS3 locus during neuronal maturation will only be achieved by first understanding the dynamics of gene transcription at the RGS3 locus.

An alternative view of the regulation of RGS3 isoforms is the consideration that they are under the control of different promoters, and thus like separate promoters of separate genes, could be differentially regulated by distinct transcription factors. Regardless of the mechanism(s) of RGS3 isoform expression, the end product is the same: differential expression of isoforms with increasingly truncated N termini. The importance of temporal co-linearity of RGS3 isoform expression might then not relate to a built-in transcriptional interference regulation mechanism, but rather a sequential loss of N-terminal modules which confer distinct functions.

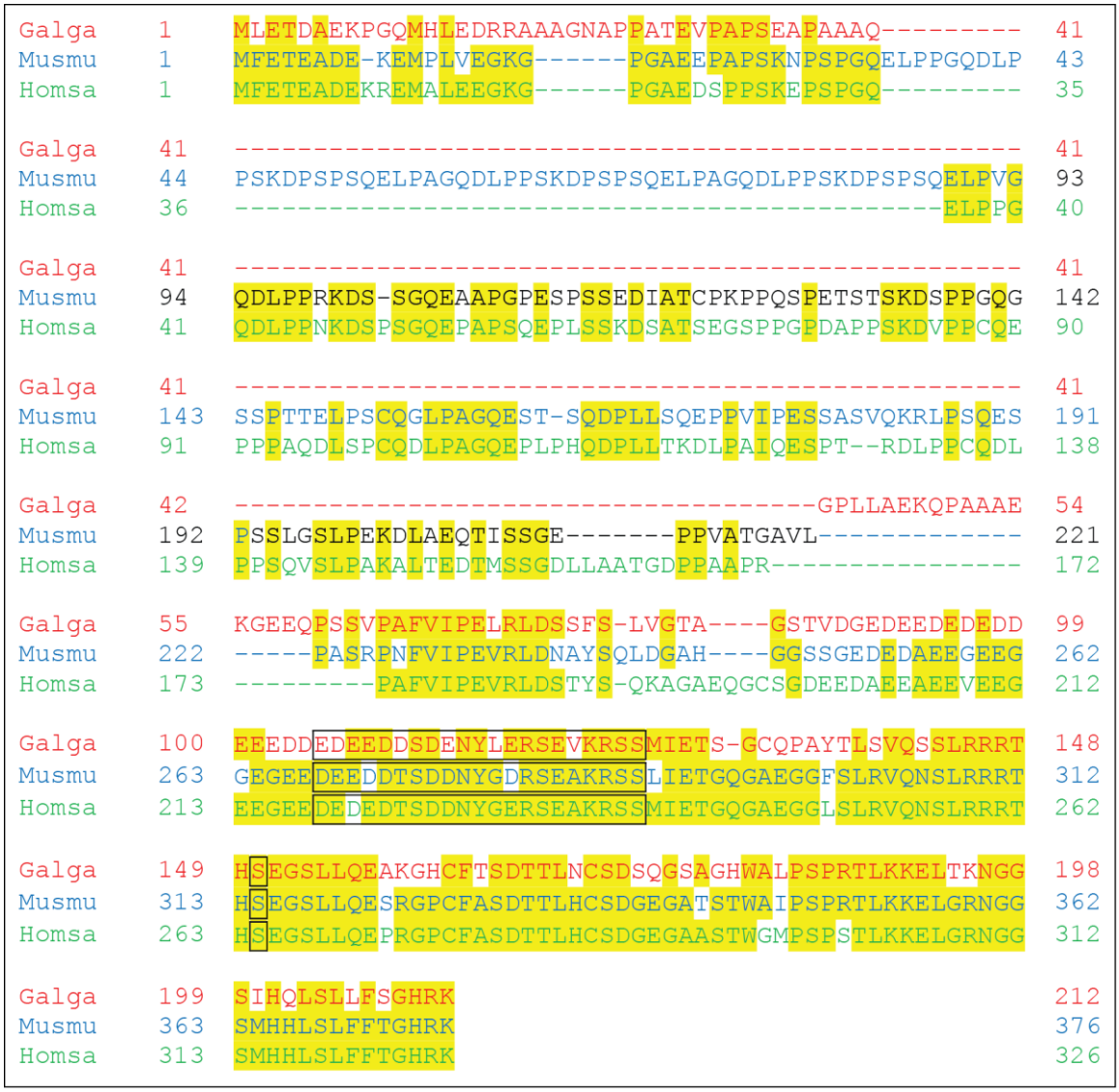


Figure 3.11. Alignment of RGS3hL Exon 20 between Chicken, Mouse and Human.
Amino acid alignment of exon 20 of RGS3hL (the first common exon of RGS3s) is shown for chicken (Galga), mouse (Musmu), and human (Homsa). Identities are highlighted in yellow. Boxes correspond to the EF Hand domain and the 14-3-3 binding serine (see Section 1.2.4.3.3), respectively. Chicken exon 20 aligns to the first ~40 and final ~150 aa of the mouse and human exons. However, an additional ~100 aa N-terminal to the final ~150 aa of chicken exon 20 are present and similar in mouse and human. In addition, a further 50 aa is present in mouse N-terminal to this sequence which is not present in human.

Chapter 4. Functional Analysis of RGS3 Isoforms in the Developing Chick Cranial Sensory Ganglia

Section 4.1 Introduction

The differential expression of RGS3 isoforms among placodal progenitors, staging area neuroblasts, and migratory neurons in the forming chick CSG suggests distinct roles of these proteins. The role of RGS3hL, C2PA and/or RGS3L (by introducing a premature stop codon before the PDZ domain with homologous recombination) has been demonstrated in the maintenance of progenitors of the developing mouse cortex (Qiu et al., 2010), consistent with its expression in the VZ (Figure 3.8C) (Lu et al., 2001). However, this function was not assessed in the placodes, nor were the roles of RGS3s or RGS3hs-HTMKE in either tissue. Furthermore, a role of any RGS3 isoform in the forming CSG of the chick has not been described.

In this chapter, I sought to dissect the distinct functions of each isoform in the three stages of neuroblast maturation (placodal progenitor, staging area neuroblast, and migratory neuron) from the chick epibranchial placodes. I first approached this with short-hairpin RNA (shRNA)-mediated knockdown. The shRNA targeted the 3' end of all isoforms (except C2PA), knocking them down simultaneously. Embryos were electroporated with these constructs prior to placode formation and incubated to stages after which the CSG had begun to form. Wholemount embryos were labelled with antibodies or via *in situ* hybridisation, and analysis was carried out on transverse sections. I first analysed the effects of shRNA knockdown on formation of all three

ganglia from the epibranchial placodes (to which expression of all isoforms except RGS3hs-HTMKE and RGS3hs-KYLER was restricted). From this point I focused my analysis on the forming petrosal ganglion, which serves as a very clear model to spatially dissect placodal progenitors, staging area neuroblasts, and migratory neurons (Figure 1.7). Phenotypes corresponding to each of these maturation states were analysed. To confirm these phenotypes were attributed to the isoforms endogenously expressed in the corresponding maturation states, I individually overexpressed each isoform. Finally, I sought to determine the specific biochemical role of each isoform by mutating or deleting functional domains. The implications for each of these loss- and gain-of-function phenotypes for the roles of RGS3 isoforms in CSG formation will be discussed in the final section.

Section 4.2 Knockdown of RGS3 Isoforms with Short-Hairpin RNA (shRNA)

Section 4.2.1 Design and Efficiency of shRNAs

To determine the functional importance of differential expression of RGS3 isoforms in the forming CSG, I first sought to determine the effects of knockdown of the isoforms. To achieve this, I used short-hairpin RNAs (shRNAs), a form of RNA interference which targets mRNA for degradation by endogenous machinery (Paddison et al., 2002). shRNAs are useful for targeted gene knockdown because they can be encoded by exogenous plasmid vectors, which allow for sustained and consistent gene knockdown (Rao et al., 2009).

To account for potential off-target effects, I designed multiple shRNAs at different sites in the RGS3 locus (see Section 2.6). Two shRNAs (termed shRNA-678 and -881 by

virtue of their positions in the RGS3L sequence) targeted exons 15 and 16 of RGS3hL, which are shared between RGS3hL, C2PA, and RGS3L (Figure 4.1). Four other shRNAs (termed shRNA-1997, -2172, -2929, and -3300) targeted the final three exons of RGS3hL, which are not present in C2PA but are present in RGS3L, RGS3s, RGS3hs, and RGS3hs-KYLER. I also aimed to knock down each isoform individually by targeting the unique exons of each isoform. However, each of these exons proved restrictively short to design shRNAs using any of the design engines. Thus, my experiments were limited to simultaneous knock down of upstream (RGS3hL, C2PA, RGS3L) or downstream (RGS3hL, RGS3L, RGS3s, RGS3hs) isoforms. Finally, I cloned a control shRNA which does not align to any sequences in the chicken transcriptome and has previously been used without perturbation on neuronal systems (Skaggs et al., 2011; Vohra et al., 2007). These constructs were cloned into p*Silencer* (Life Technologies; Section 2.6), which has previously been shown to efficiently express shRNAs and knock down endogenous gene expression in the chick embryo (Freter et al., 2008).

To determine the effects of RGS3 shRNA on the forming epibranchial ganglia, presumptive placodal ectoderm in HH11-13 embryos was electroporated *in ovo* with the p*Silencer* plasmid encoding shRNA and a plasmid encoding Green Fluorescent Protein (GFP) as a marker for electroporation efficiency. Eggs were re-sealed and embryos were incubated to HH16-18 (a further 18-26 hours), when CSG are actively forming, before dissection and fixation. Embryos with robust GFP fluorescence in one or more of the placodes were selected for further analysis.

To determine the knockdown efficiency of each shRNA, *in situ* hybridisation of the endogenous target was performed following electroportation. For knockdown of upstream isoforms, I used the RGS3hL/C2PA/RGS3L probe previously used for

expression analysis (see Section 3.3.1) (Figure 4.1A). For knockdown of downstream isoforms, I used the original EST-based probe which aligns to the shared 3' UTR (Figure 3.4L,Q) RGS3hL, RGS3L, RGS3s, and RGS3hs. Because placodes and their derivative CSG develop bilaterally, I used the unelectroporated side (the left side) as an internal control for *in situ* stain development (Figure 4.1C).

Two controls, the control shRNA plus the GFP-expressing vector, and the GFP-expressing vector alone, resulted in very few embryos perturbed in their staining of the targeted placodes using the downstream probe. However, the two upstream shRNAs were additionally insufficient to reduce staining using the upstream probe. Only two of seven shRNA-881-electroporated embryos exhibited reduction in staining compared to the unelectroporated side, and no shRNA-678-electroporated embryos showed reduced staining (Figure 4.1D). This is likely due to unpredictable RNA secondary structures or RNA-binding proteins at these sites, preventing the hybridisation of the processed shRNA with the endogenous mRNA transcript. Thus, more shRNAs need to be tested for further investigation into the effects of knockdown of upstream isoforms.

Of the shRNAs designed to knock down downstream isoforms, shRNA-1997 and -3300 reduced staining in 9/14 and 6/9 embryos, respectively. I proceeded with these shRNAs to determine the effects of knockdown of downstream isoforms, henceforth referring to them as respectively shRNA-*CDS* and shRNA-*3'UTR*, and collectively as RGS3 shRNA. Because C2PA is the only isoform not targeted by these shRNAs, I will henceforth exclude C2PA when discussing the functions of RGS3 isoforms.

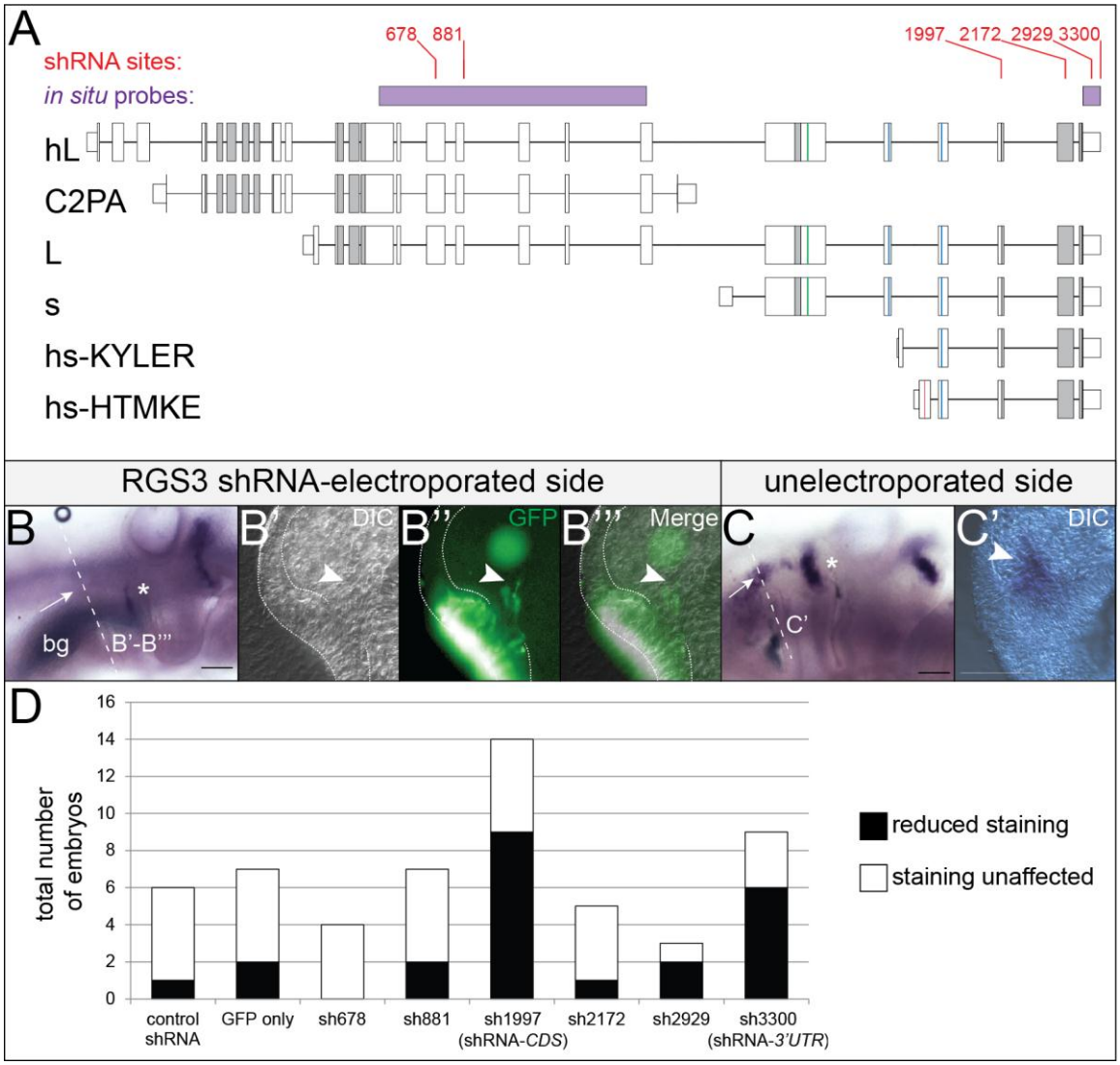


Figure 4.1. Short-Hairpin RNA Design and Efficiency.
(A) Short-hairpin RNAs (shRNA) were designed to target the upstream and downstream exons of RGS3hL, thus differentially targeting RGS3hL, C2PA and RGS3L versus RGS3hL, RGS3L, RGS3s, and RGS3hs, respectively. The positions of each targeted site are indicated. *In situ* hybridisation probes used to measure efficacy of knockdown by downstream or upstream shRNAs are shown. Coloured lines and boxes on exons correspond to those in Figure 1.11. *(B-C)* A representative embryo electroporated with shRNA-3300 and *in situ* hybridised with the downstream probe. A clear reduction *(B)* (arrow, and to a lesser extent, asterisk) can be seen compared to the unelectroporated side of the embryo *(C)*. Note: ventral staining seen in B corresponds to underlying background staining (bg). In transverse sections *(B'-B''', C')*, the reduction in staining corresponds to internally migrating GFP-positive neurons (arrowhead) *(B'',B''')*. *(D)* Total number of embryos electroporated showing either reduction (black) or no reduction (white) between electroporated and unelectroporated sides of the embryo in targeted placodes. Note: control shRNA and GFP-only electroporated embryos were stained with the downstream *in situ* hybridisation probe. Scale bars: 100 µm.

Section 4.2.2 Morphological Effects on the Forming Epibranchial Ganglia

To determine the effect of RGS3 shRNA on epibranchial ganglia development, electroporated embryos were stained in wholemount with antibodies against GFP (as a marker of electroporation) and Neurofilament-Medium chain (NFM), a neuron-specific intermediate filament component which labels neuronal projections (Blentic et al., 2011; Graham et al., 2007) (see Section 1.1.6.2.2). Embryos were then sectioned at a thickness of 100 um in the transverse plane to capture the whole migratory stream. Sections were imaged with a Zeiss 710 confocal microscope and Z-stacks were compiled for qualitative and quantitative analysis.

Intriguingly, my qualitative analysis showed that the migratory streams emanating from the epibranchial placodes developed prematurely in shRNA-*CDS*-electroporated embryos compared to stage-matched GFP-only- or shRNA control- electroporated embryos. Neurons derived from the geniculate placode normally first coalesce in a domain rostral and ventral to the forming vestibuloacoustic ganglion, then migrate and extend projections dorsally around the vestibuloacoustic ganglion toward the dorsal neural tube (Blentic et al., 2011). In GFP-only controls, some geniculate neurons were seen to migrate and project around the vestibuloacoustic ganglion. By contrast, a robust stream of geniculate neurons migrated around the vestibuloacoustic ganglion in shRNA-*CDS*-electroporated embryos, and four of six embryos showed innervation of geniculate neurons with the hindbrain (Figure 4.2B, asterisk) (compared to only one of six GFP-only-electroporated embryos).

The petrosal migratory stream, which extends in a nearly straight line from the placode to the hindbrain, was also affected by electroporation of shRNA-*CDS*. Like the geniculate stream, the dorsal part of the petrosal stream was expanded, both in terms of width and in

terms of extension toward the hindbrain (Figure 4.2C,D). Consistently, petrosal neurons had innervated the hindbrain in five of eleven shRNA-*CDS*-electroporated embryos, while this was never observed in control shRNA-electroporated embryos. A similar effect was seen in petrosal migratory streams of shRNA-*3'UTR*-electroporated embryos (n=4/8 at or near the hindbrain innervation point; not shown), confirming specificity of the phenotype to loss of RGS3 isoforms.

Lastly, an expansion of the nodose migratory stream was also observed (Figure 4.2E,F). At this stage, nodose neurons normally coalesce into a ganglion anlage before emanating a migratory stream toward the hindbrain (Begbie and Graham, 2001; Blentic et al., 2011). Control shRNA-electroporated embryos similarly formed a ganglion anlage without a migratory stream, but RGS3 shRNA-electroporated embryos displayed a prominent migratory stream in addition to the ganglion anlage.

Taken together, these data suggest that shRNA targeting all RGS3 isoforms causes a precocious formation of the epibranchial CSG.

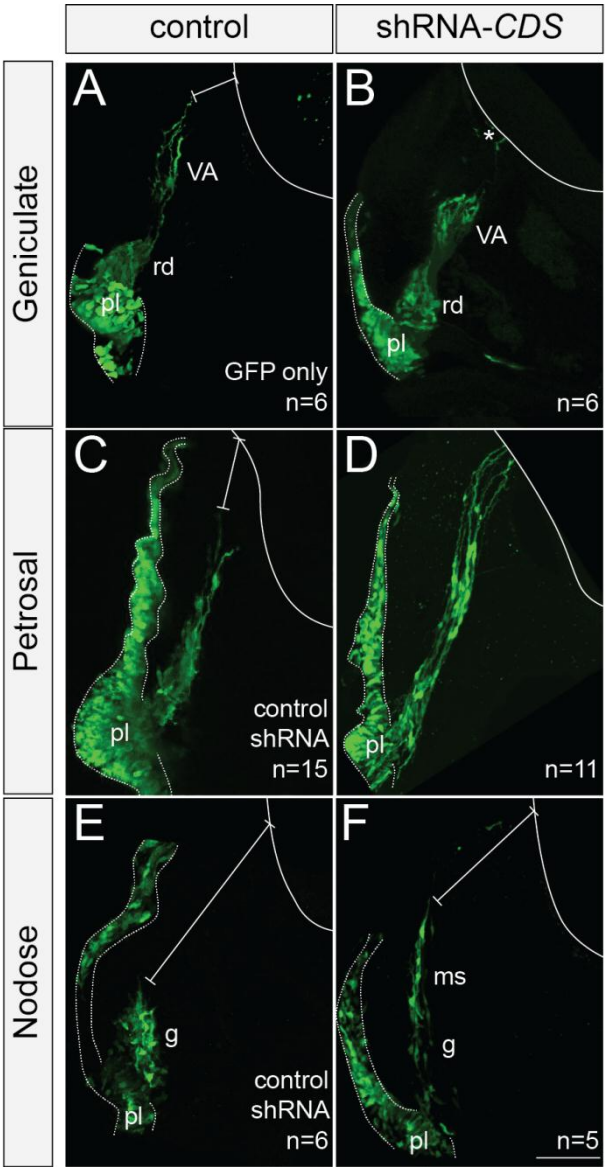


Figure 4.2. Effects of RGS3 shRNA-*CDS* on Epibranchial Ganglion Formation
Confocal stacks of transverse sections of HH17-18^{+} embryos electroporated with GFP only *(A)*, control shRNA *(C,E)* or shRNA-*CDS (B,D,F)*. αGFP staining is shown. Electroporated surface ectoderm, including the placode (pl), is indicated in dashed lines. The outline of the neural tube is indicated in solid lines. Brackets indicate distance between the migratory stream and the point of CNS innervation (the dorsal hindbrain). *(A-B)* Geniculate neurons coalesce in a rostral domain (rd) before migrating and projecting around the vestibuloacoustic (VA) ganglion. This region was more robust in shRNA-*CDS*-electroporated embryos compared to controls, and the hindbrain was innervated (asterisk) in 4/6 embryos. *(C-D)* An expansion of the petrosal migratory stream was also observed in shRNA-*CDS* electroporated embryos *(C)* compared to control shRNA-electroporated embryos *(D)*. A similar effect was seen in shRNA-*3'UTR*-electroporated embryos (n=8; not shown). *(E-F)* Lastly, an expansion of the nodose migratory stream was observed in shRNA-*CDS* electroporated embryos *(F)* compared to control shRNA-electroporated embryos *(E)*. In the control scenario *(E)*, a ganglion anlage (g) formed some distance from the dorsal neural tube (bracket), without yet projecting a stream of migratory neurons. By contrast, a migratory stream (ms) toward the dorsal neural tube from the ganglion anlage was clearly observed in shRNA-*CDS*-electroporated embryos *(F)*. Note: most of the ganglion anlage in *(F)* is on a subsequent section and is not shown. Scale bar: 100 μm.

Section 4.2.3 Effects on Placodal Neurogenesis

Precocious ganglion formation as the result of knockdown of RGS3 isoforms could relate precocious neurogenesis in the placode or precocious migration of placodal derivatives. To discriminate between these effects, I chose to focus my investigations on the forming petrosal ganglion, since it provides the clearest spatial separation between the placode, differentiating neuroblasts, and mature migratory neurons (see Section 3.2.2). For the remainder of my functional analyses, I specifically targeted the petrosal placode for electroporation.

Section 4.2.3.1 Increase in the Total Number of Neuroblasts and Neurons

To investigate whether alterations in placodal neurogenesis contributes to precocious ganglion formation, I carried out wholemount triple labelling of shRNA-electroporated embryos with antibodies against GFP, NFM, and Islet-1/2. αGFP served as a marker for electroporated cells. αNFM is a neural-specific stain which labels neuroblasts and as well as projections of differentiated neurons (Section 1.1.6.2.2). Islet-1 expression initiates early and is maintained in the neuroblast differentiation process (see Section 1.1.6.2.1), and αIsl-1/2 stains nuclei of placodal neuroblasts and differentiated neurons (Begbie et al., 2002; Freter et al., 2013) (Figure 4.3A,B). The number of Isl-1/2-positive nuclei in the staging area and migratory stream were counted in digital Z slices as described in Section 2.11.

Consistent with an expansion of the migratory stream previously observed (Section 4.2.2), an increase in the number of Isl-1/2-positive neuroblasts and neurons was observed in RGS3 shRNA-*CDS*- and shRNA-*3'UTR*-electroporated embryos compared to control shRNA-electroporated embryos (Figure 4.3C; shRNA-*CDS*: 218.50±46.00,

n=6, *p*=0.039; shRNA-*3'UTR*: 197.50±22.90, n=4, *p*=0.013; control shRNA: 115.75±14.88, n=8) (for this and all other statistical analyses, *p* values correspond to analysis with Student's T-test (Section 2.15)).

This effect could be due to an early onset of neurogenesis from the placode, or an enhanced rate of neurogenesis. To distinguish these phenotypes, I looked earlier in development to HH16^{-}-HH17 (25-31 somite stage) embryos, a stage at which petrosal neurogenesis is in its infancy (Blentic et al., 2011). At this stage, I also saw an increase in the number of Isl-1/2-positive neuroblasts and neurons compared to controls (Figure 4.3C) (shRNA-*CDS*: 109.29±12.82, n=7, *p*=0.030, *p* (to older embryos)=0.032; shRNA-*3'UTR*: 115.00±18.724, n=6, *p*=0.047, *p* (to older embryos)=0.014; control shRNA: 73.33±11.97, n=9, *p* (to older embryos)=0.022). Importantly though, there was an increase in the fold-change between control and RGS3 shRNA from young to older embryos (shRNA-*CDS*: 1.49 [young embryos] to 1.89 [older embryos]; shRNA-*3'UTR*: 1.57 [young embryos] to 1.71 [older embryos]). If the rate of neurogenesis was constant between the control and RGS3 shRNA scenarios, and the increase in Isl-1/2-positive cells was solely due to an early onset of placodal neurogenesis, the fold change between control and RGS3 shRNA should also remain constant. While the possibility of an early onset of neurogenesis cannot be eliminated, the increase in fold change between young and older embryos confirms that at least an increase in the rate of neurogenesis is responsible for this phenotype.

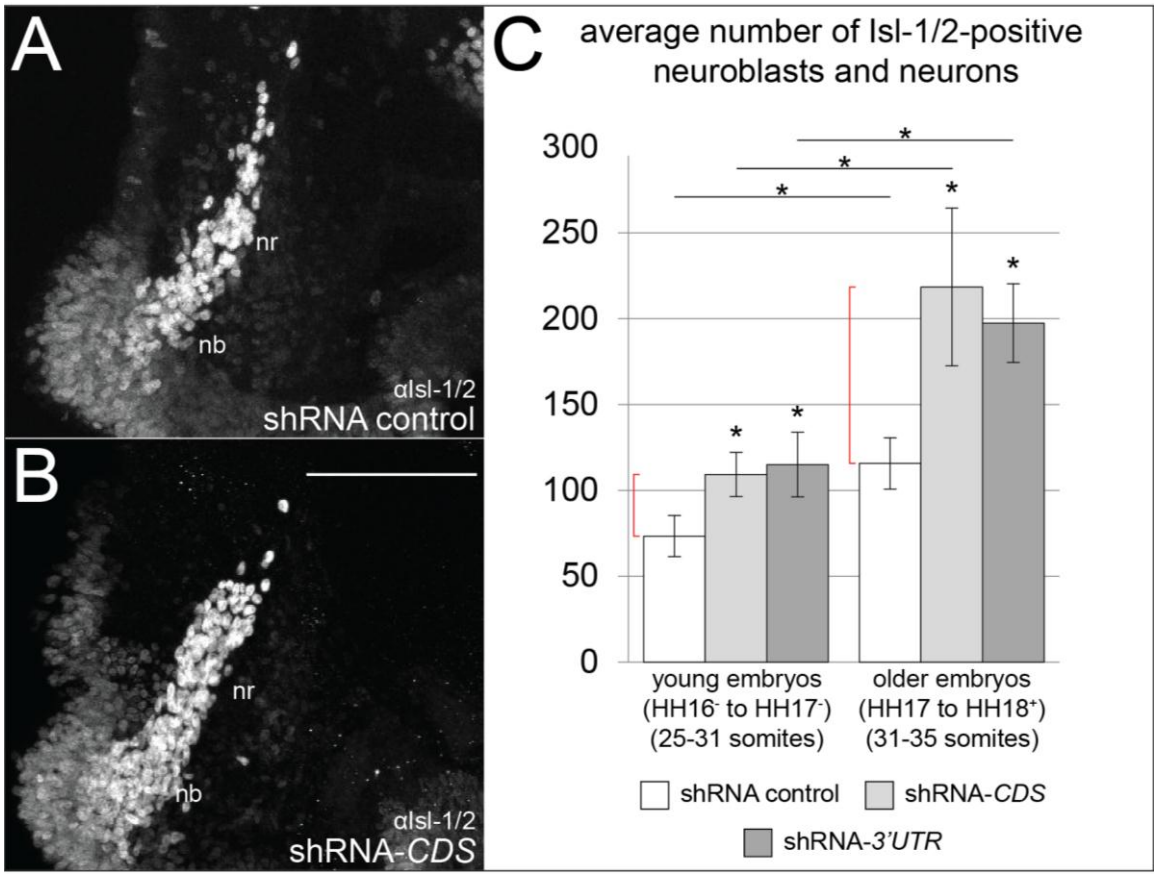


Figure 4.3. Effects of RGS3 shRNA on the Production of Neuroblasts and Neurons.
(A,B) Representative petrosal migratory streams of HH18 embryos electroporated with control shRNA *(A)* or shRNA-*CDS (B)* and stained with αIsl-1/2, showing an apparent increase in the number of Isl-1/2-positive neuroblasts and neurons. To quantify this effect, embryos electroporated at HH11-13 were incubated to young stages (HH16$^-$ to HH17$^-$) (25-31 somite stage) or older stages (HH17 to HH18$^+$) (31-35 somite stage), and the number of Isl-1/2-positive cells delaminated from the placode were counted *(C)*. At both stages, an increase in the number of Isl-1/2-positive cells was observed in RGS3 shRNA-electroporated embryos compared to control shRNA-electroporated embryos. Furthermore, the fold change between knockdown and control scenarios was seen to increase from young stages to older stages (indicated by red brackets). *=p<0.05, Student's T-test (see Section 2.15). Scale bar in *(B)*: 50 µm.

Section 4.2.3.2 Increase in Neurogenesis is Not Due to Changes in Proliferation

Based on the above data, it is possible that the increase in Isl-1/2-positive neuroblasts and neurons is due to an expansion of the placodal progenitor and/or the delaminated neuroblast pools. To investigate whether this is the case, we stained embryos with an antibody against phosphorylated Histone H3 (αpH3), a highly transient stain which specifically labels nuclei of cells in metaphase (Hans and Dimitrov, 2001) and thus serves as a marker for cell division. No change was observed in the number of pH3-/GFP-double positive placodal cells at either young or older stages between RGS3 shRNA- and control shRNA-electroporated embryos (shRNA-*CDS*: 4.33±1.26, n=6, p=0.261; shRNA-*3'UTR*: 3.50±0.50, n=6, p=0.432; control shRNA: 3.33±0.82, n=9). This was also true for divisions of delaminated neuroblasts (shRNA-*CDS*: 1.67±0.61, n=6, p=0.070; shRNA-*3'UTR*: 0.83±0.17, n=6, p=0.181; control shRNA: 0.56±0.24, n=9).

These results are consistent with αpH3 stains on the unelectroporated embryo (Begbie et al., 2002; Blentic et al., 2011; Graham et al., 2007), which show that placode and delaminated neuroblast cell divisions are infrequent. Thus in the context of the generation of placode-derived neurons, 'neurogenesis' must largely involve the commitment of placodal progenitors to the neuronal fate, independent of the cell cycle. Upon knockdown of all isoforms except C2PA, an enhancement in neurogenesis therefore implicates RGS3hL and RGS3L, the only shRNA-targeted isoforms expressed in the placode, as playing a critical role in progenitor maintenance.

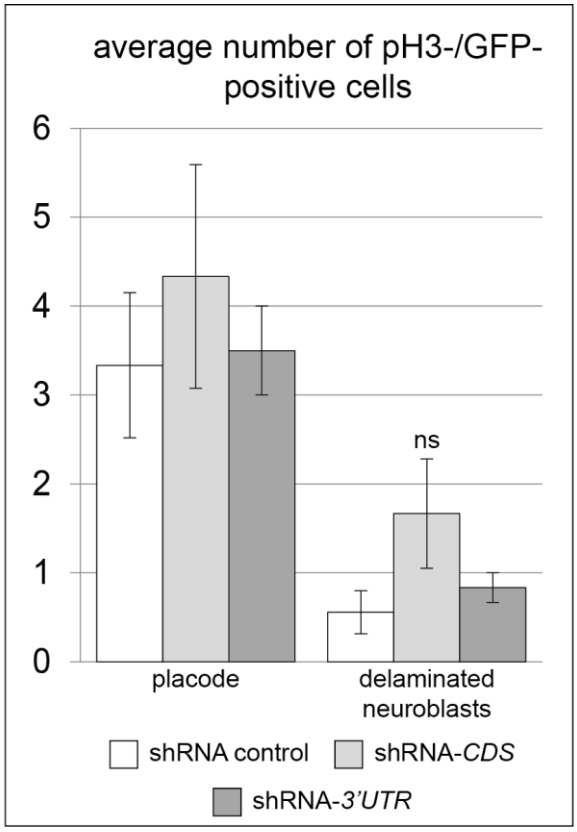


Figure 4.4. Effects of RGS3 shRNA on Proliferation of Placodal Cells and Delaminated Neuroblasts.
The number of pH3-/GFP-double positive cells in HH16^{-}-18^{+} shRNA-electroporated embryos in the placode (left) or delaminated from the placode (right) were quantified. No significant change between RGS3 shRNA and control shRNA was observed in either population. ns: *p>0.05* (not significant).

Section 4.2.4 Effects on Placodal Neuroblast Differentiation

Section 4.2.4.1 Retraction of the Neuroblast Staging Area

Since the rate of proliferation in the placode is not driving the precocious ganglion formation, I investigated whether RGS3 shRNA affected the differentiation of neuroblasts into neurons. I stained embryos with an antibody against HuC/D, a marker of post-mitotic neurons (Marusich et al., 1994). In the forming CSG, αHuC/D stains outside of the neuroblast staining area, labelling only differentiated neurons in the migratory stream (see Section 1.1.6.2.2; Figure 4.5E,K; Figure 1.7). To determine the extent of the HuC/D-negative staging area, I measured the distance between the ventral-most delaminated neuroblast and the first HuC/D-positive neuron in confocal stacks of the petrosal stream (see Section 2.12 and Figure 2.3). To account for size differences between embryos, I normalised this distance against the total distance between the ventral-most delaminated neuroblast and the dorsal neural tube, where CSG neurons will innervate the hindbrain.

In RGS3 shRNA-electroporated embryos, αHuC/D was seen to stain closer to the placode as a percentage of the total distance between the ventral-most delaminated neuroblast and the dorsal neural tube compared to control shRNA-electroporated embryos (Figure 4.5E,J,K,L) (shRNA-*CDS*: 15.55±0.93%, n=3, p=0.001; shRNA-*3'UTR*: 17.01±1.54%, n=5, p=0.007; control shRNA: 23.98±1.97%, n=14). This indicates a retraction of the staging area. In addition, preliminary data suggested that SCG10, a microtubule-binding protein which, like HuC/D, is only expressed in mature neurons (see Section 1.1.6.2.2), was expressed closer to the placode (Figure 4.5K) (shRNA-*CDS*: 14.43±4.29%, n=2, p=0.170; control shRNA: 21.02±3.64%, n=4), though greater n values will be required to determine the statistical significance of this result.

By contrast, αNFM and *in situ* hybridisation staining against Phox2b, which stain neuroblasts as soon as they delaminate from the placode (see Figure 1.7B), were not perturbed (Figure 4.5C,D,H,I,K). *In situ* hybridisation staining against NeuroM and Isl-1, which are expressed in the placode even earlier in the differentiation process (see Section 1.1.6.2.1), were also unaffected (Figure 4.5A,B,F,G,K). Together, this suggests an alteration in the spatial expression of mature neuronal markers, shrinking the staging area, without affecting the expression of early markers of neuroblast commitment.

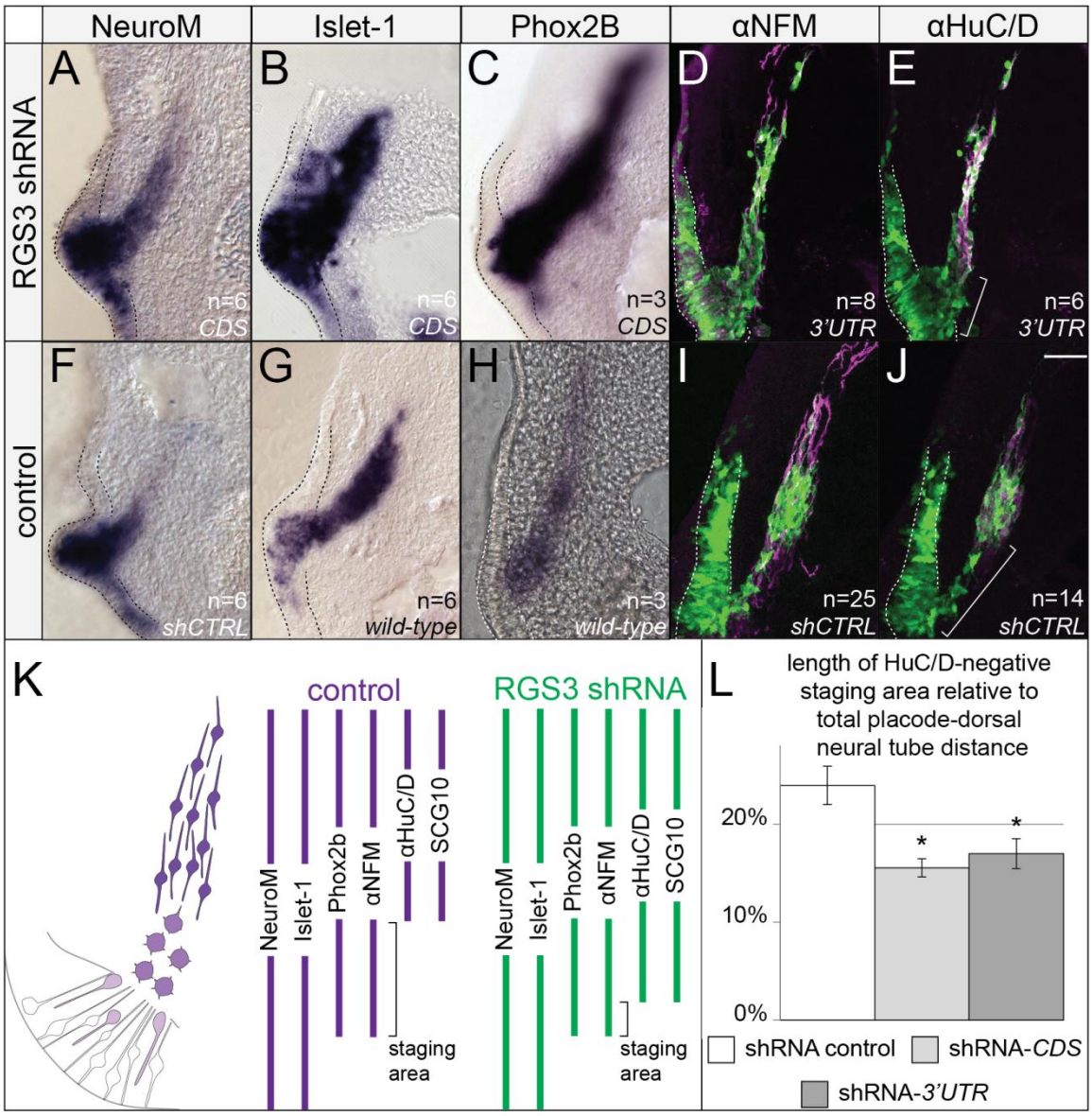


Figure 4.5. Effects of RGS3 shRNA on the Spatiotemporal Transcriptional Programme of Placodal Derivatives.

In situ hybridisation *(A-C, F-H)* or antibody stains (*D-E, I-J)* on RGS3 shRNA *(A-F)* or control *(F-J)* embryos. RGS3 shRNA embryos were electroporated with either shRNA-*CDS (A-C)* or shRNA-*3'UTR (D-E)*. shRNA-*CDS*-electroporated embryos were also stained with αNFM and αHuC/D (not shown; n=11 and n=3, respectively). Control embryos were either electroporated with control shRNA (shCTRL) *(F, I-J)* or not electroporated (*G-H)*. Embryos were *in situ* hybridised against NeuroM *(A, F)*, Islet-1 *(B, G)*, or Phox2b *(C, H)*; or stained with antibodies against NFM *(D, I)* or HuC/D *(E, J)*. Dashed lines indicate surface ectoderm, including the placode. The only marker whose spatial expression was perturbed was HuC/D, which was brought closer to the placode (compare brackets in *E* and *F*). In addition, preliminary evidence suggested SCG10 initiates closer to the placode (schematised in *K*; see text for quantification). Brackets in *(K)* indicate retraction of the HuC/D-/SCG10-negative staging area. *(L)* Quantification of length of the HuC/D-negative staging area normalised to the total distance between the ventral-most delaminated neuroblast and the dorsal neural tube, showing reduction in the HuC/D-negative staging area for shRNA-*CDS* and shRNA-*3'UTR*. Scale bar *(J)*: 50 µm. *=$p<0.05$.

Section 4.2.4.2 Increased Neuroblast Differentiation

Two possibilities could account for a retracted staging area in RGS3 shRNA embryos. First, neuroblasts could migrate more slowly, and thus in the same timeframe required for neuroblast differentiation, the position at which the neuroblast is in relation to the placode when it differentiates is closer in the RGS3 shRNA versus control shRNA scenarios. Alternatively, RGS3 shRNA-electroporated neuroblasts could have a greater proclivity to differentiate into HuC/D-positive neurons, thus resulting in more HuC/D-positive neurons relative to the total number of neuronal derivatives at any given point in time. Such an effect could expand the migratory stream at the expense of the staging area.

To test this hypothesis, I measured the ratio of electroporated neurons (GFP-, HuC/D-double positive) to total electroporated neuroblasts and neurons (GFP-, NFM-double positive). This analysis showed an increase in this proportion from control to RGS3 shRNA-electroporated embryos (Figure 4.6) (shRNA-*3'UTR*: 0.83±0.03, n=5, p=0.010; control shRNA: 0.70±0.03, n=9). Together, these data suggest a role of RGS3 isoforms in negatively regulating neuroblast differentiation. In particular, the data implicate RGS3s and/or RGS3hs-HTMKE, which are expressed in neuroblasts, in mediating this function. It is possible that this phenotype is a secondary effect from a loss of RGS3hL and/or RGS3L in the placode; however, the fact that early neuroblast commitment markers are unperturbed by RGS3 shRNA (Figure 4.5) suggests a late onset effect specific to committed neuroblasts.

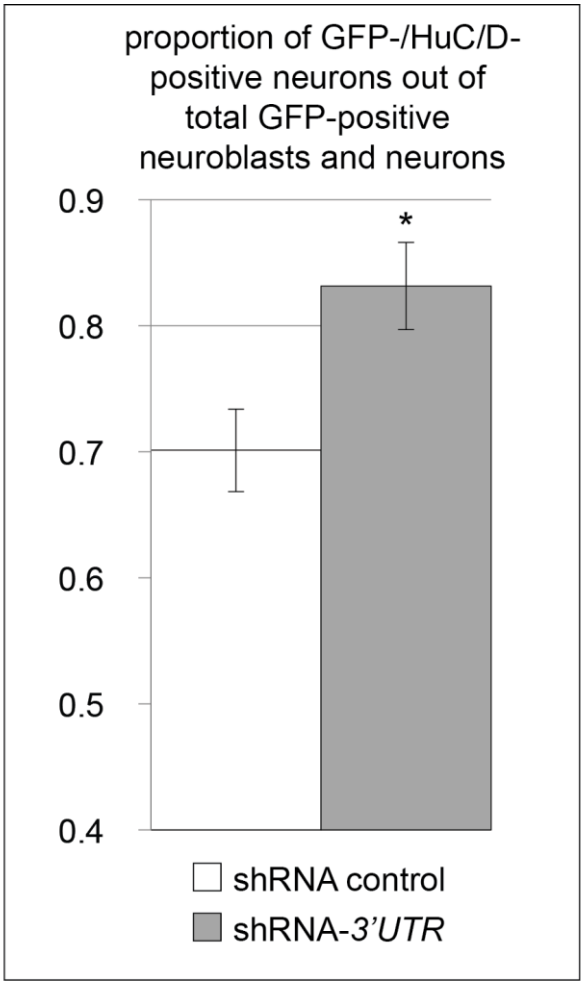


Figure 4.6. Effects of RGS3 shRNA on Neuroblast Differentiation.
The number of GFP-/HuC/D-double positive neurons were measured as a proportion of the total number of GFP-positive neuroblasts and neurons. GFP-positive, HuC/D-negative cells were confirmed as neuroblasts by αNFM antibody staining. An increase in this ratio was observed in shRNA-*3'UTR*-electroporated embryos compared to control shRNA-electroporated embryos. *=$p<0.05$.

Section 4.2.5 Effects on Placode-Derived Neuronal Migration

Neuronal migration is characterised by repeated cycles of leading process extension followed by somal translocation (Marín et al., 2010). This is in contrast to the mechanisms of axon guidance, which extend the leading process without translocating the cell body. I initially observed an extension of the migratory stream toward the dorsal neural tube (Figure 4.2D); however, this observation does not distinguish between axon guidance versus neuronal migration.

To distinguish between axon guidance and neuronal migration, I compared the position of the furthest-migrated electroporated (GFP-positive) cell body toward the dorsal neural tube in relation to its leading projection (see Section 2.12 and Figure 2.3). These measurements were analysed relative to the total distance between the ventral placode and the dorsal neural tube in a manner identical to the measurements normalising the extent of the neuroblast staging area (Section 4.2.4.1). An increase in the relative position was observed at both the cell body (Figure 4.7A) (shRNA-*CDS*: 69.97±3.75%, n=11, p=0.021; shRNA-*3'UTR*: 71.02±6.12%, n=7, p=0.042; control shRNA: 59.76±2.80%, n=15) and at the projection terminus (Figure 4.7B) (shRNA-*CDS*: 85.76±5.06%, n=11, p=0.011; shRNA-*3'UTR*: 80.30±4.03%, n=7, p=0.040; control shRNA: 70.59±3.26%, n=15). Therefore, RGS3 shRNA enhanced neuronal migration.

Furthermore, while the projection termini of leading neurons had extended a greater distance in RGS3 shRNA-electroporated embryos, the average length of these projections was not significantly greater (shRNA-*CDS*: 74.14±19.34µm, n=11, p=0.152; shRNA-*3'UTR*: 40.81±9.98µm, n=8, p=0.233; control shRNA: 51.12±9.61µm, n=15). Thus, the capacity of the cell body to translocate in response to leading process extension is equally efficient in the RGS3 shRNA versus control shRNA scenarios.

While neurons could migrate farther as a secondary consequence of enhanced neurogenesis and neuroblast differentiation, it is also possible that extent of neuronal migration and space in time is entirely intrinsic to that neuron. Since the only RGS3 isoforms expressed in migrating neurons are RGS3hs-KYLER and RGS3hs-HTMKE, this would directly implicate RGS3hs-KYLER and/or RGS3hs-HTMKE in negatively regulating neuronal migration.

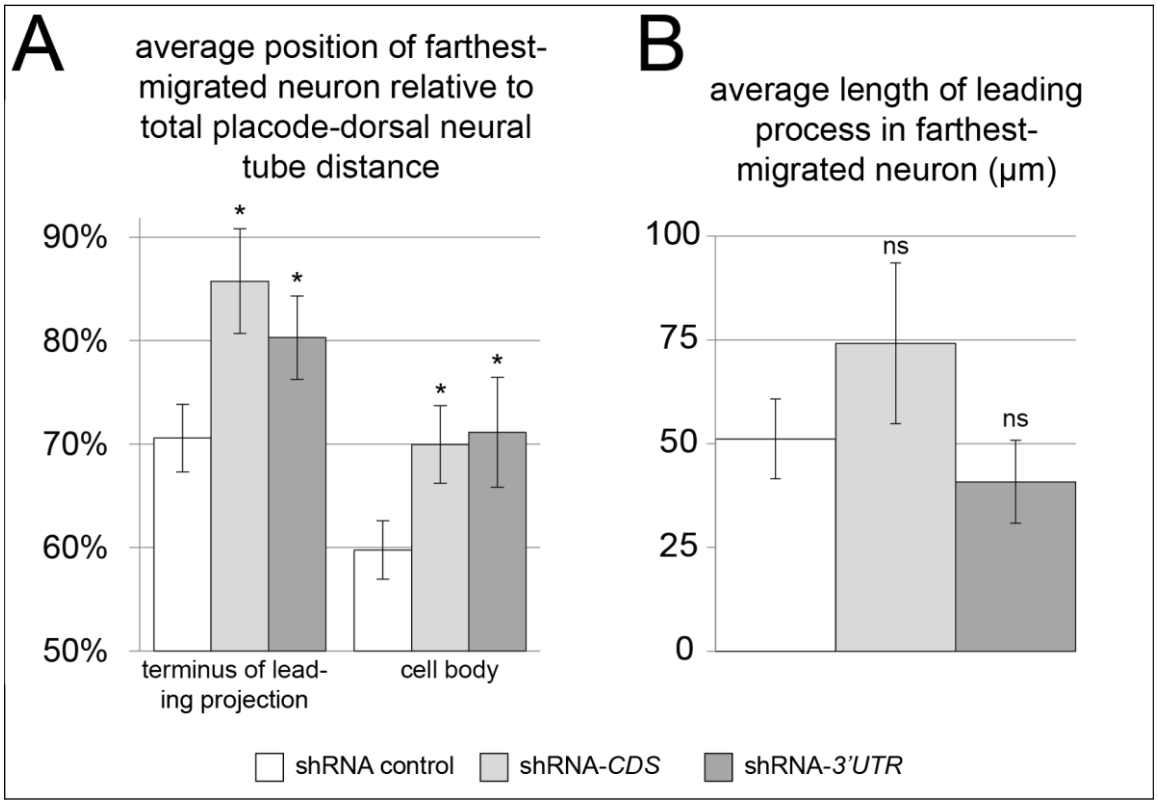


Figure 4.7. Effects of RGS3 shRNA on Neuronal Migration.
(A) The distance of the farthest-migrated neuron from the ventral-most delaminated neuroblast was measured and normalised against the total distance from the ventral-most delaminated neuroblast and the dorsal neural tube, where the neurons will innervate. This measurement was taken at the terminus of the leading process and at the position of the cell body. In both measurements, an increase in RGS3 shRNA-electroporated embryos was observed compared to control shRNA-electroporated embryos. *(B)* The distance of the farthest-migrated cell body was subtracted from this distance of its leading process to calculate the length of the leading process. No significant difference was observed in RGS3 shRNA-electroporated embryos compared to control shRNA-electroporated embryos. *=$p<0.05$. ns: $p>0.05$ (not significant).

Section 4.3 Overexpression of Each Isoform Individually

After knocking down all RGS3 isoforms simultaneously with shRNA, multiple phenotypes were observed. Intriguingly, each of these phenotypes corresponded to the three cell types in which RGS3 isoforms are differentially expressed: enhanced neurogenesis would occur in the placode, where RGS3hL and RGS3L are expressed; enhanced neuroblast differentiation would occur in the neuroblasts, where RGS3s and RGS3hs-HTMKE are expressed; and enhanced neuronal migration would occur in the neurons, where RGS3hs-HTMKE and RGS3hs-KYLER are expressed.

However, the specific functions of each isoform could not be identified by shRNA knockdown because the unique 5' sequences of each isoform are too short to design shRNAs to these regions. To dissect the specific functions of each isoform, I aimed to overexpress each isoform individually. I amplified and cloned each isoform into the overexpression vector pMES (Swartz et al., 2001). pMES contains a chicken β-actin promoter and a cytomegalovirus intermediate/early enhancer upstream of the cloning site. Downstream of the cloning site, pMES encodes an internal ribosomal entry site (IRES) followed by enhanced GFP (EGFP). This results in a bicistronic transcript which can be simultaneously translated by two ribosomes.

Although RGS3hL and C2PA later proved to be expressed in the placode (Figure 3.4B,C), I chose to focus my investigation on RGS3L because it was previously demonstrated to play a role in neuroepithelial progenitor maintenance (see Section 1.2.4.3.2) (Qiu et al., 2010). I later overexpressed RGS3hL to investigate the evolution of RGS3 (Section 5.3), and will draw comparisons when discussing the role of RGS3L.

For RGS3s and RGS3hs overexpression, I designed artificial constructs corresponding only to the shared coding sequences encoded by the terminal six exons of RGS3hL. For RGS3s, the overexpression construct lacked an N-terminal seven aa compared to the endogenous protein. These seven aa are encoded by the unique 5' exon of RGS3s, which was identified by 5' RACE (Section 3.2.2). Human and mouse do not possess these unique aa. Instead, the start codon begins with the first nucleotide of the shared coding exon (as in Figure 4.8). Thus while this construct is technically truncated, there is not a conserved importance of the truncated aa.

The first common exon of RGS3hs-HTMKE and RGS3hs-KYLER is exon 22 of RGS3hL. The fourth aa encoded by this exon is a methionine. I designed an overexpression construct that begins with this methionine, encoding the terminal 168 aa of RGS3hL. The homologous human construct has previously been shown to negatively regulate G protein signalling (Mittmann et al., 2001) (see 'RGS3S' in Table 1.2). Importantly, this construct contains the full RGS domain, and does not contain any N-terminal sequences present in RGS3s but not RGS3hs-HTMKE or RGS3hs-KYLER (Figure 4.8), which have been shown to play a number of regulatory functions (see Section 1.2.4.3.3). Henceforth I will refer to this construct as RGS3hs.

To test whether the overexpression constructs were capable of expressing stable transcripts, I ectopically expressed each vector in the non-placodal surface ectoderm and performed *in situ* hybridisation against the coding sequence. Because the pMES overexpression vector generates bicistronic transcripts, every EGFP-positive cell should also be positive for the overexpressed transcript. Indeed, in all cases, every EGFP-positive region stained positively for the respective *in situ* hybridisation probe (for n values, see legend of Figure 4.9). Furthermore, the stain in every case developed much

more quickly than endogenous stain. As a control for overexpression, empty pMES was similarly ectopically electroporated. Ectopic *in situ* hybridisation staining was never observed in pMES-electroporated embryos.

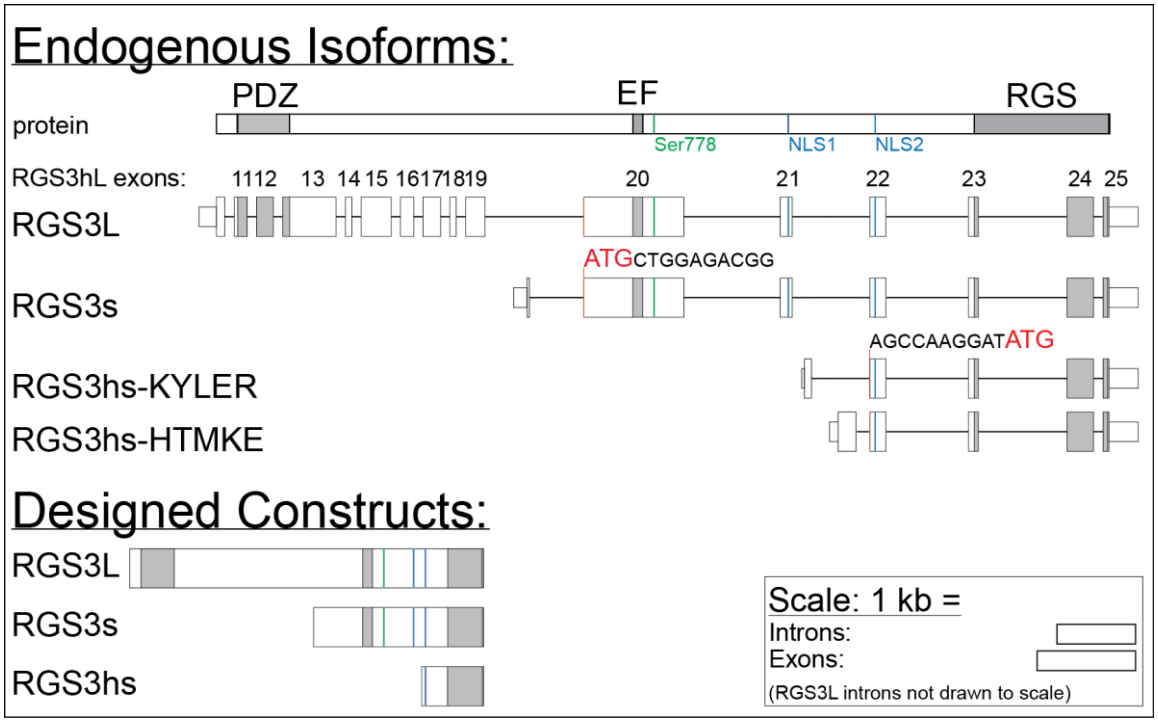


Figure 4.8. Constructs Designed for Individual Isoform Overexpression.
The RGS3L construct contained its full-length endogenous coding sequence, including the PDZ, EF Hand, and RGS domains (grey), as well as the 14-3-3-regulated Ser778 residue (green; see Section 1.2.4.3.3) and the two nuclear localisation sequences (blue). The RGS3s construct contains all of the endogenous coding sequence encoded by the final six exons of RGS3hL (exons 20-25), but lacks seven aa encoded by its unique exon. Instead, its start codon begins with the first nucleotide of RGS3hL exon 20 (red). The RGS3hs construct encodes most of the final four exons of RGS3hL. Its start codon begins at the 11th nucleotide of exon 22 (red). The resulting constructs are 799 aa, 408 aa, and 168 aa, respectively. Note: introns and exons are drawn according to the scale, but introns upstream of exon 20 are not drawn to scale.

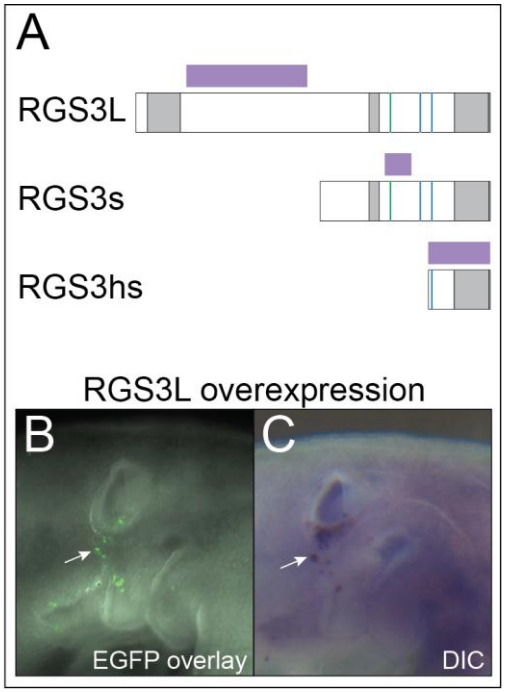


Figure 4.9. Ectopic Transcript Expression from Overexpression Constructs.
(A) Overexpression constructs were electroporated into non-placodal surface ectoderm and embryos were *in situ* hybridised with respective probes indicated in purple. Coloured vertical lines correspond to those in Figure 4.8 and Figure 1.11. *(B,C)* RGS3L shown as a representative example of ectopic transcript expression following overexpression. *(B)* EGFP fluorescence was overlaid on brightfield and imaged prior to *in situ* hybridisation, and then embryos were re-imaged after stain development *(C)*. Arrow indicates ectopic staining colocalised with EGFP fluorescence. Note: image in *(C)* corresponds to an embryo in which stain development was stopped before endogenous staining developed. In all pMES control overexpressions, ectopic staining was never observed. N values are as follows. RGS3L with RGS3L probe: n=2. RGS3L with RGS3s probe: n=1. pMES with RGS3L probe: n=7. RGS3s with RGS3s probe: n=3. pMES with RGS3s probe: n=3. RGS3hs with RGS3hs probe: n=3. pMES with RGS3hs probe: n=3.

Section 4.3.1 Overexpression of RGS3L

Section 4.3.1.1 The Role of RGS3L in Neurogenesis

RGS3L has previously been implicated in the negative regulation of neurogenesis in the cortex (see Section 1.2.4.3.2) (Qiu et al., 2010). To determine the role of RGS3L in the production of placodal neurons, I stained pMES-RGS3L-electroporated embryos with αNFM to mark neuroblasts and neurons, and αHuC/D to label neurons.

Quantitative analysis of confocal stacks showed that overexpression of RGS3L resulted in a complete abolishment of neuronal differentiation: an average of 3.25±1.57 HuC/D-positive neurons (n=8; $p=1.0x10^{-5}$) were counted compared to 80.83±10.61 in pMES controls (n=12) (Figure 4.10C), and the rare HuC/D-positive neurons observed were always EGFP-negative (Figure 4.10B, arrow). Similarly, only 1/11 embryos exhibited NFM-/EGFP-double positive neuroblasts (compared to 19/19 pMES controls). This complements the increased neurogenesis phenotype following RGS3 shRNA (Section 4.2.1), and suggests an extremely efficient role of RGS3L in the negative regulation of neuroblast commitment in the placode.

To dissect the biochemical function of RGS3L, I first compared RGS3L overexpression to overexpression of RGS3s. This construct lacks the N-terminal 391 aa of RGS3L, including the PDZ domain (see Figure 4.8). In contrast to the total lack of neurogenesis seen with RGS3L overexpression, RGS3s overexpression did not affect the average number of HuC/D-positive neurons (Figure 4.10C) (59.50±10.06, n=10, $p=0.080$), and many EGFP-positive neuroblasts and neurons were present (Figure 4.12B). A similar result was observed following overexpression of RGS3hs (Figure 4.10C; Figure 4.13B) (average number of neurons: 57.83±10.22, n=6, $p=0.070$). This demonstrates that the N-

terminal 391 aa of RGS3L is essential for its neurogenesis overexpression phenotype. Because RGS3hs encodes little more than the RGS domain, this suggests that the RGS domain is not sufficient to negatively regulate neurogenesis in the placodes.

To test whether the RGS function of RGS3L is required to negatively regulate neurogenesis, I mutated a conserved asparagine residue in the RGS domain. This asparagine (Asp740 of chicken RGS3L) was originally identified in RGS4 (a paralogue member of the R4 subfamily; see Figure 1.12) as structurally important for stabilising the water molecule used in GTP hydrolysis (Tesmer et al., 1997). A range of single-aa substitutions were subsequently tested, demonstrating an essential role of this asparagine in Gαq and Gαi binding (Posner et al., 1999). Among these, substitution with alanine was most efficient at abrogating RGS activity, so I decided to substitute AspN740 with alanine (N740A). In RGS3, this mutation has been shown to prevent Gαi binding and inhibition (Vogt et al., 2007; Yau et al., 2008). Overexpression of an RGS3L construct carrying the homologous mutation (RGS3LN470A) in the placode resulted in a similar neurogenesis phenotype to that seen with RGS3L overexpression (Figure 4.10C) (average number of neurons: 9.50±5.98, n=4, p=2.0x10^{-5}). I did observe an increase in the number of embryos which contained delaminated, EGFP-/NFM-positive neuroblasts (4/6 compared to 1/11 RGS3L-electroporated embryos; not shown). However these neuroblasts were not numerous enough to account for the decrease in number of neurons compared to control, as an average of only 4.75±1.38 EGFP-positive neuroblasts were counted in these four embryos.

Taken together, these data suggest that RGS function might be important in ectopically preventing neuroblast differentiation, but is largely dispensable for the RGS3L overexpression phenotype.

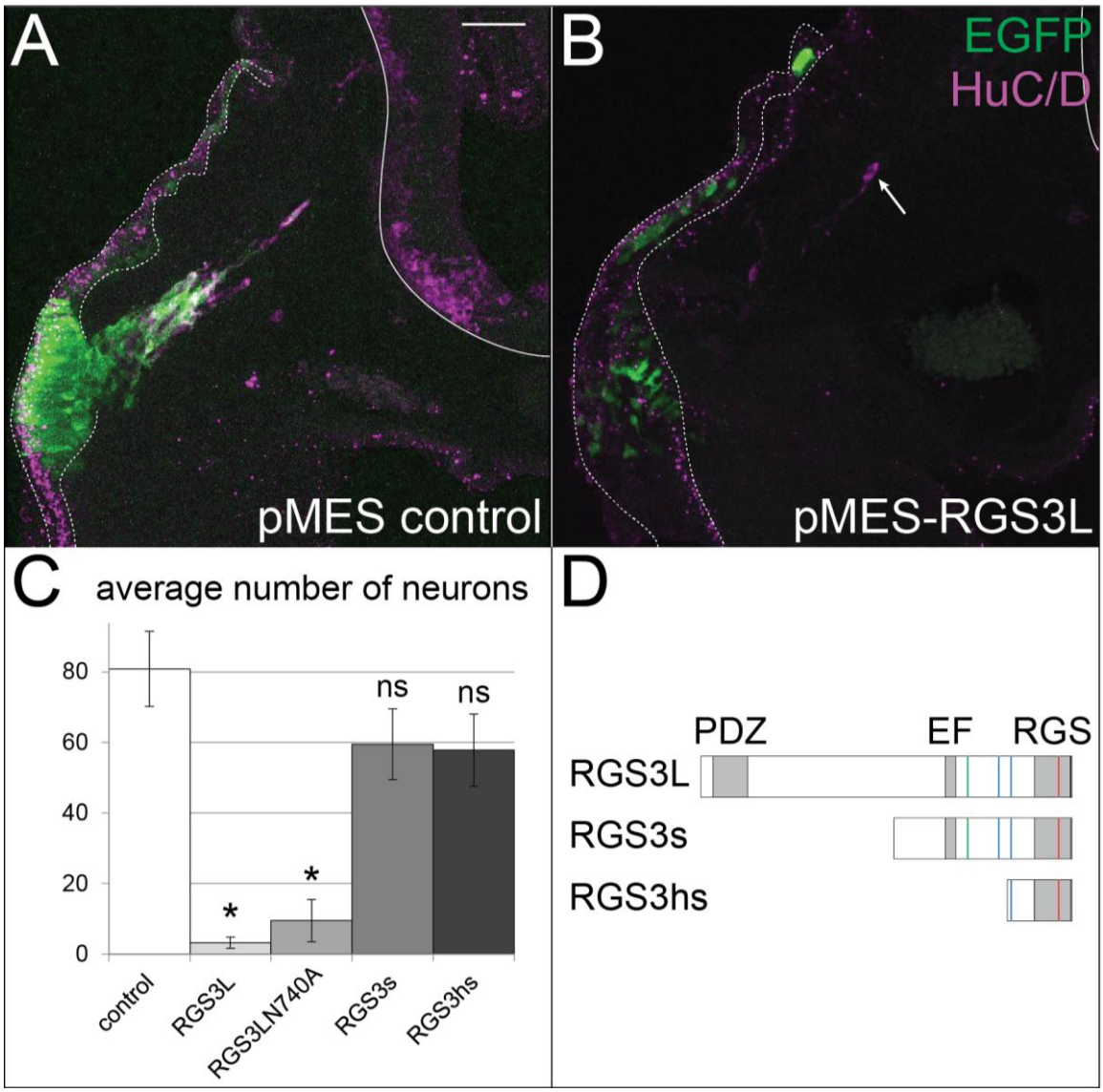


Figure 4.10. Overexpression of RGS3L Abolishes Neurogenesis.
Overexpression of RGS3L *(B)* resulted into the placodes resulted in a total lack of neurogenesis compared to empty pMES controls *(A)*, with the rare HuC/D-positive neuron (arrow) always EGFP-negative. *(C)* Quantification of this effect. Mutation of a critical asparagine residue in the RGS domain (N740A) results in a similar reduction in neurogenesis, suggesting it is dispensable to cause this effect. By contrast, RGS3s and RGS3hs do not affect neurogenesis. *(D)* Structural differences between the three isoforms. RGS3L possesses 391 aa upstream of the start of RGS3s, including a PDZ domain. Blue and green vertical lines correspond to those in Figure 4.8 and Figure 1.11. The red line indicates the position of the critical asparagine residue. n values: pMES: 12; RGS3L: 8; RGS3LN740A: 4; RGS3s: 10; RGS3hs: 6. *=p<0.05. ns: p>0.05 (not significant). Scale bar in *(A)*: 50µm.

Section 4.3.1.2 The Role of RGS3L in Epithelial Integrity

The above data show an essential role of the N-terminal 391 aa of RGS3L in negatively regulating neurogenesis. Importantly, this sequence contains a PDZ domain. PDZ domains are present in a multitude of proteins which localise to the apical surface of epithelia, including the Par-aPKC complex (Suzuki and Ohno, 2006). In neuroepithelia, maintenance of apical polarity is essential for the proper control of neurogenesis. Disruption of apico-basal polarity in the developing cortex perturbs the regulation of neurogenesis in VZ progenitors (Cappello et al., 2006; Costa et al., 2008; Srinivasan et al., 2008). Similarly, mouse embryos conditionally mutant for the small GTPase RhoA exhibit disruptions to the apical surface of the midbrain and concomitant reduction in neurogenesis (Katayama et al., 2011).

Because of its endogenous expression in the placodal epithelium and the importance of apical polarity in the regulation of neurogenesis, I hypothesised that RGS3L might play a role in regulating apical polarity. To explore this idea, I analysed the integrity of RGS3L-electroporated placodes at the apical surface. Intriguingly, I found defects in epithelial integrity in 8/11 embryos (Figure 4.11). Of these, 6 embryos exhibited protrusion of cell bodies on the apical surface of the embryo (Figure 4.11D-F). Three embryos displayed a disrupted epithelium in which the underlying mesenchyme was exposed to the outside of the embryo (Figure 4.11G-I), similar to that observed in the midbrains of RhoA knockout mice (Katayama et al., 2011). Importantly, non-placodal surface ectoderm was never observed to be defective, indicating the specificity of this phenotype to the neuroepithelial placode. Only 1/20 pMES-electroporated embryos exhibited protrusion of cell bodies at the apical surface of the placodes, and none showed epithelial disruption (Figure 4.11A-C). Of six RGS3LN740A-electroporated embryos,

two contained placodes which protruded cell bodies at the apical surface, and none exhibited epithelial disruption (not shown). This suggests that RGS3LN470A overexpression does not completely rescue the RGS3L effect on placodal integrity, but more embryos will need to be analysed to determine the extent to which the effect is ameliorated.

Interestingly, I also observed in 2/11 pMES-RGS3L-electroporated embryos ectopic EGFP-positive rosette-like epithelial structures in the mesenchyme (Figure 4.11J-L). In both cases, these structures were observed in proximity (on the same transverse section) to disrupted placodes, suggesting that they possibly formed from destabilised surface epithelial cells. Similar structures were observed in the neuroepithelium of RhoA knockout mice (Katayama et al., 2011), as well as the chick spinal cord following overexpression of Par3, an apical polarity protein which also contains a PDZ domain (Afonso and Henrique, 2006). This suggests that RGS3L might regulate epithelial integrity (as well as neurogenesis) through regulation of apical polarity. Further analysis of the localisation of apical polarity markers such as Par3 following RGS3L overexpression will shed light on this role.

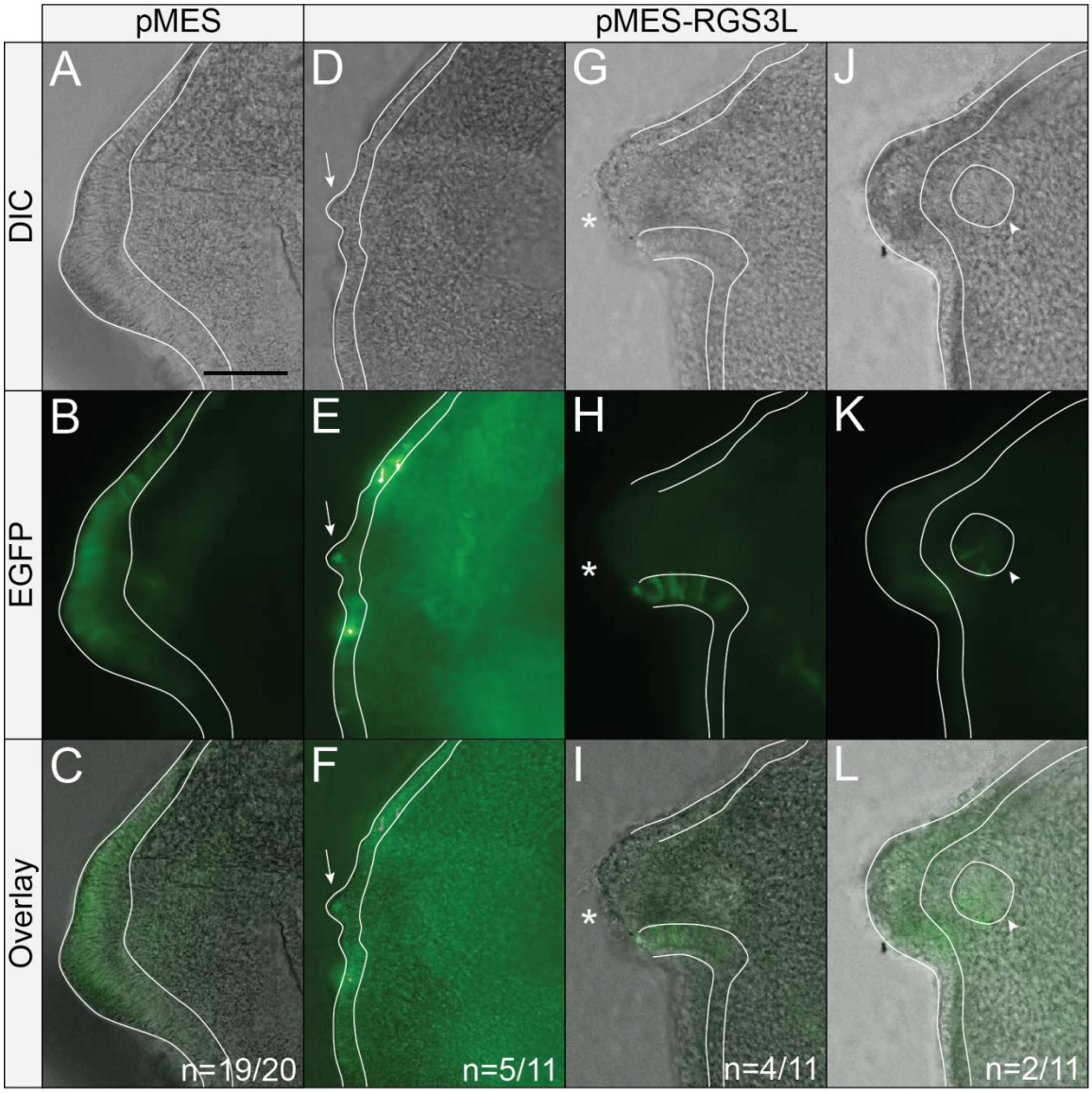


Figure 4.11. Effects of RGS3L Overexpression on Epithelial Integrity.
DIC and EGFP fluorescence imaged with an Olympus BX51 compound light microscope (Section 2.10). *(A-C)* pMES-electroporated placodes exhibited normal, pseudostratified morphology. By contrast, 8/11 pMES-RGS3L-electroporated placodes showed defects in epithelial integrity. These included protrusion of EGFP-positive cell bodies at the apical surface *(D-F)* (arrow), disruption of the apical and basal surfaces of the placode *(G-I)* (asterisk), or ectopic EGFP-positive epithelia present within the mesenchyme *(J-L)* (arrowhead). Epithelial surfaces are marked in white. Note: *(G-I)* and *(J-L)* are different focal planes of the same section. Scale bar in *(A)*: 100µm.

Section 4.3.2 Overexpression of RGS3s

Though RGS3s was the first RGS3 isoform identified (Druey et al., 1996) and the most extensively studied *in vitro,* an *in vivo* role in development has not been characterised. In different *in vitro* contexts RGS3s has been described to play a number of roles in the regulation of G protein signalling. Since G protein signalling is broadly implicated in neuronal development (Section 1.2.3.1), it was intriguing to observe a very specific expression pattern in neuroblasts in the staging area adjacent to the epibranchial placodes. The increase in neuroblast differentiation following RGS3 shRNA (Section 4.2.4.2) suggests that RGS3s might be important to mediate this function.

To investigate the role of RGS3s in placode-derived neuroblasts, pMES-RGS3s was electroporated into the placodes as described (Section 2.5). Overexpression of RGS3s did not affect ability of the placode to produce committed EGFP-positive neuroblasts and neurons (Section 4.3.1.1), and differentiated EGFP-positive neurons were normal in terms of migration and morphology (Section 4.3.3).

However, analysis of EGFP-positive neuroblasts showed that they were affected by RGS3s overexpression. When the distance between the ventral-most delaminated neuroblast and the first HuC/D-positive neuron was normalised against the total distance to the dorsal neural tube as in Section 4.2.4.1, I found that αHuC/D stained farther from the placode following RGS3s overexpression (20.54±2.62%, n=9, p=0.018) compared to controls (13.09±1.81%, n=7), indicating a protraction of the staging area (Figure 4.12C). This complements the shRNA phenotype, in which a retraction of the staging area was observed (Figure 4.5L). Consistently, whereas RGS3 shRNA increased the proportion of electroporated neurons out of the total pool of electroporated neuroblasts and neurons (Figure 4.6), RGS3s overexpression decreased this proportion (0.60±0.04, n=11,

p=0.012) compared to pMES control (0.72±0.03, n=13) (Figure 4.12D). Together this suggests that RGS3s actively inhibits neuroblast differentiation.

In either measurement, RGS3hs overexpression caused no significant difference compared to pMES controls (Figure 4.12C,D) (αHuC/D staining: 12.19±3.26%, n=5, *p*=0.409; proportion of electroporated neurons: 0.71±0.02, n=7, *p*=0.405).

This demonstrates that the N-terminal 240 aa of RGS3s which are not present in RGS3hs are essential to affect neuroblast differentiation. This region has previously been shown to regulate RGS activity of RGS3s, either indirectly by affecting subcellular localisation, or directly by promoting 14-3-3 binding (Section 1.2.4.3.3). However, it has also been shown to act independently of RGS function in the regulation of TGFβ signalling (Yau et al., 2008). To test the importance of RGS function in RGS3s-mediated inhibition of neuroblast differentiation, I introduced the previously used N740A mutation (Section 4.3.1.1) into the RGS domain of RGS3s (RGS3sN740A) and overexpressed it as before. Embryos electroporated with this construct exhibited no significant difference in the proportion of EGFP-positive neurons compared with controls (Figure 4.12D) (0.70±0.07, n=3, *p*=0.400), indicating that RGS3s requires Gα binding activity to negatively regulate neuroblast differentiation.

Together, this suggests that the RGS domain of RGS3s cooperates with the N-terminus to inhibit neuroblast differentiation. Importantly, this region contains an EF Hand domain, which binds Ca^{+} and can induce conformational change in tertiary structure (Lewit-Bentley and Réty, 2000). The EF Hand domain of RGS3s has previously been shown to be essential for its negative regulation of GABA-induced inhibition of Ca^{2+} currents (Tosetti and Dunlap, 2004; Tosetti et al., 2003). The authors of these studies proposed a

mechanism whereby the EF Hand domain activates RGS function of RGS3s, though a dependence on the RGS domain was not demonstrated.

To test whether the EF Hand domain plays an important role in the function of RGS3s, I generated an RGS3s construct in which this domain was deleted (RGS3sΔEF). Surprisingly, overexpression of this construct produced a more dramatic effect on neuroblast differentiation compared to RGS3s (Figure 4.12D), reducing the proportion of EGFP-positive neurons to 0.31±0.09 (n=5; p=0.004; p (to RGS3s)=0.015).

Taken together, these data suggest that the RGS domain of RGS3s negatively regulates neuroblast differentiation, and the EF Hand domain antagonises this function. This antagonism could be the result of an EF Hand-induced conformational change in the RGS domain, rendering it inactive. Further analysis using an EF Hand deletion-N740A double mutant construct will help to resolve this mechanism.

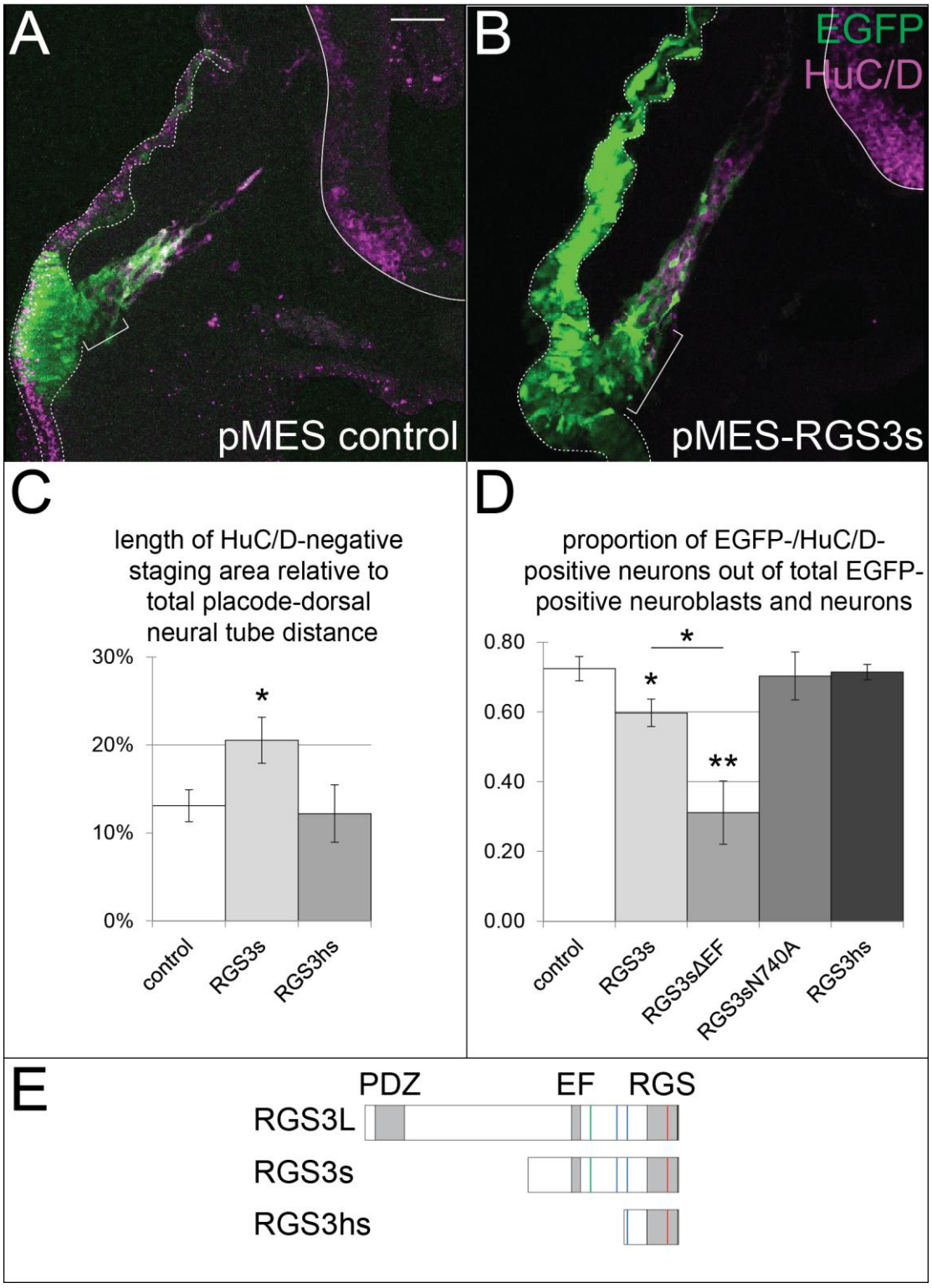


Figure 4.12. RGS3s Overexpression Affects Spatial HuC/D Expression and Neuroblast Differentiation.

Figure legend on next page.

Figure 4.12. RGS3s Overexpression Affects Spatial HuC/D Expression and Neuroblast Differentiation.
Overexpression of RGS3s *(B)* resulted in a protracted HuC/D-negative staging area relative to empty pMES control *(A)* (indicated by brackets). *(C)* Quantification of this effect. *(D)* Fewer EGFP-/HuC/D-double positive neurons were counted relative to the total number of EGFP-positive neuroblasts and neurons, suggesting a decreased proclivity for neuroblasts to differentiation. Surprisingly, deletion of the EF Hand domain (RGS3sΔEF) enhanced this effect. By contrast, mutation of a critical asparagine residue in the RGS domain of RGS3s (RGS3sN740A) suppressed the effect. Overexpression of RGS3hs had no effect. The composition of each isoform is indicated in *(E)* as in Figure 4.10. *=p<0.05. **=p<0.005. Scale bar in *(A)*: 50μm.

Section 4.3.3 Overexpression of RGS3hs

The RGS3 shRNA phenotype of enhanced neuronal migration directly implicates RGS3hs-HTMKE and/or RGS3hs-KYLER, which are the only RGS3 isoforms expressed in placode-derived migratory neurons (Section 4.2.5). To investigate the functions of both, I electroporated placodes with the pMES-RGS3hs construct containing their shared coding sequence. As described in Section 4.3.1.1 and Section 4.3.2, placodal progenitors and immature neuroblasts were unaffected by RGS3hs overexpression. However, neuronal migration was impaired (Figure 4.13C). Normalised to the total distance between the ventral placode and the dorsal neural tube (as measured in Section 4.2.4.1, Section 4.2.5, and Section 4.3.2), decreases in the average relative positions of the leading cell body (pMES: 74.86±5.41%, n=7; RGS3hs: 57.87±7.24%, n=5, p=0.048) and the terminus of its leading process (pMES: 84.61±4.33%, n=7; RGS3hs: 61.38±7.09%, n=5, p=0.014) were observed.

In addition, I observed morphological changes associated with impaired migration. Contrary to the RGS3 shRNA phenotype, in which no change in leading process length was observed compared to controls, a dramatic shortening of these processes was measured following RGS3hs overexpression compared to pMES controls (Figure 4.14A) (pMES: 47.32±12.86μm, n=7; RGS3hs: 13.99±1.13μm, n=5, p=0.021). Furthermore,

whereas pMES control neurons almost always protruded two projections in opposite directions (average number of projections: 2.05±0.05, n=19 cells of 6 embryos), neurons overexpressing RGS3hs exhibited multiple projections (Figure 4.14B) (average number of projections: 2.90±0.23, n=10 cells of 3 embryos, p=0.003).

Importantly, overexpression of RGS3s resulted in no significant difference compared to pMES controls in any of these phenotypes (cell body position: 64.28±6.05%, n=9, p=0.107; leading process terminus: 73.83±7.15%, n=9, p=0.110; projection length: 45.77±13.68, n=9, p=0.468; number of projections: 2.22±0.10, n=18 cells of 8 embryos, p=0.074). This further validates the RGS3s-specific effects observed in neuroblast differentiation (Section 4.3.2), and suggests that the effects of RGS3hs overexpression are also due to regulation of a specific substrate. Because RGS3hs contains little more than an RGS domain, I hypothesised that RGS activity was essential for its overexpression phenotype. To test this, I introduced the N740A mutation into the RGS domain of RGS3hs (RGS3hsN740A) and overexpressed it as before. Overexpression of this construct resulted in no significant difference between pMES controls (Figure 4.13C and Figure 4.14A,B) (cell body position: 63.36±3.88%, n=5, p=0.058; leading process terminus: 76.12±1.45%, n=5, p=0.0.52; projection length: 57.43±21.83, n=5, p=0.351; number of projections: 2.20±0.11, n=15 cells of 4 embryos, p=0.063).

Taken with the enhanced migration shRNA phenotype, these data suggest an important role of RGS3hs-HTMKE and/or RGS3hs-KYLER in the negative regulation of migration, and a dependence on the RGS domain to exert this function.

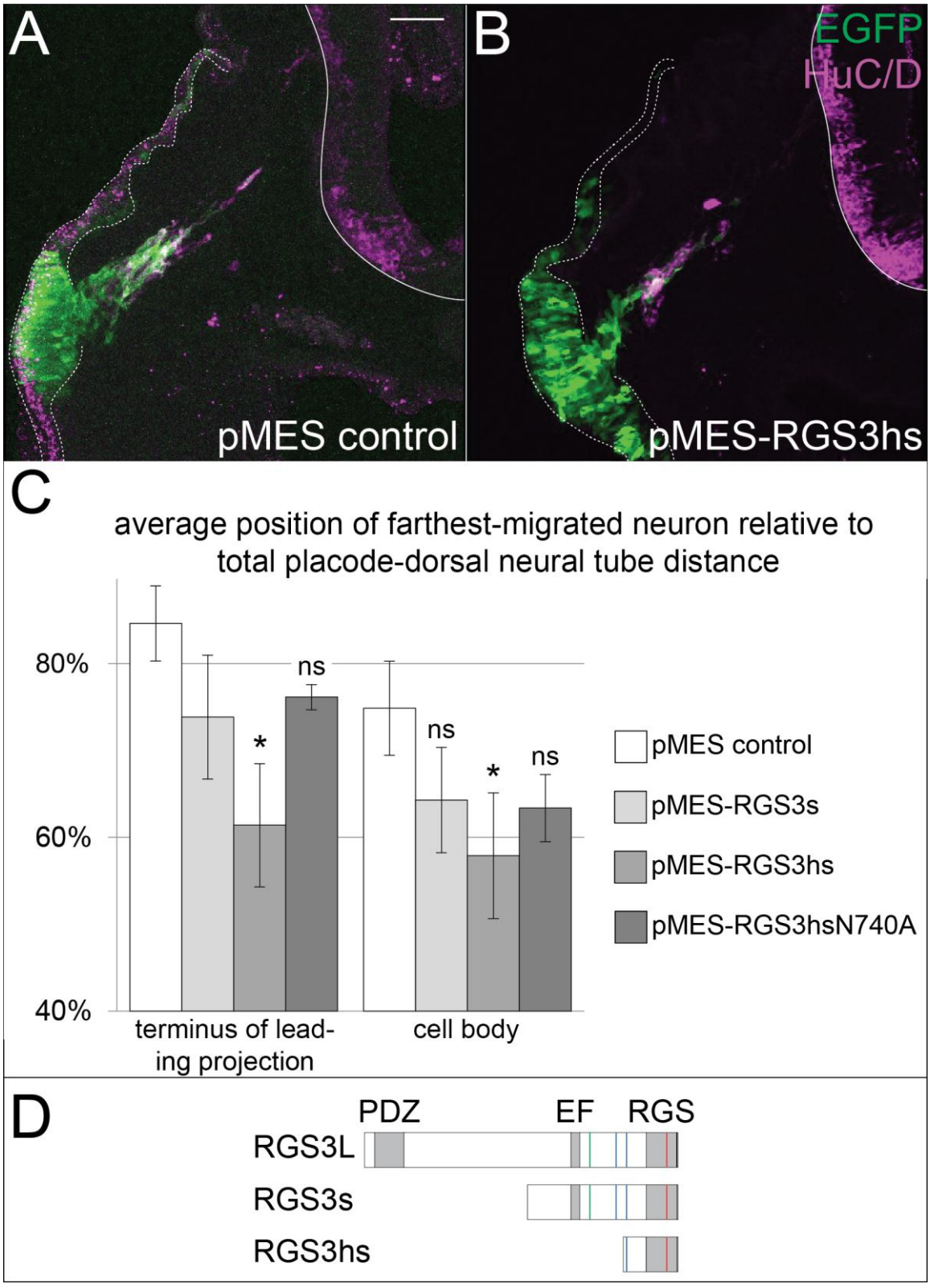


Figure 4.13. RGS3hs Overexpression Affects Neuronal Migration.
Figure legend on next page.

Figure 4.13. RGS3hs Overexpression Affects Neuronal Migration.
Overexpression of RGS3hs *(B)* resulted in decreased migration compared to pMES control *(A)*, seen at the level of the position of the leading cell body and the terminus of its leading projection. These values were normalised as a percentage against the total distance between the ventral-most delaminated neuroblast and the dorsal neural tube *(C)*. RGS3s overexpression had no significant effect compared to pMES, nor did a single aa substitution at a critical asparagine residue in the RGS domain of RGS3hs (RGS3hsN740A). The composition of each isoform is indicated in *(E)* as in Figure 4.10. *=p<0.05. ns=p>0.05 (not significant). Scale bar in *(A)*: 50µm.

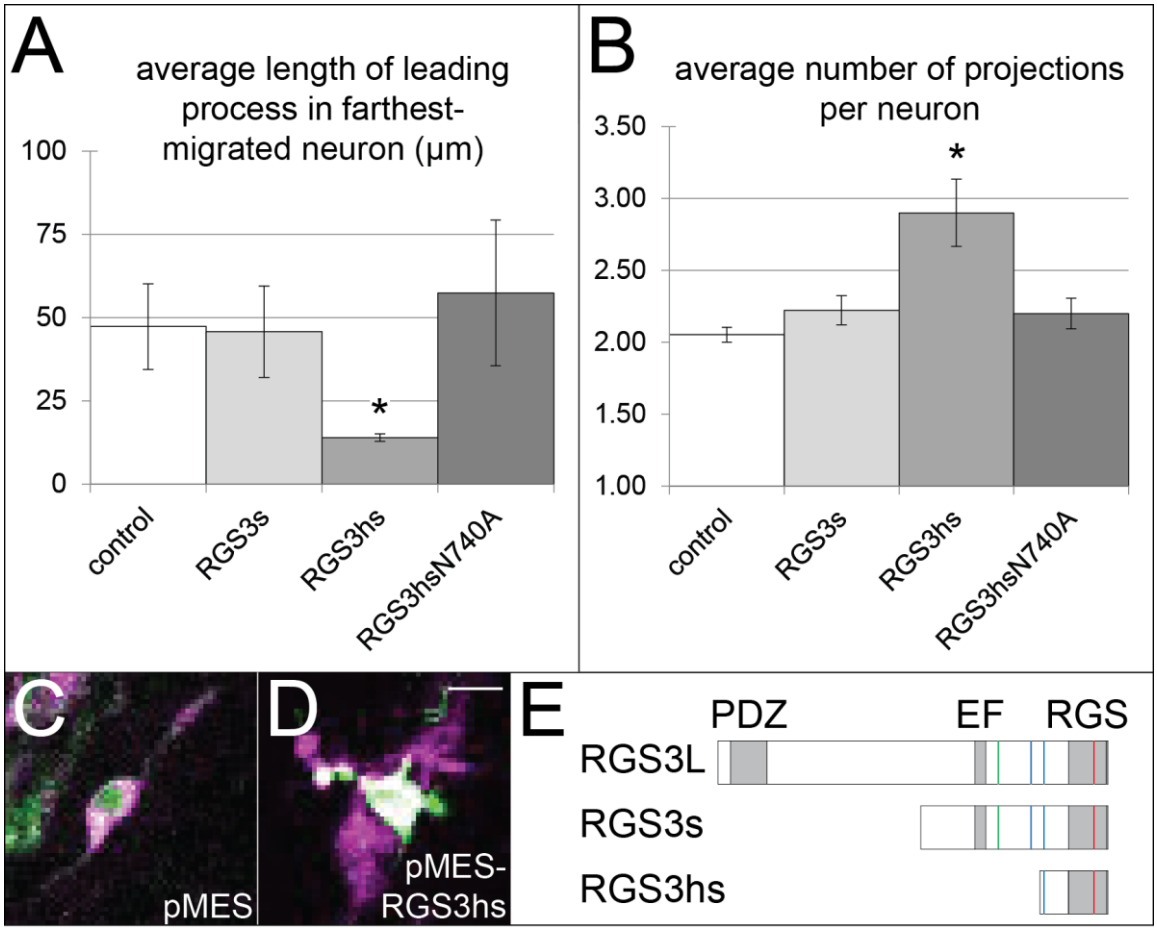


Figure 4.14. RGS3hs Overexpression Affects Neuronal Morphology.
Perturbed migration following RGS3hs overexpression observed in Figure 4.13 was associated with abnormal neuronal morphology. *(A)* The distance from the placode of the cell body of the farthest-migrating neuron was subtracted from that of the terminus of its leading process to find the average length of this process (described in Section 2.12). RGS3hs overexpression decreased this length significantly but RGS3s and RGS3hsN740A did not. *(B)* In addition, cells were more likely to be multipolar following RGS3hs overexpression compared to pMES, RGS3s or RGS3hsN740A, resulting in a greater average number of projections. *(C-D)* Optical confocal slices (1.44µm thick) of pMES or pMES-RGS3hs-electroporated embryos, showing a multipolar morphology with short projections *(D)* compared to the normal bipolar morphology *(C)*. Green: EGFP; magenta: HuC/D. The composition of each isoform is indicated in *(E)* as in Figure 4.10. *=p<0.05. Scale bar in *(D)*: 10µm.

Section 4.4 Discussion

Collectively, these data complement the differential spatiotemporal expression patterns for each RGS3 isoform observed in Chapter 3. Simultaneous knockdown of all isoforms (except C2PA) results in three distinct phenotypes relating to the three phases of neuronal differentiation: an enhanced rate of neurogenesis corresponding to commitment of placodal progenitors; an increased proportion of HuC/D-positive neurons and retraction of the staging area corresponding to differentiation of neuroblasts; and an enhanced displacement of the migratory stream toward the dorsal neural tube corresponding to migration of neurons. Consistently, overexpression of each isoform individually produces complementary phenotypes. Importantly, these experiments were conducted by introducing constructs into the placode, and thus isoforms expressed in neuroblasts and neurons were ectopically expressed. However, each overexpression experiment only affected the phase of differentiation in which the isoform is endogenously expressed: RGS3hs overexpression perturbed neuronal migration but did not affect placodal commitment or neuroblast differentiation; RGS3s overexpression inhibited neuroblast differentiation but not placodal commitment or neuronal migration; and RGS3L only affected placodal commitment. On this latter point, it is important to note that RGS3L overexpression prevented the generation of neuroblasts and neurons, and thus a potential ectopic role in these populations could not be analysed. Taken together, these experiments provide intriguing new insights into the roles of RGS3 isoforms and the processes of commitment, differentiation and migration.

Section 4.4.1 Regulation of Progenitor Commitment in the Placode by RGS3hL and RGS3L

RGS3hL, C2PA, and RGS3L are all expressed in the placode and not in delaminated neuroblasts or neurons. Simultaneous knockdown of RGS3hL and RGS3L resulted in an increase in committed neuroblasts and neurons, suggesting an endogenous role in the maintenance of the progenitor state. Overexpression of RGS3L resulted in the abolishment of neurogenesis, with a concomitant disruption of epithelial organisation. Overexpression of RGS3hL (see Section 5.3), which also encodes the PDZ, EF Hand, and RGS domains in addition to an N-terminal C2 domain (Section 1.2.4.1), preliminarily suggested a similar role. EGFP-/HuC/D-double positive neurons were never observed in three RGS3hL-overexpressing embryos, but none of these embryos exhibited epithelial defects. As this is a qualitative result, more embryos will need to be analysed to determine whether RGS3hL plays a role in epithelial organisation. However, it is clear from these data that RGS3hL and RGS3L are both sufficient to negatively regulate neurogenesis. RGS3L was previously investigated in the developing mouse cortex by using homologous recombination to insert a stop codon before the PDZ domain, creating a null RGS3L mutation without affecting RGS3s or RGS3hs sequences (Qiu et al., 2010). However, a second consequence of this mutation is the truncation of RGS3hL and C2PA, resulting in C2 domain-only isoforms. Whether both isoforms are required to prevent progenitor commitment will only be resolved with isoform-specific knockdown. Equally important will be overexpression and knockdown experiments on C2PA, which is also expressed in the placode.

It is possible that defects in epithelial integrity following RGS3L overexpression relate to activity at apical complexes, where PDZ domain- and PDZ-binding motif-containing proteins are abundant (Suzuki and Ohno, 2006). To this end, because the PDZ domain of

RGS3L is capable of recognising PDZ-binding motifs of several different proteins (Meyer et al., 2004), it could be acting dominant negatively on non-endogenous binding partners when overexpressed. However, unpublished work in our laboratory from Anna Zornoza showed antibodies recognising apical markers Par3 and aPKC label the apical surface of non-neural surface ectoderm as well as the placode. Ectopic overexpression of RGS3L in non-neural surface ectoderm did not result in perturbations to epithelial integrity, suggesting a disruption of apico-basal polarity would be specific to a binding partner specifically expressed in the placode. This suggests that RGS3L, and possibly RGS3hL, might play an endogenous role at apical complexes to regulate neurogenesis. The apical surface of neuroepithelial progenitors has recently been shown to be critical for progenitor maintenance, and failure to abscise the apical membrane prevents neurogenesis (Das and Storey, 2014). Further analysis of the subcellular localisation of RGS3L and RGS3hL and the localisation of apical markers following their overexpression will help to resolve their endogenous role(s) in apical complexes.

It remains to be seen whether the PDZ domain of RGS3L and RGS3hL is sufficient to negatively regulate neurogenesis, or if other domains play an important regulatory role. Importantly, overexpression of RGS3LN740A, which lacks GAP activity, did not revert the RGS3L overexpression phenotype. Epithelial defects were still observed (though in reduced frequency: 2/6 embryos compared to 8/11 pMES-RGS3L-electroporated embryos), as was a failure to generate neurons (though some EGFP-positive neuroblasts were generated). This is in contrast to the mouse cortex, where a homologous asparagine-to-aspartate mutation occluded the effect of RGS3L overexpression (Murai et al., 2010). However, the readout for this experiment was migration of electroporated cells into the CP (prevented by RGS3L overexpression), and neither a role in epithelial

integrity nor the neuronal identity of the electroporated cells was analysed. Furthermore, this effect was only demonstrated when RGS3L was co-overexpressed with EphrinB1. Via in situ hybridisation analysis, however, I found EphrinB1 and its paralogue EphrinB2 to be expressed in somites of HH18 chick embryos as previously reported (Koblar et al., 2000; Krull et al., 1997), but not in the placodes (not shown).

Finally, it is important to note that the functional consequence of the N740A mutation is solely an inability to bind Gα. RGS3 is independently capable of regulating Gβ1γ2 heterodimers (Shi et al., 2001; Vogt et al., 2007). In fact, the homologous asparagine-to-alanine mutation in human RGS3s was more efficient at reducing Gβ1γ2-induced downstream transcription than wild-type RGS3s, possibly because it prevented competition with Gα (Vogt et al., 2007). In addition, a similar mutation in the RGS domain preventing Gα binding did not inhibit $G\beta_1\gamma_2$ binding, and both the N and C termini (corresponding to aa 629-827 and 828-1036 of chicken RGS3hL, respectively) were sufficient to immunoprecipitate with Gβ1γ2 (Shi et al., 2001). Thus multiple modules are present between the PDZ and RGS domains of RGS3L and RGS3hL which might play important roles in the regulation of neurogenesis. An essential first step toward elucidating the C-terminal regulatory role of RGS3hL and RGS3L will be to delete the entire RGS domain, followed by other regions of the protein, and analyse the overexpression effects of these constructs.

Section 4.4.2 Regulation of Neuroblast Differentiation by RGS3s

The knockdown and overexpression experiments presented in this chapter very strongly implicate RGS3s in the regulation of neuroblast commitment. Simultaneous knockdown of all isoforms caused a retraction of the staging area, measured with αHuC/D and,

preliminarily, by *in situ* hybridisation against SCG10. Conversely, overexpression of RGS3s, but not RGS3hs, resulted in protraction of the HuC/D-negative staging area. This accompanies a decrease of the neuroblast pool following knockdown, and an increase of the neuroblast pool following overexpression, relative to the pool of differentiated neurons. Collectively this suggests that RGS3s normally negatively regulates the differentiation of neuroblasts into neurons.

The mechanism of this regulation is entirely dependent on Gα binding by RGS3s, since overexpression of RGS3sN740A caused no effect on neuroblast differentiation. A G protein regulatory role of RGS3s has not been described during neuronal differentiation, but RGS3s has been shown to negatively regulate MAPK kinase activation downstream of the G protein-coupled LPA receptor (Chatterjee et al., 1997b; Grüning et al., 1999). LPA receptor 1 (LPAR1) expression is enriched in the VZ and SVZ of the mouse cortex (Hecht et al., 1996), and LPA promotes neuronal differentiation in dissociated cortical neuroblasts (Fukushima et al., 2007). This suggests a potential G protein-coupled pathway on which RGS3s might act to negatively regulate neuroblast differentiation. I have cloned and stained *in situ* hybridisation probes for two LPA receptors (including LPAR1) and found no detectable expression in the placodes; however, the chicken genome encodes six LPA receptors (Kent et al., 2002), and the expression of the other four remains to be tested.

The finding that deletion of the EF Hand domain of RGS3s enhanced its overexpression phenotype is intriguing. It is possible that Ca^{2+} binding induces an inhibitory conformational change in the RGS domain. Alternatively, as in the case of the yeast trehalase enzyme Nth1 (Kopecka et al., 2014), it is possible that inhibitory 14-3-3 binding is mediated by the EF Hand domain (see Section 1.2.4.3.3). In conjunction with

or independent from either of these ideas, it is lastly possible that the EF Hand domain alters RGS activity by changing the subcellular localisation of RGS3s. In support of this hypothesis, the N-terminus of RGS3s was previously shown to translocate from the cytoplasm to the membrane of human mesangial cells upon treatment with a Ca^{2+} ionophore (Dulin et al., 1999).

Whatever the mechanism of EF Hand-mediated regulation of the RGS domain, these results oppose the results of previous experiments on the EF Hand domain of RGS3s, which showed a dependence on the EF Hand domain for RGS3s to cause an overexpression phenotype (Tosetti and Dunlap, 2004; Tosetti et al., 2003). Dissociated DRG neurons treated with GABA produced an inhibition of Ca^{2+} influx, and RGS3s overexpression attenuated this inhibition in a manner dependent on its EF Hand domain. However, it was not distinguished whether the Ca^{2+} response was mediated by the G protein-coupled $GABA_B$ receptor, or the ionotropic $GABA_A$ receptor. Furthermore, a dependence on RGS function of RGS3s was not demonstrated.

Instead, my data from Section 4.3.2 suggest that, via the EF Hand domain, Ca^{2+} plays an important function in negatively regulating RGS3s. This is intriguing in light of the previously characterised role of Ca^{2+} in differentiation of neuroblasts of the CNS. Undifferentiated cells of the VZ and SVZ exhibit spontaneous fluctuations of intracellular Ca^{2+} concentrations (Owens and Kriegstein, 1998). *In vitro*, undifferentiated cells dissociated from the SVZ depend on voltage-gated Ca^{2+} channels to differentiate into neurons (Lepski et al., 2013). Interestingly, a voltage-gated Ca^{2+} channel subunit, CACNG4, has been shown to be expressed in neuroblasts and neurons derived from the cranial sensory placodes (Kious et al., 2002).

Together, this suggests a mechanism by which Ca^{2+} influx in placode-derived neuroblasts promotes neuronal differentiation by binding to the EF Hand domain of RGS3s and negatively regulating it. This mechanism likely inactivates or mislocalises the RGS domain, since its activity is required for its inhibition of neuroblast differentiation. It remains to be confirmed the degree to which Ca^{2+} influx is required for placode-derived neuroblast differentiation, and the downstream pathway(s) upon which RGS3s regulates.

Section 4.4.3 Regulation of Neuronal Migration by RGS3hs

Finally, the data presented here suggest a role for RGS3 isoforms in neuronal migration. In particular, the knockdown phenotypes relating to enhanced migration suggest an endogenous role of RGS3hs-KYLER and/or RGS3hs-HTMKE, which are the only isoforms expressed in these neurons, in the regulation of this migration. This is consistent with the previously demonstrated roles of RGS3hs in negatively regulating lymphocyte migration (Reif and Cyster, 2000; Williams et al., 2013), and the negative regulation of breast cancer metastasis by its paralogue RGS4 (Mu et al., 2012; Xie et al., 2009).

However, it is possible that a greater displacement of neurons observed following RGS3 shRNA is not a result of loss of RGS3hs but rather a secondary consequence of enhanced neurogenesis and neuroblast differentiation. To address this, I overexpressed the shared coding sequence between RGS3hs-KYLER and RGS3hs-HTMKE. This resulted in a complementary effect, with a perturbation of displacement of neuronal cell bodies and their processes. In addition, cell bodies were multipolar, and the processes they projected were significantly shorter. This morphology has previously been associated with a failure to migrate in cortical neurons (Qin and Zhang, 2012).

These data potentially illuminate a mechanism by which RGS3hs negatively regulates neuronal migration. Leading process dynamics are governed by the stabilisation and destabilisation of actin filaments (Hutchins et al., 2013; Marín et al., 2010). A critical mediator of actin flow is the activation of Myosin II downstream of IP_3 signalling (Hutchins et al., 2013). IP_3 is produced from PIP_2 by the catalytic activity of PLC-β, which is activated by Gαq (see Section 1.2.2.3). Given the previously demonstrated ability of RGS3 to bind and inhibit Gαq (see Section 1.2.2.4), it is possible that RGS3hs negatively regulates this pathway in migratory neurons. This is bolstered by the complete requirement of GAP activity of RGS3hs, as pMES-RGS3hsN740-electroporated neurons resembled pMES controls in terms of migration and morphology. Hypothetically, the short projections observed following RGS3hs overexpression could be the result of perturbed Myosin II activation downstream of Gαq signalling. In the absence of RGS3hs following shRNA knockdown, leading processes would be more stable, leading to increased displacement of these processes toward the dorsal neural tube. Neuronal cell bodies would respond and translocate with the projections, leading to enhanced neuronal migration. The effects of Gαq knockdown or constitutive activation, and the dynamics of actin flow following RGS3hs overexpression, will provide important clues about the biochemical pathway downstream of RGS3hs regulation.

Lastly, it is interesting to note that while RGS3hs-HTMKE and RGS3hs-KYLER are both expressed in CSG neurons, the latter is also expressed in CNS neurons such as motor neurons and neurons of the MTN. CNS neurons do not delaminate from their origin neuroepithelium after commitment like CSG neurons do, so the mechanisms of migration between CNS neurons and CSG neurons are not necessarily identical. Thus, RGS3hs-KYLER might have a different function in CNS neurons than RGS3hs-HTMKE

does in CSG neurons. It will be interesting to compare the differences in phenotype (if any) between overexpression of the full-length sequences of RGS3hs-HTMKE versus RGS3hs-KYLER.

Chapter 5. On The Evolution of RGS3

Section 5.1 Introduction

RGS3 generates multiple isoforms from a large locus encoding a C2 domain, a PDZ domain, an EF Hand domain, and an RGS domain (Figure 1.11). RGS3 is a member of the R4 subfamily of RGS proteins by virtue of its RGS domain. However, as seen in Figure 1.12, the non-RGS domains of RGS3 are not present in other R4 subfamily members, making RGS3 stand out within this family. In fact, the other R4 members encode little more than an RGS domain, and in this respect, RGS3hs-HTMKE and RGS3hs-KYLER very closely resemble non-RGS3 R4 subfamily members. This raises intriguing questions about the evolutionary history of RGS3 and the R4 subfamily. There is evidence that suggests that the structure of RGS3 very closely resembles the R4 subfamily prior to expansion of the R4 subfamily in vertebrates from two rounds of whole-genome duplication. For example, non-RGS3 R4 subfamily members are all linked by synteny on human chromosome 1, likely resulting from tandem duplications. However, RGS3 is on human chromosome 9 at a locus paralogous to that of other R4 subfamily members. This is an indication that RGS3 and other R4 subfamily members diverged as a result of one of the two rounds of whole-genome duplication at the base of the vertebrate lineage (Holland et al., 1994; Kasahara, 2007; Shimeld and Donoghue, 2012), after which tandem duplications occurred in the non-RGS3 member (Suurväli et al., 2013). Furthermore, the R4 subfamily was originally reported to be a vertebrate novelty (Sierra et al., 2002), but an ‘R4 RGS-like’ open reading frame has since been identified in amphioxus (Suurväli et al., 2013), and domain analysis of this gene using the SMART tool reveals, like RGS3, it contains both RGS and PDZ domains.

In this chapter, I aimed to identify the evolutionary history of RGS3 and the rest of the R4 subfamily by mining available genomic and transcriptomic information from extant species across vertebrate and invertebrate taxa. To this end, I collaborated with Dr Patthey, who holds expertise in evolutionary analyses and who conducted all of the bioinformatic analyses. We determined the conservation of RGS3 in major vertebrate and invertebrate taxa, and characterised the differences in protein architecture between these taxa. We also conducted an analysis of the phylogenetic relationships of all R4 subfamily genes and determined that RGS3 is the founder gene of this family, in the sense that RGS3 has kept ancestral characteristics while the rest of the family has expanded and diversified from a common ancestral gene. Important differences between the invertebrate RGS3 and the vertebrate RGS3 protein sequences were found, prompting me to investigate the functional role of the invertebrate protein. To address this aim, I ectopically overexpressed the full-length amphioxus RGS3hL in the chick placode and compared the effects with overexpression of the full-length chicken RGS3hL. The significance of these findings with regard to the evolution of RGS3, the R4 subfamily, and the vertebrate placodes will be discussed in the final section.

Section 5.2 Evolution of RGS3 and the Expansion of the R4 Subfamily in Vertebrates

To characterise the conservation of the RGS3 gene in the Metazoan kingdom, the genomes of metazoan representatives were searched using TBLASTN with human RGS3 as a query. In addition, other members of the R4 subfamily were aligned with BLAST. Homology between hits and particular members of the R4 family was determined using reciprocal BLAST onto vertebrate datasets and/or by building phylogenetic trees. Finally, transcriptomic datasets were analysed to determine the conservation of RGS3 isoforms.

Section 5.2.1 Conservation of RGS3 in Metazoans

Section 5.2.1.1 Conservation of RGS3 in Vertebrates

In vertebrates, RGS3 genes were identified in every species listed in Figure 5.1, representing all major vertebrate taxa. In all species, at least one RGS3 gene copy was found containing the C2 and PDZ domains at its N terminus (Figure 5.1).

All gnathostomes contained the domains previously seen in human and chicken (Figure 1.11): the C2, PDZ, EF Hand, and RGS domains. In addition, a pseudo-PH domain was identified, which will be discussed in Section 5.2.1.2.

In teleost fishes, which underwent a whole-genome duplication shortly after the divergence from the rest of the ray-finned fishes (Jaillon et al., 2004), two RGS3 genes were present. One of these genes (RGS3a), however, lacks an N-terminal C2 domain, suggesting it represents the duplicated copy which lost a C2 domain during teleost evolution.

Agnathans did not have a pseudo-PH domain or an EF Hand domain. The EF Hand was also not found in any invertebrate (Figure 5.2), suggesting it is a gnathostome novelty. Interestingly, agnathans possessed four copies of RGS3: two which encoded C2-PDZ-RGS proteins, and two which only encoded only an RGS domain. This is intriguing in light of the fact that all other members of the R4 subfamily only encode an RGS domain (Figure 1.12). The implications of this finding for the evolution of the R4 subfamily will be discussed in Section 5.2.3.

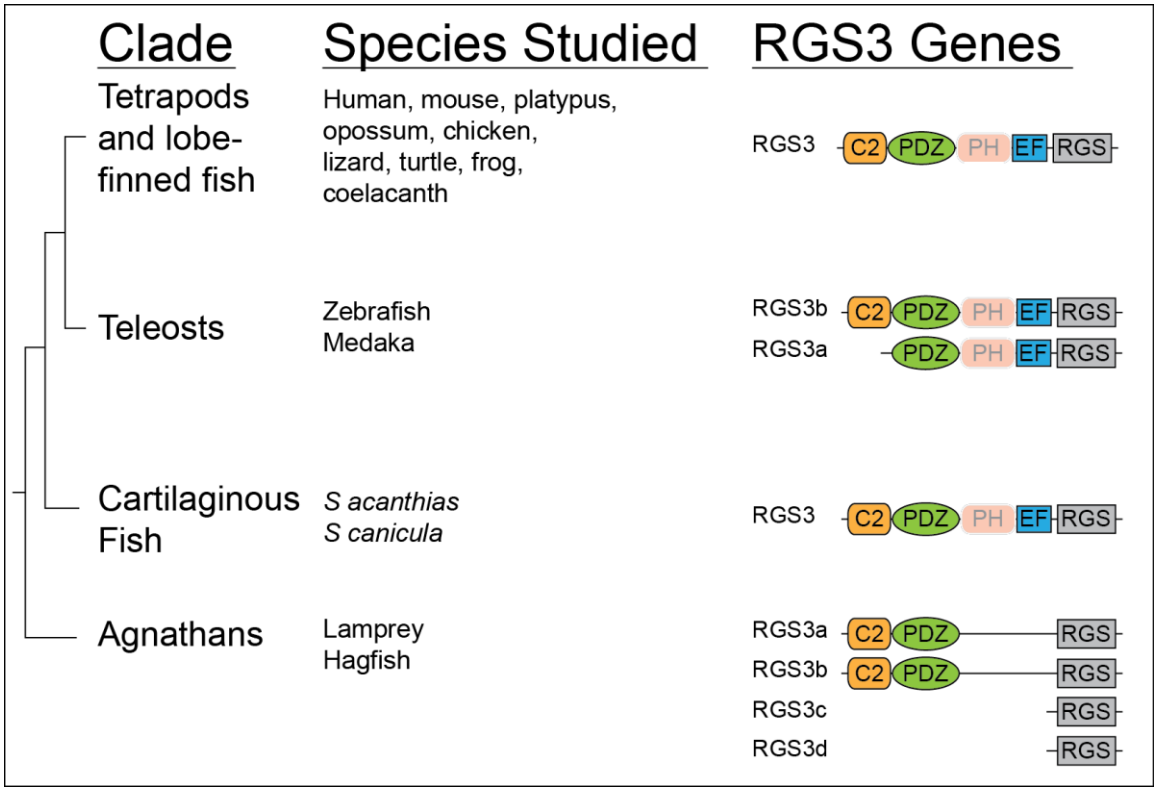


Figure 5.1. Conservation of RGS3 in Vertebrates
Clades whose species contain identical numbers and domain composition of RGS3 genes are shown. All gnathostomes possess an RGS3 gene containing a C2, PDZ, mutated PH (faded; see Section 5.2.1.2), EF Hand, and RGS domain. Teleosts have a duplication of RGS3 (RGS3a) which lacks an N-terminal C2 domain. Agnathans have four copies of RGS3, two with N-terminal C2 and PDZ domains (but lacking PH and EF Hand domains), and two with RGS domains only.

Section 5.2.1.2 Conservation of RGS3 in Non-Protostome Invertebrates

Because RGS3 was found in all vertebrate clades, we sought to determine if it has an ancestral origin in invertebrates. To this end, we investigated representative species from all major invertebrate taxa, including the poriferan *Amphimedon*, which represents the most basal extant metazoan relative to vertebrates (Figure 5.2). In this species, we found one copy of RGS3 encoding a C2, PDZ, and RGS domain, in addition to two other domains (see below). The protostome species we investigated showed an interesting divergence which will be discussed Section 5.2.1.3. Like in *Amphimedon*, every deuterostome species possessed an RGS3 gene with a C2, PDZ and RGS domain. In between the PDZ and RGS domains of hemichordates, echinoderms and cephalochordates, two additional domains were present: a pleckstrin homology (PH) domain, which is classically understood to localise proteins to phosphoinositides within the plasma membrane, but has diverse specificity highly dependent on its amino acid context (Lemmon, 2004); and a GEF domain, which replaces GDP with GTP on Gα proteins or other small GTPases (see Section 1.2.2.1).

Section 5.2.1.2.1 The PH Domain

The PH domain was not found in any vertebrate species investigated. However, a region of gnathostome RGS3 genes was detected by SMART as a PH domain but not predicted as putative because of a higher-than-threshold e-value. This reflects a poor match of the PH domain to the hidden Markov model (HMM), which measures probability of amino acids appearing at certain positions (Hughey and Krogh, 1996). We analysed the divergence of this domain by substituting human amino acid residues *in silico* with homologous residues from the amphioxus *Branchiostoma lanceolatum*. Only a few substitutions were required to raise the HMMER alignment score above threshold (Figure

5.3B), suggesting that the PH domain has been mutated in the vertebrate lineage but not lost. In fact, PH domains comprise one of the most numerous and diverse domain families, and a single tryptophan is the only residue conserved in all PH domains (Gibson et al., 1994; Musacchio et al., 1993). In the mutated PH domain of vertebrate RGS3, a valine residue is present at the homologous position of the conserved tryptophan (which is present in the PH domain of amphioxus RGS3; Figure 5.3A). The valine-to-tryptophan substitution alone was sufficient to raise the HMMER score above threshold, and the converse mutation in the amphioxus sequence reduced the HMMER score to below threshold. Together this suggests very few changes in the vertebrate PH domain. Considering the strong conservation of this new amino acid sequence across vertebrates (not shown), it seems likely that the mutated domain has in fact adopted a new function, and selective pressure to retain the new domain has been maintained. Consistent with this notion, similarly mutated PH domains were found in various clades throughout metazoan evolution (Figure 5.2).

Section 5.2.1.2.2 The GEF Domain

The GEF domain was not detected in vertebrates at all by SMART analysis. To confirm whether the GEF domain was mutated beyond detectability or truly lost, we compared the exon/intron boundaries between the human and amphioxus RGS3 genes. The nucleotide sequence at the termini of every exon, and concomitantly the position of the terminal nucleotides within the codon (the phase of the codon), were analysed (Figure 5.3C). This analysis showed that the 3' boundaries of human exons 3-12 (encoding the C2 and PDZ domains) and 15-25 (encoding the mutated PH domain and the RGS domain) were largely intact. However, between the exons of amphioxus RGS3 homologous to human exons 12 and 15, an additional 8 exons were present which

encoded the GEF domain. Thus, the GEF domain was lost from RGS3 in the vertebrate lineage.

Section 5.2.1.2.3 Divergence and Duplication of RGS3 in Tunicates

Tunicates were the only invertebrate deuterostomes to have more than one RGS3 gene. Six copies of RGS3 were found in *Ciona intestinalis*. Three of these genes only encoded an RGS domain; two encoded a C2 domain and an RGS domain but lacked PDZ, GEF or PH domains; and one encoded a C2 domain and two tandem RGS domains. The presence of these copies likely relates to the fact that tunicate genomes are highly derived (Delsuc et al., 2006). Furthermore, phylogenetic grouping placed all of these genes in an out-group separate from RGS3 and other vertebrate R4 members (Figure 5.4), suggesting that all of these genes appeared by independent duplication of the RGS3 gene in the tunicate lineage.

Section 5.2.1.2.4 Summary

Together these findings suggest that the GEF/PH-containing RGS3 gene was present in the most recent common ancestor of all metazoans, with a divergence in the gene architecture occurring in three lineages: vertebrates, which lost the GEF domain and mutated the PH domain; tunicates, which copied the gene and lost the PDZ, GEF and PH domains in their fast-evolving lineage; and protostomes (Section 5.2.1.3).

Section 5.2.1.3 Conservation of RGS3 in Protostomes

RGS3 was identified in *Lottia*, *Capitella*, and *Tribolium* (representing the major clades of protostomes) through alignment with the RGS domain of human RGS3 (Figure 5.2). However, unlike deuterostome and poriferan RGS3, this gene contained little more than an RGS domain. Interestingly, when either the C2 or PDZ domain of human RGS3 was

aligned against the translated genomes of protostomes, a separate gene was found in each species. This gene, called protostome-specific GEF (PsGEF), encodes the C2, PDZ, GEF and PH domains of RGS3 (Higuchi et al., 2009). Because the full-length C2-PDZ-GEF-PH-RGS gene is present in *Amphimedon* as well as deuterostomes, this suggests the full-length gene was present in the most recent common ancestor of deuterostomes and protostomes, and was split into two genes in the protostome lineage.

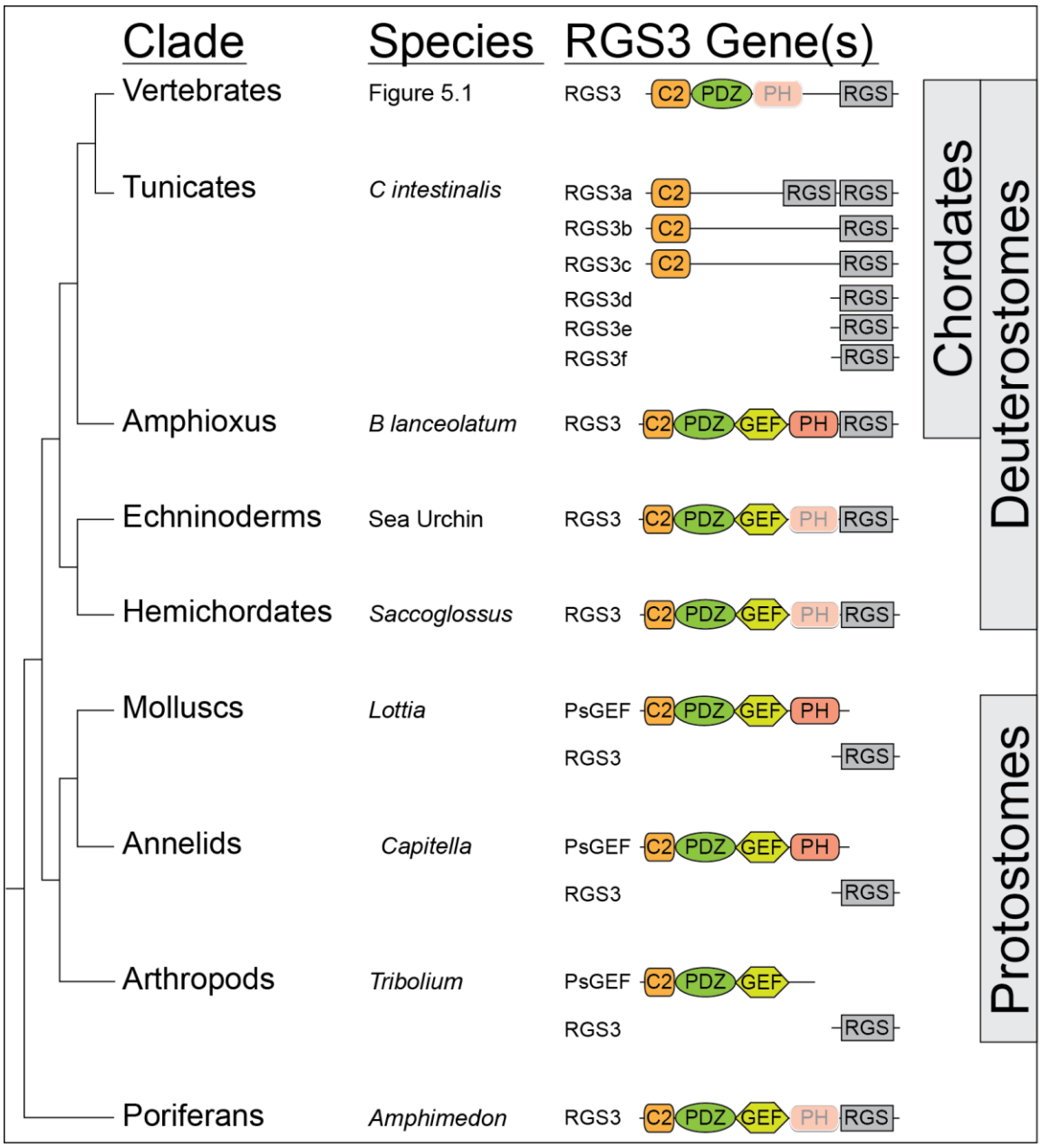


Figure 5.2. Conservation of RGS3 in Invertebrates
The domain composition and number of RGS3 genes in the major clades of invertebrates were investigated using the species listed. Vertebrates possess a C2, PDZ, PH, and RGS domain (as well as an EF Hand domain in gnathostomes; Figure 5.1). Invertebrates additionally possess a GEF domain between the C2 and PDZ domains, with several key divergences. First, tunicates do not possess the GEF, PDZ or PH domains and have multiple copies of full-length and RGS-only genes. Second, protostomes have two genes, one containing the N-terminal domains (PsGEF) and one containing only the RGS domain. In several lineages, including vertebrates, non-chordate deuterostomes, and poriferans, the PH domain (faded) was mutated to below the threshold of predictability by the SMART engine.

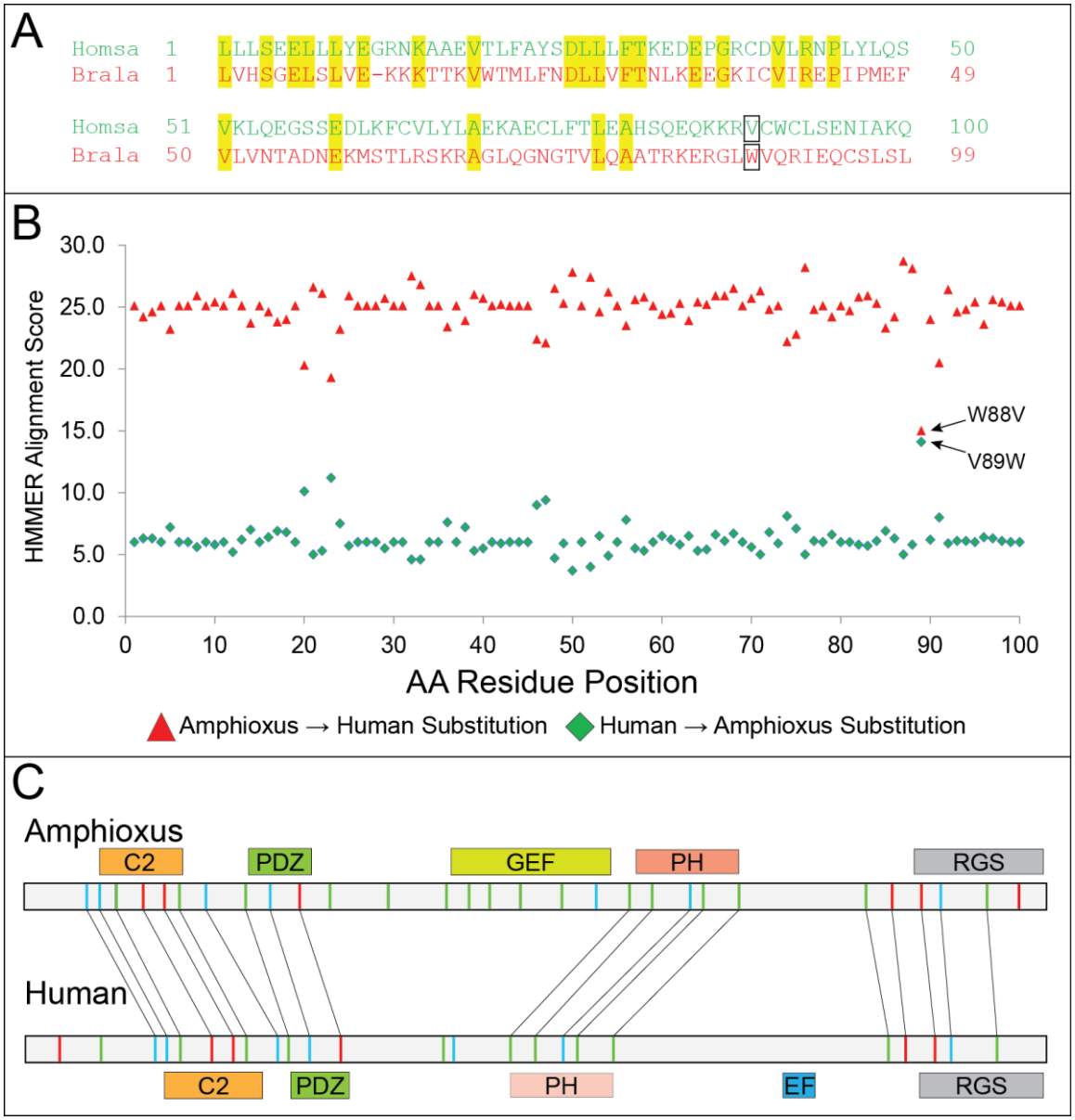


Figure 5.3. Divergence of the PH and GEF Domains from Invertebrate RGS3.
(A) Alignment of the PH domain of human RGS3 with that of amphioxus RGS3. Identical sequences are highlighted. The tryptophan (W) residue of amphioxus, which is conserved in all PH domains, and the valine (V) residue of the same position in human are boxed. *(B)* Human (green) or amphioxus (red) domains were mutated *in silico* with the residue aligned to the same position in the other species, and analysed by SMART with a HMMER score, which predicts probability of aa positioning. Substitution of the human valine boxed in *(A)* to tryptophan (V89W) was sufficient to raise the HMMER score of the human PH domain above the threshold of putative predictability; the inverse mutation in the amphioxus PH domain (W88V) similarly lowered the HMMER value below threshold. *(C)* The intron-exon boundaries between human and amphioxus RGS3 proteins were analysed by comparing the nucleotide sequences at these boundaries (not shown) as well as the phase of the codon sequence. Boundaries between exons are shown in coloured lines: green indicates that the exon terminus is in-frame (phase 0), blue indicates that the exon terminus occurs after the first nucleotide of the final codon (phase 1), and red indicates that the exon terminus occurs after the second nucleotide of the final codon (phase 2). Based on these data, homologous exon/intron boundaries are indicated with black lines.

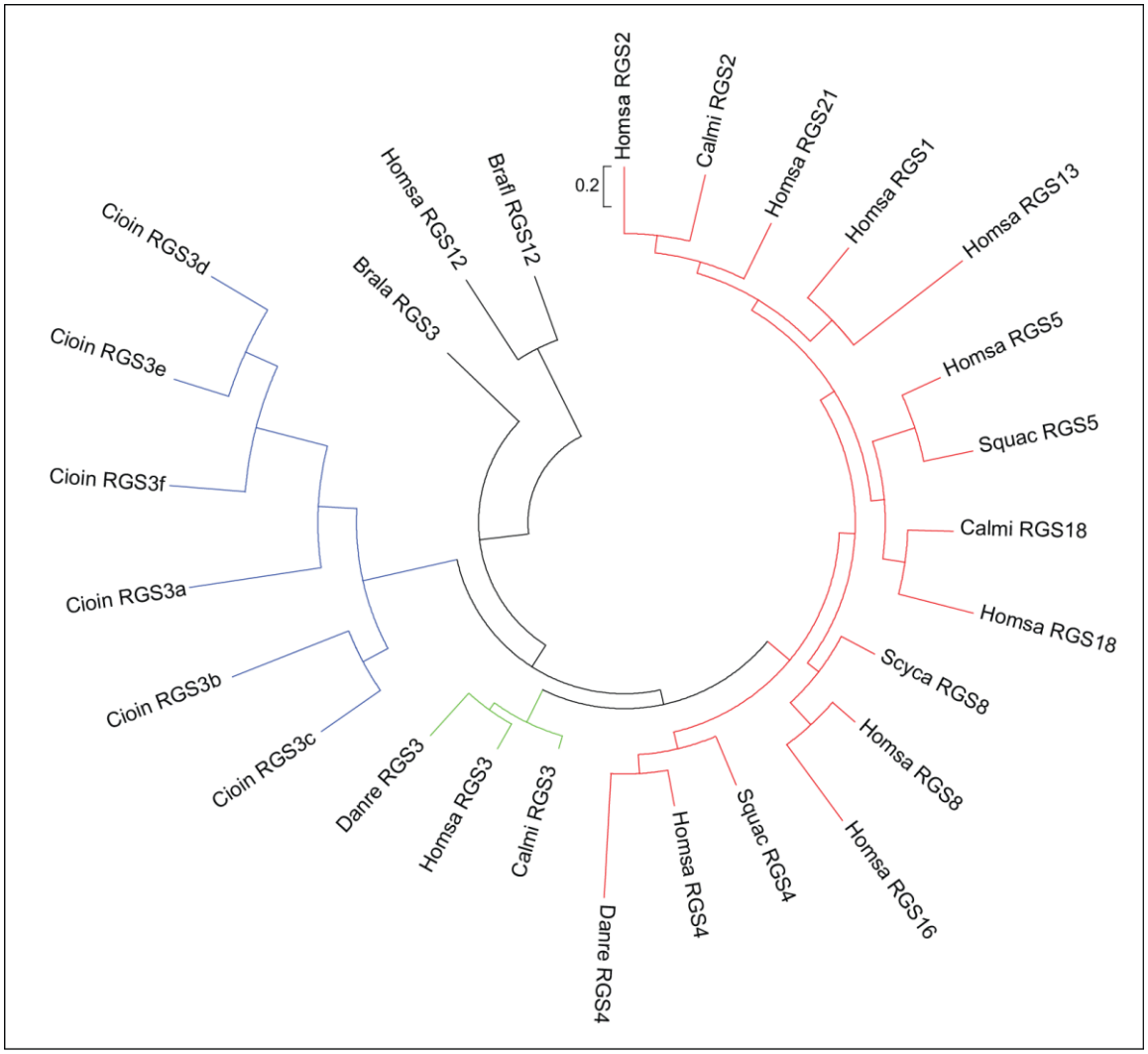


Figure 5.4. Phylogenetic Comparison of R4 Subfamily Proteins.
The RGS domain of R4 subfamily genes of amphioxus (*B lanceolatum*; Brala), tunicate (*C intestinalis*; Cioin), ghostshark (*C milii*; Calmi), catshark (*S canicula*; Scyca), dogfish (*S acanthias*; Squac), zebrafish (*D rerio*; Danre), and human (*H sapiens*; Homsa) were compared to determine their phylogenetic relationships. Amphioxus RGS3 forms the root of this phylogeny. Vertebrate RGS3 genes (green) cluster in a sister group to non-RGS3 R4 genes (red). All tunicate RGS3 genes (blue) cluster in their own out-group. The amphioxus root does not cluster with the R12 member RGS12, showing that the invertebrate RGS3 is part of its own R4 subfamily and did not branch from the R12 subfamily. Brafl: *Branchiostoma floridae* (another amphioxus species). Scale bar indicates average number of amino acid changes per position.

Section 5.2.2 Conservation of Isoform Generation in Metazoans

From this thesis and previous studies (Kehrl et al., 2002; Reif and Cyster, 2000), it is clear that multiple isoforms are generated from the RGS3 locus in human, mouse and chicken. The conservation of the RGS3 gene structure in vertebrates suggests that the generation of multiple isoforms might also be conserved. To investigate this, we analysed transcriptomic datasets available in taxa across the vertebrate lineage as well as amphioxus. Intriguingly, multiple isoforms were found in all species examined (listed in Figure 5.5A). As in human, mouse and chicken, all tetrapods and lobe-finned fish were found to contain RGS3hL, C2PA, RGS3L, RGS3s and RGS3hs isoforms. In teleosts, which contain two copies of RGS3 genes (Figure 5.1), RGS3hL and RGS3s were found to be encoded by one copy, while RGS3L and RGS3hs were encoded by the second. C2PA was not found in teleosts or any other species examined outside of tetrapods and lobe-finned fish, suggesting its expression emerged after the divergence of lobe-finned fish. Cartilaginous fish encoded RGS3hL, RGS3s, and RGS3hs, but no RGS3L isoform. In fact, no RGS3L isoform was found outside of the osteichthyes (tetrapods, lobe-finned fish and teleosts), suggesting it emerged after the divergence of this lineage. Agnathans were found to possess two C2-PDZ-RGS genes and two RGS-only genes (Section 5.2.1.1), which themselves resemble RGS3hs isoforms. Of the two C2-PDZ-RGS genes, one was found to generate an RGS3hs isoform in addition to the RGS3hL isoform.

We were able to mine the amphioxus transcriptome through unpublished data provided by Manuel Irimia (University of Toronto, Canada) and Juan-Pascual Anaya (RIKEN CDB, Japan). In this dataset, we found RGS3hL and RGS3hs isoforms, but interestingly several other isoforms were found. Two versions of RGS3s were generated: one encoding 62 unique aa upstream of the common exon (corresponding to exon 20 of

human RGS3hL) and one whose coding sequence begins 18 aa into the common exon. A truncated version of RGS3hs was also detected, which only encodes the C-terminal half of the RGS domain. Lastly, an intermediate isoform was found to be shorter than RGS3L but longer than RGS3s, encoding the PH domain and RGS domain. Because these latter two isoforms were not detected in any other species however (including vertebrates), this suggests they emerged in cephalochordates after their divergence from the rest of chordates.

Taken together, these results show a broad conservation of isoforms generated by the RGS3 locus, and do not rule out the possibility that RGS3 isoform generation dates back to even earlier-derived lineages (such as poriferans).

Section 5.2.2.1 Conservation of RGS3hs-KYLER and RGS3hs-HTMKE

The above results suggest that the generation of RGS3hs is as old as the divergence of amphioxus from the chordate lineage. However, it is not clear at which point RGS3hs-KYLER and RGS3hs-HTMKE emerged in evolution. To investigate the conservation of these isoforms, we aligned their unique N-terminal amino acid sequences to the translated genomes of vertebrates and amphioxus using BLAST.

No sequence homologous to the unique amino acid sequences of vertebrate RGS3hs-KYLER or RGS3hs-HTMKE was found in the amphioxus genome using BLAST. Consistently, the unique exon of amphioxus RGS3hs found in transcriptomic data was non-coding, and the coding sequence begins in its first common exon (not shown). Thus, amphioxus RGS3hs contains neither KYLER nor HTMKE sequences. Of the two RGS3hs-like RGS3 genes found in lamprey (Section 5.2.1.1), one contained a 5' sequence which aligned to the KYLER sequence (Figure 5.5B). The other gene did not

align to KYLER or the HTMKE sequence. The one full-length C2-PDZ-RGS lamprey gene which generated an RGS3hs isoform was found to align to KYLER. No lamprey RGS3 gene aligned to the HTMKE sequence. The RGS3 gene of cartilaginous fish did have two RGS3hs isoforms, one aligning to the KYLER and one to the HTMKE sequence. Teleost fish were found to contain two RGS3 genes but an RGS3hs isoform was only encoded by one, the N-terminal sequences of which aligned to the KYLER sequence. An HTMKE sequence was not identified in teleosts. All tetrapods investigated contained RGS3hs isoforms whose N-terminal sequences aligned to the HTMKE sequence. However, while birds, reptiles and non-eutherian mammals (including marsupials) were found to also have an RGS3hs-KYLER isoform (as identified previously in 5' RACE; Section 3.2.2), no eutherian mammal investigated possessed an RGS3hs isoform with N-terminal sequences aligning to the KYLER sequence.

Taken together, these findings suggest a model of RGS3hs evolution as follows (Figure 5.7). RGS3hs existed in invertebrates, but was not a KYLER or HTMKE version. The non-coding exon of invertebrate RGS3hs evolved to encode the KYLER sequence in early vertebrates, prior to the divergence of agnathans. After the divergence of gnathostomes, RGS3hs-HTMKE emerged. Teleosts lost RGS3hs-HTMKE during their lineage, but retained RGS3hs-KYLER. Birds, reptiles and non-eutherian mammals retained both RGS3hs-HTMKE and RGS3hs-KYLER. Finally, eutherian mammals lost RGS3hs-KYLER early in their lineage, but retained RGS3hs-HTMKE.

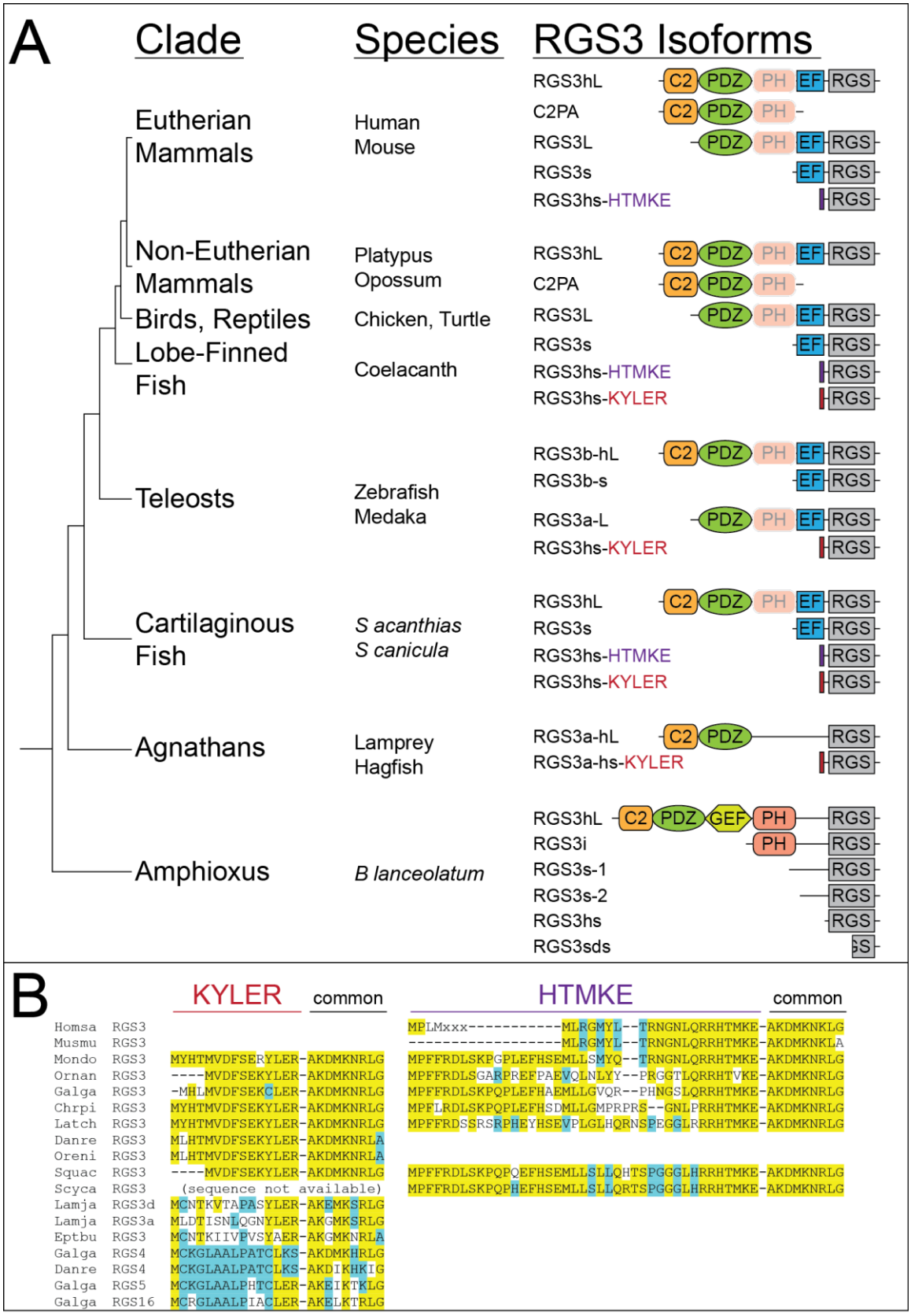


Figure 5.5. Conservation of RGS3 Isoforms in Metazoans.
Figure legend on next page.

Figure 5.5. Conservation of RGS3 Isoforms in Metazoans.
(A) Clades whose species produce the same set of RGS3 isoforms are shown, and their representative species are listed. Non-eutherian mammals, birds, reptiles, and lobe-finned fish produce all vertebrate isoforms. Eutherian mammals produce this set except for RGS3hs-KYLER. Teleosts do not produce RGS3hs-HTMKE or C2PA. Cartilaginous fish produce both RGS3hs-HTMKE and RGS3hs-KYLER, but not C2PA. Agnathans produce only RGS3hL and RGS3hs-KYLER. Amphioxus produces a number of isoforms in addition to RGS3hL. An intermediate isoform (RGS3i) is shorter than RGS3L (it does not encode the PDZ domain) but does include the PH domain. Two version of RGS3s initiate upstream of the exon homologous to human RGS3hL exon 20 as does human RGS3s. The first of these (RGS3s-1) generates a unique 5' coding exon which adds 62 aa onto the N-terminus of the protein. The second (RGS3s-2) generates a unique 5' non-coding exon, and initiates transcription 18 aa into the first common exon. Amphioxus produces an RGS3hs, but it does not have KYLER or HTMKE upstream sequences. Instead, its 5' unique exon is non-coding, and it initiates 4 aa into the common exon (homologous to the artificial overexpression construct used in Chapter 4; see Section 4.3). Finally, a truncated isoform (RGS3sds) encodes the C-terminal half of the RGS domain. *(B)* Alignment of the KYLER and HTMKE coding sequences in representative vertebrate species. Residues highlighted yellow and blue are identical. KYLER is present in all taxa except eutherian mammals. In addition, representative members of the R4 subfamily are shown to align to the KYLER sequence. HTMKE is not present in agnathans or teleosts. Chrpi: *C picta* (painted turtle); Danre: *D rerio* (zebrafish); Eptbu: *E* burger (hagfish); Galga: *G gallus* (chicken); Homsa: *H sapiens* (human); Lamja: *L japonica* (lamprey); Latch: *L chalumnae* (coelacanth); Mondo: *M domestica* (opossum); Musmu: *M musculus* (mouse); Oreni: *O niloticus* (tilapia); Ornan: *O anatinus* (platypus); Scyca: *S canicula* (catshark); Squac: *S acanthias* (dogfish).

Section 5.2.3 Non-RGS3 R4 Members Diversified After Gnathostome Evolution

In addition to RGS3, the presence of other members of the R4 subfamily was separately investigated across Metazoa (Figure 5.6). Tetrapods (including amphibians, reptiles, birds and mammals) and lobe-finned fish were found to possess every non-RGS3 R4 member identified in human: RGS1, -2, -4, -5, -8, -13, -16, -18, and -21 (Bansal et al., 2007). Teleosts were seen to possess all of these genes as well as two copies of RGS4 and RGS5. Cartilaginous fish, which diverged from other gnathostomes before the divergence of teleosts but after the divergence of agnathans, had a reduced subset of non-RGS3 R4 genes: RGS2, -4, -5, -8, and -18. In lampreys, two genes similar in domain composition to the gnathostome non-RGS3 R4 genes were found. However, we were not able to determine using phylogenetic trees or conservation of synteny whether they are orthologous to non-RGS3 R4 genes. Invertebrates similarly possessed only a single

RGS3 gene more similar to human RGS3 than other R4 members, consistent with previous investigations (Sierra et al., 2002). Thus, the non-RGS3 R4 subfamily appeared in the vertebrate lineage after the divergence of amphioxus and expanded and diversified in jawed vertebrates.

Because R4 RGS genes resemble RGS3hs in terms of primary amino acid sequence as well as intron-exon boundaries (Sierra et al., 2002), we hypothesised that non-RGS3 R4 genes have their origin in the RGS3hs isoform of the RGS3 gene of ancestral chordates. Analysis of synteny in the human genome reveals that RGS3, on chromosome 9, and the other R4 genes, all on chromosome 1, are located in paralogous syntenic regions. This is very strong evidence for a result of the whole genome duplication at the base of vertebrates (Holland et al., 1994; Kasahara, 2007; Shimeld and Donoghue, 2012). Consistently, lampreys, which share at least one whole genome duplication with vertebrates (Holland et al., 1994; Kasahara, 2007; Shimeld and Donoghue, 2012), have two genes resembling RGS3 (C2-PDZ-RGS) and two genes resembling non-RGS3 R4 genes (RGS-only; Figure 5.1). Considering these results, we suggest a model as follows (Figure 5.7). In ancestral vertebrates, the GEF and PH domains were lost and mutated (respectively) and the KYLER sequence was acquired after the divergence of cephalochordates. This single gene was duplicated two times with the two rounds of whole genome duplication, generating four paralogues. Two were lost in the gnathostome lineage, resulting in two C2-PDZ-RGS genes, both able to generate RGS3hs-KYLER isoforms. One of them became RGS3 and the other one was the founder of the non-RGS3 R4 subfamily. Since constraints were released by the duplication, the ancestral non-RGS3 R4 gene was permitted to generate only the RGS3hs isoform. Subsequently, the N-terminal sequences were lost, resulting in an RGS-only

RGS3hs- like gene. Thus, the R4 subfamily expanded from a duplication of RGS3 in proto-gnathostomes which lost its N-terminal sequences before duplicating.

This model is supported by the fact that R4 subfamily members share a common synteny which dates at least as far back as ancestral non-cartilaginous osteichthyes (Suurväli et al., 2013), while the RGS3 locus is on a separate chromosome. However, this could be explained by a convergent evolution and subsequent duplication of a closely-related member of the RZ subfamily, as previously suggested (Sierra et al., 2002) (Section 1.2.5). If the above model is correct, a signature of RGS3hs should be found in modern non-RGS3 R4 genes: namely, these genes should have an upstream sequence aligning to the KYLER sequence, as does the lamprey gene. Indeed, we found that RGS4, -5, and -16 all had conserved sequences which aligned to the KYLER sequence of RGS3hs (Figure 5.5B). Thus, the R4 subfamily expanded in the early gnathostome lineage from an RGS3 duplication.

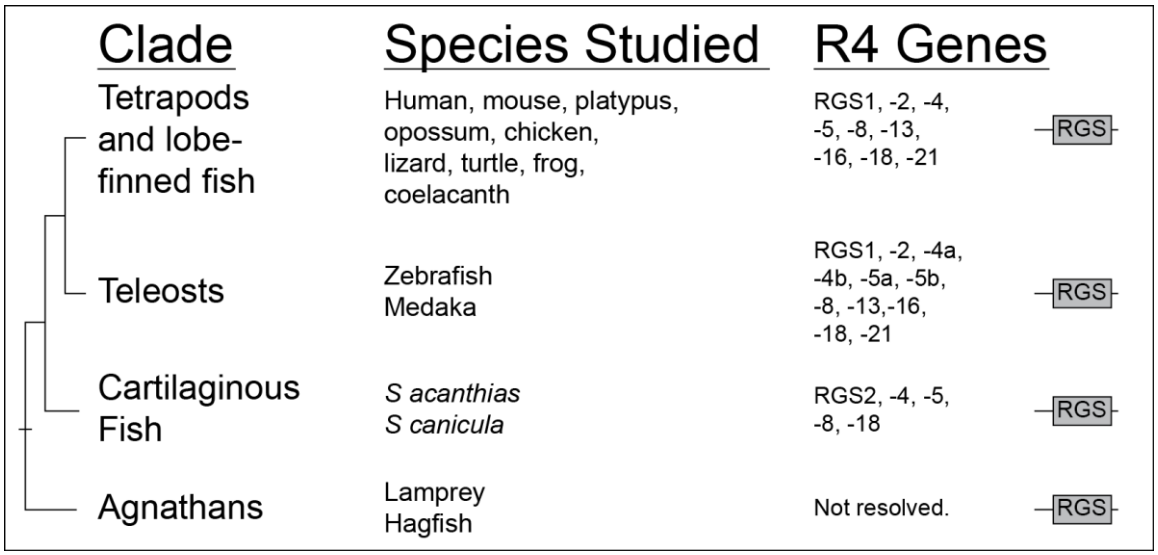


Figure 5.6. Conservation of R4 RGS Proteins in Vertebrates.
Clades whose species contain identical numbers and domain composition of R4 subfamily members are shown. In tetrapods, the largest set of R4 family members is present. Teleosts have duplications of RGS4 and RGS5. In cartilaginous fish, the R4 subfamily is reduced in number, which suggests that these genes were duplicated after in the divergence of agnathans but prior to the divergence of teleosts. The orthology of agnathan R4 genes is not resolved.

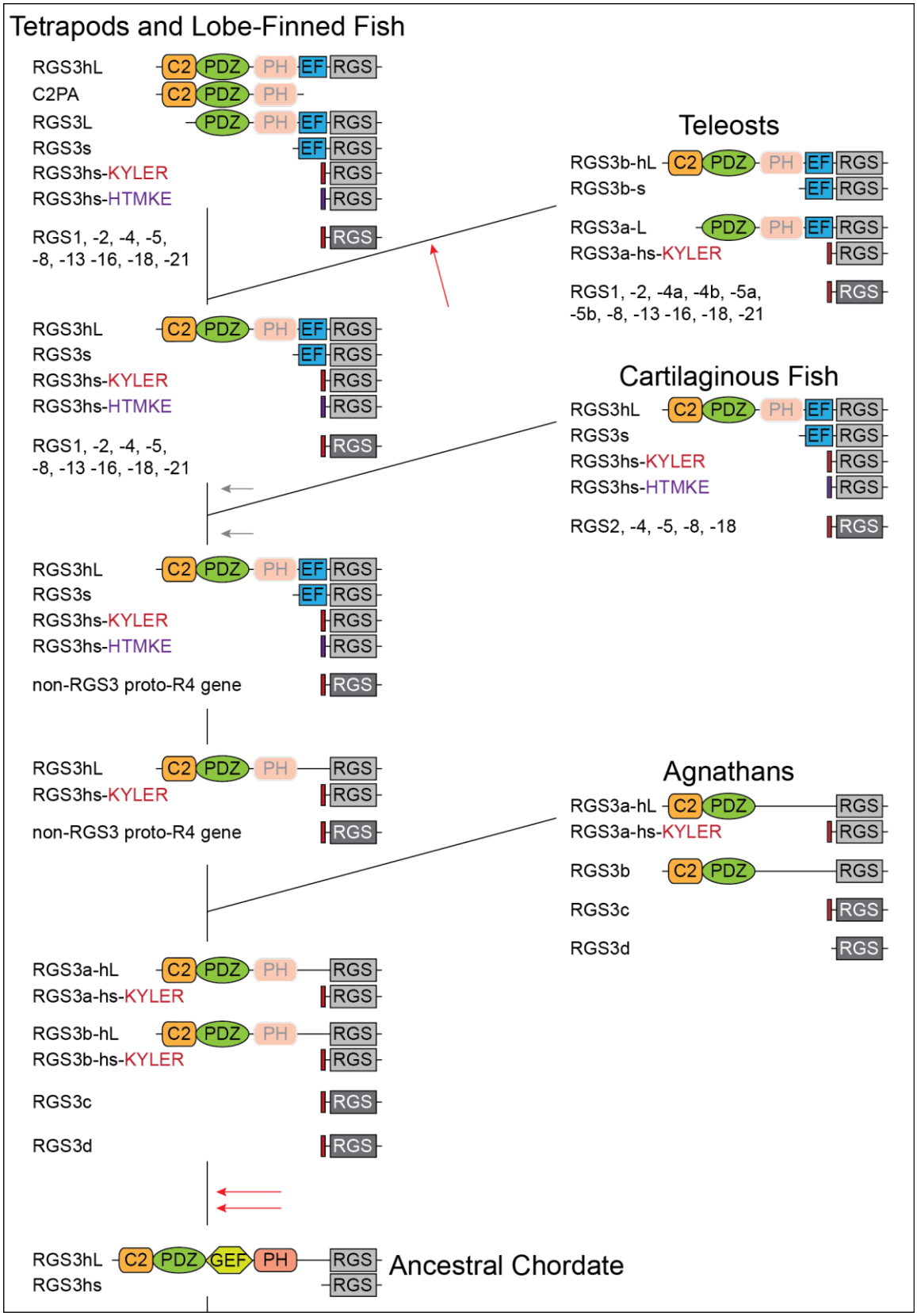


Figure 5.7. A Model for the Evolution and Expansion of the R4 Subfamily.
Figure legend on next page.

Figure 5.7. A Model for the Evolution and Expansion of the R4 Subfamily.
A theoretical explanation supported by the data presented (Section 5.2.3) for the evolution of RGS3 isoforms and the expansion of the R4 subfamily. In ancestral chordates, the R4 subfamily had one member, RGS3, which encoded a C2, PDZ, GEF, PH, and RGS domain, and generated RGS3hL and RGS3hs isoforms. Following loss of the GEF domain, mutation of the PH domain (faded), and acquisition of a KYLER sequence downstream of the RGS3hs start, one round of whole genome duplication (red arrows) (Holland et al., 1994; Kasahara, 2007; Shimeld and Donoghue, 2012) duplicated this gene. One of these genes lost N-terminal domains, probably because relieved selective pressure on the generation of RGS3hL from this gene permitted it to only express RGS3hs. A second round of whole genome duplication resulted four genes, two full-length and with RGS3hL and RGS3hs isoforms (RGS3a and RGS3b), and two with only RGS domains (RGS3c and RGS3d). In the agnathan lineage, all four genes were kept. In the gnathostome lineage, two of these four genes were lost: one full-length, and a proto non-RGS3 R4 gene (RGS-only). Through later duplications of this RGS-only gene (grey arrows), the non-RGS3 R4 subfamily expanded in gnathostomes. RGS3, meanwhile, acquired RGS3hs-HTMKE and RGS3s promoters as well as the EF Hand domain. Following divergence of the teleost lineage, a third whole-genome duplication event (red arrow) (Jaillon et al., 2004) duplicated RGS3 into two genes: RGS3b, which lost the KYLER and HTMKE promoters, and RGS3a, which lost the N-terminal C2 domain, the RGS3s promoter, and the HTMKE promoter. RGS4 and RGS5 also duplicated in this lineage. Ancestral lobe-finned fish evolved promoters for C2PA and RGS3L, and modern lobe-finned fish and tetrapods generate all six isoforms. Eutherian mammals, however, have lost the KYLER promoter (not shown).

Section 5.3 Ectopic Overexpression of Amphioxus RGS3hL in the Vertebrate Placode

All vertebrate RGS3hL proteins possess the same domain architecture with the exception of agnathans, which do not contain the PH or EF Hand domains (Figure 5.1). This is in contrast to the invertebrate RGS3hL, which lacks an EF Hand domain yet possesses a GEF domain and a PH domain with a conserved tryptophan (Section 5.2.1.2). This suggests that RGS3hL plays a conserved role in vertebrates, but plays a different role in invertebrates. Expression analysis showed that RGS3hL is expressed in the placode of the chick embryo (Figure 3.4B). A probe recognising RGS3hL as well as C2PA and RGS3L also stained the placode of the mouse embryo (Figure 3.7B,F). Furthermore, a probe recognising RGS3hL and C2PA labelled the pre-placodal ectoderm of chick embryos (Figure 3.6A,B). Thus RGS3hL might play a role in the formation and maintenance of the vertebrate placode. Amphioxus and tunicates have structures which resemble primitive placodes (Section 1.1.5.2), but these do not possess all of the

stereotypic characteristics of vertebrate placodes, and they do not contribute as much diversity of derivatives as do the vertebrate placodes (Section 1.1.5.2). We thus hypothesised that the evolution of RGS3hL in early vertebrates might relate to the evolution of the placodes. To test this hypothesis, we decided to determine the ectopic function of the invertebrate form of RGS3hL in the vertebrate placode. We chose to use the amphioxus RGS3hL because while tunicates are more closely related to vertebrates than amphioxus (Delsuc et al., 2006), the highly derived nature of the tunicate genome (Delsuc et al., 2006) means that tunicate RGS3 genes are not representative of the invertebrate sequence (Section 5.2.1.2).

I designed PCR primers to the putative translated coding sequence of full-length amphioxus RGS3hL and cloned a cDNA from mRNA extracted from *Branchiostoma lanceolatum* adults (provided by Dr Patthey). Sequencing confirmed that this transcript was amphioxus RGS3hL. I subcloned this sequence into the pMES overexpression vector (Section 4.3) for overexpression. I also cloned the chick RGS3hL coding sequence from RNA extracted from retinas of E6.0 (HH29) embryos (provided by Alexandra Smith in our laboratory). Overexpression vectors were electroporated into HH11-13 pre-petrosal ectoderm and embryos were incubated to HH16-18 as before (Section 4.2.1). The efficiency of electroporation was determined by EGFP fluorescence and staining with antibodies against EGFP and HuC/D labelled electroporated cells and differentiated neurons, respectively.

Similar to overexpression of RGS3L (Figure 4.10), which is also expressed in the placode (Figure 3.4E), overexpression of chick RGS3hL (pMES-GalgaRGS3hL) resulted in abolished neurogenesis, with no EGFP-/HuC/D-double positive neurons detected (n=3; not shown). Overexpression of amphioxus RGS3hL (pMES-BralaRGS3hL)

similarly resulted in reduced neurogenesis and no EGFP-/HuC/D-double positive neurons (n=3; not shown).

One of the prominent differences between the amphioxus non-neural epidermal field which resembles a primitive placode and the vertebrate placode is the thickened and pseudostratified nature of the vertebrate placodal epithelium compared to the columnar epithelium of the amphioxus placode (Kaltenbach et al., 2009). To examine whether ectopic amphioxus RGS3hL overexpression affects placodal morphology, I measured the maximum thickness of the electroporated placodes (usually corresponding exactly to the middle of the placode along the dorso-ventral axis) and compared it to the maximum thickness of the left (unelectroporated) placodes (Figure 5.8). Intriguingly, I found that pMES-BralaRGS3hL-electroporated placodes were dramatically thinner compared to the unelectroporated placodes, while pMES-GalgaRGS3hL-electroporated placodes were insignificantly different to the left side (pMES-BralaRGS3hL: left side: 56.43±4.68 µm, right side: 34.01±3.71 µm, n=3, p=0.011, Student's T-test (Section 2.15); pMES-GalgaRGS3hL: left side: 57.40±2.09 µm, right side: 49.20±4.20 µm, n=3, p=0.090). Similarly, placodes electroporated with pMES alone were 59.18±7.73 µm wide (left side: 55.84±5.45 µm, n=4, p=0.180), significantly larger than pMES-BralaRGS3hL-electroporated embryos (p=0.020) but not different from pMES-GalgaRGS3hL-electroporated embryos (p=0.157). Concomitantly, no more than three nuclei were present along the apico-basal axis in pMES-BralaRGS3hL-electroporated placodes, while pMES-GalgaRGS3hL and pMES-electroporated placodes had up five or six cell bodies along the apico-basal axis. This morphology is similar to that observed by Anna Zornoza (unpublished work in our laboratory) in the ectoderm of the non-placodal pharyngeal arch (indicated in Figure 5.8B'). This suggests that placodal thickening was prevented

following pMES-BralaRGS3hL overexpression and pre-placodal cells instead developed the morphology of pharyngeal arch. Together this shows that amphioxus RGS3hL, but not chicken RGS3hL, is sufficient to inhibit pseudostratification of vertebrate pre-placodal ectoderm.

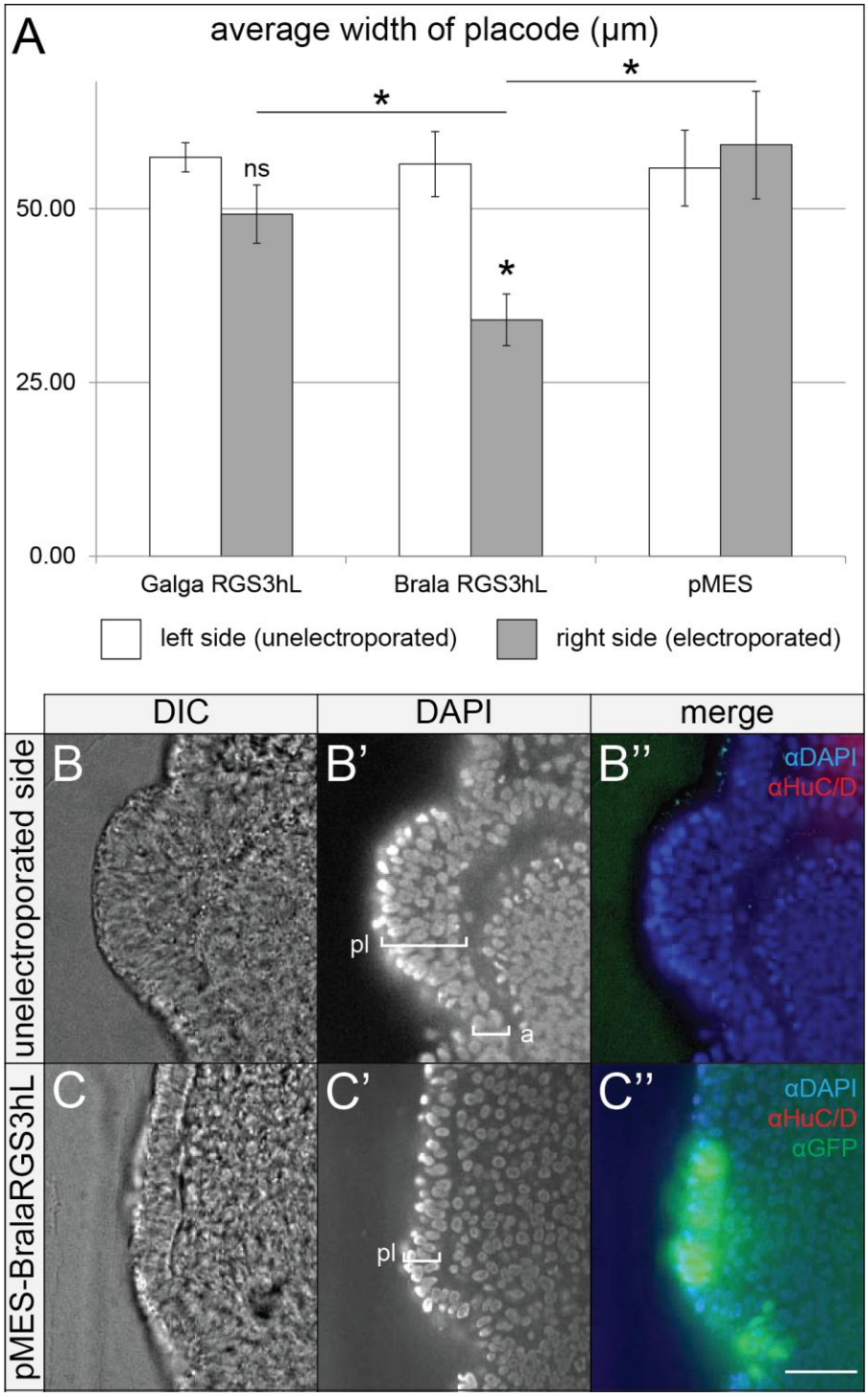


Figure 5.8. Ectopic Overexpression of Amphioxus RGS3hL Alters Morphology of the Vertebrate Placode.
Figure legend on next page.

Figure 5.8. Ectopic Overexpression of Amphioxus RGS3hL Alters Morphology of the Vertebrate Placode.
(A) The maximum widths of placodes overexpressing chicken (Galga) or amphioxus (Brala) RGS3hL (grey) and their contralateral (unelectroporated) placodes (white) were measured. Overexpression of Brala RGS3hL was observed to dramatically decrease the width of the placode compared to the contralateral side and to the pMES- and pMES-GalgaRGS3hL-electroporated placodes. *(B-C'')* DIC, DAPI, GFP and HuC/D imaged with an Olympus BX51 compound light microscope (Section 2.10). *(B-B'')* The morphology of the unelectroporated placode (pl) was thick and pseudostratified, with multiple layers of nuclei positioned along the apico-basal axis (shown with DAPI staining). More ventrally, the ectoderm of the pharyngeal arch (a) was thinner and more closely resembled a columnar morphology. *(C-C'')* By contrast, the morphology of pMES-BralaRGS3hL-electroporated placodes was indistinguishable from the epithelium of the pharyngeal arch, with an apparent thin, columnar morphology. *=p<0.05, Student's T-test (Section 2.15). ns=p>0.05 (not significant). Scale bar in *(C'')*: 50μm.

Section 5.4 Discussion

The data presented in this chapter have intriguing implications about the evolutionary importance of RGS3. RGS3 is an ancient gene, at least as old as all extant metazoans. Moreover, its ability to generate N-terminally truncated isoforms dates back at least to the divergence of cephalochordates from the chordate lineage. Such a mechanism potentially serves diverse functions. Differential RGS3 isoform production was shown in Chapter 4 to be important for the formation of the chick CSG. This is clearly a vertebrate-specific function, since the CSG are a vertebrate novelty. However, amphioxus does possess a non-neural epithelial field which resembles a placode (Section 1.1.5.2.1) and which generates migratory neurons. If the tissue-type specificity of enhancers governing RGS3hL versus RGS3hs transcription is conserved, RGS3hL would be expected to be expressed in the proto-placodal field, and RGS3hs would be expected to be expressed in the neurons migrating away from this field. Analysis of differential expression of RGS3hL and RGS3hs in amphioxus larvae would shed much light on this hypothetical function.

If this hypothesis is true, it would have profound implications for the role of RGS3hL in evolution. When overexpressed into pre-placodal ectoderm of the chick embryo,

amphioxus RGS3hL was sufficient to prevent pseudostratification of the placode, and instead resembled the columnar morphology of the pharyngeal arch. Similarly in amphioxus, the proto-placode neurogenic epithelium resembles a columnar morphology indistinguishable from the lateral surface ectoderm except by the expression of Tlx (Kaltenbach et al., 2009). Does RGS3hL actively prevent pseudostratification in amphioxus? Most likely, the acquisition of thickened placodes in the chordate lineage after the divergence of cephalochordates is related to a number of changes in protein-coding genes and non-coding regions. However, it is entirely possible that amphioxus RGS3hL, but not vertebrate RGS3hL, regulates cytoskeletal dynamics in a manner that restricts the apico-basal extension of epithelial cells. If this is true, this regulation would likely relate to the domains absent in vertebrate RGS3hL but present in amphioxus RGS3hL: namely, vertebrate RGS3hL lacks entirely the GEF domain of amphioxus RGS3hL. In support of this idea, PsGEF, which lacks the RGS domain of RGS3 but contains the C2, PDZ, GEF and PH domains, genetically interacts with the small GTPase Rac1 in the arthropod *Drosophila melanogaster* (Higuchi et al., 2009). Furthermore, the GEF domain of *Drosophila* PsGEF was sufficient to induce actin polymerisation in the immortalised human HeLa cell line, as observed by membrane ruffling. Such a phenotype is specific to constitutively active forms of Rac, but not Cdc42 or Rho, two other prominent small GTPases which are regulated by GEF domains (Ridley et al., 1992). This demonstrates that the GEF domain of PsGEF is capable of regulating specific substrates in vertebrate cells; since Rac is highly conserved across Metazoa (Cotteret and Chernoff, 2002), it stands to reason that a similar regulation occurs endogenously in the amphioxus placode and ectopically in the chick placode. To confirm this idea, a BralaRGS3hL GEF deletion construct will need to be cloned and overexpressed as before in the chick placode. If this construct fails to thin the placode,

this would highly suggest that the GEF domain of amphioxus RGS3hL is responsible for the regulation of cytoskeletal dynamics which ectopically prevents pseudostratification of the vertebrate placode.

The importance of the loss of the GEF domain of RGS3 in vertebrate evolution will only be understood by resolving the endogenous expression and function of RGS3 in amphioxus. For example, does knockdown of RGS3hL in amphioxus result in thickening of the epithelium? The purpose of pseudostratification in the vertebrate neural tube is to expand the progenitor pool by allowing more apical mitoses to occur per unit space (Fish et al., 2008). In the placode, divisions occur less frequently (Graham et al., 2007), but the pseudostratified morphology is likely similarly related to maintenance of the progenitor pool. To this end, it seems likely that pseudostratification of the placode is an evolutionary acquisition, rather than a default state of non-neural epithelia in invertebrates which is repressed by the GEF domain of RGS3hL. Instead, loss of the GEF domain of RGS3 might be one of the genomic alterations which allowed for pseudostratification to evolve in the placodes. Interestingly, tunicates (which are more closely related to vertebrates than amphioxus) also lack the GEF domain, suggesting the loss might have occurred in the most recent common ancestor between tunicates and vertebrates. Consistently, the epithelium of the atrial primordium, a proto-posterior placode (Section 1.1.5.2.2), is thickened (Mazet et al., 2005). However the production of neurons from this epithelium has not been extensively investigated, so whether epithelial thickening relates to expansion of the progenitor pool and enhanced neurogenesis in tunicates remains to be resolved.

Section 5.4.1 RGS3hs and the Expansion of the R4 Subfamily

The data presented in this chapter also bring forth a novel understanding of the expansion of the R4 subfamily of RGS proteins. Essentially, non-RGS3 R4 genes originate from RGS3hs, produced at a duplicated RGS3 locus early in the vertebrate lineage. The N-terminal sequences were lost following this duplication event, creating RGS-only genes. Importantly, the N-terminal KYLER sequences of these proteins were left intact. This could relate to a conserved function of these short polypeptide regions, and/or conservation of a regulatory region which includes the coding sequence. In support of the latter hypothesis, RGS3hs-HTMKE and other R4 subfamily members perform similar functions in the negative regulation of migration in a variety of tissues. In this study, a truncated isoform containing neither the N-terminal KYLER nor HTMKE sequences was sufficient to negatively regulate neuronal migration in the forming chick CSG (Section 4.3.3). RGS4 negatively regulates breast cancer metastasis (Mu et al., 2012; Xie et al., 2009) and is dramatically downregulated in metastatic ovarian cancer cells (Hurst et al., 2009). Finally, RGS1, -13 and -16 have been shown to negatively regulate lymphocyte migration (Bansal et al., 2007). This final example is interesting in light of the fact that non-RGS3 R4 genes share a common synteny with the major histocompatibility complex (MHC), a large protein-coding region which is highly expressed in the vertebrate immune system and which similarly expanded during vertebrate evolution (Kasahara, 2007; Suurväli et al., 2013). This suggests that non-RGS3 R4 genes might have co-evolved with the MHC in early vertebrate evolution and have been employed in the immune system to regulate lymphocyte migration; indeed, RGS2, -5, and -13 are highly expressed in lymphocytes (Moratz et al., 2004). If the conservation of KYLER sequences does correspond to an important polypeptide motif specific to the regulation of lymphocyte migration, RGS3hs-HTMKE should not be able to perform the same

biochemical function. However, RGS3hs-HTMKE overexpression in mouse lymphocytes similarly negatively regulates their migration (Reif and Cyster, 2000). Together this suggests that KYLER and HTMKE polypeptide regions are dispensable for protein function, but transcription of the isoforms is driven by different regulatory sequences.

Finally, RGS3hs might have an ancestral role in the neuronal context. Differential *in situ* hybridisation in the chick showed both isoforms expressed in the CSG, but RGS3hs-KYLER additionally expressed in other sensory neuronal subtypes (Section 3.5). Amphioxus RGS3hs encodes only the C-terminal sequence homologous to the shared sequence of RGS3hs-KYLER and RGS3hs-HTMKE (Section 5.2.2). If it is expressed in migratory neurons as postulated in the previous section, this would suggest an ancient function of RGS3hs in migratory sensory neurons, with the employment of the KYLER and HTMKE enhancers in vertebrate evolution in association with the diversification of sensory neuron subtypes.

Chapter 6. Conclusions

In this thesis, I aimed to determine the developmental and evolutionary roles of isoforms of RGS3 during neuronal differentiation. To this end, I used the forming petrosal ganglion of the chick embryo as a primary model system to spatially dissect neuroepithelial progenitors, immature neuroblasts, and differentiated neurons.

Section 6.1 Temporal Co-linearity within the RGS3 Locus

I found distinct expression and functions of RGS3 isoforms during neuroblast commitment and maturation of the forming chick CSG. In summary:

- RGS3hL and RGS3L, expressed in the progenitor placode (Figure 3.4J), negatively regulate commitment of progenitors to neuroblasts (Figure 4.3, Figure 4.10);
- RGS3s, expressed in immature neuroblasts (Figure 3.4K), negatively regulates differentiation of neuroblasts into neurons (Figure 4.6, Figure 4.12); and
- RGS3hs, expressed in differentiated neurons (Figure 3.4L,M), negatively regulates neuronal migration and morphology (Figure 4.7, Figure 4.13, Figure 4.14).

Intriguingly, the sequence of expression of these isoforms in space and time is co-linear with their genomic orientation. To our knowledge, such intragenic spatiotemporal co-linearity has not been described. However, with recent advances in transcriptome sequencing, the complexity and diversity of isoform generation is only beginning to be uncovered (Pelechano et al., 2013). Thus, this could represent the tip of the iceberg of intragenic transcriptional regulation. It remains to be seen to what extent intragenic

promoters drive N-terminally truncated isoforms as in the case of RGS3, and more importantly, to what extent these isoforms are co-linearly regulated in space and time.

However, it is clear that this mechanism of regulation has profound implications for the formation of the chick CSG. RGS3L must be expressed exclusively in the placode, likely because it has a PDZ domain which can potentially localise it to apical junctions. RGS3s must be expressed exclusively in the neuroblasts, because it can prevent differentiation but be deactivated by the EF Hand domain once intracellular Ca^{2+} levels accumulate. And RGS3hs must be expressed in the neurons, where it can inhibit a G protein signalling pathway important for cytoskeletal dynamics involved in migration (for example, mediated by Gαq) free from the regulation of N-terminal domains.

I determined the conservation of the expression of the isoforms in the forming mouse CSG and the developing mouse cortex. Importantly, the expression patterns seen in the mouse placodes and CSG neurons paralleled those of the mouse VZ and CP (respectively; Figure 3.10), suggesting the programme of RGS3 isoform expression is similar between these neuronal tissues. However, with the exception of RGS3hL, C2PA, and/or RGS3L, which were expressed in the mouse cortex as well as the placodes of both species, there were species-specific differences between the mouse and chick CSG, highlighted below.

Section 6.1.1 RGS3s

RGS3s was expressed in the neuroblast staging area outside the chick petrosal placode, consistent with its role in the negative regulation of neuroblast differentiation. In contrast, it was expressed in the differentiated neurons of the mouse CSG and CP neurons of the cortex. This suggests that mouse RGS3s serves a completely separate

biochemical function. This is not difficult to conceive, considering that mouse RGS3s possesses an extra ~150 aa in its N-terminal sequences relative to chick RGS3s (Figure 3.11). The N terminus of RGS3s includes an EF Hand domain, which I found through deletion to be important for regulation of RGS3s function (Figure 4.12). In addition, a critical serine residue has been found in the N-terminus of RGS3s to be essential for binding by 14-3-3 proteins, which negatively regulate RGS3s (Section 1.2.4.3.3). Lastly, the N-terminus of human RGS3s is sufficient to localise to the plasma membrane following treatment of a Ca^{2+} ionophore (Dulin et al., 1999). Thus the N terminus of RGS3s is in large part responsible for its regulation, and additional sequences in the mouse N terminus could alter the localisation and/or conformation of the protein in a manner which results in a new biochemical function.

Such a new function would be expected to relate to a cell-biological process of neurons, such as migration and process stabilisation. Importantly, ectopic overexpression of chick RGS3s in differentiated neurons of the chick CSG did not affect neuronal migration or morphology (Figure 4.13C and Figure 4.14A,B). If ectopic overexpression of mouse RGS3s in chick CSG neurons did affect neuronal migration and/or morphology (especially if it concomitantly did not affect neuroblast differentiation), this would provide strong evidence for a new biochemical function of mouse RGS3s.

Of course, this expression study was limited by only analysing two species. It would be interesting to compare expression of RGS3s in the forming CSG of non-galliform birds (as well as reptiles and anamniotes) and non-rodent mammals to confirm that this is not a derived clade-specific phenomenon. In parallel, it would be interesting to compare the exons of RGS3s N-terminal to the RGS domain in each species (namely, the large exon 20, which is aligned in Figure 3.11 and encodes the majority of the N-terminus of

RGS3s). If a homologous region outside of the chick sequence (such as that aligned between human and mouse in Figure 3.11) is present only in species with expression of RGS3s in CSG neurons (such as mammals), this would dramatically strengthen the idea that a new biochemical function of RGS3s, and consequent change in expression, was acquired in evolution outside of the avian phylum. Lastly, it is important to note that from the transcriptomic data available for us to mine, RGS3s was not found in agnathans (Figure 5.5A), which suggests it cannot serve a regulatory role in placode-derived neuroblasts of these species. Thus while RGS3s negatively regulates neuroblast differentiation of the chick CSG, it is not employed in this function in all vertebrates.

Section 6.1.2 RGS3hs and RGS4

The relationship between RGS3hs and RGS4 was also explored in this thesis. Importantly, RGS4 likely emerged early in the vertebrate lineage essentially as a duplication of RGS3hs-KYLER (see below). In the chick, RGS3hs-HTMKE and RGS3hs-KYLER are expressed in CSG neurons (Figure 3.4L,M), but RGS4 expression is absent from neural tissue at the stages examined (Section 3.4.1.4). In the mouse, the opposite is true. RGS3hs-KYLER is not encoded in the genome, and RGS3hs-HTMKE is not expressed in CSG or cortex neurons (Figure 3.7H, Figure 3.8E). RGS4, by contrast, is strongly expressed in CSG and cortical neurons (Figure 3.7I, Figure 3.8F). Furthermore, RGS3hs-KYLER of the chick embryo and RGS4 of the mouse embryo were expressed in similar populations of neurons outside of the CSG, such as the DRG (Figure 3.9; Section 3.5). Taken together, this suggests these three proteins are virtually interchangeable in neurons, and are differentiated by enhancers governing their differential expression.

Section 6.2 Evolution of RGS3 and the Placodes

The results in Chapter 5 of this thesis show an ancient origin for RGS3. Our analysis of the conservation of RGS3, its isoforms, and other members of the R4 subfamily of RGS proteins in metazoan phylogeny showed that:

- RGS3 is the founding member of the R4 subfamily (Figure 5.4);
- the expansion of R4 genes probably resulted from a duplication of RGS3 followed by the loss of its N-terminal domains, whilst retaining the RGS3hs sequences (Figure 5.7); and
- RGS3 lost a GEF domain after the divergence of cephalochordates from the chordate lineage (Figure 5.2).

Ectopic overexpression of the amphioxus full-length RGS3 product resulted in a thinning of the placode (Figure 5.8), suggesting that the GEF domain plays a role in preventing pseudostratification. Combined with the fact that tunicates, which lack the GEF domain (Figure 5.2), have a thickened proto-placode (Figure 1.6), this suggests that the loss of the GEF domain from the RGS3 locus might have been a critical feature in the early olfactore lineage which allowed for pseudostratified placodes to evolve. This is intriguing in light of the parallels between placodes and neuroepithelia of the neural tube, and commands a broadened expression and functional analysis of RGS3hL. The data from this thesis show that RGS3hL and/or C2PA are expressed in pre-placodal ectoderm; thus, RGS3hL could play an essential role in the establishment and maintenance of the pseudostratified morphology of the placode. Does it play a similar role in the forming neural tube? Intriguingly, loss of RGS3hL, C2PA and RGS3L by means of homologous recombination of a premature stop codon before the PDZ domain in mouse results in significant thinning of the developing cortex by E15.5 (Qiu et al., 2010). Perhaps the

loss of the GEF domain in vertebrates caused it to adopt a new function of promoting pseudostratification.

Moreover, is RGS3hL in amphioxus expressed in the ventral proto-placode, which does not exhibit a pseudostratified morphology (Figure 1.6)? If so, this could be a key indicator of the ancestral role of RGS3, and suggests a hypothesis as follows. In poriferans and more basal deuterostomes, RGS3hL could be expressed in non-neural surface ectoderm, where it would play a role in epithelial maintenance. In cephalochordates, RGS3hL could play a similar role, though the surface ectoderm tissue in which it would be expressed has evolved the capacity to generate sensory neurons. In olfactores, it is expressed in a homologous non-neural patch of surface ectoderm which generates sensory neurons; however, a deletion of the GEF domain causes it to have a different biochemical function which permits (and perhaps promotes) pseudostratification. Finally, in vertebrates, RGS3hL is expressed in pre-placodal ectoderm and perhaps developing neuroepithelia of the CNS, where it plays an important role in neuroepithelial establishment and consequent generation of neurons of the nervous system. A demonstration of the specific expression of RGS3hL in these tissues will provide a solid foundation to further investigation on the developmental and evolutionary importance of RGS3.

Section 6.3 Summary

Taken together, the findings in this thesis have profound implications for the role of RGS3 in the vertebrate nervous system, both in terms of evolution of the nervous system and in terms of development of vertebrate neurons. Above all else, the regulation of the RGS3 locus by intragenic temporal co-linearity is responsible for the graded maturation of neurons in the developing vertebrate embryo, by generating distinct isoforms, with distinct biochemical functions, exerted in distinct phases of a neuroblast's lifetime.

Chapter 7. References

Abitua, P. B., Wagner, E., Navarrete, I. A. and Levine, M. (2012). Identification of a rudimentary neural crest in a non-vertebrate chordate. *Nature* **492**, 104-107.

Abu-Elmagd, M., Ishii, Y., Cheung, M., Rex, M., Le Rouëdec, D. and Scotting, P. J. (2001). cSox3 expression and neurogenesis in the epibranchial placodes. *Developmental Biology* **237**, 258-269.

Afonso, C. and Henrique, D. (2006). PAR3 acts as a molecular organizer to define the apical domain of chick neuroepithelial cells. *Journal of Cell Science* **119**, 4293-4304.

Alberts, B., Johnson, A. and Lewis, J. (2002). Signaling through G-Protein-Linked Cell-Surface. In *Molecular Biology of the Cell*. New York: Garland Science.

Altschul, S. F., Gish, W., Miller, W., Myers, E. W. and Lipman, D. J. (1990). Basic local alignment search tool. *Journal of Molecular Biology* **215**, 403-410.

Anders, S. and Huber, W. (2010). Differential expression analysis for sequence count data. *Genome Biology* **11**, R106.

Anderson, D. J. (1999). Lineages and transcription factors in the specification of vertebrate primary sensory neurons. *Current Opinion in Neurobiology* **9**, 517-524.

Anger, T., Grebe, N., Osinski, D., Stelzer, N., Carson, W., Daniel, W. G., Hoeher, M. and Garlichs, C. D. (2008). Role of endogenous RGS proteins on endothelial ERK 1/2 activation. *Experimental and Molecular Pathology* **85**, 165-173.

Anger, T., Klintworth, N., Stumpf, C., Daniel, W. G., Mende, U. and Garlichs, C. D. (2007). RGS protein specificity towards Gq- and Gi/o-mediated ERK 1/2 and Akt activation, in vitro. *Journal of Biochemistry and Molecular Biology* **40**, 899-910.

Anger, T., Zhang, W. and Mende, U. (2004). Differential contribution of GTPase activation and effector antagonism to the inhibitory effect of RGS proteins on Gq-mediated signaling in vivo. *Journal of Biological Chemistry* **279**, 3906-3915.

Artinger, K. B., Fedtsova, N., Rhee, J. M., Bronner-Fraser, M. and Turner, E. (1998). Placodal origin of Brn-3-expressing cranial sensory neurons. *Journal of Neurobiology* **36**, 572-585.

Arvanitis, D. N., Béhar, A., Tryoen-Tóth, P., Bush, J. O., Jungas, T., Vitale, N. and Davy, A. (2013). Ephrin B1 maintains apical adhesion of neural progenitors. *Development* **140**, 2082-2092.

Bach, I. (2000). The LIM domain: regulation by association. *Mechanisms of Development* **91**, 5-17.

Badea, T. C., Williams, J., Smallwood, P., Shi, M., Motajo, O. and Nathans, J. (2012). Combinatorial expression of Brn3 transcription factors in somatosensory neurons: genetic and morphologic analysis. *Journal of Neuroscience* **32**, 995-1007.

Bae, B. I., Tietjen, I., Atabay, K. D., Evrony, G. D., Johnson, M. B., Asare, E., Wang, P. P., Murayama, A. Y., Im, K., Lisgo, S. N., et al. (2014). Evolutionarily dynamic alternative splicing of GPR56 regulates regional cerebral cortical patterning. *Science* **343**, 764-768.

Baker, C. V. and Bronner-Fraser, M. (2000). Establishing neuronal identity in vertebrate neurogenic placodes. *Development* **127**, 3045-3056.

Baker, C. V., Bronner-Fraser, M., Le Douarin, N. M. and Teillet, M. A. (1997). Early- and late-migrating cranial neural crest cell populations have equivalent developmental potential in vivo. *Development* **124**, 3077-3087.

Baker, C. V., Stark, M. R., Marcelle, C. and Bronner-Fraser, M. (1999). Competence, specification and induction of Pax-3 in the trigeminal placode. *Development* **126**, 147-156.

Baker, C. V. H. and Bronner-Fraser, M. (2001). Vertebrate Cranial Placodes I. Embryonic induction. *Developmental Biology* **232**, 1-61.

Bansal, G., Druey, K. M. and Xie, Z. (2007). R4 RGS proteins: regulation of G-protein signaling and beyond. *Pharmacology & Therapeutics* **116**, 473-495.

Begbie, J. (2008). Migration of Neuroblasts from Neurogenic Placodes. *Developmental Neuroscience* **30**, 3–35.

---- (2013). Induction and Patterning of Neural Crest and Ectodermal Placodes and their Derivatives. In *Comprehensive Developmental Neuroscience: Patterning and Cell Type Specification in the Developing CNS and PNS*, pp. 239-258. Amsterdam: Elsevier.

Begbie, J., Ballivet, M. and Graham, A. (2002). Early steps in the production of sensory neurons by the neurogenic placodes. *Molecular and Cellular Neuroscience* **21**, 502-511.

Begbie, J., Brunet, J. F., Rubenstein, J. L. and Graham, A. (1999). Induction of the epibranchial placodes. *Development* **126**, 895-902.

Begbie, J. and Graham, A. (2001). Integration between the epibranchial placodes and the hindbrain. *Science* **294**, 595-598.

Benzing, T., Yaffe, M. B., Arnould, T., Sellin, L., Schermer, B., Schilling, B., Schreiber, R., Kunzelmann, K., Leparc, G. G., Kim, E., et al. (2000). 14-3-3 interacts with regulator of G protein signaling proteins and modulates their activity. *Journal of Biological Chemistry* **275**, 28167-28172.

Bernstein, B. E., Birney, E., Dunham, I., Green, E. D., Gunter, C. and Snyder, M. (2012). An integrated encyclopedia of DNA elements in the human genome. *Nature* **489**, 57-74.

Bertrand, N., Castro, D. S. and Guillemot, F. (2002). Proneural genes and the specification of neural cell types. *Nature Reviews Neuroscience* **3**, 517-530.

Bhattacharyya, S., Bailey, A. P., Bronner-Fraser, M. and Streit, A. (2004). Segregation of lens and olfactory precursors from a common territory: cell sorting and reciprocity of Dlx5 and Pax6 expression. *Developmental Biology* **271**, 403-414.

Bhattacharyya, S. and Bronner-Fraser, M. (2008). Competence, specification and commitment to an olfactory placode fate. *Development* **135**, 4165-4177.

Bielen, H. and Houart, C. (2014). The Wnt cries many: Wnt regulation of neurogenesis through tissue patterning, proliferation, and asymmetric cell division. *Developmental Neurobiology*.

Blentic, A., Chambers, D., Skinner, A., Begbie, J. and Graham, A. (2011). The formation of the cranial ganglia by placodally-derived sensory neuronal precursors. *Molecular and Cellular Neuroscience* **46**, 452-459.

Boardman, P. E., Sanz-Ezquerro, J., Overton, I. M. and Burt, D. W. (2002). A comprehensive collection of chicken cDNAs. *Current Biology* **12**, 1965-1969.

Bone, Q. and Ryan, K. P. (1978). Cupular sense organs in Ciona (Tunicata: Ascidiacea). *Journal of Zoology* **186**, 417-429.

Bowman, E. P., Campbell, J. J., Druey, K. M., Scheschonka, A., Kehrl, J. H. and Butcher, E. C. (1998). Regulation of chemotactic and proadhesive responses to chemoattractant receptors by RGS (regulator of G-protein signaling) family members. *Journal of Biological Chemistry* **273**, 28040-28048.

Brunet, J. F. and Pattyn, A. (2002). Phox2 genes - from patterning to connectivity. *Current Opinion in Genetics & Development* **12**, 435-440.

Burighel, P., Lane, N. J., Zaniolo, G. and Manni, L. (1998). Neurogenic role of the neural gland in the development of the ascidian, Botryllus schlosseri (Tunicata, Urochordata). *Journal of Comparitive Neurology* **394**, 230-241.

Butts, T. and Graham, A. (2013). Old before their time: the ancient origins of the neural crest. *Pigment Cell & Melanoma Research*.

Candiani, S., Oliveri, D., Parodi, M., Bertini, E. and Pestarino, M. (2006). Expression of AmphiPOU-IV in the developing neural tube and epidermal sensory neural precursors in amphioxus supports a conserved role of class IV POU genes in the sensory cells development. *Development Genes and Evolution* **216**, 623-633.

Candiani, S., Pennati, R., Oliveri, D., Locascio, A., Branno, M., Castagnola, P., Pestarino, M. and De Bernardi, F. (2005). Ci-POU-IV expression identifies PNS neurons in embryos and larvae of the ascidian Ciona intestinalis. *Development Genes and Evolution* **215**, 41-45.

Cappello, S., Attardo, A., Wu, X., Iwasato, T., Itohara, S., Wilsch-Bräuninger, M., Eilken, H. M., Rieger, M. A., Schroeder, T. T., Huttner, W. B., et al. (2006). The Rho-GTPase cdc42 regulates neural progenitor fate at the apical surface. *Nature Neuroscience* **9**, 1099-1107.

Castro-Fernández, C., Brothers, S. P. and Michael Conn, P. (2003). A Galphas mutation (D229S) differentially effects gonadotropin-releasing hormone receptor regulation by RGS10, RGS3 and RGS3T. *Molecular and Cellular Endocrinology* **200**, 119-126.

Castro-Fernández, C., Maya-Núñez, G. and Méndez, J. P. (2004). Regulation of follicle-stimulating and luteinizing hormone receptor signaling by "regulator of G protein signaling" proteins. *Endocrine* **25**, 49-54.

Chahdi, A. and Sorokin, A. (2010). The role of beta(1)Pix/caveolin-1 interaction in endothelin signaling through Galpha subunits. *Biochemical and Biophysical Research Communications* **391**, 1330-1335.

Chatterjee, T. K., Eapen, A., Kanis, A. B. and Fisher, R. A. (1997a). Genomic organization, 5'-flanking region, and chromosomal localization of the human RGS3 gene. *Genomics* **45**, 429-433.

Chatterjee, T. K., Eapen, A. K. and Fisher, R. A. (1997b). A truncated form of RGS3 negatively regulates G protein-coupled receptor stimulation of adenylyl cyclase and phosphoinositide phospholipase C. *Journal of Biological Chemistry* **272**, 15481-15487.

Chen, B., Siderovski, D. P., Neubig, R. R., Lawson, M. A. and Trejo, J. (2014). Regulation of protease-activated receptor 1 signaling by the adaptor protein complex 2 and R4 subfamily of regulator of G protein signaling proteins. *Journal of Biological Chemistry* **289**, 1580-1591.

Chitnis, A., Henrique, D., Lewis, J., Ish-Horowicz, D. and Kintner, C. (1995). Primary neurogenesis in Xenopus embryos regulated by a homologue of the Drosophila neurogenic gene Delta. *Nature* **375**, 761-766.

Cho, H., Harrison, K., Schwartz, O. and Kehrl, J. H. (2003). The aorta and heart differentially express RGS (regulators of G-protein signalling) proteins that selectively regulate sphingosine 1-phosphate, angiotensin II and endothelin-1 signalling. *Biochemistry Journal* **371**, 973-980.

Christiaen, L., Burighel, P., Smith, W. C., Vernier, P., Bourrat, F. and Joly, J. S. (2002). Pitx genes in Tunicates provide new molecular insight into the evolutionary origin of pituitary. *Gene* **287**, 107-113.

Colas, J. F. and Schoenwolf, G. C. (2001). Towards a cellular and molecular understanding of neurulation. *Developmental Dynamics* **221**, 117-145.

Costa, M. R., Wen, G., Lepier, A., Schroeder, T. and Götz, M. (2008). Par-complex proteins promote proliferative progenitor divisions in the developing mouse cerebral cortex. *Development* **135**, 11-22.

Costigan, M., Samad, T. A., Allchorne, A., Lanoue, C., Tate, S. and Woolf, C. J. (2003). High basal expression and injury-induced down regulation of two regulator of G-protein signaling transcripts, RGS3 and RGS4 in primary sensory neurons. *Molecular and Cellular Neuroscience* **24**, 106-116.

Cotteret, S. and Chernoff, J. (2002). The evolutionary history of effectors downstream of Cdc42 and Rac. *Genome Biology* **3**, REVIEWS0002.

Curran, K., Lister, J. A., Kunkel, G. R., Prendergast, A., Parichy, D. M. and Raible, D. W. (2010). Interplay between Foxd3 and Mitf regulates cell fate plasticity in the zebrafish neural crest. *Developmental Biology* **344**, 107-118.

D'Amico-Martel, A. (1982). Temporal patterns of neurogenesis in avian cranial sensory and autonomic ganglia. *American Journal of Anatomy* **163**, 351-372.

D'Amico-Martel, A. and Noden, D. M. (1980). An autoradiographic analysis of the development of the chick trigeminal ganglion. *Journal of Embryology and Experimental Morphology* **55**, 167-182.

---- (1983). Contributions of placodal and neural crest cells to avian cranial peripheral ganglia. *American Journal of Anatomy* **166**, 445-468.

Darnell, D. K., Stanislaw, S., Kaur, S. and Antin, P. B. (2010). Whole mount in situ hybridization detection of mRNAs using short LNA containing DNA oligonucleotide probes. *RNA* **16**, 632-637.

Das, R. M. and Storey, K. G. (2014). Apical abscission alters cell polarity and dismantles the primary cilium during neurogenesis. *Science* **343**, 200-204.

Dauger, S., Pattyn, A., Lofaso, F., Gaultier, C., Goridis, C., Gallego, J. and Brunet, J. F. (2003). Phox2b controls the development of peripheral chemoreceptors and afferent visceral pathways. *Development* **130**, 6635-6642.

Deaton, A. M. and Bird, A. (2011). CpG islands and the regulation of transcription. *Genes & Development* **25**, 1010-1022.

Delsuc, F., Brinkmann, H., Chourrout, D. and Philippe, H. (2006). Tunicates and not cephalochordates are the closest living relatives of vertebrates. *Nature* **439**, 965-968.

Donoghue, P. C., Graham, A. and Kelsh, R. N. (2008). The origin and evolution of the neural crest. *BioEssays* **30**, 530-541.

Doupnik, C. A., Davidson, N., Lester, H. A. and Kofuji, P. (1997). RGS proteins reconstitute the rapid gating kinetics of gbetagamma-activated inwardly rectifying K+ channels. *Proceedings of the National Academy of Sciences USA* **94**, 10461-10466.

Druey, K. M., Blumer, K. J., Kang, V. H. and Kehrl, J. H. (1996). Inhibition of G-protein-mediated MAP kinase activation by a new mammalian gene family. *Nature* **379**, 742-746.

Dulin, N. O., Pratt, P., Tiruppathi, C., Niu, J., Voyno-Yasenetskaya, T. and Dunn, M. J. (2000). Regulator of G protein signaling RGS3T is localized to the nucleus and induces apoptosis. *Journal of Biological Chemistry* **275**, 21317-21323.

Dulin, N. O., Sorokin, A., Reed, E., Elliott, S., Kehrl, J. H. and Dunn, M. J. (1999). RGS3 inhibits G protein-mediated signaling via translocation to the membrane and binding to Galpha11. *Molecular and Cellular Biology* **19**.

Dupin, E., Creuzet, S. and Le Douarin, N. M. (2006). The contribution of the neural crest to the vertebrate body. *Advances in Experimental Medicine and Biology* **589**, 96-119.

Eng, S. R., Dykes, I. M., Lanier, J., Fedtsova, N. and Turner, E. E. (2007). POU-domain factor Brn3a regulates both distinct and common programs of gene expression in the spinal and trigeminal sensory ganglia. *Neural Development* **2**.

Englund, C., Fink, A., Lau, C., Pham, D., Daza, R. A., Bulfone, A., Kowalczyk, T. and Hevner, R. F. (2005). Pax6, Tbr2, and Tbr1 are expressed sequentially by radial glia, intermediate progenitor cells, and postmitotic neurons in developing neocortex. *Journal of Neuroscience* **25**, 247-251.

Etienne-Manneville, S. and Hall, A. (2002). Rho GTPases in cell biology. *Nature* **420**, 629-635.

Farley, E. K., Gale, E., Chambers, D. and Li, M. (2011). Effects of in ovo electroporation on endogenous gene expression: genome-wide analysis. *Neural Development* **6**, 17.

Fedtsova, N. G. and Turner, E. E. (1995). Brn-3.0 expression identifies early post-mitotic CNS neurons and sensory neural precursors. *Mechanisms of Development* **53**, 291-304.

Fish, J., Dehay, C., Kennedy, H. and Huttner, W. (2008). Making bigger brains-the evolution of neural-progenitor-cell division. *Journal of Cell Science* **121**, 2783-2793.

Fleenor, S. J. and Begbie, J. (2014). Neural crest cell and placode interactions in cranial PNS development. In *Neural Crest Cells: Evolution, Development and Disease*, pp. 153-165. Amsterdam: Elsevier.

Flicek, P., Amode, M., Barrell, D., Beal, K., Billis, K., Brent, S., Carvalho-Silva, D., Clapham, P., Coates, G., Fitzgerald, S., et al. (2014). Ensembl 2014. *Nucleic Acids Research* **42**, D749-755.

Florio, M. and Huttner, W. B. (2014). Neural progenitors, neurogenesis and the evolution of the neocortex. *Development* **141**, 2182-2194.

Fode, C., Gradwohl, G., Morin, X., Dierich, A., LeMeur, M., Goridis, C. and Guillemot, F. (1998). The bHLH protein NEUROGENIN 2 is a determination factor for epibranchial placode-derived sensory neurons. *Neuron* **20**, 483-494.

Fornaro, M., Geuna, S., Fasolo, A. and Giacobini-Robecchi, M. G. (2001). Evidence of very early neuronal migration from the olfactory placode of the chick embryo. *Neuroscience* **107**, 191-197.

Freisinger, C. M., Fisher, R. A. and Slusarski, D. C. (2010). Regulator of g protein signaling 3 modulates wnt5b calcium dynamics and somite patterning. *Public Library of Science Genetics* **6**, e1001020.

Freter, S., Fleenor, S. J., Freter, R., Liu, K. J. and Begbie, J. (2013). Cranial neural crest cells form corridors prefiguring sensory neuroblast migration. *Development* **140**, 3595-3600.

Freter, S., Muta, Y., Mak, S. S., Rinkwitz, S. and Ladher, R. K. (2008). Progressive restriction of otic fate: the role of FGF and Wnt in resolving inner ear potential. *Development* **135**, 3415-3424.

Freyer, L., Aggarwal, V. and Morrow, B. E. (2011). Dual embryonic origin of the mammalian otic vesicle forming the inner ear. *Development* **138**, 5403-5414.

Fukushima, N. (2004). LPA in neural cell development. *Journal of Cellular Biochemistry* **92**, 993-1003.

Fukushima, N., Shano, S., Moriyama, R. and Chun, J. (2007). Lysophosphatidic acid stimulates neuronal differentiation of cortical neuroblasts through the LPA1-G(i/o) pathway. *Neurochemistry International* **50**, 302-307.

Gans, C. and Northcutt, R. G. (1983). Neural crest and the origin of vertebrates: a new head. *Science* **220**, 268-273.

Gardiner-Garden, M. and Frommer, M. (1987). CpG islands in vertebrate genomes. *Journal of Molecular Biology* **196**, 261-282.

Geach, T. J., Faas, L., Devader, C., Gonzalez-Cordero, A., Tabler, J. M., Brunsdon, H., Isaacs, H. V. and Dale, L. (2014). An essential role for LPA signalling in telencephalon development. *Development* **141**, 940-949.

George, L., Kasemeier-Kulesa, J., Nelson, B. R., Koyano-Nakagawa, N. and Lefcort, F. (2010). Patterned assembly and neurogenesis in the chick dorsal root ganglion. *Journal of Comparitive Neurology* **518**, 405-422.

Gibson, T. J., Hyvönen, M., Musacchio, A., Saraste, M. and Birney, E. (1994). PH domain: the first anniversary. *Trends in Biochemical Sciences* **19**, 349-353.

Götz, M. and Huttner, W. B. (2005). The cell biology of neurogenesis. *Nature Reviews Molecular Cell Biology* **6**, 777-788.

Götz, M., Stoykova, A. and Gruss, P. (1998). Pax6 controls radial glia differentiation in the cerebral cortex. *Neuron* **21**, 1031-1044.

Graham, A. and Begbie, J. (2000). Neurogenic placodes: a common front. *Trends in Neuroscience* **23**, 313-316.

Graham, A., Blentic, A., Duque, S. and Begbie, J. (2007). Delamination of cells from neurogenic placodes does not involve an epithelial-to-mesenchymal transition. *Development* **134**, 4141-4145.

Graham, A. and Shimeld, S. M. (2013). The origin and evolution of the ectodermal placodes. *Journal of Anatomy* **222**, 32-40.

Green, M. J., Myat, A. M., Emmenegger, B. A., Wechsler-Reya, R. J., Wilson, L. J. and Wingate, R. J. (2014). Independently specified Atoh1 domains define novel developmental compartments in rhombomere 1. *Development* **141**, 389-398.

Greger, I. H., Aranda, A. and Proudfoot, N. (2000). Balancing transcriptional interference and initiation on the GAL7 promoter of Saccharomyces cerevisiae. *Proceedings of the National Academy of Sciences USA* **97**, 8415-8420.

Grillet, N., Dubreuil, V., Dufour, H. D. and Brunet, J. F. (2003). Dynamic expression of RGS4 in the developing nervous system and regulation by the neural type-specific transcription factor Phox2b. *Journal of Neuroscience* **23**, 10613-10621.

Grillet, N., Pattyn, A., Contet, C., Kieffer, B. L., Goridis, C. and Brunet, J. F. (2005). Generation and characterization of Rgs4 mutant mice. *Molecular and Cellular Biology* **25**, 4221-4228.

Grocott, T., Tambalo, M. and Streit, A. (2012). The peripheral sensory nervous system in the vertebrate head: a gene regulatory perspective. *Developmental Biology* **370**, 3-23.

Groves, A. K. and Bronner-Fraser, M. (2000). Competence, specification and commitment in otic placode induction. *Development* **127**, 3489-3499.

Groves, A. K. and Fekete, D. (2012). Shaping sound in space: the regulation of inner ear patterning. *Development* **139**, 245-257.

Grüning, W., Arnould, T., Jochimsen, F., Sellin, L., Ananth, S., Kim, E. and Walz, G. (1999). Modulation of renal tubular cell function by RGS3. *American Journal of Physiology* **276**, F535-543.

Gummalla, M., Galetti, S., Maeda, R. K. and Karch, F. (2014). Hox gene regulation in the central nervous system of Drosophila. *Frontiers in Cellular Neuroscience* **8**.

Hamburger, V. and Hamilton, H. L. (1992). A series of normal stages in the development of the chick embryo. 1951. *Developmental Dynamics* **195**, 231-272.

Hans, F. and Dimitrov, S. (2001). Histone H3 phosphorylation and cell division. *Oncogene* **20**, 3021-3027.

Hans, S., Liu, D. and Westerfield, M. (2004). Pax8 and Pax2a function synergistically in otic specification, downstream of the Foxi1 and Dlx3b transcription factors. *Development* **131**, 5091-5102.

Hao, J., Michalek, C., Zhang, W., Zhu, M., Xu, X. and Mende, U. (2006). Regulation of cardiomyocyte signaling by RGS proteins: differential selectivity towards G proteins and susceptibility to regulation. *Journal of Molecular and Cellular Cardiology* **41**, 51-61.

Harlow, D. E. and Barlow, L. A. (2007). Embryonic origin of gustatory cranial sensory neurons. *Developmental Biology* **310**, 317-328.

Harlow, D. E., Yang, H., Williams, T. and Barlow, L. A. (2011). Epibranchial placode-derived neurons produce BDNF required for early sensory neuron development. *Developmental Dynamics* **2**, 309-323.

Haubensak, W., Attardo, A., Denk, W. and Huttner, W. B. (2004). Neurons arise in the basal neuroepithelium of the early mammalian telencephalon: a major site of neurogenesis. *Proceedings of the National Academy of Sciences USA* **101**, 3196-3201.

Hecht, J. H., Weiner, J. A., Post, S. R. and Chun, J. (1996). Ventricular zone gene-1 (vzg-1) encodes a lysophosphatidic acid receptor expressed in neurogenic regions of the developing cerebral cortex. *Journal of Cell Biology* **135**, 1071-1083.

Heintzman, N. D., Stuart, R. K., Hon, G., Yutao, F., Ching, C. W., Hawkins, R. D., Barrera, L. O., Van Calcar, S., Qu, C., Ching, K. A., et al. (2007). Distinct and predictive chromatin signatures of transcriptional promoters and enhancers in the human genome. *Nature Genetics* **39**, 311-318.

Henrique, D., Adam, J., Myat, A., Chitnis, A., Lewis, J. and Ish-Horowicz, D. (1995). Expression of a Delta homologue in prospective neurons in the chick. *Nature* **375**, 787-790.

Higuchi, N., Kohno, K. and Kadowaki, T. (2009). Specific retention of the protostome-specific PsGEF may parallel with the evolution of mushroom bodies in insect and lophotrochozoan brains. *BMC Biology* **7**.

Hirabayashi, S., Ohno, H., Iida, J. and Hata, Y. (2002). C2PA is a nuclear protein implicated in the heat shock response. *Journal of Biological Chemistry* **87**, 65-74.

Hiscock, J. and Straznicky, C. (1986). The development of the neurons of the glossopharyngeal (IX) and vagal (X) sensory ganglia in chick embryos. *Histology and Histopathology* **1**, 129-137.

Holland, P., Garcia-Fernàndez, J., Williams, N. and Sidow, A. (1994). Gene duplications and the origins of vertebrate development. *Development (Supplement)*, 125-133.

Hughey, R. and Krogh, A. (1996). Hidden Markov models for sequence analysis: extension and analysis of the basic method. *Computer Applications in the Biosciences* **12**, 95-107.

Hurst, J., Mendpara, N. and Hooks, S. (2009). Regulator of G-protein signalling expression and function in ovarian cancer cell lines. *Cellular & Molecular Biology Letters* **14**, 153-174.

Hutchins, B. I., Klenke, U. and Wray, S. (2013). Calcium release-dependent actin flow in the leading process mediates axophilic migration. *Journal of Neuroscience* **33**, 11361-11371.

Ikeda, M., Hirokawa, M., Satani, N., Kinoshita, T., Watanabe, Y., Inoue, H., Tone, S., Ishikawa, T. and Minatogawa, Y. (2001). Molecular cloning and characterization of a steroid receptor-binding regulator of G-protein signaling protein cDNA. *Gene* **2**, 207-214.

Ikeda, M., Inoue, S., Muramatsu, M. and Minatogawa, Y. (2007). Characterization and identification of a steroid receptor-binding protein, SRB-RGS. *Biological and Pharmaceutical Bulletin* **30**, 1056-1064.

Irvine, S. Q., Cangiano, M. C., Millette, B. J. and Gutter, E. S. (2007). Non-overlapping expression patterns of the clustered Dll-A/B genes in the ascidian Ciona intestinalis. *Journal of Experimental Zoology* **308**, 428-441.

Ishii, Y., Abu-Elmagd, M. and Scotting, P. J. (2001). Sox3 expression defines a common primordium for the epibranchial placodes in chick. *Developmental Biology* **236**, 344-353.

Itoh, M., Nagatomo, K., Kubo, Y., Sugimoto, M. and Saitoh, O. (2005). Molecular cloning and characterization of a new RGS protein of Medaka. *Gene* **345**, 165-171.

Jaén, C. and Doupnik, C. A. (2005). Neuronal Kir3.1/Kir3.2a channels coupled to serotonin 1A and muscarinic m2 receptors are differentially modulated by the "short" RGS3 isoform. *Neuropharmacology* **49**, 465-476.

---- (2006). RGS3 and RGS4 differentially associate with G protein-coupled receptor-Kir3 channel signaling complexes revealing two modes of RGS modulation: precoupling and collision coupling. *Journal of Biological Chemistry* **281**, 34549-34560.

Jaillon, O., Aury, J. M., Brunet, F., Petit, J. L., Stange-Thomann, N., Mauceli, E., Bouneau, L., Fischer, C., Ozouf-Costaz, C., Bernot, A., et al. (2004). Genome duplication in the teleost fish Tetraodon nigroviridis reveals the early vertebrate proto-karyotype. *Nature* **431**, 946-957.

Jansson, L. C. and Akerman, K. E. (2014). The role of glutamate and its receptors in the proliferation, migration, differentiation and survival of neural progenitor cells. *Journal of Neural Transmission*.

Kalcheim, C. and Le Douarin, N. M. (1986). Requirement of a neural tube signal for the differentiation of neural crest cells into dorsal root ganglia. *Developmental Biology* **116**, 451-466.

Kaltenbach, S. L., Yu, J. K. and Holland, N. D. (2009). The origin and migration of the earliest-developing sensory neurons in the peripheral nervous system of amphioxus. *Evolution & Development* **11**, 142-151.

Karakoula, A., Tovey, S. C., Brighton, P. J. and Willars, G. B. (2008). Lack of receptor-selective effects of either RGS2, RGS3 or RGS4 on muscarinic M3- and gonadotropin-releasing hormone receptor-mediated signalling through G alpha q/11. *European Journal of Pharmacology* **587**, 16-24.

Kasahara, M. (2007). The 2R hypothesis: an update. *Current Opinion in Immunology* **19**, 547-552.

Katayama, K., Melendez, J., Baumann, J. M., Leslie, J. R., Chauhan, B. K., Nemkul, N., Lang, R. A., Kuan, C. Y., Zheng, Y. and Yoshida, Y. (2011). Loss of RhoA in neural progenitor cells causes the disruption of adherens junctions and hyperproliferation. *Proceedings of the National Academy of Sciences USA* **108**, 7607-7612.

Katoh, K. and Standley, D. M. (2013). MAFFT multiple sequence alignment software version 7: improvements in performance and usability. *Molecular Biology and Evolution* **30**, 772-780.

Kehrl, J. H., Srikumar, D., Harrison, K., Wilson, G. L. and Shi, C. S. (2002). Additional 5' exons in the RGS3 locus generate multiple mRNA transcripts, one of which accounts for the origin of human PDZ-RGS3. *Genomics* **79**, 860-868.

Kent, W. J., Sugnet, C. W., Furey, T. S., Roskin, K. M., Pringle, T. H., Zahler, A. M. and Haussler, D. (2002). The human genome browser at UCSC. *Genome Research* **12**, 996-1006.

Kious, B. M., Baker, C. V., Bronner-Fraser, M. and Knecht, A. K. (2002). Identification and characterization of a calcium channel gamma subunit expressed in differentiating neurons and myoblasts. *Developmental Biology* **243**, 249-259.

Koblar, S. A., Krull, C. E., Pasquale, E. B., McLennan, R., Peale, F. D., Cerretti, D. P. and Bothwell, M. (2000). Spinal motor axons and neural crest cells use different molecular guides for segmental migration through the rostral half-somite. *Journal of Neurobiology* **42**, 437-447.

Koelle, M. R. and Horvitz, H. R. (1996). EGL-10 regulates G protein signaling in the C. elegans nervous system and shares a conserved domain with many mammalian proteins. *Cell* **84**, 115-125.

Kopecka, M., Kosek, D., Kukacka, Z., Rezabkova, L., Man, P., Novak, P., Obsil, T. and Obsilova, V. (2014). Role of the EF-hand like motif in the 14-3-3 protein-mediated activation of yeast neutral trehalase Nth1. *Journal of Biological Chemistry* **[Epub ahead of print]**.

Kourakis, M. J., Newman-Smith, E. and Smith, W. C. (2010). Key steps in the morphogenesis of a cranial placode in an invertebrate chordate, the tunicate Ciona savignyi. *Developmental Biology* **340**, 134-144.

Kourakis, M. J. and Smith, W. C. (2007). A conserved role for FGF signaling in chordate otic/atrial placode formation. *Developmental Biology* **312**, 245-257.

Krüger, M. and Braun, T. (2002). The neuronal basic helix-loop-helix transcription factor NSCL-1 is dispensable for normal neuronal development. *Molecular and Cellular Biology* **22**, 792-800.

Krull, C. E., Lansford, R., Gale, N. W., Collazo, A., Marcelle, C., Yancopoulos, G. D., Fraser, S. E. and Bronner-Fraser, M. (1997). Interactions of Eph-related receptors and ligands confer rostrocaudal pattern to trunk neural crest migration. *Current Biology* **7**, 571-580.

Kulesa, P. M., Bailey, C. M., Kasemeier-Kulesa, J. C. and McLennan, R. (2010). Cranial neural crest migration: new rules for an old road. *Developmental Biology* **344**, 543-554.

Kurabayashi, N., Nguyen, M. D. and Sanada, K. (2013). The G protein-coupled receptor GPRC5B contributes to neurogenesis in the developing mouse neocortex. *Development* **140**, 4335-4346.

Kuratani, S., Tanaka, S., Ishikawa, Y. and Zukeran, C. (1988). Early development of the hypoglossal nerve in the chick embryo as observed by the whole-mount nerve staining method. *American Journal of Anatomy* **182**, 155-168.

Lacalli, T. C. and Hou, S. (1999). A reexamination of the epithelial sensory cells of amphioxus (Branchiostoma). *Acta Zoologica* **80**, 125-134.

Ladds, G., Goddard, A., Hill, C., Thornton, S. and Davey, J. (2007). Differential effects of RGS proteins on G alpha(q) and G alpha(11) activity. *Cellular Signalling* **19**, 103-113.

Ladher, R. K., O'Neill, P. and Begbie, J. (2010). From shared lineage to distinct functions: the development of the inner ear and epibranchial placodes. *Development* **137**, 1777-1785.

Lazarov, N. E. (2007). Neurobiology of orofacial proprioception. *Brain Research Reviews* **56**, 362-383.

Le Douarin, N. M. and Kalcheim, C. (1999). *The Neural Crest*. New York: Cambridge University Press.

Lee, H. J. and Zheng, J. J. (2010). PDZ domains and their binding partners: structure, specificity, and modification. *Cell Communication & Signaling* **8**, 8.

Lemmon, M. A. (2004). Pleckstrin homology domains: not just for phosphoinositides. *Biochemical Society Transactions* **32**, 707-711.

Lepski, G., Jannes, C. E., Nikkhah, G. and Bischofberger, J. (2013). cAMP promotes the differentiation of neural progenitor cells in vitro via modulation of voltage-gated calcium channels. *Frontiers in Cellular Neuroscience* **7**, 155.

Lewit-Bentley, A. and Réty, S. (2000). EF-hand calcium-binding proteins. *Current Opinion in Structural Biology* **10**, 637-643.

Lin, D., Gish, G. D., Songyang, Z. and Pawson, T. (1999). The carboxyl terminus of B class ephrins constitutes a PDZ domain binding motif. *Journal of Biological Chemistry* **274**, 3726-3733.

Linares, J. L., Wendling, C., Tomasetto, C. and Rio, M. C. (2000). C2PA, a new protein expressed during mouse spermatogenesis. *FEBS Letters* **480**, 249-254.

Lo, L., Dormand, E. L. and Anderson, D. J. (2005). Late-emigrating neural crest cells in the roof plate are restricted to a sensory fate by GDF7. *Proceedings of the National Academy of Sciences USA* **102**, 7192-7197.

Lodish, H., Berk, A. and Zipursky, S. L. (2000). Section 20.3, G Protein –Coupled Receptors and Their Effectors. In *Molecular Cell Biology*. New York: W. H. Freeman.

Logan, C., Wingate, R. J., McKay, I. J. and Lumsden, A. (1998). Tlx-1 and Tlx-3 homeobox gene expression in cranial sensory ganglia and hindbrain of the chick embryo: markers of patterned connectivity. *Journal of Neuroscience* **18**, 5389-5402.

López-Bendito, G., Cautinat, A., Sánchez, J. A., Bielle, F., Flames, N., Garratt, A. N., Talmage, D. A., Role, L. W., Charnay, P., Marín, O., et al. (2006). Tangential neuronal migration controls axon guidance: a role for neuregulin-1 in thalamocortical axon navigation. *Cell* **125**, 127-142.

Lu, Q., Sun, E. E. and Flanagan, J. G. (2004). Analysis of PDZ-RGS3 function in ephrin-B reverse signaling. *Methods in Enzymology* **390**, 120-128.

Lu, Q., Sun, E. E., Klein, R. S. and Flanagan, J. G. (2001). Ephrin-B reverse signaling is mediated by a novel PDZ-RGS protein and selectively inhibits G protein-coupled chemoattraction. *Cell* **105**, 69-79.

Lu, T. M., Luo, Y. J. and Yu, J. K. (2012). BMP and Delta/Notch signaling control the development of amphioxus epidermal sensory neurons: insights into the evolution of the peripheral sensory system. *Development* **139**, 2020-2030.

Lui, J. H., Hansen, D. V. and Kriegstein, A. R. (2011). Development and evolution of the human neocortex. *Cell* **146**, 18-36.

Ma, Q., Chen, Z., del Barco Barrantes, I., de la Pompa, J. L. and Anderson, D. J. (1998). neurogenin1 is essential for the determination of neuronal precursors for proximal cranial sensory ganglia. *Neuron* **20**, 469-482.

Ma, Q., Fode, C., Guillemot, F. and Anderson, D. J. (1999). Neurogenin1 and neurogenin2 control two distinct waves of neurogenesis in developing dorsal root ganglia. *Genes & Development* **13**, 1717-1728.

Mackereth, M. D., Kwak, S. J., Fritz, A. and Riley, B. B. (2005). Zebrafish pax8 is required for otic placode induction and plays a redundant role with Pax2 genes in the maintenance of the otic placode. *Development* **132**, 371-382.

Mackie, G. O. and Singla, C. L. (2003). The capsular organ of Chelyosoma productum (Ascidiacea: Corellidae): a new tunicate hydrodynamic sense organ. *Brain, Behavior and Evolution* **61**, 45-58.

Maddison, D. R. and Schulz, K. S. (2007). In *The Tree of Life Web Project.*

Maier, E., Saxena, A., Alsina, B., Bronner, M. E. and Whitfield, T. T. (2014). Sensational placodes: neurogenesis in the otic and olfactory systems. *Developmental Biology* **389**, 50-67.

Marín, O., Valiente, M., Ge, X. and Tsai, L. H. (2010). Guiding neuronal cell migrations. *Cold Spring Harbor Perspectives in Biology* **2**, a001834.

Marusich, M. F., Furneaux, H. M., Henion, P. D. and Weston, J. A. (1994). Hu neuronal proteins are expressed in proliferating neurogenic cells. *Journal of Neurobiology* **25**, 143-155.

Mattar, P., Langevin, L. M., Markham, K., Klenin, N., Shivji, S., Zinyk, D. and Schuurmans, C. (2008). Basic helix-loop-helix transcription factors cooperate to specify a cortical projection neuron identity. *Molecular and Cellular Biology* **28**, 1456-1469.

Mazet, F., Hutt, J. A., Milloz, J., Millard, J., Graham, A. and Shimeld, S. M. (2005). Molecular evidence from Ciona intestinalis for the evolutionary origin of vertebrate sensory placodes. *Developmental Biology* **282**, 494-508.

Melliti, K., Meza, U., Fisher, R. and Adams, B. (1999). Regulators of G protein signaling attenuate the G protein-mediated inhibition of N-type Ca channels. *Journal of General Physiology* **113**, 97-110.

Meulemans, D. and Bronner-Fraser, M. (2007). Insights from amphioxus into the evolution of vertebrate cartilage. *Public Library of Science One* **2**, e787.

Meyer, G., Varoqueaux, F., Neeb, A., Oschlies, M. and Brose, N. (2004). The complexity of PDZ domain-mediated interactions at glutamatergic synapses: a case study on neuroligin. *Neuropharmacology* **47**, 724-733.

Milligan, G. and Kostenis, E. (2006). Heterotrimeric G-proteins: a short history. *British Journal of Pharmacology* **Suppl 1**, S46-55.

Mittmann, C., Chung, C. H., Höppner, G., Michalek, C., Nose, M., Schüler, C., Schuh, A., Eschenhagen, T., Weil, J., Pieske, B., et al. (2002). Expression of ten RGS proteins in human myocardium: functional characterization of an upregulation of RGS4 in heart failure. *Cardiovasculature Research* **55**, 778-786.

Mittmann, C., Schüler, C., Chung, C. H., Höppner, G., Nose, M., Kehrl, J. H. and Wieland, T. (2001). Evidence for a short form of RGS3 preferentially expressed in the human heart. *Naunyn-Schmiedeberg's Archives of Pharmacology* **363**, 456-463.

Miyata, T. (2008). Development of three-dimensional architecture of the neuroepithelium: role of pseudostratification and cellular 'community'. *Development, Growth & Differentiation* **50**, S105-112.

Miyata, T., Kawaguchi, A., Saito, K., Kawano, M., Muto, T. and Ogawa, M. (2004). Asymmetric production of surface-dividing and non-surface-dividing cortical progenitor cells. *Development* **131**, 3133-3145.

Molnár, Z. (2011). Evolution of cerebral cortical development. *Brain, Behavior and Evolution* **78**, 94-107.

Montelius, A., Marmigère, F., Baudet, C., Aquino, J. B., Enerbäck, S. and Ernfors, P. (2007). Emergence of the sensory nervous system as defined by Foxs1 expression. *Differentiation* **75**, 404-417.

Moratz, C., Harrison, K. and Kehrl, J. (2004). Role of RGS proteins in regulating the migration of B lymphocytes. *Archivum Immunologiae Et Therapiae Experimentalis* **52**, 27-35.

Morin, X., Cremer, H., Hirsch, M. R., Kapur, R. P., Goridis, C. and Brunet, J. F. (1997). Defects in sensory and autonomic ganglia and absence of locus coeruleus in mice deficient for the homeobox gene Phox2a. *Neuron* **18**, 411-423.

Mu, X. M., Shi, W., Sun, L. X., Li, H., Wang, Y. R., Jiang, Z. Z. and Zhang, L. Y. (2012). Pristimerin inhibits breast cancer cell migration by up- regulating regulator of G protein signaling 4 expression. *Asian Pacific Journal of Cancer Prevention* **13**, 1097-1104.

Murai, K., Qiu, R., Zhang, H., Wang, J., Wu, C., Neubig, R. R. and Lu, Q. (2010). Gα subunit coordinates with ephrin-B to balance self-renewal and differentiation in neural progenitor cells. *Stem Cells* **28**, 1581-1589.

Musacchio, A., Gibson, T., Rice, P., Thompson, J. and Saraste, M. (1993). The PH domain: a common piece in the structural patchwork of signalling proteins. *Trends in Biochemical Sciences* **18**, 343-348.

Nakamura, H., Katahira, T., Matsunaga, E. and Sato, T. (2005). Isthmus organizer for midbrain and hindbrain development. *Brain Research Reviews* **49**, 120-126.

Nalefski, E. A. and Falke, J. J. (1996). The C2 domain calcium-binding motif: structural and functional diversity. *Protein Science* **5**, 2375-2390.

Neill, J. D., Duck, L. W., Sellers, J. C., Musgrove, L. C. and Kehrl, J. H. (2001). A regulator of G protein signaling, RGS3, inhibits gonadotropin-releasing hormone (GnRH)-stimulated luteinizing hormone (LH) secretion. *BMC Cell Biology* **2**.

Niu, J., Scheschonka, A., Druey, K. M., Davis, A., Reed, E., Kolenko, V., Bodnar, R., Voyno-Yasenetskaya, T., Du, X., Kehrl, J., et al. (2002). RGS3 interacts with 14-3-3 via the N-terminal region distinct from the RGS (regulator of G-protein signalling) domain. *Biochemical Journal* **365**, 677-684.

Noctor, S. C., Martínez-Cerdeño, V., Ivic, L. and Kriegstein, A. R. (2004). Cortical neurons arise in symmetric and asymmetric division zones and migrate through specific phases. *Nature Neuroscience* **7**, 136-144.

Nomaksteinsky, M., Kassabov, S., Chettouh, Z., Stoeklé, H. C., Bonnaud, L., Fortin, G., Kandel, E. R. and Brunet, J. F. (2013). Ancient origin of somatic and visceral neurons. *BMC Biology* **11**.

Norlin, E. M. and Berghard, A. (2001). Spatially restricted expression of regulators of G-protein signaling in primary olfactory neurons. *Molecular and Cellular Neuroscience* **17**, 872-882.

Northcutt, R. G. (2005). The New Head Hypothesis Revisited. *Journal of Experimental Zoology* **304B**, 274–297.

O'Leary, D. D. and Wilkinson, D. G. (1999). Eph receptors and ephrins in neural development. *Current Opinion in Neurobiology* **9**, 65-73.

Obsilova, V., Kopecka, M., Kosek, D., Kacirova, M., Kylarova, S., Rezabkova, L. and Obsil, T. (2014). Mechanisms of the 14-3-3 protein function: regulation of protein function through conformational modulation. *Physiological Research* **63**, S155-164.

Olesen, C., Nyeng, P., Kalisz, M., Jensen, T. H., Møller, M., Tommerup, N. and Byskov, A. G. (2007). Global gene expression analysis in fetal mouse ovaries with and without meiosis and comparison of selected genes with meiosis in the testis. *Cell and Tissue Research* **328**, 207-221.

Osborne, N. J., Begbie, J., Chilton, J. K., Schmidt, H. and Eickholt, B. J. (2005). Semaphorin/neuropilin signaling influences the positioning of migratory neural crest cells within the hindbrain region of the chick. *Developmental Dynamics* **232**, 939-949.

Owens, D. F. and Kriegstein, A. R. (1998). Patterns of intracellular calcium fluctuation in precursor cells of the neocortical ventricular zone. *Journal of Neuroscience* **18**, 5374-5388.

Paddison, P. J., Bernstein, e., Bernstein, E., Hannon, G. J. and Conklin, D. S. (2002). Short hairpin RNAs (shRNAs) induce sequence-specific silencing in mammalian cells. *Genes & Development* **16**, 948-958.

Patthey, C. and Gunhaga, L. (2011). Specification and regionalisation of the neural plate border. *European Journal of Neuroscience* **34**, 1516-1528.

Patthey, C., Schlosser, G. and Shimeld, S. M. (2014). The evolutionary history of vertebrate cranial placodes - I: Cell type evolution. *Developmental Biology* **389**, 82-97.

Pattyn, A., Morin, X., Cremer, H., Goridis, C. and Brunet, J. F. (1997). Expression and interactions of the two closely related homeobox genes Phox2a and Phox2b during neurogenesis. *Development* **124**, 4065-4075.

---- (1999). The homeobox gene Phox2b is essential for the development of autonomic neural crest derivatives. *Nature* **399**, 366-370.

Pelechano, V., Wei, W. and Steinmetz, L. M. (2013). Extensive transcriptional heterogeneity revealed by isoform profiling. *Nature* **497**, 127-131.

Pieper, M., Eagleson, G. W., Wosniok, W. and Schlosser, G. (2011). Origin and segregation of cranial placodes in Xenopus laevis. *Developmental Biology* **360**, 257-275.

Placzek, M. and Briscoe, J. (2005). The floor plate: multiple cells, multiple signals. *Nature Reviews Neuroscience* **6**, 230-240.

Pollard, K. S., Hubisz, M. J., Rosenbloom, K. R. and Siepel, A. (2010). Detection of nonneutral substitution rates on mammalian phylogenies. *Genome Research* **20**, 110-121.

Posner , B. A., Mukhopadhyay, S., Tesmer, J. J., Gilman, A. G. and Ross, E. M. (1999). Modulation of the affinity and selectivity of RGS protein interaction with G alpha subunits by a conserved asparagine/serine residue. *Biochemistry* **38**, 7773-7779.

Qin, S. and Zhang, C. L. (2012). Role of Kruppel-like factor 4 in neurogenesis and radial neuronal migration in the developing cerebral cortex. *Molecular and Cellular Biology* **32**, 4297-4305.

Qiu, R., Wang, J., Tsark, W. and Lu, Q. (2010). Essential role of PDZ-RGS3 in the maintenance of neural progenitor cells. *Stem Cells* **28**, 1602-1610.

Qiu, R., Wang, X., Davy, A., Wu, C., Murai, K., Zhang, H., Flanagan, J. G., Soriano, P. and Lu, Q. (2008). Regulation of neural progenitor cell state by ephrin-B. *Journal of Cell Biology* **181**, 973-983.

Raft, S. and Groves, A. K. (2014). Segregating neural and mechanosensory fates in the developing ear: patterning, signaling, and transcriptional control. *Cell and Tissue Research*.

Rao, D. D., Vorhies, J. S., Senzer, N. and Nemunaitis, J. (2009). siRNA vs. shRNA: similarities and differences. *Advanced Drug Delivery Reviews.* **61**, 746-759.

Reif, K. and Cyster, J. G. (2000). RGS molecule expression in murine B lymphocytes and ability to down-regulate chemotaxis to lymphoid chemokines. *Journal of Immunology* **164**, 4720-4729.

Rétaux, S., Bourrat, F., Joly, J. S. and Hinaux, H. (2013). Perspectives in Evo-Devo of the Vertebrate Brain. In *Advances in Evolutionary Developmental Biology* (ed. J. T. Streelman). Hoboken, New Jersey, USA: John Wiley & Sons.

Rezabkova , L., Boura, E., Herman, P., Vecer, J., Bourova, L., Sulc, M., Svoboda, P., Obsilova, V. and Obsil, T. (2010). 14-3-3 protein interacts with and affects the structure of RGS domain of regulator of G protein signaling 3 (RGS3). *Journal of Structural Biology* **170**, 451-461.

Rezabkova, L., Man, P., Novak, P., Herman, P., Vecer, J., Obsilova, V. and Obsil, T. (2011). Structural basis for the 14-3-3 protein-dependent inhibition of the regulator of G protein signaling 3 (RGS3) function. *Journal of Biological Chemistry* **286**, 43527-43536.

Ridley, A., Paterson, H., Johnston, C., Diekmann, D. and Hall, A. (1992). The small GTP-binding protein rac regulates growth factor-induced membrane ruffling. *Cell* **70**, 401-410.

Rifkin, J. T., Todd, V. J., Anderson, L. W. and Lefcort, F. (2000). Dynamic expression of neurotrophin receptors during sensory neuron genesis and differentiation. *Developmental Biology* **227**, 465-480.

Robins, H. and Press, W. H. (2005). Human microRNAs target a functionally distinct population of genes with AT-rich 3' UTRs. *Proceedings of the National Academy of Sciences USA* **102**, 15557-15562.

Ryan, K., Butler, K., Bellefroid, E. and Gurdon, J. B. (1998). Xenopus eomesodermin is expressed in neural differentiation. *Mechanisms of Development* **75**, 155-158.

Sánchez-Fernández, G., Cabezudo, S., García-Hoz, C., Benincá, C., Aragay, A. M., Mayor, F. J. and Ribas, C. (2014). Gαq signalling: the new and the old. *Cellular Signalling* **26**, 833-848.

Santos-Rosa, H., Schneider, R., Bannister, A. J., Sherriff, J., Bernstein, B. E., Emre, N. C., Schreiber, S. L., Mellor, J. and Kouzarides, T. (2002). Active genes are tri-methylated at K4 of histone H3. *Nature* **419**, 407-411.

Sauka-Spengler, T., Meulemans, D., Jones, M. and Bronner-Fraser, M. (2007). Ancient evolutionary origin of the neural crest gene regulatory network. *Developmental Cell* **13**, 405-420.

Scheschonka, A., Dessauer, C. W., Sinnarajah, S., Chidiac, P., Shi, C. and Kehrl, J. H. (2000). RGS3 is a GTPase-activating protein for g(ialpha) and g(qalpha) and a potent inhibitor of signaling by GTPase-deficient forms of g(qalpha) and g(11alpha). *Molecular Pharmacology* **58**, 719-728.

Schlosser, G. (2005). Evolutionary origins of vertebrate placodes: insights from developmental studies and from comparisons with other deuterostomes. *Journal of Experimental Zoology Part B: Molecular and Developmental Evolution* **304**, 347-399.

---- (2006). Induction and specification of cranial placodes. *Developmental Biology* **294**, 303-351.

Schneider, R., Bannister, A. J., Myers, F. A., Thorne, A. W., Crane-Robinson, C. and Kouzarides, T. (2004). Histone H3 lysine 4 methylation patterns in higher eukaryotic genes. *Nature Cell Biology* **6**, 73-77.

Schreiber, R., Kindle, P., Benzing, T., Walz, G. and Kunzelmann, K. (2001). Control of the cystic fibrosis transmembrane conductance regulator by alphaG(i) and RGS proteins. *Biochemical and Biophysical Research Communications* **281**, 917-923.

Schultz, J., Milpetz, F., Bork, P. and Ponting, C. P. (1998). SMART, a simple modular architecture research tool: identification of signaling domains. *Proceedings of the National Academy of Sciences USA* **95**, 5857-5864.

Sharman, J. L., Benson, H. E., Pawson, A. J., Lukito, V., Mpamhanga, C. P., Bombail, V., Davenport, A. P., Peters, J. A., Spedding, M., Harmar, A. J., et al. (2013). IUPHAR-DB: updated database content and new features. *Nucleic Acids Research* **41**, D1083-1088.

Shearwin, K. E., Callen, B. P. and Egan, J. B. (2005). Transcriptional interference--a crash course. *Trends in Genetics* **21**, 339-345.

Shi, C. S., Huang, N. N. and Kehrl, J. H. (2012). Regulator of G-protein signaling 3 isoform 1 (PDZ-RGS3) enhances canonical Wnt signaling and promotes epithelial mesenchymal transition. *Journal of Biological Chemistry* **287**, 33480-33487.

Shi, C. S., Lee, S. B., Sinnarajah, S., Dessauer, C. W., Rhee, S. G. and Kehrl, J. H. (2001). Regulator of G-protein signaling 3 (RGS3) inhibits Gbeta1gamma 2-induced inositol phosphate production, mitogen-activated protein kinase activation, and Akt activation. *Journal of Biological Chemistry* **276**, 24293-24300.

Shimeld, S. M. and Donoghue, P. C. (2012). Evolutionary crossroads in developmental biology: cyclostomes (lamprey and hagfish). *Development* **139**, 2091-2099.

Sierra, D. A., Gilbert, D. J., Householder, D., Grishin, N. V., Yu, K., Ukidwe, P., Barker, S. A., He, W., Wensel, T. G., Otero , G., et al. (2002). Evolution of the regulators of G-protein signaling multigene family in mouse and human. *Genomics* **79**, 177-185.

Skaggs, K., Martin, D. M. and Novitch, B. G. (2011). Regulation of spinal interneuron development by the Olig-related protein Bhlhb5 and Notch signalling. *Development* **138**, 3199-3211.

Skelton, N. J., Kördel, J., Akke, M., Forsén, S. and Chazin, W. J. (1994). Signal transduction versus buffering activity in Ca(2+)-binding proteins. *Nature Structural Biology* **1**, 239-245.

Smrcka, A. V. (2008). G protein βγ subunits: central mediators of G protein-coupled receptor signaling. *Cellular and Molecular Life Sciences* **65**, 2191-2214.

Soshnikova, N. and Duboule, D. (2009). Epigenetic temporal control of mouse Hox genes in vivo. *Science* **324**, 1320-1323.

Srinivasan, K., Roosa, J., Olsen, O., Lee, S. H., Bredt, D. S. and McConnell, S. K. (2008). MALS-3 regulates polarity and early neurogenesis in the developing cerebral cortex. *Development* **135**, 1781-1790.

Streit, A. (2002). Extensive cell movements accompany formation of the otic placode. *Developmental Biology* **249**, 237-254.

---- (2007). The preplacodal region: an ectodermal domain with multipotential progenitors that contribute to sense organs and cranial sensory ganglia. *International Journal of Developmental Biology* **51**, 447-461.

---- (2008). The cranial sensory nervous system: specification of sensory progenitors and placodes. In *StemBook, ed.* (eds F. Watt & F. Gage): The Stem Cell Research Community.

Strobl-Mazzulla, P. H. and Bronner, M. E. (2012). Epithelial to mesenchymal transition: new and old insights from the classical neural crest model. *Seminars in Cancer Biology* **22**, 411-416.

Sun, W., Kim, H. and Moon, Y. (2010). Control of neuronal migration through rostral migration stream in mice. *Anatomy & Cell Biology* **43**, 269-279.

Suurväli, J., Robert, J., Boudinot, P. and Rüütel Boudinot, S. (2013). R4 regulators of G protein signaling (RGS) identify an ancient MHC-linked synteny group. *Immunogenetics* **65**, 145-156.

Suzuki, A. and Ohno, S. (2006). The PAR-aPKC system: lessons in polarity. *Journal of Cell Science* **119**, 979-987.

Swartz, M. E., Eberhart, J., Pasquale, E. B. and Krull, C. E. (2001). EphA4/ephrin-A5 interactions in muscle precursor cell migration in the avian forelimb. *Development* **128**, 4669-4680.

Tabata, H. and Nakajima, K. (2003). Multipolar migration: the third mode of radial neuronal migration in the developing cerebral cortex. *Journal of Neuroscience* **23**, 9996-10001.

Tamura, K., Peterson, D., Peterson, N., Stecher, G., Nei, M. and Kumar, S. (2011). MEGA5: molecular evolutionary genetics analysis using maximum likelihood, evolutionary distance, and maximum parsimony methods. *Molecular Biology and Evolution* **28**, 2731-2739.

Tang, W. J., Chen, J. S. and Zeller, R. W. (2013). Transcriptional regulation of the peripheral nervous system in Ciona intestinalis. *Developmental Biology* **378**, 183-193.

Tatenhorst, L., Senner, V., Püttmann, S. and Paulus, W. (2004). Regulators of G-protein signaling 3 and 4 (RGS3, RGS4) are associated with glioma cell motility. *Journal of Neuropathology & Experimental Neurology* **63**, 210-222.

Tesmer, J. J., Berman, D. M., Gilman, A. G. and Sprang, S. R. (1997). Structure of RGS4 bound to AlF4--activated G(i alpha1): stabilization of the transition state for GTP hydrolysis. *Cell* **89**, 251-261.

Theveneau, E., Marchant, L., Kuriyama, S., Gull, M., Moepps, B., Parsons, M. and Mayor, R. (2010). Collective chemotaxis requires contact-dependent cell polarity. *Developmental Cell* **19**, 39-53.

Thiery, J. P., Acloque, H., Huang, R. Y. and Nieto, M. A. (2009). Epithelial-mesenchymal transitions in development and disease. *Cell* **139**, 871-890.

Thompson, H., Blentic, A., Watson, S., Begbie, J. and Graham, A. (2010). The formation of the superior and jugular ganglia: insights into the generation of sensory neurons by the neural crest. *Developmental Dynamics* **239**, 439-445.

Toro-Castillo, C., Thapliyal, A., Gonzalez-Ochoa, H., Adams, B. A. and Meza, U. (2007). Muscarinic modulation of Cav2.3 (R-type) calcium channels is antagonized by RGS3 and RGS3T. *American Journal of Phyisology Cell Physiology* **292**, C573-580.

Torres, R., Firestein, B. L., Dong, H., Staudinger, J., Olson, E. N., Huganir, R. L., Bredt, D. S., Gale, N. W. and Yancopoulos, G. D. (1998). PDZ proteins bind, cluster, and synaptically colocalize with Eph receptors and their ephrin ligands. *Neuron* **21**, 1453-1463.

Tosetti, P. and Dunlap, K. (2004). Assays of RGS3 activation and modulation. *Methods in Enzymology* **390**, 99-119.

Tosetti, P., Pathak, N., Jacob, M. H. and Dunlap, K. (2003). RGS3 mediates a calcium-dependent termination of G protein signaling in sensory neurons. *Proceedings of the National Academy of Sciences USA* **100**, 7337-7342.

Tovey, S. C. and Willars, G. B. (2004). Single-cell imaging of intracellular Ca2+ and phospholipase C activity reveals that RGS 2, 3, and 4 differentially regulate signaling via the Galphaq/11-linked muscarinic M3 receptor. *Molecular Pharmacology* **66**, 1453-1464.

Vogt, A., Lutz, S., Rümenapp, U., Han, L., Jakobs, K. H., Schmidt, M. and Wieland, T. (2007). Regulator of G-protein signalling 3 redirects prototypical Gi-coupled receptors from Rac1 to RhoA activation. *Cellular Signalling* **19**, 1229-1237.

Vohra, B. P., Fu, M. and Heuckeroth, R. O. (2007). Protein kinase Czeta and glycogen synthase kinase-3beta control neuronal polarity in developing rodent enteric neurons, whereas SMAD specific E3 ubiquitin protein ligase 1 promotes neurite growth but does not influence polarity. *Journal of Neuroscience* **27**, 9458-9468.

Wada, H., Saiga, H., Satoh, N. and Holland, P. W. (1998). Tripartite organization of the ancestral chordate brain and the antiquity of placodes: insights from ascidian Pax-2/5/8, Hox and Otx genes. *Development* **125**, 1113-1122.

Walther, C. and Gruss, P. (1991). Pax-6, a murine paired box gene, is expressed in the developing CNS. *Development* **113**, 1435-1449.

Wang, Q., Liu, M., Mullah, B., Siderovski, D. P. and Neubig, R. R. (2002). Receptor-selective effects of endogenous RGS3 and RGS5 to regulate mitogen-activated protein kinase activation in rat vascular smooth muscle cells. *Journal of Biological Chemistry* **277**, 24949-24958.

Wang, X., Tsai, J. W., LaMonica, B. and Kriegstein, A. R. (2011). A new subtype of progenitor cell in the mouse embryonic neocortex. *Nature Neuroscience* **14**, 555-561.

Ward, R. J. and Milligan, G. (2005). A key serine for the GTPase-activating protein function of regulator of G protein signaling proteins is not a general target for 14-3-3 interactions. *Molecular Pharmacology* **68**, 1821-1830.

Watson, N., Linder, M. E., Druey, K. M., Kehrl, J. H. and Blumer, K. (1996). RGS family members: GTPase-activating proteins for heterotrimeric G-protein alpha-subunits. *Nature* **383**, 172-175.

Williams, J. W., Yau, D., Sethakorn, N., Kach, J., Reed, E. B., Moore, T. V., Cannon, J., Jin, X., Xing, H., Muslin, A. J., et al. (2013). RGS3 controls T lymphocyte migration in a model of Th2-mediated airway inflammation.

American Journal of Physiology Lung Cellular and Molecular Physiology **305**, L693-701.

Wilson, S. W. and Houart, C. (2004). Early steps in the development of the forebrain. *Developmental Cell* **6**, 167-181.

Xiang, M., Gan, L., Zhou, L., Klein, W. H. and Nathans, J. (1996). Targeted deletion of the mouse POU domain gene Brn-3a causes selective loss of neurons in the brainstem and trigeminal ganglion, uncoordinated limb movement, and impaired suckling. *Proceedings of the National Academy of Sciences USA* **93**, 11950-11955.

Xie, Y., Wolff, D. W., Wei, T., Wang, B., Deng, C., Kirui, J. K., Jiang, H., Qin, J., Abel, P. W. and Tu, Y. (2009). Breast cancer migration and invasion depend on proteasome degradation of regulator of G-protein signaling 4. *Cancer Research* **69**, 5743-5751.

Yang, J., Mani, S. A., Donaher, J. L., Ramaswamy, S., Itzykson, R. A., Come, C., Savagner, P., Gitelman, I., Richardson, A. and Weinberg, R. A. (2004). Twist, a master regulator of morphogenesis, plays an essential role in tumor metastasis. *Cell* **117**, 927-939.

Yau, D. M., Sethakorn, N., Taurin, S., Kregel, S., Sandbo, N., Camoretti-Mercado, B., Sperling, A. I. and Dulin, N. O. (2008). Regulation of Smad-mediated gene transcription by RGS3. *Molecular Pharmacology* **73**, 1356-1361.

Zhou, Y., Falenta, K. and Lalli, G. (2014). Endocannabinoid signalling in neuronal migration. *International Journal of Biochemistry and Cell Biology* **47**, 104-108.

Zhuo, H., Ichikawa, H. and Helke, C. J. (1997). Neurochemistry of the nodose ganglion. *Progress in Neurobiology* **52**, 79-107.

Zirlinger, M., Lo, L., McMahon, J., McMahon, A. P. and Anderson, D. J. (2002). Transient expression of the bHLH factor neurogenin-2 marks a subpopulation of neural crest cells biased for a sensory but not a neuronal fate. *Proceedings of the National Academy of Sciences USA* **99**, 8084-8089.

Zou, D., Silvius, D., Fritzsch, B. and Xu, P. X. (2004). Eya1 and Six1 are essential for early steps of sensory neurogenesis in mammalian cranial placodes. *Development* **131**, 5561-5572.